12-2012

Induced Elastic Matrix Synthesis within 3-Dimensional Collagen Constructs

Lavanya Venkataraman
Clemson University, lvenkat@clemson.edu

INDUCED ELASTIC MATRIX SYNTHESIS WITHIN 3-DIMENSIONAL COLLAGEN CONSTRUCTS

A Dissertation
Presented to
the Graduate School of
Clemson University

In Partial Fulfillment
of the Requirements for the Degree
Doctor of Philosophy
Bioengineering

By
Lavanya Venkataraman
December 2012

Accepted by:
Anand Ramamurthi, Ph.D (Research Advisor)
Martine LaBerge, Ph.D (Committee Chair)
Naren R. Vyavahare, Ph.D
Jiro Nagatomi, Ph.D

ABSTRACT

Elastin, a primary component of elastic arteries, maintains structural stability of the cyclically recoiling artery, and critically regulates vascular cell behavior. Accelerated degradation of elastic matrix, such as that seen in vascular pathologies like abdominal aortic aneurysms (AAA), can therefore severely compromise vessel homeostasis. Tissue engineering and in-situ matrix repair strategies evaluated so far are primarily limited in inducing adult vascular cells to replicate the complex elastic matrix assembly process, and restore lost matrix integrity. Previously, our lab established the elastogenic benefits of concurrent delivery of TGF-β1 and HA-oligomers (together termed elastogenic factors, EFs), within 2D cultures of rat aortic smooth muscle cells (SMCs). Since SMCs are known to switch to a synthetic, highly matrix producing phenotype, in a manner that cannot be replicated *in vivo*, we sought to develop a relevant 3D *in vitro* model system, where the benefits of EFs can be replicated. We chose a 3D collagen-gel model since the presence of a collagenous matrix is centric to replicating vascular tissue architecture and mechanics. Further, vascular cells, regardless of the choice of scaffolds, robustly synthesize collagen. Examining the impact of a pre-existing collagenous microenvironment on the ability of the SMCs to synthesize fibrous elastic matrix in response to provided EFs, is pertinent to its clinical translation.

In the first set of studies, we examined a dose range of EFs on inducing rat SMCs-seeded within 3D collagen gel constructs. Relative to untreated control, all the three doses tested showed up to a 2-fold up-regulation in gene expression of the elastin crosslinking enzyme, lysyl oxidase, and increased the accumulation of matrix elastin up

to 5-fold. The lowest dose combination of 0.1 ng/ml TGF-β1 and 0.2 μg/ml HA-o, was evaluated to be most elastogenic, and this was utilized in subsequent studies. Next, we evaluated the application of cyclic strains at varying frequencies in improving EF-induced elastic matrix output, and to obtain matrix and cell orientation in a manner similar to that required *in vivo*. Further, we tested this system on human SMCs seeded within tubular collagen-gel constructs, to examine if they respond to EF-treatment similar to rat SMCs. A bimodal trend in elastic matrix output was observed with increasing frequencies. Relative to static controls, constructs treated with EFs at 2.5% strains and 1.5 Hz were found to improve contractile SMC phenotype, up-regulate elastin gene expression up to 7-fold, and increase elastic matrix content by 5-fold. These parameters were therefore chosen for application in subsequent studies. The presence of high concentrations of matrix degrading proteases, such as MMPs-2 and -9, inherent to AAA wall, as well as within our 3D system, can compromise the accumulation and efficient assembly of newly synthesized elastic matrix components. In the next set of studies, we demonstrated that addition of Doxycycline (DOX), a non-specific MMP inhibitor, along with EFs, suppressed MMP-2 gene expression, within static and dynamic (2.5% strain at 1.5 Hz) tubular constructs, and markedly improved overall elastic matrix synthesis.

Since the effects of EFs and DOX are highly dose-dependent, the successful *in vivo* translation of their benefits relies on their controlled and targeted delivery specifically to the site of disease. In the final set of studies, we tested the effects of TGF-β1 and DOX released from PLGA nanoparticles, incorporated within the cyclically stretched tubular 3D model optimized in previous studies. We were able to successfully

demonstrate that such localized delivery was able to induce elastogenesis in a manner similar to exogenous delivery of the same factors.

Overall, these results will be useful towards addressing a fundamental and widely absent aspect in vascular engineering, that of inducing adult vascular cells to replicate biological and structural mimics of native elastic fiber networks.

ACKNOWLEDGEMENTS

I would first like to thank my advisor Dr. Anand Ramamurthi, for his utmost support, mentorship and guidance throughout the course of my time as a Ph.D. student. He has been extremely understanding and supportive even during times when I have been very undeserving of it. His perspectives as a scientist, as well as that as an individual, have played an important role in shaping mine, and will always remain a source of inspiration. It is also thanks to his career path, that I have had the privilege to meet and be amidst some very fine scientists and individuals in 3 great institutes and cities.

I would next like to thank my academic advisor, Dr.Martine LaBerge. She has always been highly encouraging and has at several occasions, gone out of her way to show me support. I would next like to thank my committee members, Dr. Naren Vyavahare and Dr.Jiro Nagatomi, who have given many valuable suggestions in shaping my thesis work.

I would next like to thank Ryan, Barry, Kevin, Dr.Gao and all members of the Design and Prototype core who have played a huge role in kick starting my bioreactor studies. I have learnt a great deal from them. I would also like to thank Diane and Mei from the Imaging Core for their help with histology and TEM.

Among my peers, I would first like to start off by thanking ex-members of the Ramamurthi lab, Emily and Carmen. My fundamentals and values as a scientist would not have been as strong had it not been for their mentorship and insight, which I must add, might have been very frustrating for them at times. In Emily, especially, I have found a great friend and a source of inspiration. I would next like to thank Chris, especially for

his help with all the mechanical testing procedures and PCR. I would also like to thank Bala and Pratik for their help and support through all the frustrating days of nanoparticle study optimization. All of their support and work has greatly contributed to my thesis. I would also like to thank other members of the Ramamurthi lab who have in many ways contributed to my learning curve- Durba, Shyam, Dennis, Sahithya, Ganesh, and last but not the least, Partha. Partha will always remain a great source for energy boosters, and a great friend. I have learnt a great deal from them in many facets of my time as a member of this lab, and also had fun in the process.

I would also like to thank all the faculty and staff members of Clemson BioE and MUSC, and staff and scientists at the Cleveland Clinic. They have all in their own ways, played an important role in shaping my perspectives as a scientist.

Lastly, I would like to thank my family, my extended family, and my small circle of close friends, for whose love, support, distractions, prayers, and belief in me and my abilities, I will always be indebted to. My parents, Venkataraman and Pushpa, my sister, Sukanya, and my husband, Sathya have been my greatest sources of inspiration, love and support. Anything I say beyond this would only do injustice to just how much of a role they have played in all facets of my life, especially in the last four years of my time as a PhD. student.

TABLE OF CONTENTS

TABLE OF CONTENTS (CONT.)

TABLE OF CONTENTS (CONT.)

TABLE OF CONTENTS (CONT.)

LIST OF FIGURES

LIST OF FIGURES (CONT.)

LIST OF FIGURES (CONT.)

LIST OF FIGURES (CONT.)

LIST OF TABLES

CHAPTER ONE

INTRODUCTION

1.1. BACKGROUND

Elastin is one of the primary structural proteins found in the ECM of several connective tissues. It crucially maintains configurations of tissues and regulates cell signaling pathways involved in morphogenesis, injury response, and inflammation[1-2]. Specifically, within elastic arteries, it comprises of 50% of the dry tissue weight, playing a major role in maintaining overall vascular homeostasis[3-4]. While the elastic matrix is responsible for providing vessels the necessary recoil and compliance to accommodate blood flow[5], intact elastic fibers also regulate vascular smooth muscle cell (VSMC) behavior through mechano–transduction[1], particularly during morphogenesis and disease progression[2].

Innate homeostatic maintenance of elastin within the extracellular matrix (ECM) is a lifelong process that involves its early synthesis and maturation, slow degradation/ turnover, and limited replacement of structural and signaling proteins involved in elastogenesis[6-7]. Once injured, the elastic matrix is not actively repaired, due to (a) poor elastin precursor (tropoelastin) synthesis by adult cells, (b) inefficient recruitment, crosslinking and organization of tropoelastin into an intact, mature elastic matrix, and (c) further degradation due to the generated matrix metalloproteases (MMPs) and elastin-peptides[7-10] Accelerated degradation of the matrix, as encountered in several vascular diseases such abdominal aortic aneurysms (AAA)[11], coupled with the inability of adult

vascular smooth muscle cells (SMCs) to regenerate lost matrix[8], can thus severely compromise vascular tissue integrity and even result in fatal rupture of vessel wall[12]. Therefore, the failure to reinstate a healthy elastic matrix, when damaged by injury or disease, or when congenitally malformed or absent, such as that seen within abdominal aortic aneurysms, can adversely impact vascular tissue homeostasis [13-15].

AAAs are conditions wherein localized thinning and dilation of the wall of abdominal aortae occur, leading to gradual loss of elasticity, resultant local increase in diameter, which can ultimately lead to rupture[11]. A vessel that has expanded in diameter by at least 50% is generally considered to be aneurismal[16-17]. Initiation and progression of AAA has been attributed primarily to chronic matrix proteolysis by MMPs and inflammatory cells that infiltrate the vessel wall in response to smoking, chronic vasculitis, atherosclerosis, calcified lipid deposits, vascular hypertension, and less frequently, inherited conditions[11, 16]. This is coupled with the absence of intrinsic signals in adult vascular cells to regenerate lost elastic matrix or to successfully repair the disrupted aortic vessel wall matrix[18]. The accelerated loss of elastic matrix and vessel wall integrity, and continuous fluctuations in hemodynamic pressures lead to the abnormal ballooning of an aneurysm[19]. AAAs typically grow about 1 cm/year to catastrophically rupture causing hemorrhage and embolisms. In the United States alone, the estimated incidence for AAAs is about 60 in every 100,000 people per year[16, 20], with a fatality rate of more than 15,000 individuals a year, i.e. about 80% of AAA patients[17, 21]. While advances in high resolution CT and MRI techniques now enable early detection of AAAs, the conditions are frequently asymptomatic until well developed[22].

Currently the most common approach to treat aortic aneurysms is the surgical replacement of the diseased section of the vessel using synthetic grafts, either by an open surgical repair, or more recently, by Endovascular Aneurysm Repair (EVAR)[23]. Although synthetic grafts help to isolate the aneurysm and prevent vessel rupture by providing an alternative pathway for blood flow, they do not accommodate for the loss of functional properties of elastic matrix, pose additional complications due to compliance mismatch between the synthetic graft material and the native blood vessels, and do not aid in regression of the diseased state[24]. Several device-related complications such as lack of endothelialization, prevalence of various types of endoleaks, implant migration and fatigue affect long-term patency of the implant, necessitating surgical intervention (> 30% of cases within 6 years)[25-26]. Synthetic grafts continue to have a failure rate of > 50% within 10 years[26].

Restoring an intact elastic matrix is essential not only to sustain the structural requirements of the vessel wall, but also to maintain healthy vascular cell functioning, both of which are equally critical for vascular homeostasis[14, 18]. Tissue engineering (TE) and matrix regenerative strategies have therefore been extensively investigated to develop biomechanically functional and self-renewing vessel components with the aim to mimic a viable elastic aorta[27]. However, a large body of this work has been unsuccessful in inducing substantial synthesis or regeneration of intact, mature, matrix elastin[10, 28-33]. Studies observing reasonable induction of elastogenesis have done so only by utilizing naturally elastogenic neonatal or juvenile SMCs; success in inducing elastogenesis in adult cells has been limited to demonstrating moderate increases in mRNA expressions of

tropoelastin[34-36]. The translational ability of these vascular TE approaches is therefore limited. Strategies for successful tissue engineering of elastic matrix-rich vascular constructs by adult SMCs are critical and currently unmet.

Previously, our lab established the elastogenic benefits of exogenous hyaluronan oligomers (HA-o; ~756 Da) and TGF-β1 in 2-D-cultures of healthy rat aortic SMCs (RASMCs) [37]. TGF-β1 has shown to increase elastin mRNA levels (by ~ 30-fold) and enhance production of LOX, critical for crosslinking collagen and elastin, and fiber organization *in situ*[38-39]. It has also shown to decrease proteolysis by reducing MMP expression and up-regulating TIMP-1, 2, and 3 mRNA expressions[40-41]. Hyaluronan (HA) also appears to stabilize elastin fibers once formed, against elastase degradation. In addition to this, HA is known to enhance formation of mature matrix elastin by 1) coacervating soluble tropoelastin via their positive lysine residues and 2) facilitating lysyl oxidase (LOX)-mediated oxidation and crosslinking of tropoelastin into insoluble elastic fibers[42-43]. Studies from our lab have also confirmed such up-regulation and demonstrated elastogenic synergy between HA oligomers (~ 756 Da) and growth factors such as TGF-β1[37, 44].

The two primary criteria to be satisfied in order to obtain a highly organized and mature elastic matrix *in vitro*, or to restore lost matrix via *in situ* repair, are 1) inducing VSMCs to synthesize and organize sufficient elastic matrix, and 2) maintaining a balance between increase in matrix production and suppression of degradative proteases. While TGF-β1- HA-o dose combinations enhance elastin synthesis several fold, their insufficiencies in suppressing MMP activity limits the accumulation of mature-matrix.

Studies in our lab have therefore investigated dose-specific benefits of Doxycycline (DOX), a modified tetracycline, in combination with the above factors, to improve elastic matrix output. Known to be a global, non-specific MMP inhibitor, systemic delivery of DOX has been clinically shown to reduce the rate of AAA growth and progression of disease, a likely outcome of reduced elastic matrix proteolytic disruption[45-47].

One of the main limitations of previous studies testing the efficacy of various elastogenic factors was that they were all performed in 2D cultures of VSMCs. VSMCs are known to take up a highly synthetic phenotype, displaying significantly higher proliferation ratios and increased ability to synthesize ECM proteins compared to that seen *in vivo*. Moreover, the matrix ultrastructure in such environments is not replicative of that needed within intact tissues *in vivo*. It is therefore important to test the effects of the elastogenic factors within micro-environmental conditions that more closely evoke the native vascular tissue.

1.2. 3D CULTURE MODEL FOR INDUCED ELASTIN SYNTHESIS

The presence of collagenous matrix is centric to replicating vascular tissue architecture and mechanics[48]. Collagen gels have been extensively investigated as 3-D scaffolding models for vascular TE since the pioneering work of Weinberg and Bell in 1986[49-50]. SMC-seeded collagen gels are actively remodeled in a process called fibrillogenesis, emulating a 3-D environment similar to that seen in the arterial media *in vivo*[51]. SMCs seeded within such scaffolds can therefore be expected to behave in a manner more representative of a healthy phenotype[52-53], compared to other synthetic or

natural scaffolds such as polyglycolic acid (PGA)[54] or fibrin[28]. Moreover, vascular cells, regardless of the choice of scaffolds, robustly synthesize collagen[10, 27]. This is also true in case of auto-regenerative phenomena within proteolytically-disrupted vascular tissues *in vivo*, such as AAAs, where a fibrotic collagen-rich matrix first accumulates[16, 55]. It is therefore further imperative to examine the impact of a pre-existing collagenous microenvironment on the ability of VSMCs to synthesize fibrous elastic matrix in response to provided elastogenic factors[56].

As described in the previous section, one of the limitations of elastic matrix engineering approaches is the lack of sufficient conversion of induced elastin synthesis into an organized and aligned elastic ECM, similar to that needed *in vivo*. Numerous studies in literature point towards benefits of cyclic dynamic conditioning to significantly influence cell phenotype, alignment, matrix deposition, and growth factor release by both native and cultured SMCs[57-59].

Lastly, it is important to note that the factors that have been tested so far *in vitro* can only be translated *in vivo* when their delivery is highly localized at the site of disease. This is important not only to ensure higher availability for efficient and timely response, but more so since the cellular response to these factors are very different depending on their location in the vasculature. For example, while the effects of TGF-β1 delivery generate a highly desirable response by VSMCs in AAAs, within thoracic aortae, it is involved in initiation and progression of aneurysms[60-61]. Moreover, the therapeutic concentrations can be more sensitively controlled and sustained via a localized delivery from polymeric scaffolds such as nanoparticles.

The 3D model system that we have utilized in this thesis is therefore comprised of 1) collagen gel constructs seeded with adult vascular cells, which are 2) subjected to cyclic mechanical distensions, and 3) treated with various dose combinations of TGF-β1, HA-o and DOX, with and without their delivery through nanoparticles.

The results will be useful towards addressing a fundamental and widely absent aspect in vascular tissue engineering, that of being able to engineer elastic tissue constructs containing biological and structural mimics of native elastic fiber networks.

1.3. STUDY OBJECTIVES AND AIMS

The specific aims are designed based on the background and results from previous studies discussed in the sections above. They are as follows:

Aim 1: Investigate basal and induced elastogenesis in static, 3-D collagen gel constructs. A range of TGF-β1 and HA-o dose-combinations will be exogenously delivered to investigate elastin regeneration and matrix orientation by healthy adult RASMCs within static, 3-D constructs of collagenous microenvironments.

Aim 2: (A) Determine benefits of cyclic distension on induced elastogenesis within tubular collagen constructs. Healthy human aortic SMCs (HASMCs) will be cultured within tubular collagen-gel constructs subjected to cyclic strains over a range of frequencies within a pulsatile bioreactor. The most significantly elastogenic dose combination of TGF-β1 and HA-o selected from **Aim 1** will be concurrently delivered to the cultures under dynamic straining. Static cultures with and without TGF-β1 and HA-o will serve as the biologic controls.

(B) Demonstrate that inhibition of matrix metalloproteases improves elastic matrix output and quality. HASMCs cultured under dynamic conditions that are most conducive to elastic matrix deposition in **Aim 2A** will be further cultured in the presence of exogenous DOX, a modified tetracycline that inhibits synthesis and activity of MMPs. Cultures without DOX treatment will serve as controls.

Effects of the above conditions on elastin synthesis, gelatinase synthesis and activity, matrix deposition and orientation, matrix yield and overall architecture will be evaluated in comparison to the respective biological controls.

Aim 3: Evaluate benefits of localized, controlled delivery of elastogenic factors and Doxycycline within tubular collagen-gel cultures over exogenous delivery: Nanoparticle encapsulation and *in vitro* release study of TGF-β1, HA-o and DOX will be performed. These nano-particles will then be incorporated within collagen gels (at concentrations optimized in **Aims 1 and 2** prior to gel polymerization, for localized and sustained delivery of these factors to HASMC cultures within.

1.4. PROJECT INNOVATION AND IMPORTANCE

Poor elastogenic potential of adult vascular cells combined with lack of strategies to efficiently improve mature elastic matrix yield have thus far deterred successful regenerative efforts in elastic vasculature. This study therefore aims at addressing these issues by 1) utilizing the elastogenic potential of TGF-β1 and HA-o in combination with 2) dynamic conditioning for enhancing matrix assembly within 3-D collagen gel constructs seeded with adult vascular SMCs. **Aim 1** of this study would first establish an

optimum dose combination of TGF-β1 and HA-o within collagen gels maintained under static strains. Following this, **Aim 2** will utilize the benefits of the above factors in the presence of cyclic strains in order to achieve a well aligned, mature elastic matrix. The application of cyclic strains in combination with targeted delivery of optimized factors will be studied in **Aim 3**. Translational potential of the above methods will also be reflected in **Aims 2 and 3** with the utilization of adult human VSMCs.

The results will be most useful towards addressing a fundamental and widely absent aspect in vascular tissue engineering, that of reinstating an intact, mature and viable elastic matrix by adult vascular cells.

1.5. ORGANIZATION OF DISSERTATION

Chapter 2 presents an overview of elastin and elastic matrix components of the vasculature, their roles in regulating vascular mechanics and cell behavior during development, aging and disease, and a review of current strategies for vascular elastic matrix regeneration and repair.

Chapter 3 evaluates outcomes of induced elastogenesis of adult rat SMCs seeded within 3D collagen gel constructs maintained under static tension, to a range of TGF-β1 and HA-o dose combination. The most elastogenic dose combination (**termed elastogenic factors or EFs**) is chosen from the outcomes of this study for application in subsequent studies of this project.

Chapter 4 discusses outcomes of combined effects of EF-treatment and varying cyclic strain frequencies within human aortic SMC-seeded tubular collagen gel constructs,

towards improving matrix assembly and alignment. The cyclic strain frequency most conducive to elastic matrix synthesis and alignment is evaluated and utilized in subsequent studies.

Chapter 5 evaluates how Doxycycline-mediated MMP suppression within cyclically strained and EF-treated SMCs seeded in tubular collagen gel constructs further improve outcomes of crosslinked, mature matrix elastin.

Chapter 6 discusses the benefits of localized delivery of TGF-β1 and Doxycycline from PLGA nanoparticles, over their exogenous delivery, within cyclically stretched SMC-seeded tubular collagen constructs.

Finally Chapter 7 details overall conclusions derived from this project and suggestions for future directions based on this work.

CHAPTER TWO

LITERATURE REVIEW

2.1. ELASTIN: PRIMARY COMPONENT OF ELASTIC FIBER ECM

Elastin is distributed throughout the body, however it is primarily found in elastic fibers of circulatory, respiratory and integumentary system that require elastic resilience to maintain important tissue functions[3, 62]. Ultrastructure analysis of elastic fibers reveal two morphologically distinct parts: a 10-12 nm microfibrillar component, primarily fibrillin-1, surrounding the more abundant, amorphous core of elastin[8]. During early stages of fetal development, the elastin precursor, tropoelastin, is deposited within these fibrillin-rich microfibril templates within the extracellular space[6-7]. This helps the monomer units to coalesce, allowing the Copper-dependent Lysyl oxidase (LOX) enzyme to crosslink the units forming a mature elastic matrix[43].

2.1.1. Distribution of Elastin

The elastic property of various connective tissues such as arteries, lungs, elastic cartilage and skin is provided by a complex three dimensional network of elastic fibers within their ECM[63]. These fibers are primarily made up of structural proteins such as elastin and microfibrils, along with various glycosaminoglycans (GAG) and proteoglycans[63-64].

Elastin, the main contributor to the elastic recoil in these tissues, is the predominant protein of mature elastic fibers[65]. The distribution, structural organization and the elastin : microfibril ratio vary between tissues of different organs depending on

physiological role, their mechanical functions and age of tissue[8, 66]. Elastic fibers are associated with other essential ECM proteins like collagen, surrounded by GAGs and proteoglycans, which support the mechanical properties specific to the tissue and help maintain their native cell physiology [8]. In the medial layer of elastic arteries, elastic fibers form concentric fenestrated lamellae separated by collagen and smooth muscle cell (SMC) layers, which impart resilience to the vessel wall during systolic pressures, and recoil during diastole, maintaining blood flow and volume[5]. Within mammalian skin, elastin is found primarily in the reticular dermis as large, flat, undulated and perforated sheets, running parallel to the skin surface, which are replaced by a more microfibril-rich elaunin fibers in the middle dermis, and oxytalan fibers in the papillary dermis consisting only of microfibrillar glycoproteins[7]. The alveolar expansion and recoil during breathing is supported by thin, highly branched elastic fibers present along the blood vessel walls throughout the respiratory tree[62]. While thick elastic fibers ~ 100μm are found in elastic ligaments of the vertebral column, a thin network of elastic fibers, ~57μm, interspersed with collagen fibers is found within elastic and articular cartilage[5, 67].

2.1.2. Chemical Composition of Elastin

Purified elastin is found to be rich in hydrophobic amino acids such as glycine (33%), alanine (24%), valine (15%) and proline (11%), has very low acidic and basic amino acids, and contains no hydroxylisine residues[3, 68-69]. The hydrophobic segments of the elastin polypeptide, present as β-sheets, alternate with the crosslinking α-helical domains rich in lysine and alanine residues[3]. The highly stable elastic characteristics are

maintained by the presence of disulfide bonds and tetrafunctional, heterocyclic desmosine (and its isoforms) crosslinks within the α-helical domains[6, 68].

2.1.3. Elastin Synthesis and Assembly into Elastic Fibers

In humans, elastin is synthesized as tropoelastin, a 72kDa alkali-soluble protein, by the elastin gene present as a single copy on chromosome 7[70-71]. Tropoelastin consists of about 750-800 residues, typically grouped into 'hydrophobic' domains that alternate with lysine-rich 'crosslinking' domains. The hydrophobic sequences are highly repetitive and usually consist of overlapping di-, tri-, tetra-, penta-, hexa-and nano-peptides of aliphatic amino acids like proline (P), alanine (A), valine (V), leucine (L), isoleucine (I)and glycine (G), of which G and V are more commonly found. The crosslinking domains consist of lysyl residues within P-and A-rich regions. These domains are coded for by the 36 exons of the gene, which have more than 70% homology among various species of vertebrates[72]. The variations are primarily seen in the hydrophobic regions, while domains that contribute to important structural features remain conserved. The most conserved region of the translated protein is the positively charged, hydrophilic C-terminus, which consists of the only two cysteine residues found in the protein. This aids in the formation of disulfide bonds[3, 8, 69].

Intracellularly, like most other proteins, tropoelastin is secreted post-transcriptionally by the endoplasmic reticulum, hydroxylated on a number of proline residues and packaged by Golgi apparatus, following which, it is transported to the extracellular space by transcytosis, where it coascervates on microfibrillar pre-scaffolds.

Tropoelastin transport is mediated by the elastin binding complex, a group of three cell membrane proteins. Two of its subuints, 55 and 61kDa, form a transmembrane link between the cytoskeleton and intracellular compartment. The third subunit, a 67kDa protein called elastin-binding protein (EBP), binds the hydrophobic VGVAPG sequence on tropoelastin, the cell membrane and galactosugars on microfibrils[73]. This binding of galactosugars to the lectin site on EBP lowers its affinity for both tropoelastin and the cell-binding site. The bound tropoelastin is therefore released, coascervated on fibrillin scaffold and EBP dissociates from the membrane (**Figures 2.1 and 2.2**).

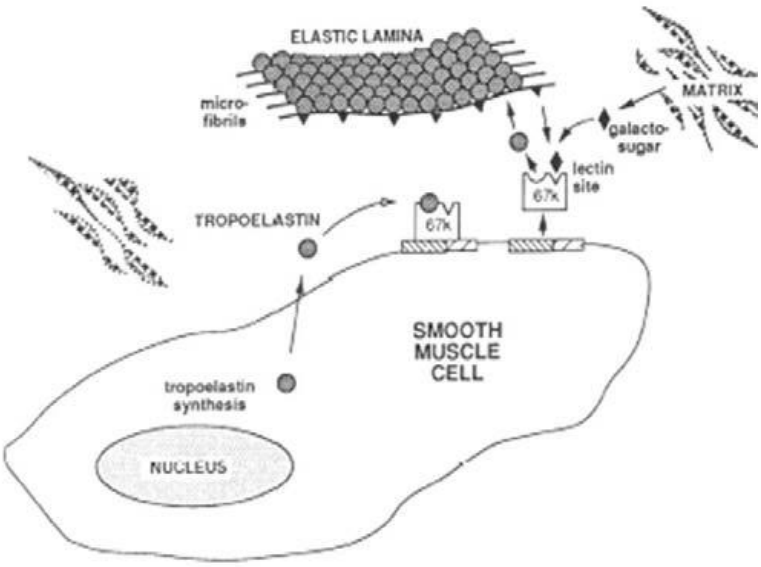

Figure 2.1: Schematic of tropoelastin transport into the extracellular space mediated by the three subunits of elastin binding protein (EBP)[73]

Though galactosugar-containing microfibrillar proteins aid in coordinated release of tropoelastin, an excess of galactose-containing components such as glycoproteins, glycosaminoglycans, or galactolipids in the ECM may adversely affect elastin assembly

by inducing premature release of tropoelastin and elastin-binding protein from the cell surface[8, 74]. Secreted tropoelastin molecules aggregate in the extracellular space on loose, pre-existing bundles of microfibrils that behave as scaffolds for elastic matrix assembly. Microfibrils (fibrillin 1, 2, fibulin 4, 5), appear as 12nm long, electron dense tubes, grouped in small bundles near the plasma membrane. Within each bundle, tropoelastin molecules gradually coalesce, generating a central core of elastin. As the fibers mature, these bundles slowly move towards the periphery[8, 66].

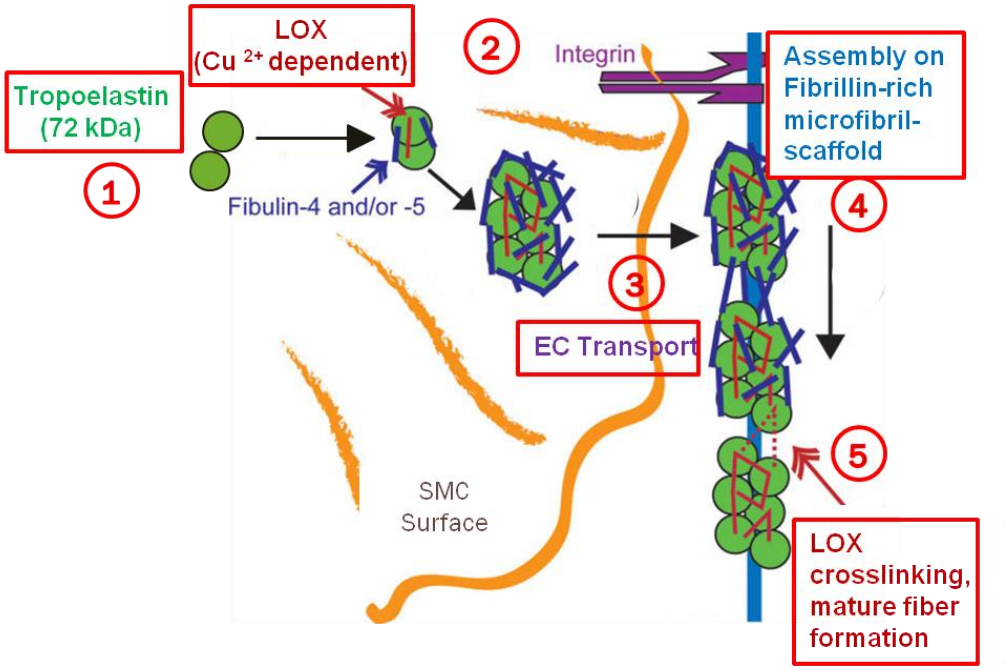

Figure 2.2: Overview of steps involved in tropoelastin transport and assembly on microfibrillar scaffolds in ECM. Adapted from *Wagenseil, J.P., et.al, 2007*[8]

According to conventional electron microscopy, it was long believed that electron dense microfibrils surround an amorphous matrix core. However, recently it was shown that the amorphous appearance of elastin core was in fact an artifact, and that elastin

molecules are organized as 5-nm thick filaments forming a three-dimensional network along the fiber. Further studies have shown that, besides elastin, a number of matrix constituents such as vitronectin, LOX, decorin, osteopontin and biglycan epitopes are also present within normal elastic fibers, which are perhaps equally important in maintaining elastic fiber integrity.

Crosslinking of elastin is initiated by a family of copper dependent enzymes called lysyl oxidase (LOX), which catalyze oxidative deamination of lysine residues into allysine. Specifically, lysyl ε-amino groups present on the α-chain domains of adjacent tropoelastin molecules are oxidized into a δ-aldehyde, an allysine. Approximately 40 lysine residues in 16 crosslinking domains of tropoelastin have been estimated to eventually participate in forming the bi-, tri-, and tetra functional crosslinks of the polymer that equips it with high resilience. LOX mediated crosslinking occurs early in the assembly phase and is critical for matrix elastin formation[43, 75-76]. Subsequent formation of the elastin crosslinks by isodesmosine and desmosine occur as a series of spontaneous condensation reaction[77]. Inhibition of LOX activity through copper deficiency or through the administration of enzymatic inhibitors results in weakened connective tissue throughout the body[78].

2.1.4. Elastic Fiber Maturation, Breakdown and Turnover

Studies have shown that most of the elastic matrix deposited as a neonate, and elastic fibers mature into completely formed matrix by around 16 years of age, following which, very little remodeling of the matrix occurs in a healthy adult vasculature **(Figure 2.3)**[7].

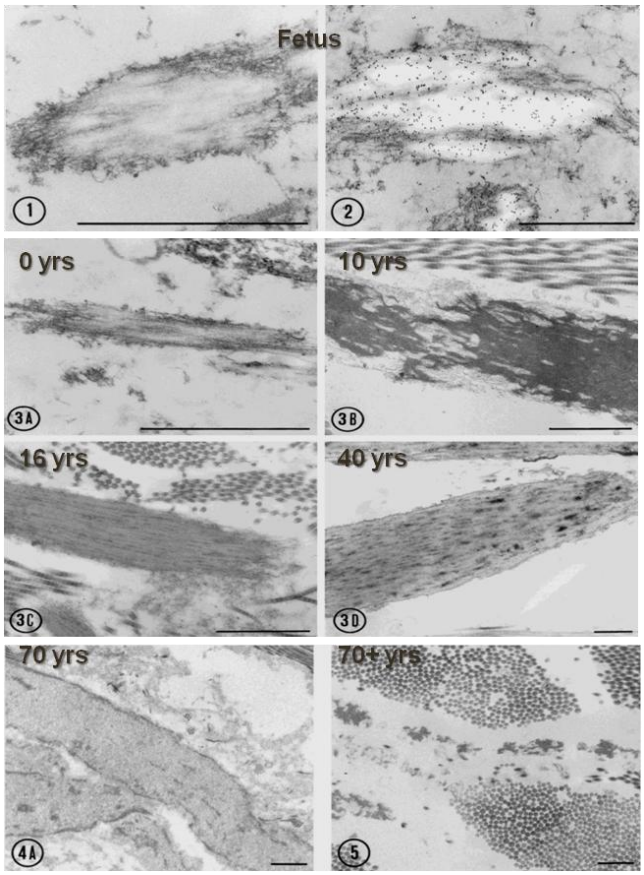

Figure 2.3: Scanning electron micrographs showing elastic fiber formation and breakdown with age. (1), (2) Elastin is assembled on microfibrillar scaffolds at the fetal stage. (3 A, B and C) Mature elastic fiber bundles are formed until 16 years of age. After this elastic fibers start to slowly and progressively degrade with age (3D, 4A, 5). Adapted from *Pasquali-Ronchetti , et al., 1997*[7]

As minimal turnover occurs in healthy tissues, half life of vascular elastin is very long (approximately 70 years). The degradation of elastin is the result of a proteolytic cascade that involves the cooperation of several degradative enzyme types such as serine proteases, matrix metalloproteinases, and cysteine proteases. These may be present in latent forms under healthy physiologic conditions, and can become activated following vessel wall injury[79-80].

Matrix-metalloproteases (MMPs), a family of Zinc-dependent enzymes, are typically involved in elastin turnover in healthy vessels[81]. Vascular SMCs release numerous MMPs that are capable of digesting individual components of the ECM and are normally regulated by tissue inhibitors of metalloproteases (TIMPs)[82]. A balance between MMPs and TIMPs is maintained at all times within healthy tissues to ensure healthy matrix reorganization for cell migration and structural homeostasis of the vessel[80, 83-84]. Integrins are the primary ECM receptors for mechano-transduction, responsible for mediating matrix remodeling, either directly or indirectly[85].

2.2. ELASTIN AND THE VASCULATURE

The largest arteries branching out from the heart, the aorta of systemic circulation, and pulmonary artery of the pulmonary circulation, along with their main branches, the branchiocephalic, common carotid, subclavian, thoracic, abdominal and common iliac arteries are classified as elastic arteries. Elastin constitutes 50% of dry tissue weight of the these arteries and plays a crucial role in maintaining unidirectional flow of blood. They typically have an internal diameter >10 mm. These arteries further branch out into the muscular arteries that have a lower elastic matrix content, higher number of smooth muscles cells and a thinner intima. They have an internal diameter of 0.1-10 mm. These further branch out to the arterioles (< 0.1 mm diameter) and the capillaries (~5 µm diameter), that have thinner walls, more cells and serve to transport blood through all tissues[67].

2.2.1. Elastic Arteries: Structure and Function

The elastic arteries have three main structural and functional layers: (1) the innermost *tunica intima*, (2) the *tunica media* or the middle layer and (3) *tunica adventitia* or the outermost layer (**Figure 2.4**). Each layer has a specific cell type and a distinct ECM composition, which together play a role in maintaining circulation and homeostasis throughout the body[67].

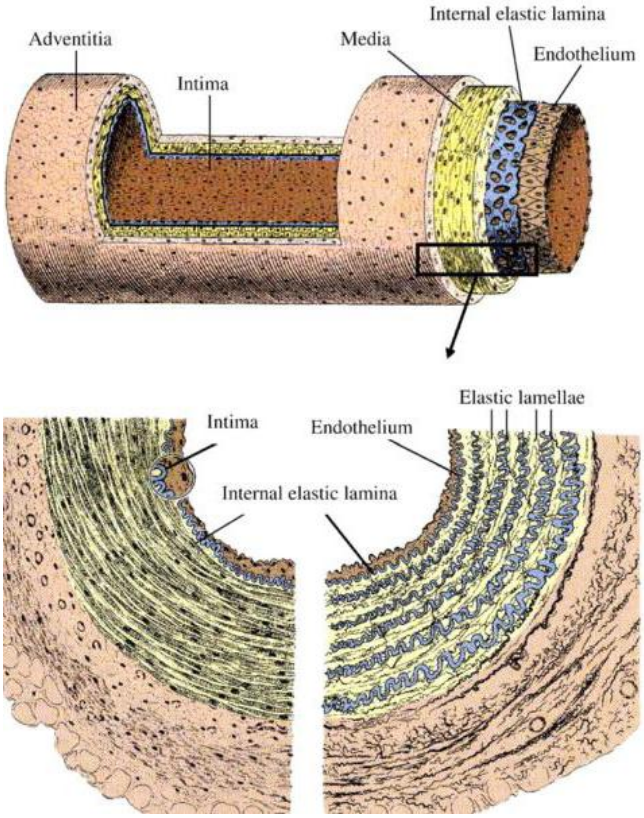

Figure 2.4: Anatomy elastic artery showing the three layers of the blood vessel, tunica intima, tunica media, and tunica adventitia. *Adapted from Patel et.al., 2006*[10]

Tunica intima consists of a layer of endothelial cells resting on a basement membrane, surrounded by a sub-endothelial space and a less conspicuous internal elastic

lamina, which separates intima from the medial layer. The endothelial cells have flat, elongated squamous epithelial cell morphology, with their long axis parallel to the direction of blood flow. They are 10-20 μm in diameter and 1-2 μm thick[67]. These cells are highly resistant to shear stress imparted by continuous flow of blood. Along with the adjoining basement membrane, this layer regulates important functions to maintain vascular homeostasis including 1) maintaining selective transport of cells and molecules across the vessel wall, 2) preserving a non-thrombogenic barrier between blood and the sub-endothelial layers by secreting various anti-thrombogenic substances and anticoagulants like prostacyclin and thrombomodulin respectively, 3) modulating blood flow and vascular resistance by secreting vascodilators like NO and constrictors like endothelin, 4) regulating cell growth, immune response and lipoprotein oxidation, and 5) maintaining extracellular matrix of the basal lamina. Any injury or abnormality in the endothelial layer would therefore disrupt the vessel wall integrity and homeostasis as seen in inflammatory diseases of the vasculature such as aortic aneurysms[86].

Tunica Media is usually the thickest layer of the elastic vessel wall. It is defined by the internal elastic lamina (IEL) following the intima and external elastic lamina (EEL) adjoining the adventitia. Elastin is distributed as fenestrated sheets or lamellae, the number and thickness of which vary linearly with the blood pressure and cyclic tension experienced by the wall[5, 87]. Concentric layers of SMCs, collagen fibers and thin layers of proteoglycan-rich ECM are present between the elastic lamellae. This layer helps accommodate the pulsatile flow of blood and provide mechanical resilience to the vessel. While elastin acts a reservoir of tensile load, distributing stresses evenly throughout the

vessel wall, collagen bears the tensile load and restricts the extent of distension[5]. The SMCs are spindle shaped with an elongated nucleus, arranged in a low-pitch spiral with respect to the long axis of the vessel[67]. Though it was found that their elimination from the wall of a mature aorta does not significantly alter its static mechanical properties, the cells actively respond to changes in cyclic stretch, endothelial growth factors and inflammatory processes, in remodeling the medial ECM[9]. The secretion of collagen and elastin by these cells is dependent on the frequency, magnitude and duration of cyclic strain transmitted to the SMCs[5]. Under normal homeostatic conditions, they remain in a contractile, non-proliferating phenotype, expressing surface markers such as SM-α-actin, calponin, SM22, SM-myosin heavy chain etc[88]. However under pathologic conditions such as hypertension, injury to endothelium, inflammatory reactions, response to various growth factors such as transforming growth factor-β1 (TGF−β1), tumor necrosis factor-α (TNF-α), platelet-derived growth factor (PDGF), basic fibroblast growth factor (bFGF), insulin-like growth factor-1 (IGF-1), interleukin-1 (IL-1) etc, SMCs can switch to a proliferating, synthetic phenotype, which in turn also alter the vascular matrix composition and mechanics[89-90]. This has been discussed in detail in subsequent sections.

Tunica adventitia is the outermost layer of the vessel wall, defined as the region outside the EEL in elastic arteries. It consists of fibroblasts that maintain a matrix rich in collagen type-I, which helps prevent rupture of the vessel at high pressures. Vasa-vasorum, the small blood vessels providing nourishment to large elastic and muscular arteries and vessel innervations are usually present in this layer. Recent studies have shown that this layer may possess injury-sensing capabilities and home progenitor cells

capable of differentiating into SMCs[67]. Recent studies have shown that the adventitia may be sensitive to injury and may also house progenitor cells capable of repopulating the media and intima[91].

Functionally, the elastic arteries facilitate in maintaining the uniform flow of blood through the vasculature, while at the same time maintaining blood volume and pressure. During the systolic phase, the ventricles contract and pump blood into the elastic arteries, and simultaneously, the arterial wall distends. The extent of distension is limited by the presence of collagen fibers in the medial and adventitial layers. Following this, during diastole, when the heart does not generate additional pressure, these vessels recoil due to the presence of elastic fibers, therefore maintaining blood flow, restoring baseline pressure and triggering the closure of the semilunar valves to prevent back-flow of blood into the heart, while the cycle continues. In effect, these arteries store a portion of the stroke volume with each systole and release the same during diastole. This helps decrease the load on the heart, minimizes systolic flow and maximizes diastolic flow through the arterioles, a phenomenon called 'windkessel effect'[5].

2.2.2. Matrix and Cellular Components of elastic arteries and their roles

While on the one hand, the vascular ECM is responsible for supporting the structural and mechanical properties of the vessel wall, they also provide instructions to regulate cellular phenotype by binding to specific cell receptors to activate gene expressions, control growth factor activity and maintain cell functions. The ECM comprises of three main components: (a) structural proteins like elastin and collagen, (b)

fibrous proteins like fibrillin, laminin etc, and (c) proteoglycans. These interact with each other, the cellular components and the surrounding environment to maintain homeostasis.

Collagen is present within the ECM of all three layers of the vessel wall and is primarily responsible for its load bearing properties. It consists of three α-helical polypeptide chains, composed of Gly-Pro and 4-Hydroxyproline, of which the side chains of Gly alone occupy the interior of the helix, while that of Pro and Hydroxy-pro face outward, helping in coalescing and crosslinking pro-collagen molecules[92]. 17 different collagen types have been identified in a mouse aorta depending on the helical size, of which collagen types I, III, IV, V and VI were found to have highest expression levels, whose distribution varies depending on the region in the vasculature. Types I, III and IV are fibrillar collagen, of which I and III are mainly load bearing. While type I is predominant in the media and type III is primarily found in the adventitia[4]. Mutations in genes encoding either of the two types result in fragile blood vessels prone to rupture. Type V collagen is found within the media and basement membranes, and plays a role in collagen fibril nucleation and assembly. This has been demonstrated in mice deficient in this gene that die during early stages of embryogenesis due to lack of fiber formation. Type VI is also a fibrillar collagen that associates with fibrillin-1 of oxytalan fibers, connecting the elastic lamellae with the basement membrane and the SMCs with other ECM components[92]. Lysyl oxidase helps crosslink fibrillar collagen, by converting the lysine and hydrozylysine residues in the non-helical telopeptides into aldehydes, forming bi-functional crosslinks. 1-4 crosslinks are found per collagen unit. This helps aggregate the 10–30 nm diameter collagen fibrils into densely packed 500-3000 nm thick fiber

bundles for achieving much higher tensile properties[43, 76, 93-94]**(Figure 2.5)**.

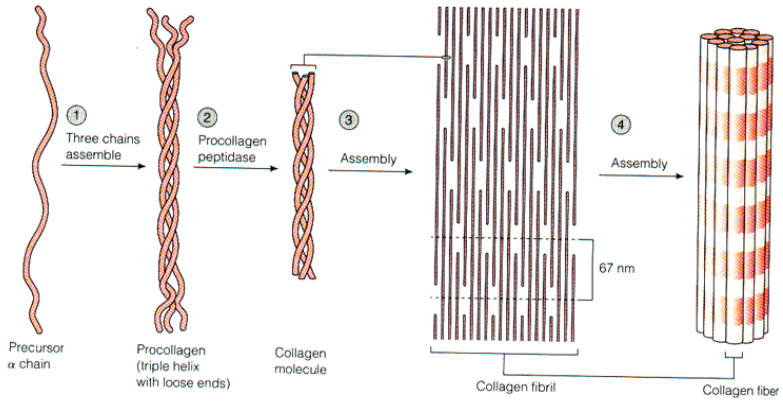

Figure 2.5: Schematic of collagen fiber assembly showing aggregation of collagen fibrils into densely packed 500-3000 nm thick fibers[95]

The amorphous ground substance surrounding cells of the vasculature consist of glycosaminoglycans (GAGs) and proteoglycans (PGs). GAGs (e.g., hyaluronan, chondroitin sulfate, dermatan sulfate, heparin sulfate, and keratin sulfate) are long un-branched polysaccharides consisting of a repeating disaccharide unit of an N-acetyl-hexosamine and hexuronic acid, either or both of which may be sulfated[95-96]. PGs are complex macromolecules that contain a core protein, covalently bound to at least one GAG chain[97]. They are closely associated with collagen and elastic fibers in the ECM . These molecules are characterized by high anionic charge densities, due to the presence of sulfate and carboxylate groups on their uronic acid residue[95]. These polysaccharides can therefore become highly hydrated and resist compressive forces, while at the same time permit diffusion of nutrients, hormones and metabolites between blood and tissue. The importance of these properties is obvious in certain avascular tissues like cartilages[95-96].

As discussed in the previous section, in elastic arteries, and most muscular arteries,

elastin contributes up to 50% of the tissue's dry weight. Within these vessels, elastin is organized as concentric fibers and lamellae around the vessel lumen, that alternate with layers of SMCs and collagen within the tunica media. The roles of elastin in elastic arteries is discussed in detail in the following section[3].

2.2.3. Role of Elastin in Physiochemical Regulation of Vascular Cells

ECM-cell interactions in all tissues is synergistic that tightly regulate developmental transitions, response to injury and overall homeostasis. Elastin, being an important ECM component of elastic tissues, therefore contributes to both structural and biochemical state of a tissue and the cells within. This section elaborates the various functions of elastin as an ECM protein.

SMCs interact with their ECM components through anchoring junctions like adherins and hemidesmosomes[98]. This in turn regulates their proliferation, migration, and in general, cell viability[99]. Mature, intact elastin also affects actin stress fiber orientation within SMCs. The integrity of the ECM is therefore important for regulating cell phenotype. For example, in healthy, mature vascular tissues, SMCs exist in a quiescent state, whose migration is inhibited by the intact, elastin-rich ECM. The matrix remodeling maintained by a tight balance between MMPs and TIMPS, is also achieved through SMC interaction with intact elastin. However, during an injury to the media, that causes degradation of the elastic matrix, the healthy SMC phenotype is found to switch to a synthetic, non-contractile, proliferative phenotype, characterized by increased migration, proliferation and secretion of disorganized, fibrous ECM[18]. In several *in vitro* studies, this

phenomenon was supported by the observation that exogenous elastin added to healthy or diseased SMCs cultured within collagen gels, inhibited their proliferation and migration in a dose dependent manner[100].

Elastin peptides, generated as a result of elastin breakdown, also increase SMC motility and proliferation. These peptides are known to induce tyrosine-dependent phosphorylation of β-tubulin, various microtubule associated proteins, α-actin and troponin-T, which increase SMC cytoskeletal reorganization and motility. Additionally, elastin derived peptides are also known to induce MMP release, which further contribute to matrix remodeling[98, 101].

Arterial calcification, a common phenomenon in various inflammatory vascular pathologies localized to regions of intima and media, usually occurs following lipid deposition, macrophage infiltration and SMC proliferation[102]. Studies have shown that genetic or induced aberration of the lamellar elastin, or the associated microfibrils that mediate SMC interaction with elastin, can interrupt SMC-elastin signaling and induce SMCs to assume an inflamed, synthetic phenotype, characterized 44,45 by increased Ca^{2+} influx, subsequent calcium deposition and matrix hardening[80, 103]. Elastin peptides interact with the elastin-laminin receptor (ELR) present on the surface of various cell types like fibroblasts, lymphocytes, SMCs and ECs. When activated, the ELR receptor induces a G-protein linked activation of phospholipase C[104-105]. This results in the increase in intracellular concentration of calcium, which in turn phosphorylates MAP kinase, triggering a series of events like overexpression of MMPs, increased ionic influx etc[106-107].

2.2.4. Contribution of Elastin to Vascular Mechanics and Vascular Homeostasis

The stresses imparted on a vessel wall include (1) shear stress from blood flow across the lumen, (2) longitudinal stress from surrounding tissue and (3) circumferential stress from surrounding tissue[5]. SMCs of adult elastic arteries contribute little to the passive mechanical properties of the vessel, unlike in smaller vessels. The complex ECM they synthesize, therefore defines the mechanical properties of a mature vessel. These include: (a) high resilience, that restore a large portion of the energy utilized during systole, by elastic recoil during diastole, (b) subsequent low hysteresis or energy loss during cardiac cycles, and (c) non-linear elasticity, that protect the wall from rupture by stiffening with increasing pressure. This non-linearity exists due the deformation of elastin at low strains, and collagen at higher strains. For the same reason, single constants like Young's modulus cannot be used to describe vascular wall properties. It is therefore represented in terms of physiologic modulus, which corresponds to incremental elastic stress values within the physiological strain values. Physiologic modulus for a human thoracic aorta is 0.6-1MPa (**Figure 2.6**)[5].

The medial elastin, woven into an interconnecting lamellar network, transfers stress uniformly throughout the vessel wall. Collagen, arranged in bundles between the lamellar networks, become circumferentially aligned as pressure increases, but lack a definite arrangement at physiological pressures[108]. Physiologic pressure is the region in a stress-strain curve, where the stresses are transferred from the elastic to the inextensible components of the wall[5]. Elastin has high reversible distensibility and deforms to large extensions with small forces. Its properties of recoil are said to be 'rubber' like, i.e., when

unstretched, it has maximum disorder, therefore maximum entropy. When stretched, order is introduced in the direction of stretch, reducing entropy. When the external force is removed, recoil occurs spontaneously, to return to the original state of maximum entropy and disorder[65, 80, 109-110].

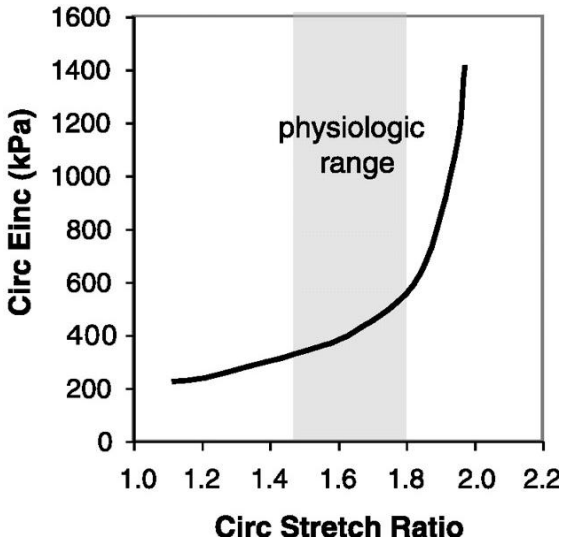

Figure 2.6: Non-linear tensile properties of elastic arteries. Elastin is the primary load-bearing protein of these vessels within physiologic strains[5]

To establish the importance of elastin in vascular mechanics, a study was conducted in a knock out model of mice deficient in elastin gene (*ELN*). It was observed that these mice had tortuous, stenotic and stiff vessels that showed little diameter change between systole and diastole. Due to the absence of elastic recoil, the ventricular pressures increased in an attempt to maintain cardiac output, and SMCs proliferated on the luminal side to lower wall stress by increasing wall thickness and decreasing inner diameter. The proliferation continued till the lumen was completely occluded[18].

SMCs continually respond to changes in hemodynamic pressures and remodel the ECM to normalize stresses across the wall. During development, while these changes are important to layout the required vessel matrix, in adult tissues, these responses often result in pathological remodeling of the vessel. Since collagen is the ECM protein most expressed by SMCs, remodeling involves deposition of collagen, which increases wall stiffness. This can further change hemodynamics of the vessel wall and start a negative feedback cycle that can lead to multiple cardiovascular complications[5].

2.3. VASCULAR ELASTINOPATHIES

Abnormalities of vascular matrix elastin may be broadly classified into two types: (a) genetic and/or congenital, and (b) acquired vascular disease. While most genetic diseases lack the required signaling pathway to lay down a mature elastic matrix, acquired diseases usually involve an injury induced inflammation, where macrophage-derived proteases degrade the vascular elastin. In either of these cases, elastin-smooth muscle cell (SMC) signaling pathways are disrupted, causing SMCs to switch to an activated, synthetic phenotype. This in turn causes downstream effects of SMC hyper-proliferation and medial thickening, further results in decreased arterial compliance and pathogenesis of the vasculature[14].

2.3.1. Genetic Disorders

Genetic abnormalities affecting the elastic matrix can occur due to mutations in the genes encoding elastin, fibrillin (*FBLN*), such as in Marfan's syndrome[111], and fibulin-4 (*FBN4*)[112]. While, defects in the elastin gene (*ELN*), such as Williams-Beuren

syndrome[113], Supravalvular Aortic Stenosis (SVAS)[114], and Autosomal recessive Cutis Laxa[115], directly result in impaired synthesis and deposition of mature elastic fibers, mutations in fibulin and fibrillin genes lead to defective microfibrillar scaffolds, which in turn impair matrix assembly[15]. These defects primarily affect the cardiovascular system, and can often be fatal. They are discussed in further detail in **Table 2.1**.

Disease	Mutant gene	Effects
Williams–Beuren[113] Syndrome, SVAS[114]	Elastin gene on chromosome 7q11	Abnormal deposition of elastin in arterial walls, increased proliferation of SMCs, formation of hyperplastic intimal lesions; elastinolytic enzymes secreted by arterial smooth muscle cells contribute to arterial lesions
Marfan's syndrome[111]	Fibrillin-1 gene on chromosome 15q21.1	Defective elastic-fiber assembly; increased microfibril/elastic fiber degradation; enhanced TGF-b signaling, Results in Vascular disease, including aortic aneurysms and dissections, and skeletal and ocular defects
Autosomal recessive Cutis Laxa[115]	Elastin gene on chromosome 7q11	Abnormal structure of dermal and vascular elastic fibers Results in inelastic skin, severe aortic disease and pulmonary emphysema

Table 2.1: List of genetic abnormalities affecting the elastic matrix proteins

2.3.2. Acquired Disorders: Abdominal Aortic Aneurysms

Vascular pathologies arising from any injury to an intact vessel wall or in the presence of calcified or lipid deposits would elicit a cascade of inflammatory response starting with the infiltration of various MMPs and lymphocytes[16, 61, 83]. This results in phenotypic variations in SMC behavior and response, massive proteolysis and matrix reorganization. Under such conditions, the elastic matrix is degraded at an accelerated

rate resulting in generation of elastin peptides (EP) [104]. EP, through their interaction with elastin-laminin receptors (ELR) on various inflammatory cells, further elicit a variety of pathologic effects such as MMP over-expression, greater Ca^{2+} influx, enhanced vasorelaxation and chemotactic activity[19, 107, 116]. Studies have shown that soon after the initiation of an inflammatory response, mRNA expressions of both tropoelastin and pro-collagen increase within vascular SMCs[48]. While sufficient deposition of collagen matrix is observed due to regeneration associated with fibrotic cell response, elastic matrix regeneration is highly deficient relative to proteolytic elastin degradation. The failure to reinstate a healthy matrix, when damaged by injury or disease (as seen in aortic aneurysms), or when congenitally malformed or absent (Marfan's syndrome), can therefore severely compromise tissue homeostasis[14].

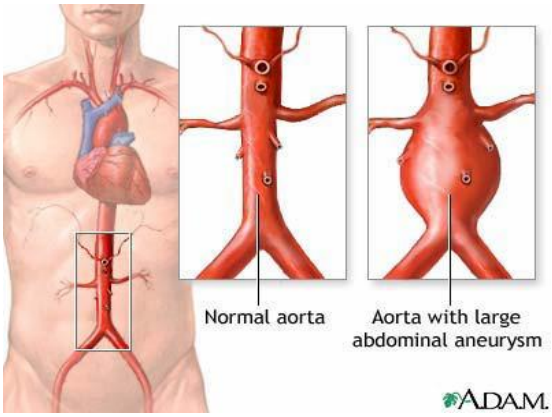

Figure 2.7: Cartoon representing AAA. AAAs are characterized by a localized dilatation of abnomial aortic wall to > 50% their diameter

AAA is defined as localized thinning and dilation of aortic walls of abdominal aortae leading to more than 50% increase in their original diameter (**Figure 2.7**) [16-17]. Initiation and progression of AAA has been attributed primarily to chronic matrix

proteolysis by MMPs and inflammatory cells that infiltrate the vessel wall in response to atherosclerosis, calcified lipid deposits, vascular hypertension or inherited conditions[11, 16]. This is coupled with the absence of intrinsic signals in adult vascular cells to regenerate lost elastic matrix or to successfully repair diseased vessel wall[18]. The accelerated loss of elastic matrix and vessel wall integrity, and continuous fluctuations in hemodynamic pressures lead to abnormal ballooning of an aneurysm[19]. As mentioned earlier, AAAs typically grow about 1 cm/year to catastrophically rupture causing hemorrhage and embolisms, with fatality rates of approximately 80%. In the United States alone, the estimated incidence for AAAs is about 60 in every 100,000 people per year[16, 20].

2.4. STRATEGIES TO RESTORE ELASTIC MATRIX

As discussed so far, elastin plays important roles in maintaining vascular homeostasis, which when compromised can lead to various complications, and even be fatal. Its restoration is therefore crucial in reinstating homeostasis. Various strategies have been developed so far that directly and indirectly target elastin restoration. These can be broadly grouped into (a) preservative, (b) replacement and (c) regenerative strategies.

2.4.1. Strategies to Replace Diseased Vessel Wall

When stability of a diseased vascular wall is severely compromised and aneurysms dilate beyond a critical diameter, vascular grafts are surgically introduced to isolate the aneurysm and reduce the load on the vessel wall to prevent its rupture.

Vascular grafts for elastic arteries can be allogenic, xenogenic or artificial polymeric grafts. Autologous grafts like saphenous vein and mammary artery are usually used for replacing vessels with smaller diameters[117]. Allogenic grafts from deceased fetuses, cryopreserved tissues, cadavers umbilical cords have long been investigated as suitable tissue replacements for aortic aneurysms, among many other tissues due to similarities in size and mechanical properties. However issues like donor-specific immune rejection and high demand-supply ratio of these grafts have made them less popular alternatives[118]. Despite developments to improve donor-rejection like uptake of immune-suppressors by the recipient, decellularization and removal of immunoreactive epitopes and globular proteins from the grafts prior to implantation, their long-term stability and compatibility continues to be a problem[119].

To minimize donor-recipient supply ratio for transplants, xenogenic grafts have long been an attractive alternative. However, these grafts experience higher levels of immune rejection, primarily through complement activation[119]. Additional issues like disease transmission, permanent alternation to genetic code, higher thrombogenecity due to lack of endothelialization, compliance mismatch and mechanical stiffening post-transplantation, physiological and biochemical variations in blood viscosity, liver metabolism and incompatibility of coagulation factors further lead to long-term graft rejection and implant-based complications[120-121]. New strategies to improve long term graft compatibility like transgenic modifications in pigs to express human complement-regulatory proteins are currently being researched[122].

Replacement of an aneurismal vessel using synthetic grafts is currently the most

common approach to treat aortic aneurysms. While they are able to overcome the immune-rejection issues of allogenic and xenogenic grafts, they are also readily available and have lower risk of implant-related disease transmission[123]. The stent-grafts currently in the market follow similar designs. They primarily consist of a metal skeleton called 'stent' that provides a frame for a polymeric 'graft', which are either sutured or bonded together. The graft is usually an elastomer like Dacron™ or poly(tetrafluoroethylene) (PTFE), while metal alloys like cobolt-chromium and stainless steel make up the stents[24]. Various stent-grafts currently available in the market are FDA approved (Zenith® Endovascular Graft, Cook Inc.; Gore Excluder®, WL Gore & Associates Inc.) while several others are under various stages of clinical trials, as depicted in[124]. The grafts are implanted either by a highly invasive open surgery, or a minimally invasive, catheter-delivered endovascular repair (EVAR), as shown in (**Figure 2.8)**. Both these techniques have their own benefits and shortcomings, and the choice of stent-graft or the delivery mode depends on the morphology of the disease, the patient and the surgeon[26]. Though synthetic grafts help isolate the aneurysm and prevent vessel rupture by providing an alternative conduit to blood flow, they are faced with several device-related issues like lack of endothelialization, various types of endoleaks, implant migration and fatigue, which affect long-term patency of the implant, and often require additional surgical intervention[25-26]. Moreover the graft materials have higher tensile properties compared to native vessel (~170Mpa for a graft vs. 800-1000 kPa for native aorta) which also lead to compliance mismatch[24]. While these grafts may replace the structural role of a blood vessel, they do not accommodate for the functional properties of elastic vessel ECM,

neither do they regress the disease[25].

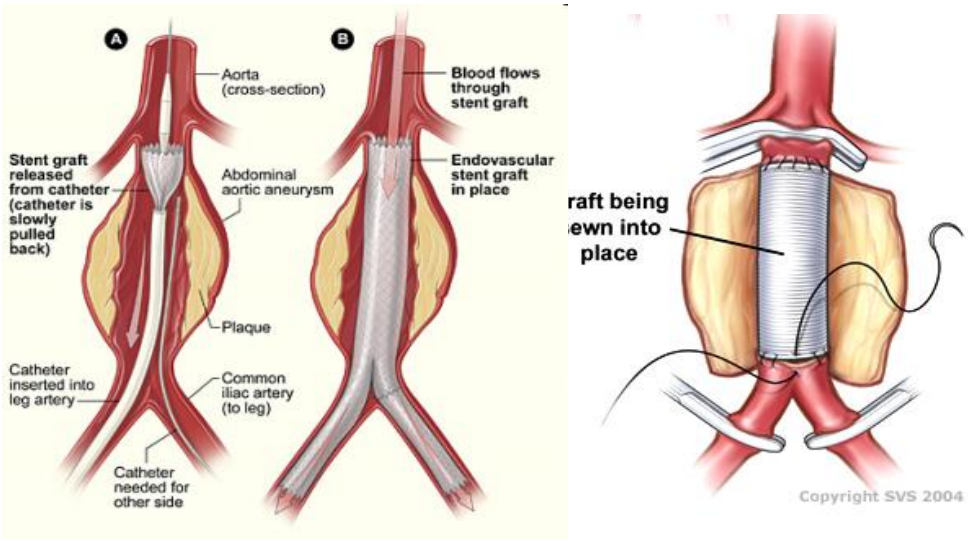

Figure 2.8: Cartoon representation of EVAR (left) vs. open surgical repair to treat AAA using synthetic vascular grafts. Adapted from *Encyclopedia of Science*

2.4.2. Strategies to Prevent Matrix Degradation

As discussed earlier, matrix degradation is accelerated at the site of aneurysm, primarily due to the presence of inflammation induced MMP activity. Preservative strategies therefore target decelerating, or ideally, arresting matrix degradation to prevent or prolong the need for surgical intervention. These strategies mainly use pharmacological methods to regulate transcription factors, inhibit MMP and other protease activity, and introduce crosslinking agents etc. that stabilize matrix degradation. While these approaches slow down the rate of aneurysm progression and reduce medical expenses, they do not restore matrix integrity, and are also associated with several side effects.

Expression and production of various MMPs by resident SMCs and fibroblasts at

the site of aneurysm accelerates matrix degradation. MMPs 2 and 9 in particular have been found to accelerate elastin degradation[12, 125]. Blocking MMP production therefore has been an obvious strategy to prevent matrix degradation. Various anti-inflammatory drugs, antibiotics, exogenous tissue-inhibitors of metalloproteases (TIMPs) and inhibitors of MMP transcription factors have been investigated to inhibit MMP synthesis and activity at the site of injury[20].

Doxycycline (DOX) is a modified tetracycline compound that has been widely administered as a broad-spectrum antibiotic[126]. Known to be a global, non-specific MMP inhibitor, systemic delivery of DOX has been clinically shown to reduce the rate of AAA growth and progression of disease[45-47]. Studies exploring the mechanisms of MMP inhibition have found DOX to significantly reduce protease activity both at transcription and translation steps of the protein synthesis[127-128]. Several groups have also specifically evaluated its effects on gelatinases, i.e., MMPs -2 and -9, proteases that are up-regulated most in the aneurysm wall and primarily responsible for elastolytic activity, both *in vivo* and *in vitro*[129-130]. In addition to reducing mRNA expression and total protein production, DOX also alters the conformation of both the zymogen and the active enzyme by binding enzyme-associated Ca^{++}[131]. This makes the proteins more susceptible to proteolysis, resulting in their fragmentation into smaller molecular weight fractions and an irreversible loss of enzyme activity[131-132]. Studies on *in vivo* rodent models of AAA[133-134] and aortic organ cultures[135-136] have shown a direct correlation between DOX-mediated suppression of gelatinase activity and significant reduction in elastin degradation in the vessel wall.

Anti-inflammatory drugs like Aspirin and stanins are commonly used by patients with AAA[20]. Other inhibitors of MMP activity like indomethacin, dexamethasone and green tea catechins for MMP 9 and trapidil for MMP 2 have also been studied[20]. Use of exogenous TIMPs in the form of either synthetic TIMP or an adenoviral vector with a native TIMP1 cDNA have shown to inhibit SMC migration and reduce neointimal hyperplasia formation in a vascular injury model in rats[12]. Inhibitors of MMP mRNA transcription like NF-κβ have also been investigated towards preventing matrix degradation[137].

Under healthy conditions, various protease inhibitors bind to proteolytic enzymes like elastases, and prevent uncontrolled matrix degradation. Absence of such inhibitors, such as serine-protease inhibitors seen in anti-trypsin deficiency, confirms the importance of these inhibitors. Another strategy to prevent elastin degradation therefore involves the use of exogenous elastase inhibitors or transfection of vascular SMCs with genes like α-1 antitrypsin[138].

Stabilization of matrix elastin within an aneurysm and prevention of further degradation by the use of chemical crosslinking agents is another approach to preserve elastin. Pentagalloyl glucose (PGG), a polyphenol derived from tannic acid, delivered periadventitially in a vascular injury model in rats, is shown to preserve elastic matrix integrity by specifically binding to arterial elastin, therefore inhibiting elastin degeneration attenuating aneurismal progression. PGG however is not shown to interfere with pathologies related to the disease like inflammation and calcification[139].

2.4.3. Strategies for *In vitro* Tissue Engineering and *In situ* Repair of Vascular Elastic Matrix

The strategies discussed so far only address replacing mechanical properties of an elastic tissue, but are unable to compensate for the physiochemical roles of elastin. Tissue engineering techniques offer potential alternatives to address both these essential requirements for successful restoration of an elastic vascular wall. Though a large section of tissue engineering research has been devoted to regenerating completely functional blood vessels, obtaining a mature elastic matrix continues to be a challenge. So far, scientists have not created a viable vascular graft that possesses the necessary complex mechanical properties as well as mimics the biological function of a native artery, specifically elastin, but much progress has been made.

Elastic fiber formation involves several steps of coordinated intracellular and extracellular activities. Strategies to regenerate elastin have used various combinations of cell types, culture environments, scaffold materials, growth factors and dynamic conditioning, each of which, independently and in combination, contribute to different levels of elastin synthesis and matrix deposition[10]. Each of these parameters influencing elastic matrix output are discussed in further detail as follows.

2D vs. 3D Microenvironments: SMCs in native arteries exist within a 3-dimensional collagen matrix, interspersed with lamellar elastin. Isolated SMCs within a 2-dimensional culture environment would therefore evoke different responses in terms of cell phenotype and morphology, expression of various cell markers and growth factors, and type and

ultrastructure of matrix produced. Several studies have compared SMC behavior in 2-D culture plates to a 3-D scaffold environment. In one such study, RASMCs cultured on hyaluronic acid based scaffolds (gels) demonstrated an increased amount of elastin production, both soluble and insoluble, on the hyaluronan gels, compared to polystyrene culture plates. Microscopic analysis of the elastin structure further showed smooth, highly fenestrated sheets composed of fibers, visible along the sheet edges[34]. In another study, SMCs cultured within 3-D collagen gels showed lower rates of cell proliferation and matrix deposition, both collagen and elastin, compared to that seen in 2D collagen matrices. Similar trends were observed in synthetic scaffolds such as polyglygolic acid (PGA) and poly-lactic-co-glycolic acid (PLGA) as well. It has been shown that the cells acquire a more contractile, non-proliferative phenotype, much like in an *in vivo* condition, as opposed to a synthetic, proliferative phenotype within 2-D cultures[140].This was additionally confirmed with the observation that tyrosine phosphorylation of FAK and the number of focal adhesions were far lesser in cells within 3-D collagen matrix, than those in 2-D cultures. Gene expressions of p21 and TGF-β1 were also shown to be higher in 3-D cultures[141].

Though SMC behavior within 3-D cultures also depend on the nature of scaffold used, apart from several other culture conditions, it is reasonable to believe that to translate elastogenic response into vascular graft application, 3-D cultures would be imperative[28].

Growth Factors—Induced Elastogenesis: Of the many growth factors investigated in the

field of regenerative strategies, insulin-like growth factor-1 (IGF-1)[142-144], TGF-β family of growth factors[38, 145] and human recombinant interleukin (IL-1β)[146] are found to be elastogenic at various levels of elastin synthesis and matrix formation. Several methods of delivering these growth factors have also been explored in various tissue engineering applications, for example, surface tethered or microsphere encapsulated growth factor delivery. Variables that determine efficiency of release profile include polymer used, its pore size, concentration and molecular weights of factors delivered and solvent the release profile is studied in. However, no direct correlation between delivery mode and elastogenesis has been established[147].

Several studies have demonstrated dose-dependent elastogenic induction of IGF-1 in both confluent cell cultures and *in vivo* delivery to rats, primarily in terms of tropoelastin synthesis and mRNA expression. Elastogenic benefits of *in vivo* administration of IGF-1 to rats (1.2 mg/kg/day), was found to be tissue and age specific. While increased tropoelastin synthesis and matrix deposition was observed in the rat aorta, lung tropoelastin mRNA levels were unaffected. This phenomenon, though observed throughout the lifetime of the rat, was found to diminish with age[142-144].

Studies have also established the contribution of TGF-β family of growth factors to elastin synthesis during fetal development and in tissue repair. One such study examined the effects of TGF-β1 and TGF-β2 on human elastin mRNA abundance, promoter activity, and mRNA stability in cultured human skin fibroblasts and found that with varying concentrations of TGF-β1 or TGF-β2 for 24 h resulted in a dose dependent increase in the elastin mRNA steady-state levels, with a maximum enhancement of

approximately 30-fold being noted with 1 ng/mL. These results demonstrate that TGF-β1 and TGF-β2 are potent enhancers of elastin gene expression and that this effect is mediated, at least in part, post-transcriptionally[38, 145]. In addition, TGF-β augments LOX-mediated crosslinking of soluble tropoelastin into a mature, insoluble matrix layer[38].

Besides growth factors, various biomolecules such as LOX helps to crosslink the tropoelastin to give elastic fibers[148]. In the absence of LOX, tropoelastin tends to associate with GAGs due to the presence of amino groups in the elastin lysine residues, which offer positive charges for binding with negative charges of GAGs[43]. Besides, in the absence of LOX, such electrostatic interaction could be important and prevent newly synthesized tropoelastin molecules from spontaneous random aggregation far from the cell surface. Elastogenic benefits of Cu ions/nanoparticles[149], calcitriol and retinoic acid have also been demonstrated in several studies[150-152].

HA as an Elastogenic Stimulator: HA is a type high molecular weight GAG found in the ECM of many tissues. It consists of N-acetyl-D-glucosamine (GlcNAc) and D-glucuronic acid (GlcA) repeats linked by a β1-4 glycosidic bond. The disaccharide units are linked by β1-3 bonds to form the HA chain[153-155]. HA is known to influence various physiologic functions such as morphogenesis, embryonic development, tissue stability, cell proliferation, remodelling, migration, differentiation, angiogenesis and wound healing. This is suggested to be achieved through its interaction with a set of HA-binding matrix and cell surface receptor proteins called hyaladherins[156-158]. Among them, CD44, a cell surface glycoprotein with a molecular weight of ~85 kDa, is known to play an important

role in HA binding to the cell surface[156, 159]. The presence of pro-inflammatory cytokines like IL-1, and growth factors like EGF, TGF-β and BMP-7, is further known to increase transcription levels of CD-44, therefore improving cell-HA interaction[154-155]. Studies in vascular, pulmonary and dermal tissues have reported a close association between GAGs such as HA and heparin sulfate, and proteoglycans such as versican[160]. Unlike GAGs like dermatan and chondroitin sulfates, HA was found to support elastic fiber formation by playing a key role in the synthesis, organization, and stabilization of elastin by VSMCs[42]. This is attributed, in part, to the role of HA in synthesis and organization of microfibrils (fibrillin), a precursor for elastic fiber deposition, and in part, to its binding of versican, which in turn interacts with microfibrillar proteins like fibulins-1 and-2, and elastin-associated proteins to form higher-order macromolecular structures important for elastic fiber assembly[158]. Recent studies also provide evidence that due to the presence of charged lysine residues, soluble tropoelastin molecules are coecervated on the highly anionic surfaces of HA, to facilitate LOX-mediated crosslinking into an insoluble matrix. HA is also known to stabilize elastin fibers against degradation by elastases[43]. Several studies have also been conducted to explain the size-specific effects of HA. Native HA is a long-chain, stable polymer, with molecular weight > 1000kDa (HMW HA). It hydrates the ECM and binds growth factors and smaller GAGs. On the other hand, smaller fragments of HA like Low molecular weight HA (LMW HA) ~100 kDa, and HA oligosaccharides (HA-o) ~ 2-10 kDa, are capable of binding to cell surface receptors in a monovalent manner resulting in the stimulation of specific cell signaling cascades, thus influencing their metabolic functions[161]. LMW HA are synthesized from enzymatically

digested HMW HA and are found in association with proliferating ECs and SMCs. Recent studies have also reported that HA 4-mer is the minimum size for HA-SMC interaction[153] . Previous studies conducted in our lab have established size-specific effects on elastogenesis by RASMCs[44, 162-163].

Role of Mechanical Stimulation In Matrix Assembly: Mechanical conditioning is another consideration for tissue engineering vascular grafts. Elastin synthesis by vascular SMCs is very sensitive to magnitude, frequency, duration and type of strain applied[164-165]. Numerous studies have been conducted to study the effects of dynamic conditioning on elastogenesis. While shear stresses induce apoptosis and detrimental cell response in VSMCs, the application of cyclic mechanical stretch simulating distension experienced by medial SMCs *in vivo* significantly influence the phenotype, alignment, matrix deposition, and growth factor release by both native and cultured SMCs[58, 164-165]. Recent studies have demonstrated that SMCs, isolated from both rat and human aortae, respond positively to radial and cyclic strains of < 10% by improving collagen compaction, tensile strength, circumferential alignment of cells and matrix, and up to a 2-fold increase in elastin mRNA production [57, 59, 164-166]. Changing the frequency of cyclic strains was found to play a more significant role in regulating the alignment of vascular SMCs in an intact actin filament-dependent manner; frequency of 1.25 Hz for cyclic strains between 2.5%-10% was found to be most effective in influencing SMC response[167-169]. Cyclic stretch-induced matrix synthesis has been found to be regulated by a tyrosine-kinase dependent TGF-β pathway[170]. A mentioned earlier, integrins play a primary role in

mechanotransductive effects of external stimuli on vascular cell response[85, 171]. Excessive strains of over 10% and beyond 5 Hz frequency have been found to induce apoptotic response mediated via integrins[164].

Scaffolding Materials for Elastic Matrix Engineering: Scaffolds provide a 3-D template for cellular infiltration and neo-tissue synthesis. Once the desired tissue is formed, the scaffold material must ideally degrade into non-toxic byproducts. Scaffolds can be broadly classified into (a) natural and (b) synthetic scaffolds. Apart from the type of scaffold used, various culture parameters like addition of biomolecules, cell type, duration of culture, application of mechanical stimuli etc., are interdependent and impact final outcomes of elastic matrix. **Table.2.2** gives an overview of various scaffolds investigated so far in combination with these parameters towards elastic matrix outcomes.

Targeted Delivery of Elastogenic Factors: In the previous sections, we discussed various biomolecules as that have been demonstrated, or have the potential for use in elastic matrix regeneration and repair. The primary considerations in translating their benefits demonstrated *in vitro*, into *in vivo* clinical use is determining an effective dose range, and more importantly the mode of delivery. This is especially true with the use of biomolecules that induce a variety of repose depending on their concentrations and tissue within AAA, at similar doses, TGF-β1 induces antagonistic and adverse reactions within TAA[60, 185]. It is therefore crucial to develop strategies that can specifically target a tissue site and have precise control over their delivery[186-188]. Strategies for targeted delivery of

Scaffold	Cell source, culture duration	Culture conditions	Elastogenic outcome	References
Collagen Type I	Human aortic SMCs, 4-8 days	10% Radial, cyclic strain	↑ 2-fold mRNA expression	172
	RASMCs, 5 weeks	2.5% - 10% Cyclic strain	Matrix elastin aligned circumferentially	59
	Adult RASMCs, 3 weeks	Static strain, TGF-β1, HA-o	Tropoelastin differences negligible, 5-fold ↑ matrix elastin, elastic fibers oriented in direction of strain	173
Fibrin	RASMCs, neonatal RASMCs, 4 weeks	TGF-β1, insulin	↑ Matrix elastin and fibrillin 1 deposition compared to control and collagen scaffolds	28, 31-32
Silk fibroin-based scaffolds	Human aortic ECs+ SMCs, 15 days	-	High mRNA expression, low matrix elastin	33
	Rat SPC-derived SOCs, 3 weeks	Platelet-derived growth factor-BB		174
Hyaluronic acid based scaffolds	Neonatal RASMCs, 3 weeks	Micro-textured hylan surfaces	Differences in matrix elastin content insignificant, elastin present as fenestrated sheets and loose fibers (~400 nm)	34, 175
	Adult RASMCs, 3 weeks	Surface tethered HA	↑ tropoelastin, matrix elastin, desmosine crosslinks, tightly continuous and fenestrated elastin sheets within fibrillin microtubules	44, 162-163
PGA	Canine Carotid SMCs, 25 days	5 % strain, 75 beats/min	Matrix elastin around regions of high cell densities alone	176

PGA+Polycaprolactone	Bovine ECs+ SMCs+fibroblasts, 2 weeks	Concentric layers of cells-seeded PCL and PGA, graduated Pulsatile perfusion	Elastic matrix layout similar to native arteries	[177]
Polyurethane	Human coronary artery SMCs	TGF-β1	↑ Tropoelastin mRNA expression, matrix elastin compared to 2D scaffold	[178]
Polyhydroxyalkanoate	Rabbit aortic SMCs, 16 days	-	↑ Insoluble elastin levels in higher 4HB content	[179]
PCL	Adult RASMCs, 16 days	Electrospun PCL, TGF-β1, HA-o	Negligible mRNA expression changes, ↑ matrix elastin	[180]
Poly(glycerol sebacate) (PGS)	Baboon aortic SMCs, 3 weeks	Pulsatile perfusion	Circumferentially aligned elastic fibers, 19% of total arterial elastin	[169, 181]
Cell sheets	Tubular layers of rat aortic SMCs transfected with splice variant versican (V3)	Absence of ascorbate in medium	↑ mRNA expression of tropoelastin, fibulin-5, fibrillin-1, ↓ LOX mRNA expression, ↑ deposition of tropoelastin, matrix elastin and desmosine crosslinking	[182]

Table 2.2: Strategies using various combinations of scaffolds, dynamic stimulation, and cell type and culture duration, towards elastic matrix engineering. *Adapted from Bashur et.al., 2012*[183]

various biomolecules have been achieved through release from polymeric nano- or micro- carriers[189-192], from scaffolds[193-200] on which they are surface tethered, or through a combination of both[201-206]. Several factors such as topography, degradation products and their effects, carrier chemistry etc. play a critical role in efficient delivery as well as in regulating cell response[207-209]. For example, topography, compliance and scaffold

chemistry closely regulate cell attachment via integrin signaling[210-211]. Biomolecules encapsulated within polymeric carriers, especially growth factors are sensitive to processing steps as well as the byproducts of polymer degradation, and can often result in loss of bioactivity[60, 212]. Along with scaffold chemistry, surface charge is also shown to influence release profiles as well as efficient uptake of released factor depending on the tissue site. For example, for targeted delivery within the vasculature, and scaffolds functionalized with a positive surface charge have shown to improve uptake and retention[213-214].Cationic surfaces have shown to positively influence outcomes in elastic matrix engineering as well. It has been hypothesized that cationic functionalization enables interaction with hydrophobic domains in elastin and the crosslinking enzyme, LOX, while at the same time repels cationic elastase and MMPs, thereby suppressing proteolytic activity[215-216].

While a lot of progress has been made towards vascular matrix engineering and *in situ* repair of compromised vessels, regeneration of elastic matrix is still insufficiently addressed. Nonetheless, various parameters summarized in this chapter, especially when used in combination, hold promise towards development of successful elastic matrix engineering strategies for vascular pathologies.

CHAPTER THREE

INVESTIGATING INDUCED ELASTOGENESIS BY VASCULAR SMCS IN AN *IN VITRO* 3-D COLLAGEN-GEL MICROENVIRONMENT

3.1. INTRODUCTION

As discussed in detail in the previous chapters, the elastic matrix is responsible for providing vessels the necessary recoil and compliance to accommodate blood flow, and at the same time also regulates vascular smooth muscle cell (SMC) behavior through mechano–transduction[1], particularly during morphogenesis and disease progression[2]. Once injured, the elastic matrix is not repaired, due to (a) poor elastin precursor (tropoelastin) synthesis by adult cells, (b) inefficient recruitment and crosslinking of tropoelastin into an elastic matrix, and (c) further organization into elastic fibers[10]. The failure to reinstate a healthy matrix, when damaged by injury or disease, or when congenitally malformed or absent, can therefore severely compromise tissue homeostasis. This is one of the reasons why synthetic graft replacements (e.g. ePTFE) for such diseased segments, though capable of reinstating vessel elasticity and compliance, are unable to provide biologic stimuli to restore healthy vascular cell phenotype and tissue homeostasis.

Alternative strategies to tissue engineer elastic vessel replacements using autologous adult vascular SMCs seeded on biodegradable scaffolds, natural or synthetic, have been challenged by poor elastogenicity of these cell types, and lack of knowledge of materials and methods to biomimetically replicate and enhance tropoelastin synthesis,

recruitment, crosslinking, and matrix assembly[10]. The problem of poor elastic matrix deposition is especially severe in cellular microenvironments within such tissue–engineered constructs invariably rich in regenerated collagen, which switch SMCs to a less synthetic, and even less elastogenic phenotype[56].

Of potential benefit to overcoming the poor elastogenicity of adult vascular cells, our laboratory previously determined the synergistic benefits of HA–o and TGF–β1 to elastin precursor synthesis, elastic matrix deposition, and fiber formation by cultured adult rat and human SMCs[148, 184]. We also showed that TGF–β1 increases expression levels of mRNA for tropoelastin, and that of the matrix crosslinking enzyme, lysyl oxidase (LOX), while suppressing the activity of matrix degrading matrix metalloproteinases (MMPs) [148, 217]. Negatively-charged HA is also thought to coacervate tropoelastin molecules for more efficient localized crosslinking and organization of these precursors into mature fibers, much like the role of glycosaminoglycans (GAGs) in a developing aorta[34, 42]. Our prior data also suggests that oligomeric forms of HA, specifically 4– and 6– mers, also enhance elastin mRNA expression. The presence of collagenous matrix is centric to replicating vascular tissue architecture and mechanics[48], and vascular cells, regardless of the choice of scaffolds, robustly synthesize collagen[10, 27]. It is therefore imperative to examine the impact of a pre-existing collagenous microenvironment on the ability of the cells to synthesize fibrous elastic matrix on their own and also their response to provided elastogenic factors[56]. Towards utilizing the above factors to enable and enhance elastic matrix deposition within collagenous tissue, in the present study, we investigate the effect of these factors at different dose

combinations within statically loaded 3–dimensional (3–D) cellularized collagen constructs.

3.2. MATERIALS AND METHODS

3.2.1. Isolation and Culture of Rat Aortic Smooth Muscle Cells

Abdominal aortae were harvested from adult Sprague–Dawley rats according to animal protocols approved by the *Medical University of South Carolina*, where this work was performed. After scraping out the intima and the adventitia, the medial layers of the aortae were minced into 1–2 mm–long pieces, incubated first in DMEM–F12 (Gibco–Invitrogen, Carlsbad, CA) containing 20% v/v fetal bovine serum (PAA Scientific, Dartmouth, MA), 1% v/v Penstrep (Thermo Scientific, Rockford, IL) and 175 U/ml collagenase II (Worthington Biochemicals, Lakewood, NJ) for one hour at 37 °C. The pieces were then incubated in a second digestion mixture containing the above solution supplemented with 0.25 mg/ml of elastase III (Worthington Biochemicals, Lakewood, NJ) for 45 minutes. The digestate was finally centrifuged at 200g for 5 minutes, and the pellet re–constituted and cultured in DMEM–F12 containing 20% v/v serum and 1% v/v Penstrep. Primary rat aortic SMCs (RASMCs) thus obtained, were cultured and passaged in T–75 flasks. Cells of low passage (P3 – P5) were used to seed the collagen constructs.

3.2.2. Fabrication of Cellularized Collagen Constructs

The inherent nature of cell–seeded collagen to shrink and form a compacted gel was utilized to fabricate 3–D constructs. Collagen–cell mixtures were aliquoted within

rectangular (3.8 mm × 2 mm × 1.5 mm) silicone rubber (Smooth–On, Inc., Easton, PA) wells cast in 100 mm diameter glass petri–dishes[218-219]. The molds/dishes were steam–sterilized at 121 ºC for 30 minutes. In order to obtain directed compaction of the collagen gels under static tension, polyurethane tubes anchored with stainless steel pins (both sterilized in 1 N HCl for 20 minutes and rinsed in sterile PBS) were anchored to the ends of each well.

Acid–solubilized type I collagen (BD Biosciences, Bedford, MA) was mixed with 5 × DMEM/F12 and 0.1 N NaOH and added drop wise to titrate the mixture to physiological pH. RASMCs (passages 3–5) were trypsinized, centrifuged, and re–suspended in medium and added to the above solution to obtain a final concentration of 2 mg/ml collagen, 1×10^6 cells/ml, 20% v/v serum and 1% v/v Penstrep in DMEM–F12. All mixing was performed on ice to prevent premature polymerization of collagen when physiologic pH was attained. Equal volumes of this collagen-SMC mixture were then aliquoted into each well and cultured in a CO_2 incubator at 37 °C. Within a few hours, the collagen–cell mixture started to gel and anchor around the polyurethane end holders. These holders prevented longitudinal gel contraction, but enabled contraction in a direction perpendicular to the long axis of the wells (**Figure 3.1**).

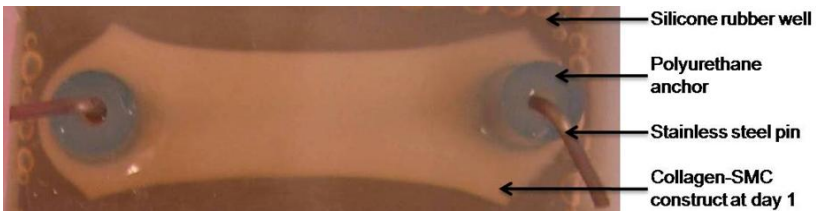

Figure 3.1: Statically loaded RASMC–seeded 3–D collagen gels. Gels, shown at day one of culture, were cast within silicone wells and anchored to polyurethane end–holders

A sterile cocktail of HA–o and TGF–β1 (Peprotech, Rocky Hill, NJ) was exogenously supplemented in the growth medium, at six different dose combinations (0.1, 1 and 10 ng/ml of TGF–β1, each with 0.2 and 2 μg/ml of HA–o). Since this is a pioneering study utilizing a combination of HA–o and TGF–β1 for elastic matrix synthesis by SMCs within 3-D cultures, there is lack of literature indicating appropriate doses for such a model. We have therefore extrapolated the dose range for the current study from our outcomes in 2-D cultures, and utilized a range to include concentrations of an order of magnitude lower and higher than that used in 2-D cultures in order to evaluate optimum conditions[37, 139, 220]. HA oligomer mixtures used in this study primarily consisted of 4–mers (~ 75%) with 6–mers and 8–mers forming the balance. They were prepared by digesting high molecular weight HA (1.5×10^6 Da, Genzyme Biosurgery, Cambridge, MA) with testicular hyaluronidase (40 U/mg at 37 °C; Worthington Biochemicals, Lakewood, NJ) as we have described previously[163]. The constructs were cultured for 21 days and spent medium changed every two days. Spent medium from each well was pooled with aliquots previously removed from the same wells, and frozen at –20 °C until biochemically analyzed at the end of the culture period.

3.2.3. Construct Compaction

All constructs were photographed at regular intervals using a digital camera and their central widths measured using Image–J (NIH, Bethesda, MD) imaging software. The extent of contraction (compaction ratio) of each construct was measured as a

percentage difference in width of the well and the central width of the construct at day 21. At least three measurements were made on each construct.

3.2.4. DNA Assay for Cell Quantification

The DNA content of RASMCs within the collagen constructs was measured at 21 days of culture to estimate to estimate increases to cell number relative to that at seeding. Briefly, the gels were detached from the holders and digested in 10 mg/ml proteinase–K (Gibco–Invitrogen, Carlsbad, CA) at 65 °C for 10 hours until the matrix structure was completely solubilized. The enzyme was inactivated by boiling the solution for ten minutes. The digested solution was then sonicated for 3 minutes on ice to lyse cells, and DNA content was measured using a flourometric assay. Cell numbers were calculated assuming 6 pg of DNA/ cell[221]. Results were represented in terms of cell proliferation ratio (cell count at 21 days/ initial seeding density) and as a fold–change in this ratio compared to control.

3.2.5. RT-PCR for mRNA expression of Tropoelastin, Collagen and LOX

Constructs were harvested in RNA-Later stabilization solution (Qiagen, Valencia, CA) after 21 days of culture, homogenized using a needle and syringe, RNA extracted using an RNeasy kit (Qiagen, Valencia, CA), and samples loaded onto RNeasy mini columns. Total RNA was eluted with 40 μL of RNase-free water, its concentration determined by absorbance measurement at 260 nm using a Ribo-green assay kit (Invitrogen, Carlsbad, CA). 200 ng of RNA was reverse transcribed with iScript cDNA

synthesis kit (Biorad, Hercules, CA) according to the manufacturers' instructions. Samples (40 μL) were incubated at 42 ºC for 5 minutes and then reverse transcriptase (RT) inactivated at 85 ºC for 35 minutes. Gene expression for collagen, elastin and LOX were evaluated using 1 μl of cDNA with Power SYBR®Green Master Mix (Applied Biosystems, Foster, CA) (n = 6/case) in the ABI 7500 Real Time PCR System (Applied Biosystems). A comparative threshold method [222] was used to quantify the mRNA expression of these genes and was reported as $2^{-\Delta\Delta Ct}$, with *18s* serving as the internal control. The sequences of all primers are listed in **Table 3.1**.

3.2.6. Fastin Assay for Elastin Content

Total elastin synthesized by RASMCs was measured using a commercially available Fastin assay kit (Accurate Scientific and Chemical Corporation, Westbury, NY). Three distinct elastin fractions were assayed for, namely, (a) tropoelastin, the soluble precursor of elastin synthesized by cells, present within medium fractions, (b) the less crosslinked, alkali–soluble matrix elastin, and (c) the highly crosslinked, alkali–insoluble matrix elastin. Volume fractions from the pooled culture medium were directly used to measure tropoelastin. To measure matrix elastin, the constructs were first treated with 0.1 N NaOH at 95 °C for one hour and centrifuged. The resulting supernatant consisted of alkali–soluble matrix elastin, while the pellet comprised of alkali–insoluble matrix elastin. The soluble matrix fraction was neutralized with an equal volume of 6 N HCl at 110 °C for 16 hours, dried overnight, reconstituted in water and quantified using the kit. Since the Fastin kit measures only soluble, α–elastin (~ 60 kDa), the insoluble matrix pellet was

first solubilized with 0.25 M oxalic acid at 95 °C for one hour, and then filter–centrifuged with 10 kDa cut–off membranes (Millipore, Billerica, MA). The solubilized matrix elastin retained above the filters was then quantified with the assay kit. Tropoelastin and total matrix (alkali –soluble + –insoluble) thus measured were normalized to the cell count within respective constructs. The matrix yield (i.e. the ratio of matrix elastin/ (tropoelastin + matrix elastin) × 100) was calculated.

Gene	Primer Sequence (5'→3')		T_m (°C)	Size (bp)	Accession no. (Source)
18S	Forward	CGGACAGGATTGACAGATTG	59	185	V01270 (Real Time Primers)
	Reverse	GGACATCTAAGGGCATCACA			
Elastin (*ELN*)	Forward	TCC TGG AGC CAC TCT TAC AG	58	165	NM_007925 (Real Time Primers)
	Reverse	CTC TCT CTC CCC AAT TAG CC			
Lysyl Oxidase (*LOX*)	Forward	TGC CAA CAC ACA GAG GAG AG	58	223	NM_010728 (Real Time Primers)
	Reverse	CCA GGT AGC TGG GGT TTA CA			

Table 3.1: Forward and reverse sequences of primers for rat *ELN*, *LOX*, and the house-keeping gene, *18S*

3.2.7. Western Blotting for LOX and MMPs –2 and –9

Western blotting was performed to semi–quantitatively compare the amounts of LOX enzyme protein and of the elastolytic MMPs –2 and –9, synthesized by RASMCs within constructs subjected to different treatment conditions. At day 21, harvested constructs were ground into powder in liquid nitrogen, extracted in RIPA lysis buffer (750 µl, Invitrogen, Carlsbad, CA) with a protease inhibitor cocktail (Thermo Scientific,

Rockford, IL), and then assayed for total protein content using a BCA assay kit (Thermo Scientific, Rockford, IL)[223]. Volumes equivalent to 3 μg of protein were loaded under reduced conditions into 4–12% SDS PAGE gel for LOX analysis and 10% SDS PAGE gel for MMP analysis, along with a pre–stained molecular weight ladder (Invitrogen, Carlsbad, CA). The gels were then transferred wet onto PVDF membranes. Following this, the membranes were blocked in *TBST* (*T*ris–*B*uffered *S*aline with 0.01% v/v *T*ween 20, pH 7.4) containing 5% w/v milk for an hour, immunostained using polyclonal antibodies (1:1000 for 1.5 hours) against LOX (**Santa Cruz Biotechnology, Inc.** Santa Cruz, CA), MMP–2 (Abcam, Cambridge, MA) and MMP–9 (Millipore, Billerica, MA), HRP–conjugated secondary antibody (1:10,000 for one hour) (GE Healthcare Biosciences, Pittsburgh, PA) and detected using an ECL–plus chemiluminogen detection kit (GE Healthcare Biosciences, Pittsburgh, PA). The blotted membranes were then stripped and re–probed with β–actin loading control (Abcam, Cambridge, MA). Bands were quantified using Image–J software (NIH, Bethesda, MD), expressed as relative density units (RDU) and normalized to control. Analysis was performed on bands generated from 3 blots per condition.

3.2.8. Gelatin Zymography for Detection of MMP–2 and –9

Volumes containing 5 μg proteins from the digested constructs were loaded per lane of 10% gelatin zymograms (Invitrogen, Carlsbad, CA) and run alongside a pre–stained protein ladder (10 kDa–190 kDa; Invitrogen, Carlsbad, CA), and purified protein standards of MMPs -2 and -9 (Anaspec, Fremont, CA), for 2 hours at 125 V. The gels

were then washed in 2.5% v/v Triton X– 100 for 30 minutes to remove SDS, following which they were incubated overnight in a substrate buffer to activate MMPs. The gels were then stained in Coomassie Brilliant Blue solution (Sigma, St. Louis, MO) for 45 minutes and de–stained (40% v/v methanol, 10% v/v glacial acetic acid) for 1.5 hours until clear bands were visible against a blue background[223]. The band intensities were quantified using Image–J and expressed as RDU values of the experimental cases normalized to RDU values of control cultures. Analysis was performed on the bands generated from 3 gels per condition.

3.2.9. Visualization of Elastic Matrix and Mineralization

At 21 days of culture, the constructs were fixed in 4% w/v formalin and embedded in paraffin. Tissue sections (5 μm thick) were then stained for elastin using a Verhoeff Van Gieson (VVG)–based elastic–stain kit (ScyTek Laboratories, Inc., Cache, UT). To visualize elastin using immuno–fluorescence, the sections were incubated in 0.05% w/v Pontamine sky blue (Sigma, St. Louis, MO) for 30 minutes, mounted using Vectashield containing DAPI (Vector Laboratories, INC. Burlingame, CA), cover–slipped and observed with a visible–red (Texas red) fluorescent filter. Pontamine sky blue quenches the auto–fluorescence of elastin and collagen in the visible–green region of the emission spectrum, and transfers the auto–fluorescence of elastin alone to the red region of the spectrum[224]. Elastin–specific fluorescence of sections labeled in this manner was confirmed by detecting elastic matrix in separate sections from the same sample with a rabbit anti–rat elastin antibody. Sections were imaged using a fluorescent microscope and

alignment of elastic fibers in the constructs were quantified by calculating their angular standard deviation[225]. Length and angle of individual fibers were measured using Image Pro software (Bethesda, MD). Elastin deposits with aspect ratio greater than 2 (long axis: short axis) were assumed to be fibers and only these were used for quantification.

The presence/absence of calcific deposits within constructs was ascertained by labeling sections with a Von Kossa–based calcium–staining kit (ScyTek Laboratories Inc., Cache, UT).

3.2.10. Mechanical Testing of 3-D Constructs

Uniaxial mechanical testing was performed on constructs treated with 4 selected dose combinations: 0.1 ng/ml, 1 ng/ml and 10 ng/ml TGF-β1, each with 0.2 μg/ml HA-o (n = 10/ case) using Instron 5943 under a 10 N load cell. Only 4 experimental cases were chosen to perform the mechanical testing based on the observations made using the various biochemical tests described above: 1) untreated control, 2) 0.2 μg/ml HA-o and 0.1 ng/ml TGF-β1, 3) 0.2 μg/ml HA-o and 1 ng/ml TGF-β1, and 4) 0.2 μg/ml HA-o and 10 ng/ml TGF-β1. The width of constructs was measured optically using a stereoscope, and thickness measurements using a liner variable differential transducer (LVDT). The constructs were gripped between serrated metal grips after wrapping the ends with three layers of paper towel and testing was performed in a saline bath maintained at 37 °C. Specimens were first preconditioned at a rate of 4 mm/s for 10 cycles followed by load to failure at an extension rate of 10 mm/min. Load vs. displacement and stress vs. strain curves were calibrated and elastic moduli calculated for each construct. Failure loads

were calculated if the specimens do not fail at the grips or due to other artifacts. Tensile modulus was calculated between 15%-30% strains (85 data points for all constructs).

3.2.11. Statistical Analysis

All quantitative results were analyzed from n = 6 independent repeats of each case and reported as mean ± standard deviation. Statistical significance between groups was determined from a one-way analysis of variance (ANOVA) and for ρ values ≤ 0.05. Power analysis of our prior data indicates that n = 6 replicates for cell/tissue cultures with 3 independent measurements for each parameter, is sufficient to reliably detect quantitative differences in outcomes, with a power of ≥ 0.95 (i.e., $\rho = 0.05$, i.e., 5% chance of claiming a false null hypothesis as true and $\rho = 0.05$, i.e., 5% false negative rate)[226].

3.3. RESULTS

3.3.1. Cell Quantification

As seen in **Figure 3.2**, cell numbers were highest (4.2 ± 0.8 –fold increases over 21 days; 1.4 ± 0.1 –fold vs. non–factor treated control) in constructs cultured with the lowest dose combination of TGF–β1 (0.1 ng/ml) and HA–o (2 μg/ml), and lowest (1.96 ± 0.23 fold increase over 21 days; 63 ± 13% of cell counts in control cultures at day 21) within constructs cultured with the highest dose of factors, i.e., TGF–β1 (10 ng/ml) and HA–o (2 μg/ml).

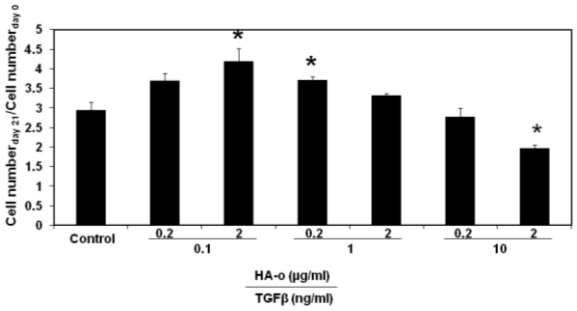

Figure 3.2: Effect of elastogenic factors on cell proliferation ratio. Cell numbers were calculated based on the estimate of 6 pg of DNA per cell, as calculated from DNA assay, at 0 and 21 days post–seeding, and their ratios determined and compared to. Differences were deemed to be significant from control cultures for $p < 0.05$ (*)

3.3.2. Elastic Matrix Content

Elastic matrix outcomes were quantified in terms of mRNA expressions of tropoelastin and LOX, quantity of the soluble precursor i.e., tropoelastin, quantity of matrix components of elastin i.e., alkali-soluble and –insoluble elastin, and LOX protein content. As seen in **Figure 3.3**, mRNA expression of elastin remained unchanged relative to control in all treatment conditions ($\rho > 0.4$). Cells within the control constructs synthesized 4.4 ± 0.5 ng/cell of tropoelastin, 9.4 ± 3.4 pg/cell of matrix elastin, comprising 4.5 ± 1.8 pg/cell of alkali–soluble matrix elastin and 1.5 ± 1.1 pg/cell of alkali–soluble fraction. Tropoelastin synthesis per cell was unaffected by culture with TGF–β1 and HA–o, except at the highest provided dose combination (10 ng/ml TGF–β1 and 2 µg/ml HA–o) at which significant increases (1.5 ± 0.2 – fold vs. control) were noted (**Figure 3.4 A**). Consistent with the tropoelastin content though, this difference was

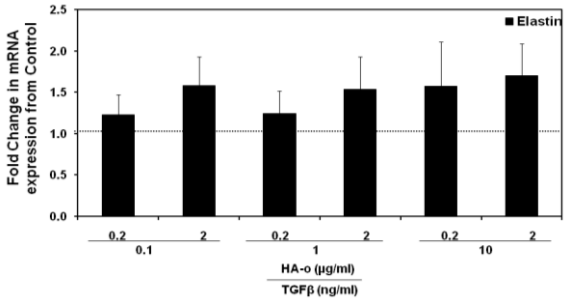

Figure 3.3: Effect of treatment conditions of mRNA expression of elastin relative to control constructs. No significant differences were observed between different conditions (n = 6)

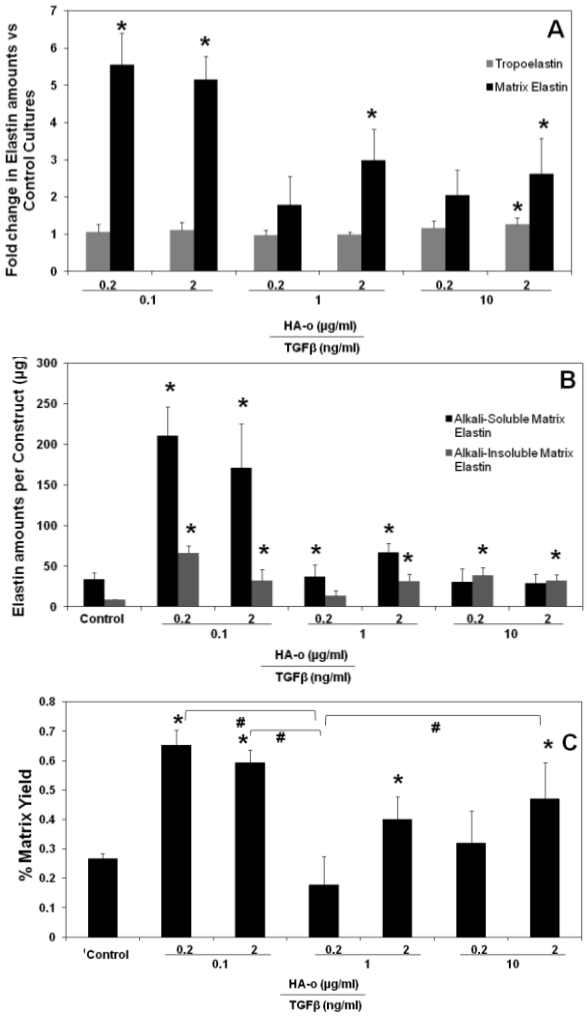

Figure 3.4: Effect of TGF–β1 and HA–o on elastin synthesis. (A) Differences in synthesis of tropoelastin and total matrix elastin per construct in samples cultured with HA–o and TGF–β1 relative to control cultures. (B) Effect of factor treatment on synthesis of alkali–soluble matrix elastin and crosslinked, alkali–insoluble matrix elastin. (C) Effect of factor treatment on yields of matrix elastin, i.e. the fraction of total elastin amounts produced by cells that is deposited in the matrix. '*' indicates differences from controls significant for $p < 0.05$, and '#' between cases as indicated (n = 6 for each case)

most pronounced in the cases with highest TGF–β1 doses (up to 26.2 ± 2.4 fold increase compared to control). This increase was significantly higher compared to the lower dose-

combinations as well (14.5 ± 3.4 in 0.1 ng/ml TGF–β1, and 11.2 ± 3.1 in 1 ng/ml TGF–β1). Differences in addition of HA-o with equal doses of TGF–β1 were insignificant in all cases.

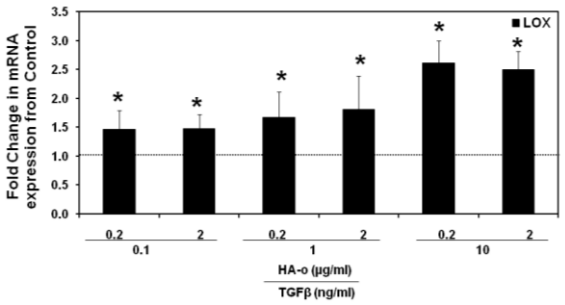

Figure 3.5: Effect of treatment conditions of mRNA expression of LOX relative to control constructs. Significant differences, indicated by '*' were observed in all treatment conditions relative to control (n = 6), $p < 0.05$

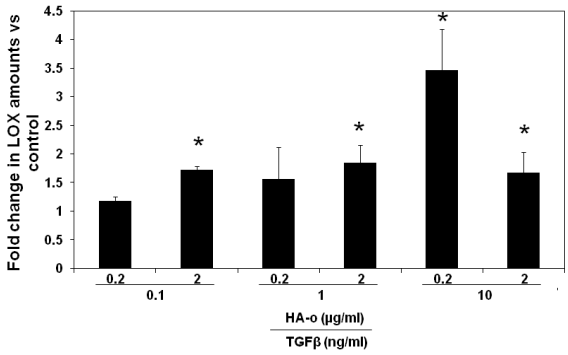

Figure 3.6: Fold change in protein levels of LOX in cultures with TGF–β1 and HA–o factors compared to untreated control cultures, as determined by western blotting. Differences from control were deemed significant (*) for $p < 0.05$ (n = 3 per case).

On the other hand, elastic matrix deposition per cell was also significantly greater in most experimental cases compared to control, with greatest increases (5.4 ± 0.8 and 5.3 ± 1.1 – folds vs. control) noted in constructs cultured with the lower dose combinations of TGF–β1 (0.1 ng/ml) and HA–o (0.2 µg/ml or 2 µg/ml) (**Figure 3.4 B**). Also noted was that increases in matrix elastin, especially at the lower provided doses of factors, were

associated more with increases in the less crosslinked, alkali–soluble matrix elastin fraction than with the more robustly–crosslinked, alkali–insoluble fraction. At the highest provided dose combinations, fold increases in both fractions compared to control were similar, i.e. the ratios of alkali- insoluble to –soluble elastin were the highest (**Figure 3.4 C**). This finding was consistent with mRNA expression and western blotting analysis for LOX enzyme (31 kDa) synthesis within cultured constructs. mRNA expression of LOX was elevated in all treatment conditions relative to control ($\rho < 0.05$), with the highest increase in constructs with 10 ng/ml TGF-β1 with both doses of HA-o (2.56 ± 3.5 –fold, $\rho < 0.001$, relative to control), as seen in **Figure 3.5**. LOX protein content was also highest in constructs cultured with 10 ng/ml of TGF–β1 and 0.2 μg/ml of HA–o (3.5 ± 0.5 –fold vs. control). LOX protein synthesis was elevated in all factor-treated cases compared to control (**Figure**s **3.6** and **3.7**). Matrix yields (**Figure 3.4 C**) were greatest in constructs cultured with the lower dose combination of factors, i.e. 0.1 ng/ml TGF–β1 with 0.2 μg/ml (0.6 ± 0.2%) 2 μg/ml of HA–o (0.6 ± 0.1%) respectively.

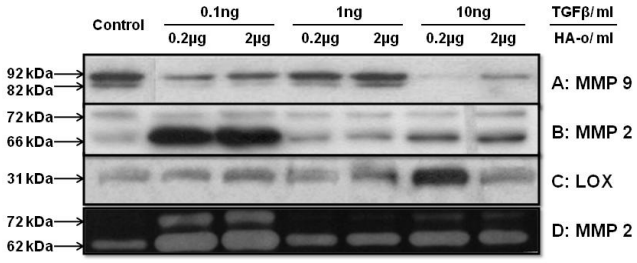

Figure 3.7: Effect of factors on enzyme synthesis and active forms. Representative immunoblots of (A) MMP–9 and (B) MMP–2 indicating the active and inactive protein bands for each case, and (C) LOX. (D) Representative gelatin zymogram of MMP–2 indicating the active and inactive bands

3.3.3. MMP Protein Analysis

Figure 3.7 shows representative immunoblots of MMPs –2 and –9 and zymogram of MMP–2. **Figure 3.8** compares MMP –2 and –9 amounts measured within collagen constructs treated with TGF–β1 and HA–o factors, with that measured within untreated control constructs.

MMP 2 was detected on the Western blots as two distinct bands corresponding to the zymogen form (~ 72 kDa) and active form (~ 62 kDa). MMP–9 was also detected in its zymogen (~ 92 kDa) and active (~ 82 kDa) forms. The greatest increases in total (active and inactive forms) MMP–2 protein amounts over controls was observed within constructs cultured with the lower dose combinations of the factors In general, MMP–9 synthesis was decreased in factor–treated constructs relative to control, though the decreases were greatest and statistically significant for constructs cultured with the highest TGF–β1 factor (10 ng/ml of TGF–β1 and 0.2 μg/ml or 2 μg/ml of HA–o) and with the lowest dose combination (0.1 ng/ml TGF–β1 and 0.2 μg/ml HA–o).

Figure 3.9 compares active and inactive forms of MMP–2 in factor–treated constructs with that in control constructs. MMP–9 activity is not shown since the bands were absent or too faint to be reliably quantified. In general, MMP–2 zymogen levels were very low, both in control and factor–treated constructs, except those cultured with low doses of HA–o (0.2 or 2 μg/ml) and TGF–β1 (0.1 ng/ml). The quantities of the active form of MMP–2 were also mostly similar between constructs, excepting those cultured with low doses of HA–o (0.2 or 2 μg/ml) and TGF–β1 (0.1 ng/ml), in which significant increases in enzyme activity was measured.

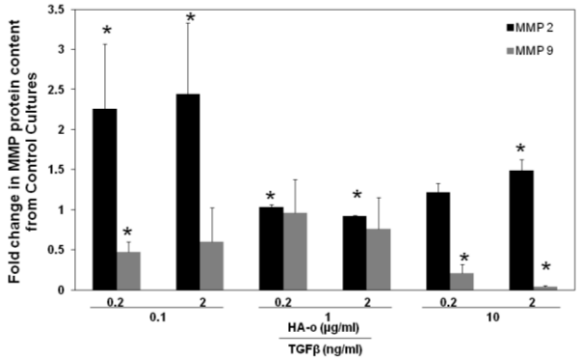

Figure 3.8: Differences in total protein synthesis of MMPs –2 and –9 in experimental cases compared to control, as determined from immunoblotting of the two proteases. '*' indicates statistical difference compared to control for $p < 0.05$ (n = 3 per case)

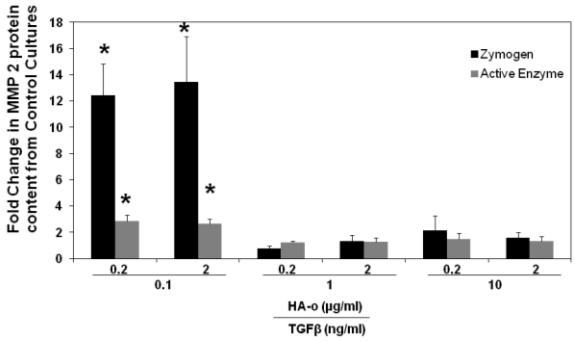

Figure 3.9: Effect of factors on MMP–2 quantities as determined by gelatin zymography. Data represents a fold change in relative density units of zymogram bands in experimental cases compared to control cultures. Significance in differences compared to control is indicated by '*' for $p < 0.05$ (n = 3 per case)

3.3.4. Mechanical Properties of Constructs

The compaction ratio of constructs cultured with the various dose combinations of TGF–β1 and HA–o was less than that of control constructs cultured without the factors (**Figure 3.10**). Compaction ratios were the lowest in constructs that received one of the two lowest dose combinations, specifically, 0.1 ng/ml TGF–β1 and 2 µg/ml HA–o (46.57 ± 4.12 %, $p < 0.05$).

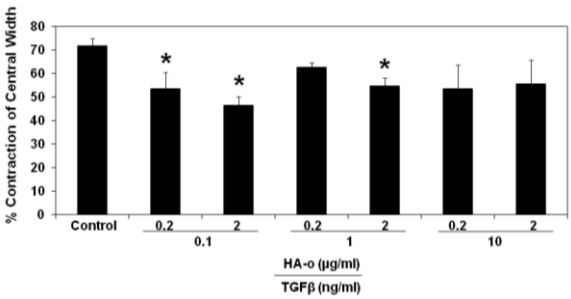

Figure 3.10: Percentage change in central widths of constructs at day 21 compared to day 0 (n = 6 per case). * indicates significance of differences compared to control cultures, deemed for $p < 0.05$

Tensile testing of constructs (**Figure 3.11**) revealed non-linear stress strain curves, typical of collagenous tissues. Addition of factors did not significantly alter the modulus of the constructs, in both the elastic toe region, as well as the plastic region. The highest elastic moduli were observed in untreated control constructs (740.7 ± 81.2 kPa), and the lowest in constructs with 0.1 ng/ml TGF–β1 and 0.2 µg/ml HA-o (632.6 ± 61.3 kPa). However, these differences were not statistically significant, compared to control or between constructs. The toe region of the constructs at the start of load to failure test phase was inconsistent. Therefore tensile modulus at this region was not calculated. Almost all constructs failed at the grips, and therefore the yield properties could not be accurately and consistently determined.

3.3.5. Visualization of Elastic Matrix

VVG staining for elastin (**Figure 3.12**) and immuno–fluorescence labeling after Pontamine sky–blue quenching (**Figure 3.13**) showed the presence of elastic fibers in all the constructs treated with factors, although due to the limited thickness of the sections,

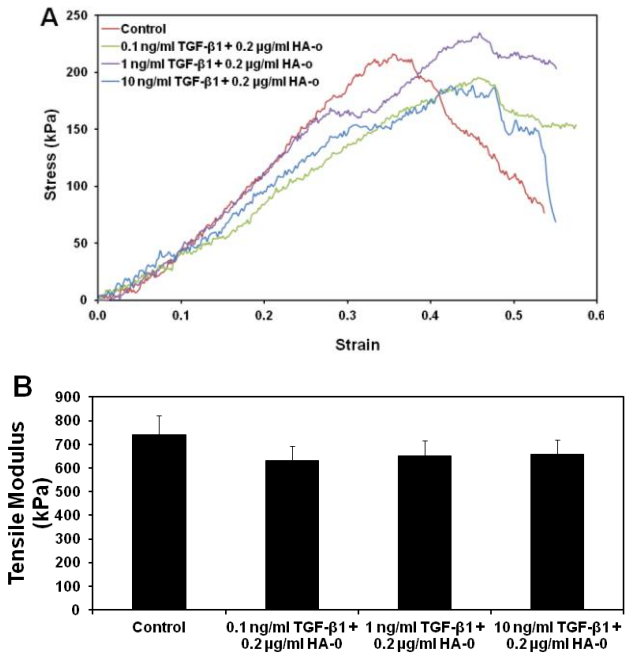

Figure 3.11: Effect of select doses of treatment conditions on tensile properties of constructs. (A) Representative stress vs. strain curves of constructs at the 4 treatment doses. Toe regions were not consisently seen in all constructs. All constructs failed at the grips. Tensile modulus calculated between 15%-30% strains were not statiscally different between cases (B).

the continuity and total length of individual fibers could not be ascertained. Elastic fibers were more abundant and appeared more complete towards the edges of the constructs.

Elastic fiber alignment, calculated in terms of angular standard deviation, did not differ between the various culture conditions (**Figure 3.14 A)**. However, there were a significantly greater number of elastic fibers (**Figure 3.14 B**) present in all cultures that received the elastogenic factors, (except cultures that received 1 ng/ml of TGF–β1 and 2 µg/ml of HA–o). Von Kossa staining (**Figure 3.15**) for calcific deposits indicated lack of matrix mineralization in all constructs.

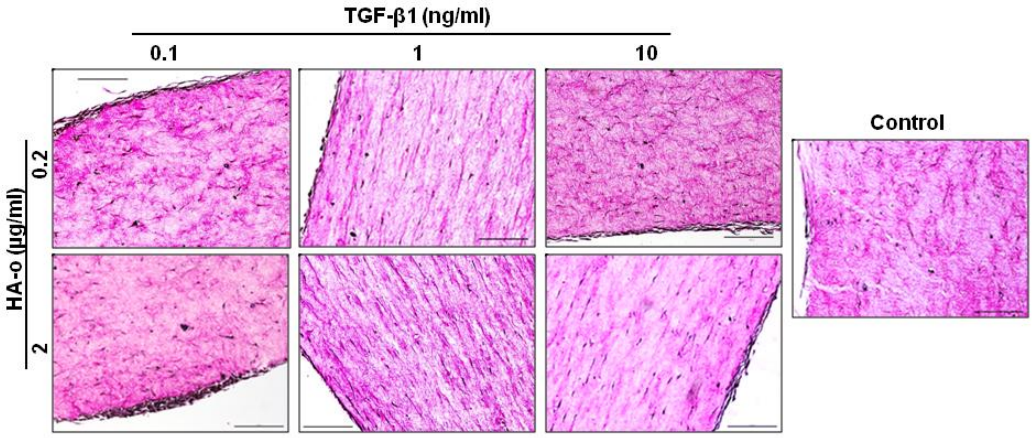

Figure 3.12: Representative images of 5 µm sections stained for elastin with modified VVG at 20 × magnification (scale bar = 200 µm). Elastic fibers are stained purple and surrounding collagen is stained pink

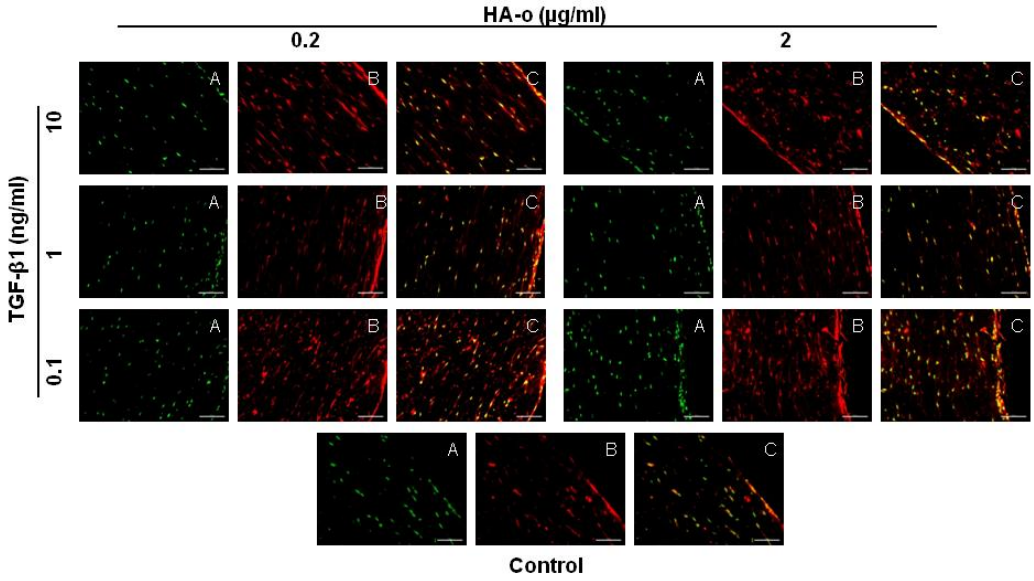

Figure 3.13: Representative fluorescence micrographs of construct sections showing distribution of nuclei in green (A), elastin/elastic fibers in red (B), and the overlay of the two (C). Paraffin embedded sections were treated with Pontamine sky blue to quench autofluorescence of collagen and shift that of elastin to the red wavelengths. Nuclei were stained with DAPI. Magnification: 20 × (scale bar = 100 µm)

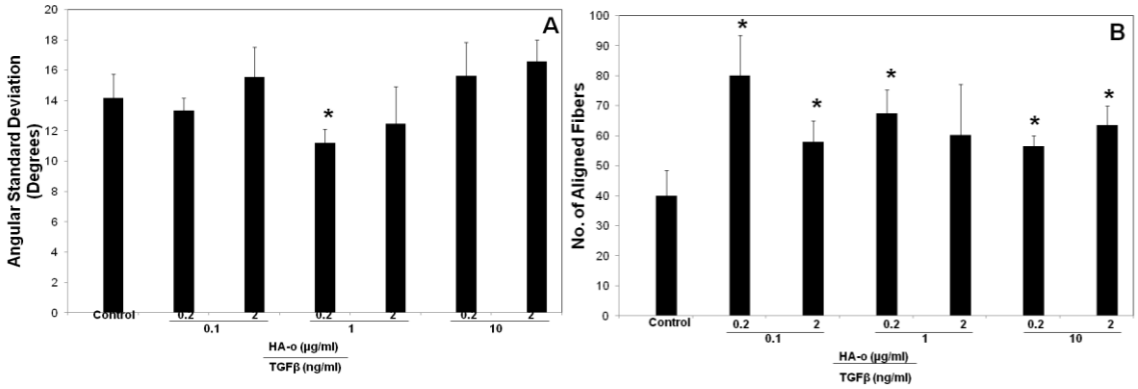

Figure 3.14: Elastic fiber alignment in collagen gel constructs represented by angular standard deviation in degrees (A) and no. of aligned fibers (B). '*' represents significance in difference from control cultures

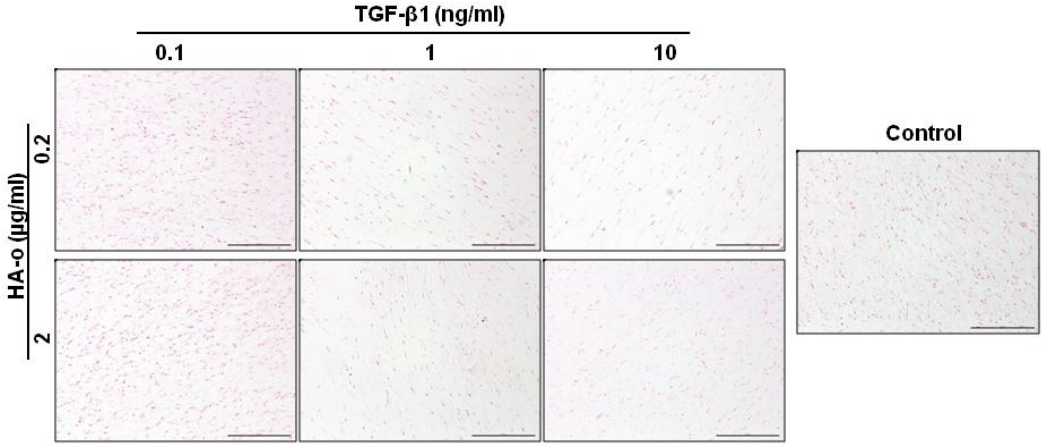

Figure 3.15: Von Kossa staining for mineral deposits. The absence of any black spots/deposits indicates lack of TGF–β1–induced matrix mineralization in the dose range studied. The kit used stains nuclei red. Magnification: 10 × (scale bar = 500 µm)

3.4. DISCUSSION

Attempts at engineering elastic tissue constructs, such as vascular replacements, thus far, have been challenged by poor ability of post–neonatal cell types to synthesize tropoelastin and crosslink the precursors into a fibrous matrix[227-228]. It is also evident

from literature that the extracellular microenvironment critically influences cell phenotype and behavior. In this context, a large body of work attests to the contractile phenotype of SMCs within the intact vessel wall, and the switch to a more synthetic (i.e. proliferative and ECM–generating) phenotype, when these SMCs are isolated and cultured *in vitro*[56, 141], either on tissue culture polystyrene (TCPS), or within scaffolds created from one of the many natural (e.g. fibrin[227]) or synthetic (e.g. Polyglycolic acid (PGA)[52]) polymers. From the standpoint of elastin regeneration, vascular SMCs in contact with these scaffolds have been found to enhance tropoelastin synthesis. Although the cellular scaffolds may provide the initial framework for cell adherence and proliferation, the expectation is that the scaffold would gradually biodegrade, and cell–synthesized ECM would accumulate and assume primary load–bearing roles. Key among these ECM proteins is collagen, which cells are able to abundantly and preferentially synthesize and deposit, beginning at a fairly early stage in culture. While such collagen fiber deposition is favorable from the standpoint of replicating the 3–D collagenous matrix within the aorta, there is also significant and irrefutable evidence that this microenvironment promotes a more quiescent, contractile phenotype amongst SMCs (compared to other scaffolding materials like PGA and fibrin), which is not particularly conducive to their ability to synthesize elastin and lay down elastic matrix structures[49, 52-53, 229]. Thus, efforts to engineer soft elastic tissues, such as vascular tissues, will tremendously benefit from an elastin–regenerative stimulus that can overcome the unfavorable microenvironment for elastin synthesis imposed by a collagenous matrix, standard to most applications.

Previously, our lab established the elastogenic benefits of TGF–β1and HA–o towards increasing tropoelastin precursor production and crosslinked–matrix deposition by RASMCs[37, 148, 217, 230]. However these studies were performed on RASMC layers cultured on 2–D TCPS surfaces, on which SMCs are known to assume a more proliferative, synthetic phenotype than what they exhibit within intact vessels. In order to translate the specific benefits of the above mentioned factors to a culture model more closely evocative of a collagenous 3–D matrix microenvironment, naturally present within decellularized vascular tissue–based scaffolds, and that generated by cells seeded on other scaffolds, we studied the effect of the above mentioned factors on adult RASMCs seeded within 3–D collagen constructs maintained under static tension.

Relative to untreated control constructs, cell numbers within constructs cultured with HA–o and TGF–β1 were in general slightly greater, with the significant differences being only for the intermediate factor doses. A significant attenuation in the increase in cell count was noted only at the highest provided dose (i.e. 10 ng/ml of TGF–β1 and 2 μg/ml of HA–o). While these results are consistent with observations of other groups, wherein increasing TGF–β1 concentrations was found to lower cell densities[231], the results contrast substantially from our previous observations of a dose–dependent inhibition of SMC proliferation on TCPS surfaces[184]. The present results suggest that (a) interaction with the collagenous ECM alters SMC behavior compared to 2–D cultures, and (b) such collagen–SMC interaction de–sensitizes the cells to TGF–β1 and HA–o, attested to by a significant decrease in cell number only at the highest provided doses. It is also apparent from our results that similar to our recently published observations in 2–

D cultures, TGF–β1 effects dominate with a biphasic dose–dependent proliferative response to TGF–β1 at both HA–o doses[232]. However, from the standpoint of a tissue engineering application, wherein growth in tissue mass is contingent on increased availability of ECM–generating cells, the HA–o/TGF–β1 dose combination that provides greater impetus to SMC proliferation (i.e. 0.1 ng/ml of TGF–β1 and 0.2 or 2 μg/ml of HA–o), is most desirable.

Within a collagenous 3–D matrix, SMCs are likely to switch to a more contractile phenotype characterized by reduced ECM synthesis, which has been previously reported[49, 52-53, 229]. Concurrently, our results indicated that within 3–D collagen constructs, HA–o and TGF–β1 together had mostly no effects on tropoelastin synthesis. The sole exception was the highest factor dose which induced a moderate, but significant increase. While this lies in complete contrast with our prior published studies in 2-D culture, wherein we noted even the lowest dose combination of factors we test here, to induce multi–fold increase in tropoelastin synthesis compared to non–additive controls, and the differences could be attributed to a switch in SMC phenotype between 2-D and 3-D cultures.

HA–o and TGF–β1 in this study appear to influence the process of tropoelastin crosslinking and matrix deposition to a greater extent than tropoelastin synthesis itself; the enhancement of elastic matrix deposition appears to be the predominant effect of the factors, though in the absence of information as to an exact mechanism by which the factors elastogenically induce the cells, this currently remains an unsubstantiated observation. As seen in **Figure**s 4A and 4B, at both HA–o doses (i.e. 0.2 and 2 μg/ml), a

classic biphasic TGF–β1 dose response is seen with regard to elastic matrix deposition, with significant (~ 5 fold) increases noted at the lowest tested TGF–β1 dose (0.1 ng/ml) and much smaller increases noted at higher TGF–β1 doses. Our results also suggest that at higher doses, HA–o reduces this biphasic elastic matrix synthesis response to TGF–β1; especially at higher TGF–β1 doses (i.e. 1 and 10 ng/ml), increasing HA–o dose led to a significant increase in elastic matrix deposition. Matrix elastin increases were primarily associated with enhanced deposition of the less crosslinked alkali–soluble fraction.

In the majority of cases, we found the factors to enhance significantly relative to controls, the synthesis of LOX enzyme, which is believed to play a central role in crosslinking tropoelastin into a mature elastic matrix. This is in agreement with our prior published findings[37, 233] where we showed HA–o/TGF–β1 to enhance mRNA expression, protein synthesis and activity of the elastin crosslinking enzyme. However, the most significant increase in LOX synthesis was observed in cell cultures treated with 0.2 μg/ml of HA-o and 10 ng/ml of TGF-β1 (see **Figures 3.6** and **3.7**). Likewise, in comparing ratios of amounts of alkali-insoluble (i.e., highly crosslinked) matrix elastin to amounts of the alkali-soluble fraction (see **Figure 3.4**), we find that the ratios are far less than 1, for all cases, especially for cultures treated with the lower doses of the factors, but greater than 1 in the singular case wherein LOX synthesis was most significantly enhanced (i.e., 0.2 μg/ml of HA-o and 10 ng/ml of TGF-β1). We thus hypothesize that the increases in amounts of LOX protein contribute to more efficient crosslinking of elastic matrix into an alkali-insoluble form.

A very interesting observation is that the matrix yield (i.e. mass % of total elastin output crosslinked into a matrix) in control collagen constructs is much lower (~ 0.2%) than what we have observed with the same cell type in 2–D cultures on non-collagenous substrates (10–15%). While we have shown a multi-fold increase in matrix yields in the presence of TGF–β1 and HA–o factors, most significantly at the lowest tested doses, the yields remain < 1%. One possible reason for the low levels of elastic matrix deposited, which will confirm in a future study, might be over-production of GAGs such as chondroitin sulfate by the SMCs, which as studies by Hwang et al.[38] and Allison et al.[39] have shown, to inhibit elastin synthesis and assembly, and shown to correlate with increased collagen matrix deposition. Regardless, despite the likely LOX–mediated crosslinking of tropoelastin in the presence of HA-o and TGF-β1, the poor elastic matrix yields obtained in this study indicate that there is room for improvement in terms of enhancing the deposition of the more robustly crosslinked, and hence the more stable alkali–insoluble elastic matrix fraction.

In the context of enhancing elastin matrix within 3–D collagenous constructs, leading to tissue engineering of a clinically sufficient, implantable tissue, it might thus be necessary to seed the scaffolds at much higher cell densities to overcome the poor matrix yield obtained per cell (even when elastogenically induced) or alternatively co–deliver elastin–crosslink–promoting factors (e.g. LOX or LOX–activity enhancing copper nanoparticles), which we have shown to be very useful for the purpose[148-149].

MMPs –2 and –9 represent a class of Zn^{2+} dependent gelatinases that degrade matrix proteins, specifically elastin[12]. Since intact elastic fibers serve as nucleation sites

for organization of new elastic matrix structures, and since net accumulation of elastic matrix is dependent on much attenuated matrix degradation relative to its regeneration, minimizing MMP production/activity is desirable[83]. In this context, our study showed that the lowest, but the most elastogenic dose combination of TGF–β1 and HA–o significantly attenuate MMP–9 synthesis, but enhance MMP–2 production by SMCs. At the highest provided dose, also deemed to be elastogenic, but less so, MMP–9 production was negligible and MMP–2 levels were similar to untreated controls. Likewise, active forms of MMP–2 protein was enhanced at the lowest TGF–β1 and HA–o dose combinations, and remained unaffected at higher doses. While it is yet undetermined as to whether the above mentioned increases in synthesis of MMP–2 protein quantities (both zymogen and active forms) at the lowest tested TGF–β1 and HA–o doses are significant enough on absolute terms to actually compromise the matrix; if it is so, providing MMP–inhibiting culture conditions, or alternatively, providing the higher, non–MMP–enhancing factor dose might be a desirable approach.

Another favorable observation of culturing SMCs within statically loaded collagen gels was the high degree of alignment in the synthesized elastic fibers, as seen in **Figure 3.14**. While the degree of alignment was more or less uniform irrespective of the culture conditions, all cultures that received the elastogenic factors, except those with 1 ng/ml of TGF–β1 and 2 μg/ml of HA–o, consisted of significantly larger number of aligned fibers compared to non-additive control cultures.

TGF–β1, when over–expressed, especially in a sustained manner, can induce SMCs to assume a more osteogenic phenotype, and enhance matrix calcification[139].

However, our study did not show any calcification, even in constructs cultured with the highest dose of 10 ng/ml TGF–β1.

3.5. CONCLUSIONS

This study demonstrates elastogenic induction of RASMCs with HA–o and TGF–β1 factors within non-elastogenic 3-D constructs of statically loaded collagen gel constructs. While a much higher dose combination than that shown useful in earlier studies within 2-D cultures is necessary to enhance both tropoelastin and matrix synthesis, compared to other studies performed on SMCs in collagen gels, we have demonstrated that synthesis of significant amounts of matrix elastin is possible in the presence of these factors. A major challenge to our ability to obtain the optimum amount of elastin, that engineering of tissue constructs for human use demand, is the rather poor elastic matrix yield (< 1%), and requires addressing.

CHAPTER FOUR

IMPACT OF DYNAMIC CONDITIONING ON INDUCED ELASTOGENESIS BY CELLS IN 3D COLLAGENOUS MICROENVIRONMENTS

4.1. INTRODUCTION

In the previous chapter we demonstrated that EF-stimulation of adult vascular cells towards *de novo* synthesis of elastic matrix components can be achieved even in a quiescent 3D collagenous microenvironment not particularly conducive to elastogenesis. We also showed that cell alignment achieved in the predominant direction of applied static strain, positively influenced orientation and alignment of both the pre-existing collagen matrix, and the cell-synthesized elastic matrix. However, due to the particular design of the 3D collagen gel system that applies strain along the longitudinal axis, the orientation of the synthesized matrix is tangential to the circumferential orientation exhibited *in vivo* by the elastic arteries. In this study, we therefore wanted to further modify this 3D model system such that the orientation of cells, and as a result, the synthesized elastic matrix would mimic that contained in vascular tissues. Several studies have demonstrated the benefits of cyclic mechanical stretch towards inducing orientation of SMCs. Studies have also demonstrated that cells behave differently under uniaxial tension within 3D constructs similar to that incorporated in our previous study[57, 234], compared to when they are cultured within tubular constructs. While cells are shown to orient in the direction of uniaxial tension, cells within tubular constructs experience radial and circumferential stretch, and orient in a direction perpendicular to stretch, therefore

conforming to circumferential alignment, similar to that seen *in vivo*. We therefore chose to use a tubular collagen gel model to which cyclic distension could be applied with the aim of achieving circumferential orientation of cells and thereby, enabling deposition of newly synthesized elastic matrix in a circumferential orientation as in intact blood vessels.

The three important factors that influence mechano-transductive response by cells, and as a result, cell phenotype and final matrix output, are strain amplitude, frequency and duration of cyclic stretch[164, 235]. To date, most studies utilizing cyclic stretch parameters have primarily used strain levels of > 2.5%, and a majority of them have used 10% strains[57, 59, 166, 236]. However, most of these studies were also targeted towards generating small diameter vascular tissue equivalents that typically respond to much higher strains than do elastic arteries[5]. Moreover, the synthesis and enzymatic activity of the predominant elastolytic protease MMP-2, has been reported to increase at higher strains[237-238]. While it is argued that MMP-2 is important for matrix reorganization[237], its enzymatic activity can at the same time however, also degrade newly synthesized elastic matrix, and prevent its maturation and assembly within the scaffolds[10, 83]. Another limitation of applying these higher strains, especially in a collagenous hydrogel environment that has not yet completely been remodeled to have sufficient fibrillar matrix, is the irrecoverable creep that the scaffold would experience under repeated cyclic loading[59]. This would also lead to the cells perceiving constantly changing levels of strains, and not the set strain levels intended to transduce the cells. Alternatively, studies have also demonstrated the importance of frequency of strain

perceived by cells, and that changing the frequency of cyclic strains was found to play a significant role in regulating the alignment of vascular SMCs in an intact actin filament-dependent manner[167-168]. In order to minimize the detrimental effects of high strain levels, and at the same time promote cell and matrix alignment, we therefore chose to subject SMC-seeded tubular collagen constructs to 2.5% cyclic strain applied at frequencies of 0.5 Hz, 1.5 Hz and 3 Hz for 21 days of culture. The doses of the EFs used to elastogenically stimulate cells in this study, were based on the results obtained in Chapter 1, where the dose combination of 0.1 ng/ml TGF-β1 and 0.2 μg/ml HA-o was concluded to be most elastogenic. In light of results of other studies in our lab that human aortic SMCs (HASMCs) respond to elastogenic stimulation by EFs[239], we transitioned to study of these cell types to render our outcomes more clinically relevant.

4.2. MATERIALS AND METHODS

4.2.1. Design, Construction and Principle of Operation of Bioreactor for Dynamic Cell Culture

A bioreactor was constructed to deliver cyclic, tangential strains to the tubular collagen gel constructs and the SMCs seeded within it. The set up (**Figure 4.1.**) consisted of (a) tubular tissue-culture-chambers with centrally placed silicone tubing (around which the collagen gel constructs would compact) connected to (b) compressible metallic bellows distended cyclically by (c) a stepper motor whose motion was controlled by (d) a custom-programmed motor-controller. The motor and controller were powered by a standard 3 amp power supply. The system was fabricated at the Device Prototype Core

(Design, Electronics and Polymer cores) at the Cleveland Clinic. All bioreactor parts were either made in house at the Device Prototype Core, or purchased from Cole Parmer (Vernon Hills, IL) or McMaster Carr (Aurora, OH).

Principle of Operation: The segment of the bioreactor that was filled with water (from the sealed end of the bellows to the sealed ends of silicone tubes within the culture chamber in **Figure 4.1**) was a closed, air-tight unit, within which the inner silicone tubes are the only compliant parts.

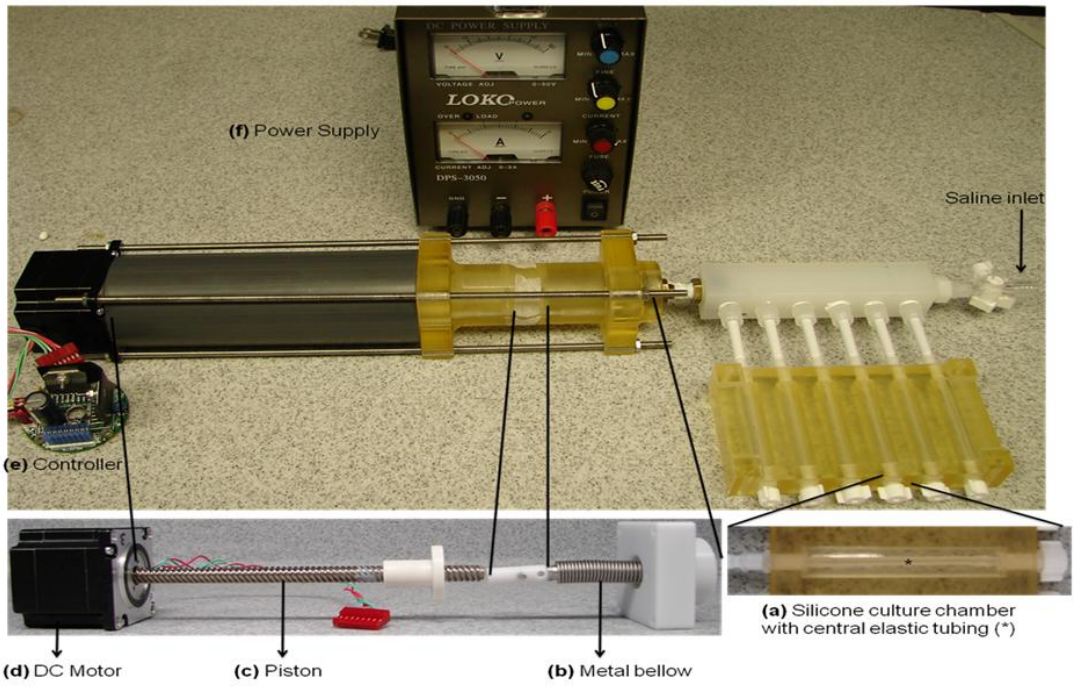

Figure 4.1: Bioreactor set-up for applying 2.5 % stains. The tissue culture chamber with inner silicone tubing (a), is connected via a manifold to the bellows (b), which are in turn coupled to the shaft (c) of the DC motor (d). The forward and backward movement of the shaft of the motor is controlled by the motor controller (e), powered by an external power supply (f). The volume spanning the region within the silicone tubing starting from the tissue culture chamber, to the end of the bellow is a closed loop into which sterile water is purged in via a leur lock inlet.

The system therefore worked on the principle that when the bellows are compressed by the motor shaft, the change in volume will be experienced only by the elastic silicone tubes and compensated by a resultant change in diameter of the tube. This cyclic change in diameter therefore induced circumferential strains on the SMCs cultured within the collagen-gel constructs surrounding the tube.

The increase in volume within the silicone tubes in order to deliver the required strains is proportional to distance travelled by motor shaft to compress the bellows which will displace that same change in volume, resulting in generation of strains at the silicone tube. It was crucial to ensure that the system was completely devoid of any air bubbles and maintained airtight throughout the culture duration in order to deliver accurate strains to the constructs.

Tissue Culture Chamber: The tissue culture chamber of the bioreactor (**Figure 4.2**) consisted of tubular compartments, 5 cm length, 8 mm diameter each, cast out of silicone rubber. Silicone rubber tubes (4 cm length, 4 mm outer diameter, 1 mm thickness) were inserted across the length of each compartment, and held taut in place by friction. Silicone rubber is easy to sterilize and provides a non-adherent surface to prevent cell-attachment. The collagen gel constructs were polymerized and contracted within these chambers such that a 5 ml volume of the collagen-cell mixture would be equally distributed around the circumference of central silicone tubing. The compartments with the silicone tubes were sealed at one end with lour fittings, and connected to a 6-channel polycarbonate manifold at the other end, which was in-turn connected to the bellows of

the bioreactor. A leur-lock was fitted to either ends of the manifold to remove air and fill the circuit with sterile water. All parts of the system directly in contact with the culture chamber were either constructed out of autoclavable polypropylene or silicone rubber.

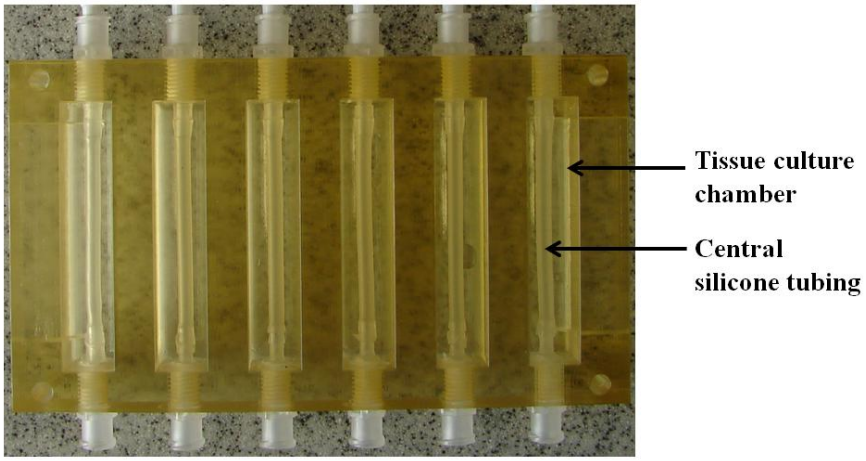

Figure 4.2: Tissue culture chamber of the bioreactor showing 6 parallel culture chambers with central silicone tubing around which the sell-seeded collagen gels would contract

Motor Controller and Generation of Strains: Stainless steel bellows were mechanically coupled to the shaft of the stepper motor (EZStepper, All Motion, Union City, CA), such that as the shaft rotates clock-wise or anti-clockwise, the bellows compress or expanded proportionately. The speed of rotation, number of steps moved forward or backward by the shaft, and the minimum and maximum limits (of shaft movement and current drawn) were controlled by the stepper motor-controller supplied with the motor, custom-programmed to deliver the required strains and frequencies. The compressibility of bellows and the stepper motor specifications were set such that the system would deliver a maximum of 5% strain at 5 Hz frequency, sufficient to meet the requirements of our study. The motor was first programmed to generate linear motion according to the

manufacturer's instructions. The parameters in the program were then set up in order to deliver the 2.5 % strains at the three chosen frequencies of 0.5 Hz, 1.5 Hz and 3 Hz. Each bioreactor set up delivered cyclic strains to 6 collagen gel constructs cultured in parallel (as seen in **Figure 4.2).** In order to confirm the settings and optimize the parameters, test runs of the strain delivery in the chambers were performed under a stereoscope (Olympus SZ61; Olympus, Center Valley, PA) connected to a CCD camera (Infinity-2, Electron Microscopy Sciences, Hatfield, PA). The strain in the silicone tubes were recorded, calculated using Image J software (NIH, Bethesda, MD) and confirmed based on the difference in outer diameter per cycle for the three frequencies.

The motor, shaft and the bellows were enclosed in a plastic casing for ease of handling. The controller was connected to a PC with its software via a USB cable and to start and stop the program alone, but not at other times. Each bioreactor was individually connected to an external power supply (0-30 V, 1-3 amps). The system drew less than 0.3 amps and its running voltage was ~ 20 V. During tissue culture, only the tissue culture chamber with its connections to the bellows and motor were placed inside a sterile CO_2 incubator maintained at 37 °C, while the controllers and power supplies were placed outside.

4.2.2. Fabrication of Tubular Collagen Gel Constructs

Before starting the cultures, the single-use central silicone tubing within each tissue culture chamber (**Figure 4.2**) was first inserted and held taut in place to prevent sagging. A leak test was then performed to ensure that there were no holes in the tubing

and it did not pop out of the chamber at the strains delivered. The chambers containing the silicone tubes were then steam sterilized (121 °C, 45 minutes). Parts (b) and (c) (mentioned in **Section 4.2.1**) were then assembled and attached to the polypropylene manifold. A leak test was separately performed for these parts to ensure a tight seal. Even though the closed circuit (containing bellows, manifold, silicone tubing and the connecting parts, **Figure 4.1**) in which water is stored to deliver the strains, is isolated from the cultures, it was ensured that they were maintained relatively clean as well. To do this, after the leak test, the entire circuit was incubated with 70% v/v ethanol (10 minute × 3 change) and then rinsed in sterile water (3 ×) . These parts were then attached to the tissue culture chamber inside a sterile hood. Sterile water was then slowly pumped into the closed circuit via the leur locks using a syringe to completely fill the volume with water. A leak test was again performed to ensure a tight, closed loop to remove any residual air bubbles. The set up was positioned upright overnight in the sterile hood, during which time any residual air bubbles from the circuit arose, to be easily removed by slowly pumping in more sterile water into the circuit.

Acid solubilized rat tail collagen-I was brought to neutral pH and kept on ice as described in **Section 3.2.2.** Adult healthy human aortic SMCs (HASMCs) (Cell Applications, San Diego, CA) were trypsinized at passage 4 and mixed with the collagen solution at a final concentration of 0.5×10^6 cells/ml and 2 mg/ml collagen. Due to the high collagen gel volumes and number of replicates, cell seeding density used in this study was 50% of that used in the experiments using rat cells detailed Chapter 3. Preliminary studies performed to test the extent of contraction between 1×10^6 cells and

0.5×10^6 HASMC/ml indicated comparable degrees of contraction when evaluated 5 days after seeding. The lower cell seeding density is also relevant in the context of our studies since prior studies have suggested that tropoelastin synthesis tends to be higher on a per cell basis with lower cell densities[28]. An aliquot of the cell-collagen mixture (5 ml) was then added slowly to each culture chamber such that the mixture uniformly distributed itself around the circumference of the tube. Culture medium was changed after 24 hours. At 48 hours, the medium was changed yet again and fresh medium with the stated EF doses (**Table 4.1**), and dynamic culture conditions were provided. Day one of the culture was therefore corresponding to 72 hours post-seeding of the constructs. Optimized EF doses of 0.1 ng/ml TGF-β1 and 0.2 μg/ml HA-o were added exogenously to the culture medium, similar to that described in Chapter 3. The five experimental and control conditions are listed in **Table 4.1.** Constructs that did not receive EFs and were cultured under static conditions (no EFs, static) were considered to be biological controls for all normalization purposes. Culture medium was changed every two days and spent medium was removed, pooled with prior aliquots from the same well, and frozen at -20 °C for later analysis.

After 21 days of treatment, i.e., 24 days post-seeding, the constructs were harvested for analysis. The constructs were first rinsed in three quick changes of sterile PBS. Each construct was then cut with the silicone tube, removed from the chamber, and placed into a dish containing sterile PBS. Constructs were transversely cut into four equal parts to be further processed for the various biochemical assays listed below.

Mechanical testing and PCR were performed on a different set of constructs, than those cultured for biochemical analysis discussed in the following sections. RT-PCR was performed on approximately 0.8 cm segments of the same constructs seeded for mechanical testing. In the procedure followed for other assays, for each batch of trypsinized cells, an equal number of constructs were seeded for each culture condition, including treatment controls. However, for these analyses, we staggered seeding and harvesting of constructs corresponding to individual test cases by a few days. All factors related to initial seeding that may contribute to any variability of construct outcomes such as cell count, final pH, volumes pipetted etc., were however maintained the same.

Group	**0.1 ng/ml TGF–β1+ 0.2 µg/ml HA-o**	**Frequency of 2.5% Cyclic strain (Hz)**
No EFs, static (control)	-	Static
EFs, static	+	Static
EFs + 0.5 Hz	+	0.5
EFs + 1.5 Hz	+	1.5
EFs + 3 Hz	+	3

Table 4.1: Experimental conditions: impact of dynamic conditioning on induced elastogenesis in 3D tubular collagen gel constructs

4.2.3. Compaction of Tissue Constructs

All constructs were photographed weekly and their lengths and central widths measured using Image J software (NIH, Bethesda, MD). At least 5 measurements for central width and 3 measurements for the length were made per construct. Construct

compaction was measured and reported as the aspect ratio (length : outer diameter) on the day of harvest.

4.2.4. DNA Assay for Cell Quantification

One segment of each construct was snap-frozen in liquid nitrogen and lyophilized for 24 hours, following which dry weights of the segments were measured. The segments were then digested in 750 μl of 5mg/ml proteinase-K (Gibco–Invitrogen, Carlsbad, CA) in a 65 °C water bath for 10 hours. The samples were then boiled for 10 minutes above 75 °C to neutralize the enzyme. After cooling the samples down to room temperature (~ 25 °C), they were sonicated on ice 5 second cycles for 45 seconds, with a 10 second lag between each sonication cycle. DNA content was then measured in these samples using a Hoechst-dye based flourometric assay as described in **Section 3.2.4**[221]. Cell count was measured based on the estimate of 6 pg DNA/cell, and was normalized to mg weights of constructs (n = 6/case).

4.2.5. RT-PCR for mRNA Expression of SMC Phenotypic Markers and Matrix Proteins

One segment of each construct (n = 6/case) was cut into 1 mm thick pieces and snap frozen until processing. Samples were reconstituted in RLT buffer provided with the RNeasy mRNA isolation kit (Qiagen, Valencia, CA) with 1% v/v 2-mercaptoethanol and homogenized using a 21-guage needle and syringe. mRNA was isolated from the homogenized samples as per the instructions provided in the RNeasy kit manual. Isolated

Gene	Primer Sequence (5'-3')		T_m (°C)	Size (bp)	Accession no. (Source)
18S	Forward	TCAAGAACGAAAGTCGGAGG	58	488	NR_003286 (Real Time Primers)
	Reverse	GGACATCTAAGGGCATCACA			
Elastin (*ELN*)	Forward	CAGTTGGTACCCAAGCACCT	58	158	NM_000501 (Real Time Primers)
	Reverse	AGGTGGCTATTCCCAGTGTG			
Fibrillin- 1 (*FBLN1*)	Forward	GCTCCAGATCCATACAACAC	58.5	145	NG_008805. 2 (Applied Biosystems)
	Reverse	ACACCTTCCTCCATTGAGAC	59.5		
Fibulin-5 (*FBLN5*)	Forward	CATTGCAGTGATATGGACGA	58	207	NM_06329 (Real Time Primers)
	Reverse	GAAGCCCCCTTGTAAATTGT			
Lysyl Oxidase (*LOX*)	Forward	CAGAGGAGAGTGGCTGAAGG	58	223	NM_002317 (Real Time Primers)
	Reverse	CCAGGTAGCTGGGGTTTACA			
Collagen-1 (*COL1A1*)	Forward	AAGGGACACAGAGGTTTCAG	59.7	189	NG_007400. 1 (Applied Biosystems)
	Reverse	TAGCACCATCATTTCCACGA	59.5		
Matrix Metalliproteinase-2 (*MMP2*)	Forward	TTGACGGTAAGGACGGACTC	60	153	NM_004530 (Real Time Primers)
	Reverse	ACTTGCCGTACTCCCCATCG			
Matrix Metalliproteinase-9 (*MMP9*)	Forward	CTCTGGAGGTTCGACGTG	58	183	NM_00994 (Real Time Primers)
	Reverse	GTCCACCTGGTTCAACTCAC			
α-Smooth Muscle Actin-2 (*ACT2*)	Forward	AGTTACGAGTTGCCTGATGG	58	165	NM_001613 (Real Time Primers)
	Reverse	GAGGTCCTTCCTGATGTCAA			
Caldesmon (*CALD1*)	Forward	CCCAAACCTTCTGACTTGAG	58.6	162	NG_029186.1 (Applied Biosystems)
	Reverse	CGAATTAGCCCTCTACAACTG	59.7		
Osteopontin-1 (*OPN1*)	Forward	TGTGCCATACCAGTTAAACAG	58.7	147	NG_030362.1 (Applied Biosystems)
	Reverse	ACTTACTTGGAAGGGTCTGTG	59.8		

Table 4.2: Forward and reverse primer sequences for genes analyzed in this study

RNA (120 ng) was converted into cDNA using iScript cDNA synthesis kit (Biorad, Hercules, CA), as outlined in **Section 3.2.8**. Gene expressions of various SMC markers such as SMA, caldesmon and osteopontin, elastic matrix proteins such as elastin, fibrillin-1, fibulin-5 and LOX, and MMPs -2 and -9, were estimated in 1 µl cDNA (in duplicates), using the comparative threshold method with 18 s as the normalizing gene, as described in the previous chapter. Primers for all genes were either purchased as optimized primer sets from Real Time Primers (Elkins Park, PA), or designed using the NIH software PerlPrimer®, as listed in **Table 4.2**.

4.2.6. Fastin Assay for Elastin Content

One segment from each construct was lyophilized for 24 hours and their dry weights were measured. Lyophilized constructs were first digested in 1 ml of 0.1 N NaOH for 1 hr in a 98 °C water bath to convert alkali-soluble matrix elastin into an α-elastin form in order to be measured using the Fastin assay kit (Accurate Scientific and Chemical Corporation, Westbury, NY). The samples were then centrifuged at 5000 rpm for 10 minutes, and supernatants collected to analyze for alkali-soluble elastin content (200 µl per sample in duplicates). The pellets were resuspended in 500 µl of 0.25 M oxalic acid and digested for 1 hr in a 98 °C water bath to convert alkali-insoluble matrix elastin into the α-elastin form. Digested samples were then filter–centrifuged with 10 kDa cut–off membranes (Millipore, Billerica, MA) at maximum speed for 10 minutes. The solubilized matrix elastin retained above the filters (40–50 µl) were then reconstituted to a total volume of 1000 µl and then quantified with the assay kit (300 µl per sample in

duplicates). Matrix elastin content measured as alkali-soluble and –insoluble elastin was reported after normalizing to mg dry weights of construct (duplicate readings, n = 6/case).

4.2.7. Western Blotting for Cellular and Matrix Proteins

One segment from n = 3 constructs from each case were lyophilized, and the cut into small pieces to speed up homogenization. Cold RIPA lysis buffer (750 µl, Invitrogen, Carlsbad, CA) with a protease inhibitor cocktail (Thermo Scientific, Rockford, IL) was then added to each of the samples, following which they were homogenized on ice for 10–15 minutes (until the pieces appeared to have been homogenized). The samples were then agitated at 4 °C for 2 hours to completely homogenize and solubilize the proteins. The digested samples were then centrifuged at 10,000 rpm for 20 minutes, and supernatants collected for further analysis. A BCA assay was performed to measure total protein concentration in each sample using a commercially available kit (Thermo Scientific, Rockford, IL).

Western blotting was performed to compare expression of phenotypic markers of contractile SMCs such as smooth muscle α-actin (SMA; an early-stage marker), Smooth muscle-22-α (SM22; a mid-stage marker), myosin heavy chain (MHC; a late-stage marker), and calponin and caldesmon (both mid-stage markers), elastic matrix proteins such as LOX, fibrillin-1 and fibulins -4 and -5, and matrix proteases MMPs-2 and -9. Volumes equivalent to 5 µg protein were loaded under reduced conditions into 4–12% SDS PAGE gels for LOX, fibulin, SMA, SM22, calponin and caldesmon, with MES

running buffer, and 10% SDS PAGE gels for MMPs, fibrillin and MHC with MOPS running buffer, along with a pre–stained molecular weight ladder (either 3.5 kDa–250 kDa, or 10 kDa–190 kDa). The gels were then transferred onto nitrocellulose membranes using an iBlot® Transfer system according to the manufacturer's instructions. Blots were then blocked for one hour using a commercially available blocking solution (Li-Cor, Lincoln, NE), then incubated overnight in primary antibodies, and one hour in secondary antibody solutions (Li-Cor). Blots were imaged using an Odyssey® Imaging System (Li-Cor) which enabled the simultaneous measurement of 2 proteins in the same blot. β-actin was used as a normalizing protein for every blot. All primary antibodies were purchased from Abcam (Cambridge, MA), except LOX, fibrillin-1 and fibulin-5 (Santa Cruz, CA), and MMP-9 (Millipore, Billerica, MA), and all western blotting supplies purchased from Invitrogen (Carlsbad, CA), unless otherwise mentioned.

Protein band intensities were measured using Image-J (NIH, Bethesda, MD) software in terms of RDU, normalized to the corresponding β-actin bands in the same blots and reported as a fold change in normalized RDU values relative to treatment control samples. Samples from three biological replicates were analyzed for each protein, except for the SMC markers (n = 1 blot each), whose bands were not quantified.

4.2.8. Gelatin Zymography for Detection of Enzyme Activities of MMPs -2 and -9

Gelatin zymography (as described in **Section 3.2.8**) in was performed on the RIPA buffer lysed samples as described in **Section 3.2.7**. Volumes equivalent to 6 μg protein were loaded into each lane of a 10 % gelatin zymogram (Invitrogen, Carlsbad,

CA), alongside a pre-stained protein ladder (10 kDa–190 kDa; Invitrogen, Carlsbad, CA), and purified protein standards of MMPs -2 and -9 (Anaspec, Fremont, CA). Gels were developed and destained to estimate the activity of MMPs-2 and -9 proportional to the extent of gelatin digestion bands in the gels. Band intensities were quantified and reported as outlined in S**ections 3.2.8 and 4.2.7.** Band intensities of samples from n = 3 biological replicates were used to analyze results.

4.2.9. Visualization of Elastic Matrix

One segment from each experimental case was fixed and paraffin-embedded as detailed in **Section 3.2.9.**, at the Imaging Core of the Cleveland Clinic. Sections (10 µm thick) were deparaffinized, epitope-retrieved in 10 mM citrate buffer in a 100 °C water bath for 40 minutes. Sections were then blocked in 5% v/v goat serum for 30 min, immunolabeled for elastin (1:100 primary, overnight, 4 °C) and fibrillin-1 (1:50 primary, overnight, 4 °C), with Alexa Flour®-633 (Invitrogen, Carlsbad, CA) secondary antibody (1:1000, 1 hour RT). The labeled sections were mounted in Vectashield with DAPI (Vector Laboratories, INC. Burlingame, CA) to stain for nuclei, cover-slipped and visualized under a Cy5 filter for elastin and fibrillin. Both cross-sections and longitudinal-sections of the constructs were labeled and imaged.

Additionally, 30─µm cross- and longitudinal-sections were stained using a commercially available VVG-based staining kit (ScyTek Laboratories Inc., Cache, UT) to visualize elastic fibers.

Longitudinal and cross section of one construct from each treatment condition were also processed for Transmission Electron Microscopy (TEM). Constructs harvested at 21 days of culture were fixed in 2.5% v/v gluteraldehyde and 4% v/v paraformaldehyde in 2% w/v sodium cacodylate buffer for 6 hours at RT and 6 hours at 4 °C, and stored in cacodylate buffer until further processing . Samples were then post–fixed in 1% w/v osmium tetroxide and 1% uranyl acetate (1 hour), and dehydrated in a graded ethanol series (50–100 % v/v). Fixed cell layers were embedded in Epon 812 resin and placed on copper grids embedded in pure Eponate for sectioning. Sections (85 nm thickness) were cut using a diamond knife, and stained with uranyl acetate and lead citrate. Sections were imaged using a Philips CM12 electron microscope operated at 60 kV.

4.2.10. Mechanical Testing of Constructs

Tensile properties of the tubular collagen constructs were analyzed on 0.8 cm wide ring sections of the constructs as outlined by Isenberg. et.al.[59] and Lee. et.al.[169]. Segments (2-3) from each of the 6 biological replicates per case were harvested. The initial diameter and thickness of specimens were measured on smaller ring sections (2-3 mm width) flanking each test specimen using an upright Olympus histology microscope (Pittsburgh, PA) and its accompanying imaging software, DP2. Multiple specimens (3-4) were imaged to take these measurements per biological replicate. Tensile testing was performed using an Instron BioPuls 5988 system (Norwood, MA) with a 10 N load cell, and in a 37 °C PBS bath. The ring specimens were held in place for the testing via 2

stainless steel hooks, which were placed between the metal grips of the instrument. The initial runs performed on test samples indicated that the constructs began to show plastic deformation and failure at very low loads, i.e., < 1 N. Therefore, unlike the method outlined in the Nerem study, pre-conditioning was not performed on these constructs. Load to failure tests were performed at rate of 10 mm/min. The gauge was calculated when the construct was truly in tension. This was done by dividing the circumference of the construct by 2, and then subtracting the circumference of the stainless steel hooks (half of the top and the bottom, equating to the full circumference of one hook). The thickness was considered to be twice the thickness of the construct, since the stresses were experienced by both sides of the ring. Tensile modulus and yield properties were determined from the engineering stress and strain values, plotted from the load vs. displacement data generated by the instrument. Modulus was calculated as the linear slope of the stress-strain curve, i.e., the section spanning a 20%-30% strain range with the highest modulus. A 10%-15% (i.e., 0.32 mm displacement) offset was used to calculate the yield point to determine the stress strain values.

4.2.11. Statistical Analysis

All quantitative results were analyzed from n = 6 independent biological replicate cultures and measurements made in triplicates, unless otherwise indicated, and reported as mean ± standard deviation. Statistics was performed with the help of SPSS software using a one-way ANOVA, and results were deemed significant for p values ≤ 0.05.

4.3. RESULTS

4.3.1. Compaction of Tissue Constructs

The aspect ratios (length : O.D.) of constructs in all treatment and control conditions were ~ 11 (**Figure 4.3**). No significant differences were found between groups. It should be noted that there were 1-2 constructs that exhibited aspect ratios between 8 and 9, indicating higher degrees of longitudinal contraction, but these observations were not particular to any given condition.

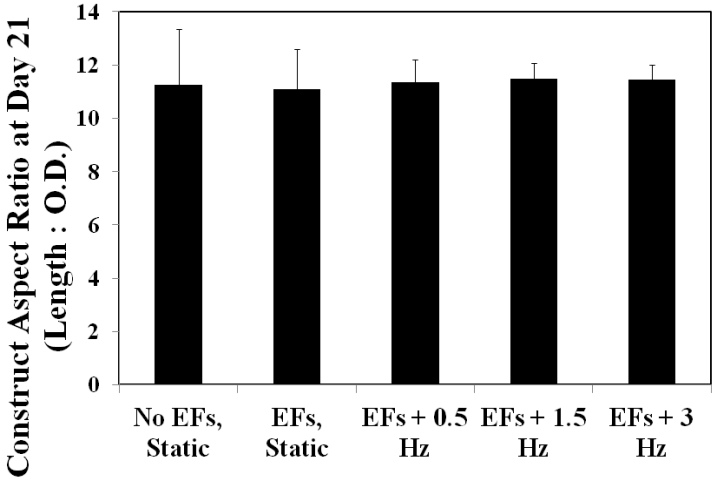

Figure 4.3: Effect of application of cyclic stretch with EFs on construct compaction. Constructs in different treatment conditions were contracted to similar levels

4.3.2. Cell Quantification

DNA assay performed on tubular collagen constructs (n = 6) indicated all constructs to have similar cell densities 21 days after treatment (**Figure 4.4**). Cell densities per mg dry weight of construct was found to range between $(1.2 \pm 0.6) \times 10^5$ cells for cases with mechanical strains at 1.5 Hz, to $(2 \pm 0.8) \times 10^5$ for cases at 0.5 Hz. Differences in cell counts between different treatment conditions were found not to be

statistically significant. Application of strains did not seem to have a positive or a negative effect on cell proliferation.

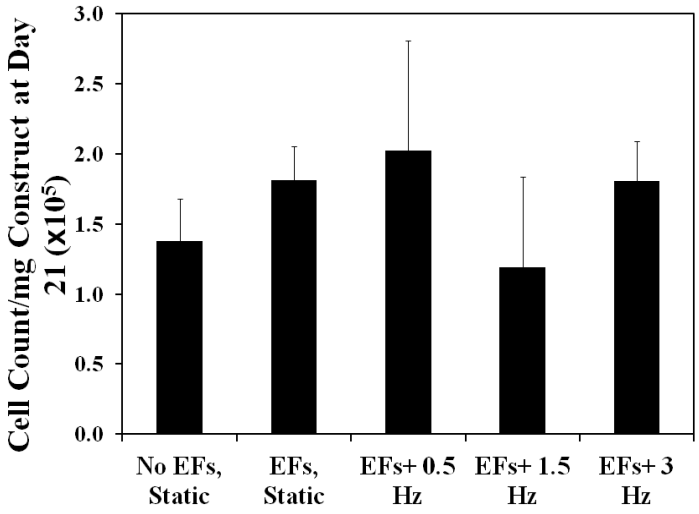

Figure 4.4: Effect of addition of EFs and dynamic conditioning on cell density after 21 days of treatment. No significant differences were observed between different treatment conditions

4.3.3. Analysis of SMC Phenotypic Markers

RT-PCR of SMC phenotypic markers SMA, caldesmon and osteopontin was performed to evaluate the effects of treatment with EFs under static and dynamic conditioning (**Figure 4.5**). While the addition of EFs did not seem to affect the expression of early-stage contractile marker within static constructs, SMA within static constructs (1.21 ± 0.3 –fold, ρ = 0.97, relative to control), a bimodal increase was observed with the addition of cyclic strains with increasing frequencies. A 2.23 ± 0.4 -fold increase from control was noted for constructs treated with EFs + 0.5 Hz (ρ = 0.004, relative to control, and 0.02 to static EFs). This was further increased to 4.13 ± 1 -fold in

constructs treated with EFs at 1.5 Hz, relative to control and static EFs constructs (ρ < 0.001 for both). However, increasing frequency to 3 Hz brought this expression down to levels similar to that in control (1.93 ± 0.23 -fold, ρ = 0.06), and static constructs with EFs (ρ = 0.19). SMA gene expression was significantly higher in constructs with EFs under 1.5 Hz relative to all treatment conditions (ρ < 0.001).

mRNA expression of caldesmon in static constructs with or without EFs remained unchanged (1.17 ± 0.28 –fold, ρ = 0.9). Relative to control, its gene expression was increased to similar extents in constructs with EFs under frequencies of 0.5 Hz (1.9 ± 0.4 –fold) and 1.5 Hz (2.2 ± 0.3 –fold), ρ < 0.001. This increase was statistically significant compared to static EFs constructs as well ($\rho \leq 0.003$). Similar to the trend seen in SMA gene expression, caldesmon gene expression in constructs with EFs under 3 Hz was again brought down to levels similar to static constructs with or without EFs (1.13 ± 0.34, relative to control, ρ > 0.95).

Expression of osteopontin remained relatively unchanged among both sets of static constructs, and dynamic constructs with EFs under 0.5 Hz and 1.5 Hz (ρ > 0.72). On the other hand, it was elevated significantly in constructs with EFs under 3 Hz frequency (2.6 ± 0.7 –fold, ρ < 0.001, relative to control). This increase was statistically significant compared to all other treatment conditions tested in this study (ρ < 0.001).

Western blotting was performed to detect protein quantities of contractile SMC phenotypic markers (**Figure 4.6**). Similar to that seen with RT-PCR, band intensities of SMA, calponin and SM22 were highly pronounced in all cases that received dynamic stimulation, and appeared similar in both static constructs. Those of MHC appeared more

elevated only in case with 0.5 Hz frequency and seemed similar within all other treatment conditions.

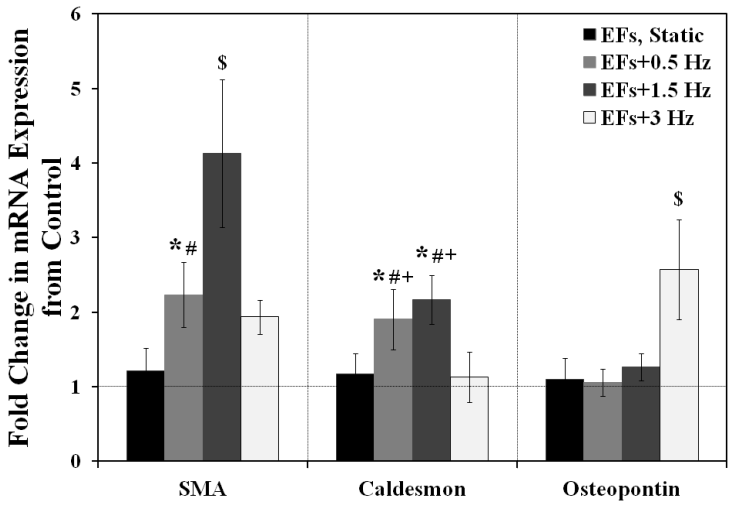

Figure 4.5: Change in mRNA expressions of SMC phenotypic markers with addition of EFs and cyclic strains relative to control. Frequency-dependent regulation of gene expressions of SMA, caldesmon and osteopontin were observed. '*' represents significant difference from control, '#' from static EFs, '+' from EFs + 3 Hz, and '$' relative to every condition, for $p \leq 0.05$

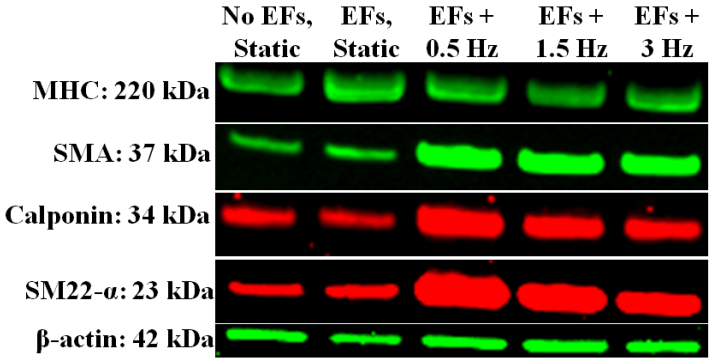

Figure 4.6: Representative western blots of contractile SMC phenotypic markers, along with normalizing protein, β-actin. Contractile marker band intensities appeared to be higher in the three stretched constructs relative to static constructs

4.3.4. Elastic Matrix Synthesis

RT-PCR was performed to evaluate the effects of EFs and cyclic strains applied at different frequencies on mRNA expressions of genes encoding various elastic matrix proteins such as elastin, fibrillin-1, fibulin-5 and LOX (**Figure 4.7**). mRNA expression of elastin was greatly influenced with the addition of EFs as well as by change in cyclic strain frequencies. Within static constructs, addition of EFs significantly increased elastin gene expression to 4.8 ± 0.4 –fold ($\rho < 0.001$), relative to control. Application of cyclic strains in addition to EFs showed a bimodal behavior in elastin gene expression with increasing frequencies. Constructs stretched at 0.5 Hz showed an increase of 3.1 ± 0.5 –fold relative to control ($\rho = 0.001$). While this increase with 0.5 Hz was lower than that seen with static constructs treated with EFs ($\rho = 0.003$), application of strain at 1.5 Hz significantly increased elastin gene expression further to 6.67 ± 1.5 –fold relative to control ($\rho \leq 0.002$ relative to all treatment conditions). On the other hand, at 3 Hz, elastin gene expression was brought down to levels similar to that with untreated controls (1.3 ± 0.2 -fold, $\rho = 0.97$, relative to control).

mRNA expression of fibrillin-1 was also influenced by the frequency of applied strain. Relative to control, while a 2 ± 0.6 –fold increase was observed in static constructs with EFs ($\rho = 0.007$), this was not mirrored under cyclic strain frequencies of 0.5 Hz (1.38 ± 0.41 –fold, $\rho = 0.7$) and 3 Hz (1.7 ± 0.32 –fold, $\rho = 0.1$). However, at 1.5 Hz stretch frequency, fibrillin-1 gene expression was increased to 1.8 ± 0.5 –fold relative to control, which was deemed statistically significant ($\rho = 0.045$). It is important to note that

among the 4 EF-treated constructs (both static and strained), differences in gene expression were not statistically significant ($\rho > 0.1$).

Addition of EFs or change in cyclic strain frequencies did not appear to influence mRNA expression of fibulin-5. Its expression levels in all treatment conditions, both static and dynamic, were similar to that in untreated static control constructs ($\rho > 0.7$).

mRNA expression of LOX showed similar trends as that seen with elastin. Addition of EFs to static constructs increased its gene expression to 2.8 ± 1.1 -fold relative to control ($\rho = 0.005$). Application of strains at 0.5 Hz and 3 Hz did not significantly alter its expression relative to control ($\rho > 0.7$). However at the median frequency of 1.5 Hz, it was elevated by 2.7 ± 1.2 –fold ($\rho = 0.01$), relative to control. The increase seen with addition of EFs to static constructs and those stretched at 1.5 Hz, were statistically similar to each other ($\rho = 0.99$) and to those stretched at 0.5 Hz ($\rho > 0.07$), but greater than those stretched at 3 Hz ($\rho < 0.02$).

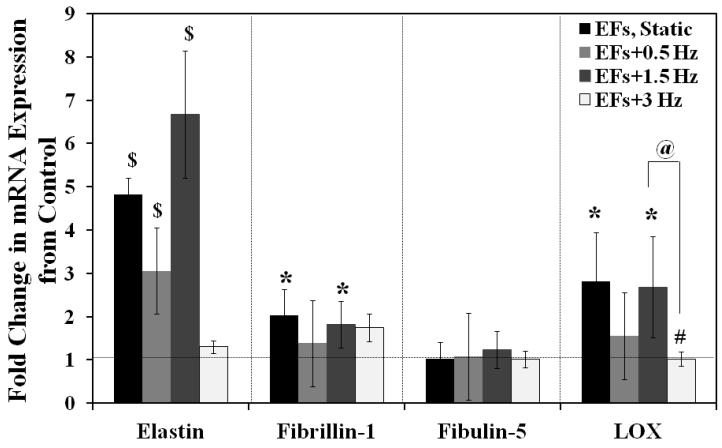

Figure 4.7: Effect of addition of EFs and varying cyclic strain frequency on mRNA expression of genes encoding elastic matrix proteins, elastin, fibrillin-1, fibulin-5 and LOX. Significant differences represented by '*' from control, '#' from static EFs, '$' relative to every treatment condition, and '@' between conditions indicated, for $p \leq 0.05$

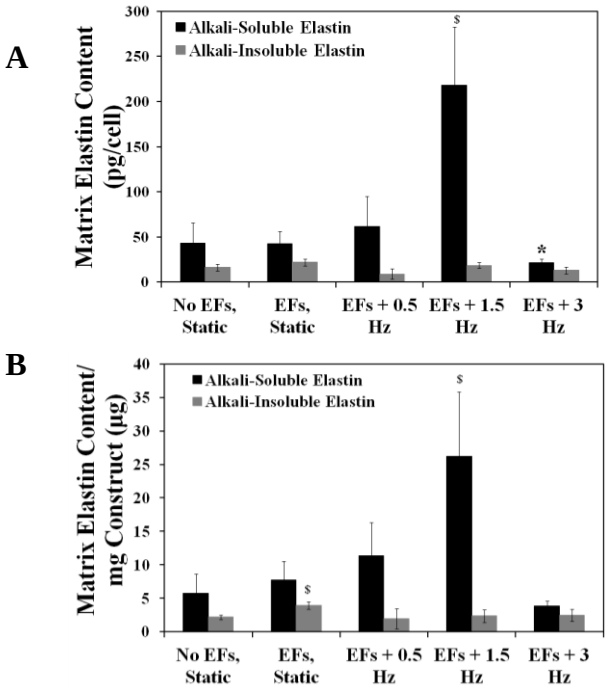

Figure 4.8: Effect of EFs treatment under static and stretched conditions on matrix elastin content. Matrix elastin measured in terms of alkali-soluble and -insoluble elastin and normalized to cell count (A) and mg dry weight of constructs (B). Significant differences represented by '*' relative to control, and '$' relative to all treatment conditions, for $p \leq 0.05$

Matrix elastin content was measured using a Fastin assay kit, in terms of alkali-soluble and –insoluble elastin. As seen in **Figure 4.8**, addition of EFs did not significantly improve alkali-soluble matrix elastin content in static cultures (ρ = 0.97). However, application of cyclic strains in the presence of EFs did significantly improve alkali-soluble matrix elastin output in a frequency-dependent manner. Relative to control, constructs treated with EFs and stretched at 0.5 Hz frequency increased alkali-soluble matrix content up to 2-fold (12.5 ± 3.3 µg/mg, compared to 5.8 ± 2.9 µg/mg in control, ρ = 0.4). A significant improvement in alkali-soluble elastin content was seen with EFs

treatment under at 1.5 Hz cyclic strains. Up to 5-fold increase relative to control, and 3-folds relative to static constructs with EFs was seen with application of stretch at 1.5 Hz (26.2 ± 9.6 μg/mg, $\rho < 0.001$ relative to both sets of static treatment). Application of stretch at 3 Hz however appeared to decrease elastic matrix output (3.8 ± 0.4 μg/mg). However, it is important to note that the differences in alkali-soluble elastin content were statistically insignificant among all treatment conditions ($\rho > 0.1$), except in constructs treated with EFs at 1.5 Hz where significantly greater quantities were deposited relative to all other conditions ($\rho < 0.001$). Insoluble matrix elastin content did not appear to benefit by the addition of cyclic strains despite treatment with EFs. There was a 1.8 fold increase observed in the static cultures treated with EFs alone (3.9 ± 0.6 μg/mg vs. 2.2 ± 0.4 μg/mg in static controls, $\rho = 0.026$). Constructs that received cyclic strains with EFs synthesized similar quantities of alkali-insoluble elastin under all three frequencies compared to untreated control ($\rho > 0.9$).

Western blotting analysis of other proteins constituting elastic matrix such as LOX, fibrillin-1 and fibulins -4 and -5 were not reliably detected at the protein concentrations tested (5 μg). It was found out from the manufacturers of the antibodies, that for the detection of fibulin in western blots, at least 50 μg protein was required, which was much higher than the protein yields obtained in our studies.

4.3.5. MMP -2 Production and Activity

RT-PCR, western blotting and zymography were performed to analyze the expression, synthesis and activity of proteases specific to elastic matrix degradation

synthesized by SMCs, i.e., MMPs -2 and -9. As seen in **Figure 4.9**, relative to control, mRNA expression of MMP-2 remained unchanged within constructs treated with EFs under static conditions and with cyclic stretch applied at 0.5 Hz and 1.5 Hz ($\rho > 0.5$). However, under EF-treatment with cyclic stretch at 3 Hz, there was a 1.9 ± 0.3 –fold increase in MMP-2 mRNA expression, relative to control. This increase was statistically significant relative to all treatment conditions ($\rho \leq 0.001$). However, as seen in **Figures 4.10 A** and **B**, western blotting performed to estimate total protein content of zymogen and active forms of MMP-2 did not reveal any significant differences among the treatment conditions, both static and dynamic. On the other hand, zymography (**Figures 4.11 A** and **B**) performed to estimate activity of secreted MMP-2 enzyme, showed more than 3-fold increase in band intensities of the zymogen form of the protease in all EF-treated constructs, relative to control ($\rho < 0.02$). This increase in zymogen content was similar in all EF-treated conditions, both static and dynamic ($\rho > 0.4$). On the other hand, no significant differences in zymogram band intensities of the active form of protease was observed in any of the treatment conditions relative to control ($\rho > 0.1$).

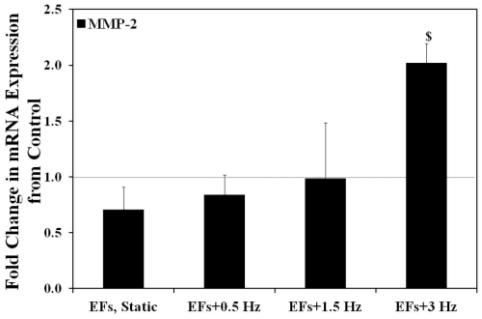

Figure 4.9: Effect of varying cyclic strain frequency and addition of EFs on MMP-2 mRNA expression relative to control. Increase in MMP-2 gene expression was significant ($) in constructs stretched at 3 Hz frequency, relative to all other treatment conditions, $p \leq 0.05$

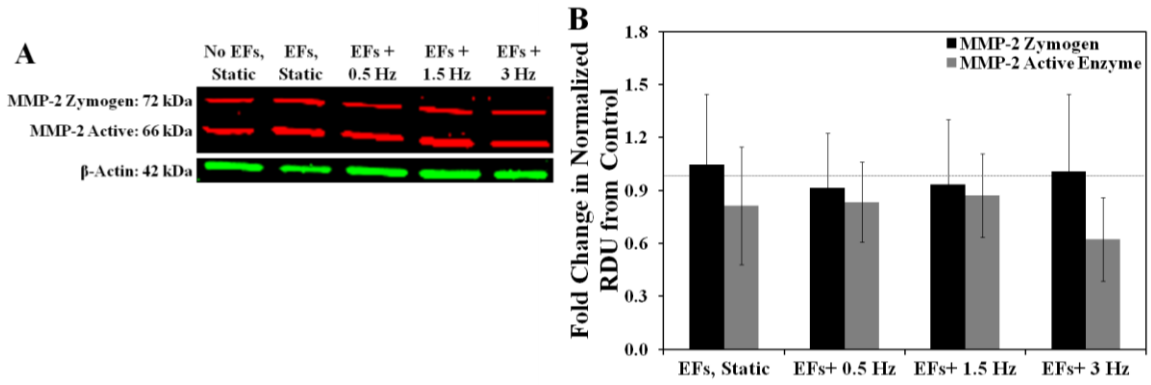

Figure 4.10: Effect of addition of EFs under static and dynamic conditions on MMP-2 protein content. (A) Representative immunoblots showing zymogen and active forms of MMP-2 protein, with normalizing protein, β-actin. (B) Semi-quantitative analysis of differences in band intensities of the 2 forms of MMP-2 protein relative to control. No significant differences were observed between different treatment conditions

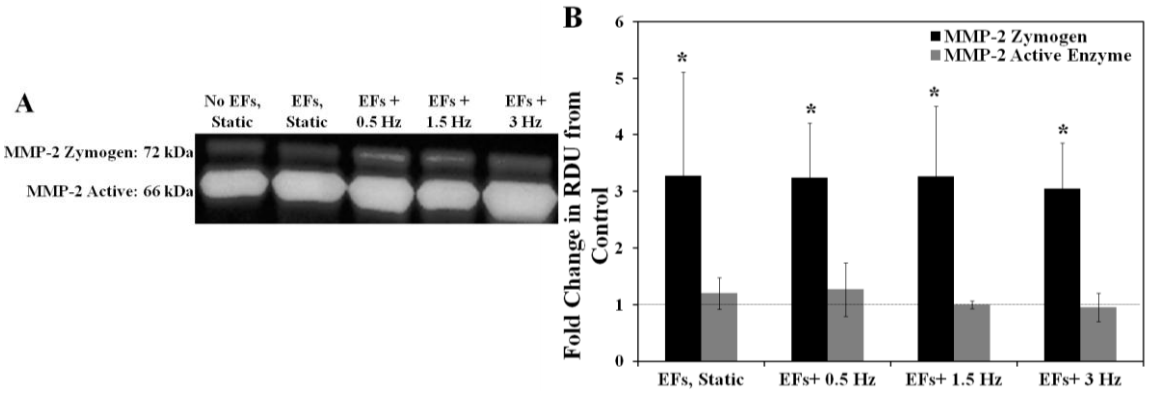

Figure 4.11: Effect of addition of EFs and change in cyclic stretch frequency on MMP-2 enzyme activity. (A) Representative zymogram showing MMP-2 band intensities at both active and zymogen forms. (B) Semi-quantitative analysis of change in MMP-2 enzyme activity relative to control. '*' indicates significant difference from control for $p \leq 0.05$

4.3.6. MMP -9 Production and Activity

mRNA expression of MMP-9 was uniformly low in all constructs, and their Ct values were at or below the detection limits of the instrument, at the cDNA concentrations tested. Therefore, it was difficult to discern differences between treatment conditions, if any existed. Similarly, bands corresponding to either active or inactive

forms of the protease were undetected by zymography, at the protein concentrations tested (5 µg/case). However, western blotting analysis of MMP-9 (**Figures 4.12 A** and **B**) showed increase in band intensities of both active and zymogen forms of the protease in EF-treated constructs subjected to cyclic stretch at frequencies of 1.5 Hz and 3 Hz. Relative to control, 1.6 ± 0.5 –fold increase in both active and inactive forms of MMP-9 were seen under 1.5 Hz ($\rho < 0.05$). With application of stretch at 3 Hz, relative to control, increase of 1.7 ± 0.5 –fold for zymogen, and 1.4 ± 0.1 –fold for active MMP-9 were seen ($\rho < 0.04$). This increase with application of 1.5 Hz and 3 Hz was statistically significant compared to static EFs and EFs + 0.5 Hz stretch as well ($\rho < 0.04$).

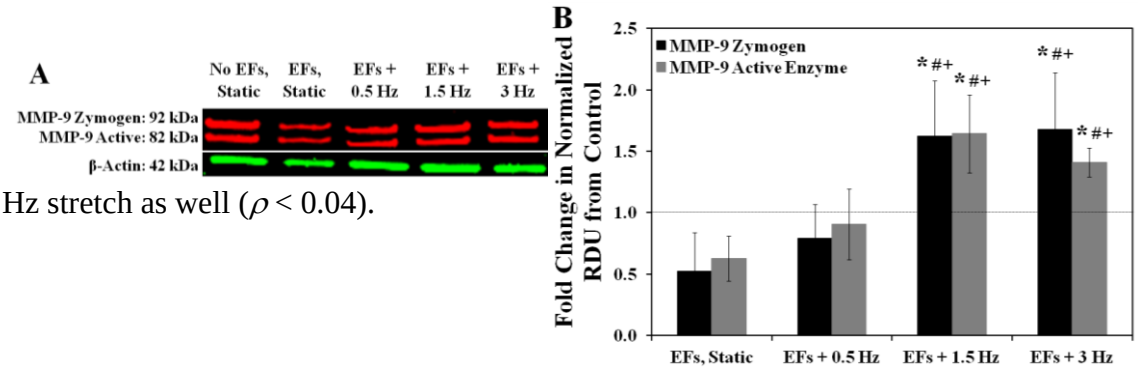

Figure 4.12: Effect of change in cyclic strain frequency and addition of EFs on MMP-9 protein content. (A) Representative immunoblot of MMP-9 showing active and zymogen forms of the enzyme. (B) Semi-quantitative analyssis of fold-change in RDU of band intensities of both forms of the protein relative to control. Significant differences are represented by '*' from control, '#' from static EFs, and '+ from EFs + 0.5 Hz, for , for $p \leq 0.05$

4.3.7. Matrix Ultrastructure

Cross- and longitudinal- sections of all treatment conditions were labeled for elastin and fibrillin proteins. As seen in **Figures 4.13** through **4.15**, cells and fibers were

found be oriented more in the longitudinal direction than in the circumferentially.

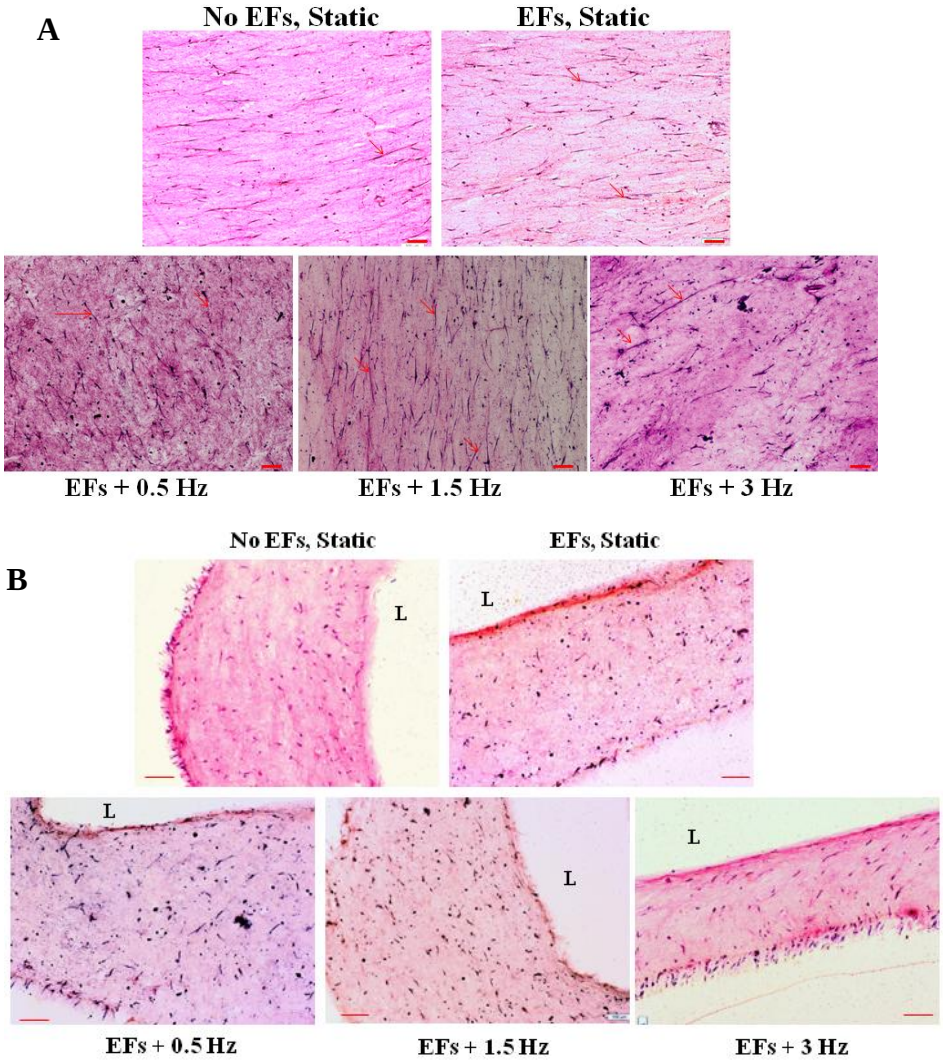

Figure 4.13: Effects of EF-treatment and variation of strain frequency on matrix assembly and orientation. Representative images of 30 µm-thick longitudinal-sections (A) and cross-sections (B) of all constructs stained with modified VVG. Elastic fibers, stained purple to black, within cyclically strained constructs appear oriented more towards the longitudinal direction, than in the circumferential direction. Alignment in the longitudinal direction appears more random with increase in strain frequency, indicating initiation of alignment perpendicular to applied strain. Circumferential alignment can be seen closer to the lumen (L) within strained constructs, which does not appear to have uniformly translated across the thickness of the constructs. More number of elastic fibers appear to be present in constructs treated with EFs compared to those without. Scale bar (in red) = 100 µm, 10 × magnification.

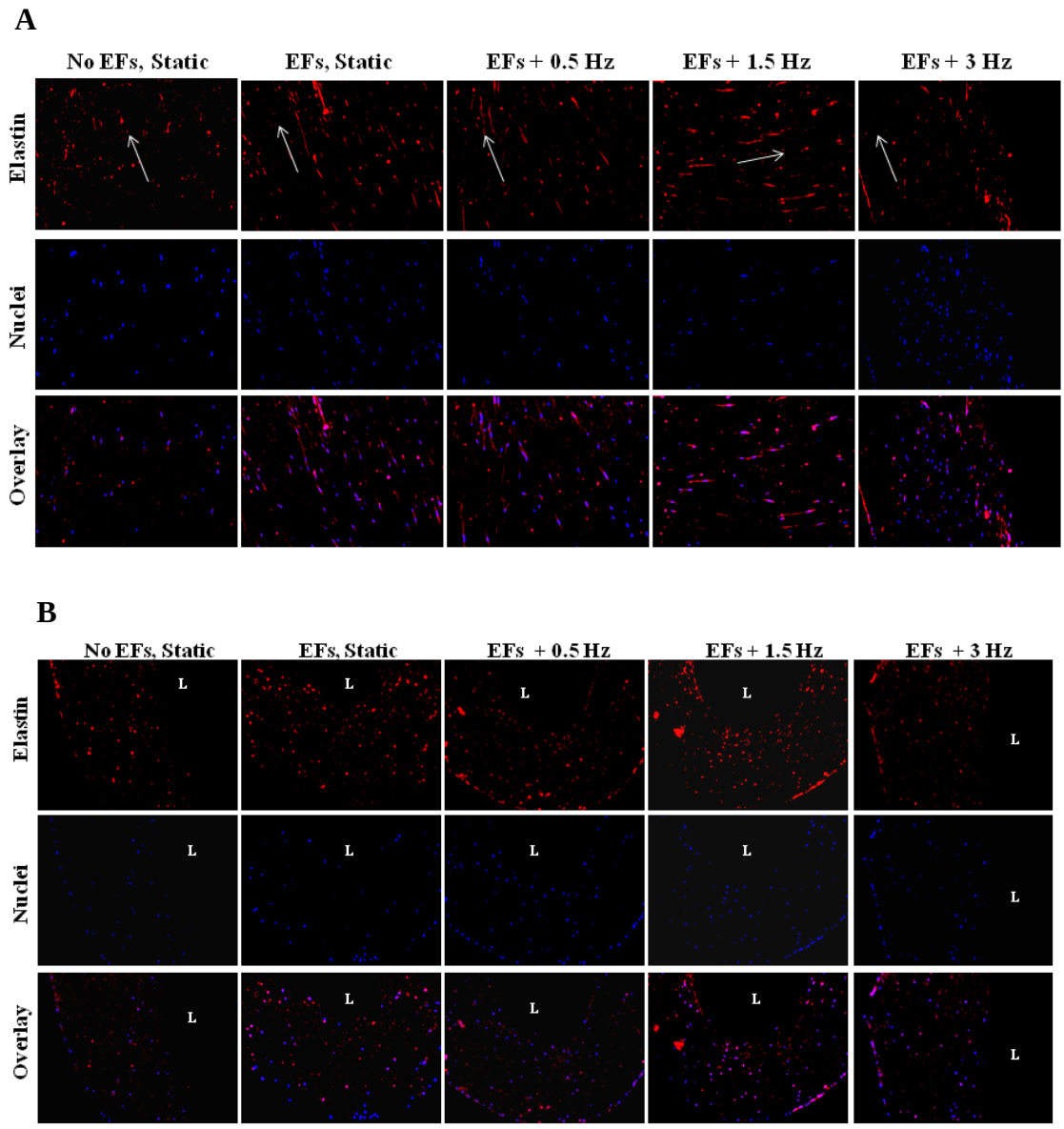

Figure 4.14: Effects of EF-treatment and cyclic strain frequency variation on synthesis and assembly of fibrillin. Representative images of 10 μm thick longitudinal- (A) and cross- (B) sections of constructs immunolabeled for elastin (red) and nuclei (blue). Longer fibers of elastin are seen in the longitudinal direction than circumferentially, similar seen in **Figure 4.13**. White arrows indicate longitudinal direction of constructs. 'L' = lumen. 10 × magnification.

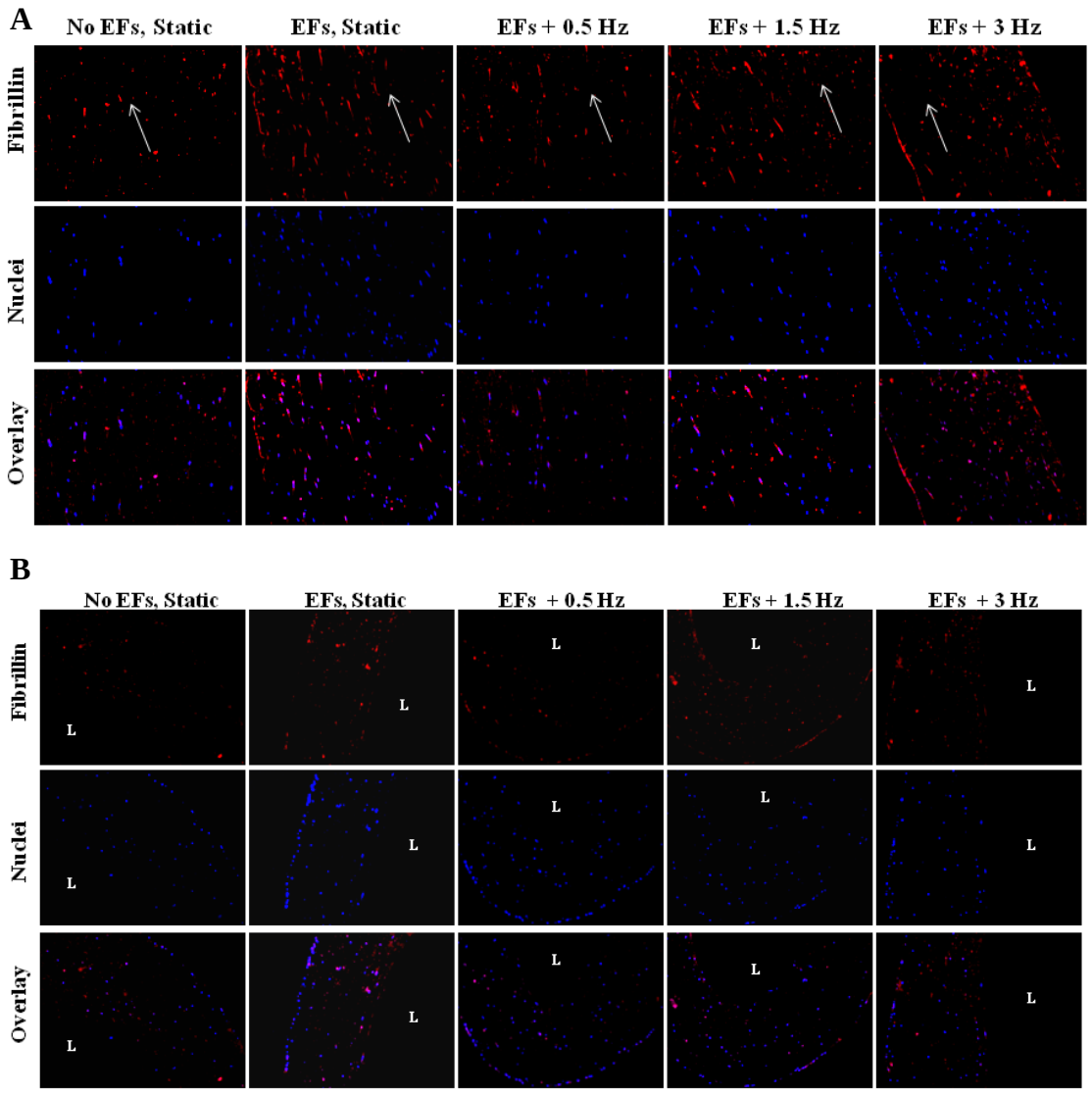

Figure 4.15: Effect of EF-treatment and varying frequency of stretch on fibrillin assembly and orientation. Representative fluorescent images of 10 μm thick longitudinal- (A) and cross- (B) sections of constructs immunolabeled for fibrillin (red) and nuclei (DAPI). White arrows indicate longitudinal direction of constructs. 'L' = lumen. 10 × magnification.

Application of stretch was found to improve orientation in the circumferential direction in the regions closer to the silicone tubing, and progressively decreased in regions further away from it. However, in the longitudinal direction, as seen in both in VVG-stained images (**Figure 4.13**) and the IF images (**Figure 4.14** and **4.15**), mature

elastic fibers were found in all the cases. Another important observation to be made is that the distribution of these fibers is not uniform across the width or circumference of the constructs; they appear to be denser in some regions more than others. Immunolabeling of elastin and fibrillin (**Figure 4.14** and **4.15)** showed that these proteins were mostly found associated with each other.

TEM was also performed on both cross- and longitudinal- sections. Representative images of longitudinal sections from a construct treated with EFs + stretch at 1.5 Hz are shown in **Figure 4.16**. Once again, what appears to be elastin assembly on fibrillin scaffolds (indicated by arrows) are seen in some regions within longitudinal-sections, but were hardly observed in the cross-sections. Cell morphology appeared normal across most regions in the section and cell membranes appeared intact.

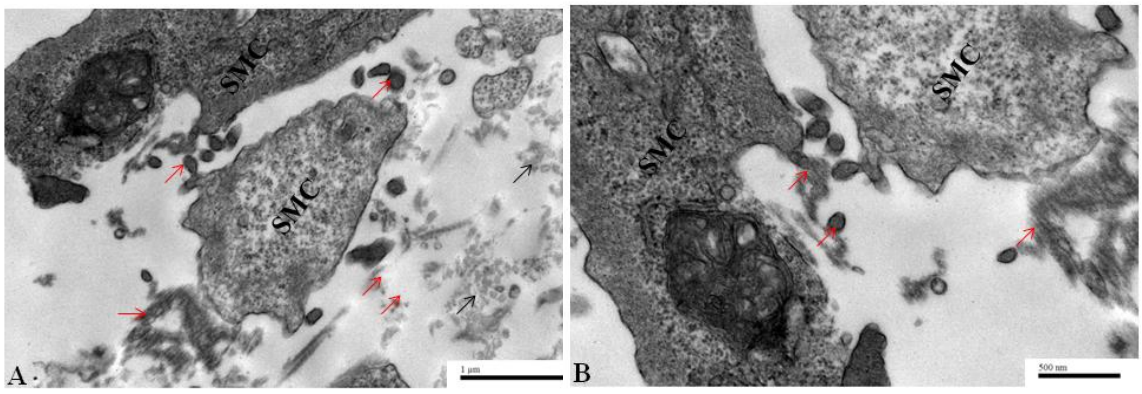

Figure 4.16: Representative TEM images of constructs conditioned with EFs and cyclic stretch at 1.5 Hz. Initiation of elastic matrix deposition (indicated by red arrows) can be seen between adjacent cells. Collagen is indicated by black arrows. Scale bars = (A) 1 µm, 25,000 × magnification, and (B) 500 nm, 40,000 × magnification.

4.3.8. Mechanical Properties of Constructs

As mentioned in **Section 4.2.2** of this chapter, mechanical testing was performed on a different set of samples than that seeded for biochemical assays discussed above. While all seeding procedures were kept constant, we observed that in the constructs seeded under the dynamic conditioning at 0.5 Hz and 1.5 Hz, the two constructs located in wells at each end of the tissue culture chambers, contracted much less than the ones seeded in the middle. We attribute this to user error that may have arisen either due to presence of residual ethanol vapors in the chambers or unequal mixing of cell-collagen solution prior to seeding. While this anomaly resulted in a decrease in mRNA yields, it did not affect the overall outcomes of our PCR results. However, the mechanical properties of these constructs cultured on either ends were quite different than the ones cultured in the three chambers towards the center. We have therefore reported results both including and excluding these constructs (**Figures 4.17** and **4.18**). We also observed a higher degree of circumferential non-homogeneity compared to previous culture sets, which is likely to have had a significant impact on the mechanical testing outcomes.

Tensile modulus was calculated over 0.873 mm displacement, corresponding to 20% - 30% strain in the constructs (**Figure 4.18 A**). Prior to excluding the end constructs, the tensile modulus was calculated to be 1.59 ± 0.97 kPa for constructs cultured at 0.5 Hz with EFs, and 1.93 ± 1.08 kPa at 1.5 Hz strains with EFs. The static constructs without EFs showed a modulus of 2.30 ± 0.39 kPa, and 2.12 ± 0.81 kPa for those with EFs. After eliminating the anomalous end constructs, the modulus was found to be 1.81 ± 1.06 kPa for 0.5 Hz and 2.48 ± 0.51 kPa for 1.5 Hz, compared to 2.41 ± 0.37 kPa for static

controls, and 1.67 ± 0.33 kPa for static cultures with EFs. The differences in the tensile modulus between cases were found to be statistically insignificant both with and without inclusion of the end constructs.

As seen in **Figure 4.18 B,** yield properties were found to be lowest in constructs with EFs at 0.5 Hz. While the yield stress showed significant decrease compared to static constructs after eliminating the end constructs (1.16 ± 0.54 kPa, ρ = 0.019), decrease in yield strain was significant prior to eliminating them (1.41 ± 0.12, ρ =). Differences in yield properties among all other constructs remained statistically insignificant.

Since the testing was started when the constructs were technically not in tension- i.e., in their original diameters, the toe region seen in the stress-strain curves primarily represent the phase where the constructs are being stretched up to a length at which they begin to experience true tension. We believe that any elastic properties of the constructs contributed by the synthesized elastic matrix may be masked by this phenomenon within this region. Therefore, unlike that reported by the Nerem group, we believe that calculating the modulus within this toe region does not provide accurate information regarding the elastic properties of the constructs. We have therefore calculated the tensile and yield properties beyond the toe region, once the constructs were in true tension.

4.4. Discussion

Among the various hemodynamic forces present in the vasculature, cyclic circumferential strains are the most prevalent forces perceived by vascular smooth muscle cells[5]. Cyclic strains are therefore also most influential in regulating

mechanotransduction-mediated effects in VSMC phenotypic state, matrix synthesis and orientation[164, 235]. Various cell surface receptors have been identified that respond to different components of external stimuli. For example, Liu et.al., have shown that strain frequency-dependent modulation of VSMC alignment is regulated by integrin β-1 receptors that activate a p38-mitogen-activated protein kinase (MAPK) pathway[167]. Alignment is elicited first in the cytoskeletal actin filaments, which ultimately results in cellular orientation. It has also been reported that such alignment is highly frequency dependent, and maximum alignment is usually obtained in frequencies between 0.5 Hz and 1.25 Hz[167-168].

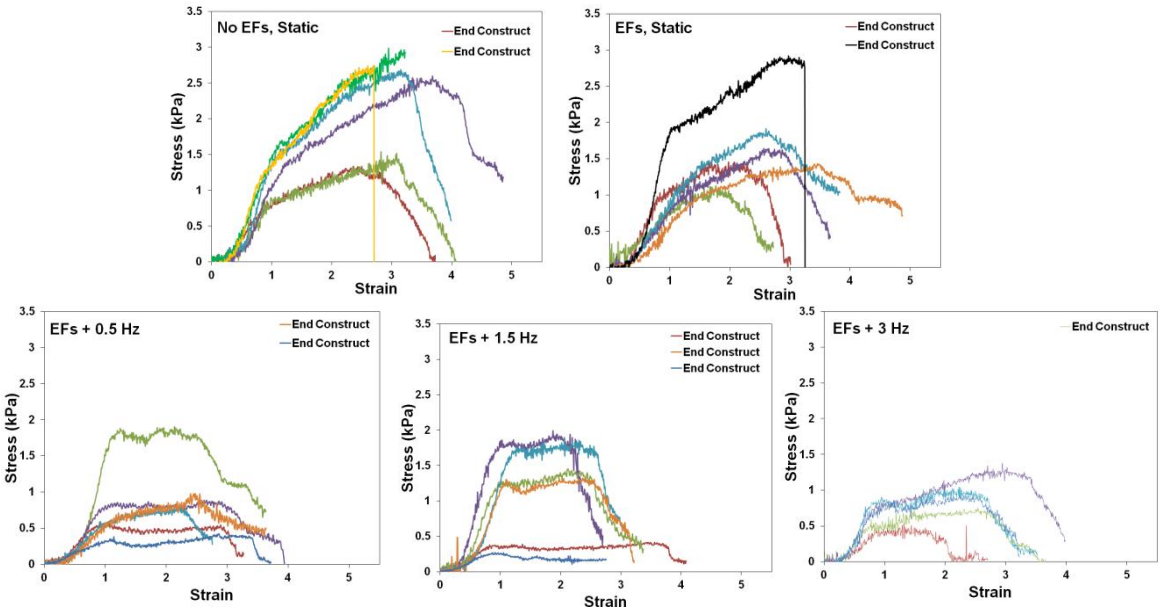

Figure 4.17: Representative stress vs. strain curves of n = 6 samples per treatment condition. The initial toe region corresponds to the phase during which constructs are truly brought under tension. All constructs demonstrated a linear phase, where their tensile properties were determined. Soon after the constructs started to fail, they continued to display plastic deformation, until they completely failed. The end constructs that did not contract as much as the ones centrally placed.

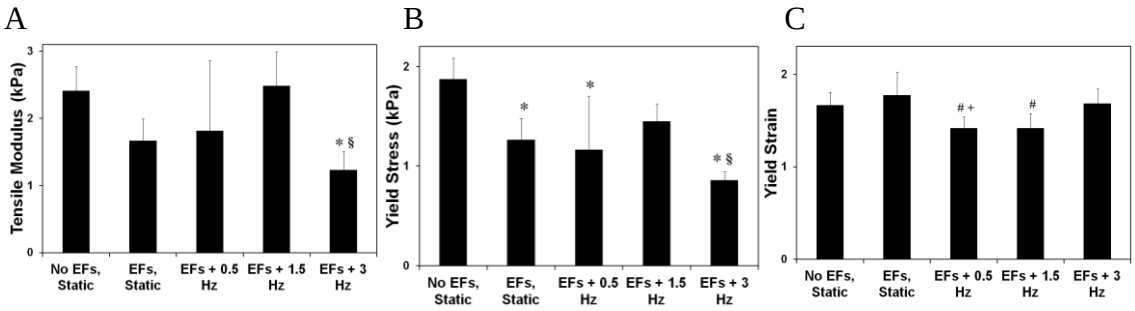

Figure 4.18: Effect of EF-treatment and cyclic strain frequencies on mechanical properties of HASMC-seeded tubular collagen gel constructs. Tensile and yield properties are represented excluding the anomalous end constructs. (A) Tensile modulus corresponding to 20%-30% strains, were found to be similar in all treatment conditions. Yield properties (B) and (C) were not improved by cyclic strains or addition of EFs. '*' represents significant difference from untreated static controls, '#' from static EFs, '§' from EFs+1.5 Hz and '+' from EFs+3 Hz, for $p \leq 0.05$

Most studies conducted so far that have explored the role of cyclic stretch to improve cell alignment and matrix output have utilized physiological levels of 10% strain at 1 Hz frequencies[57, 59, 166, 236]. These studies were also aimed towards tissue engineering small diameter vascular grafts that typically experience higher strains than elastic arteries[5]. However, as noted by the Tranquillo group, cells under these conditions *in vivo* usually remain in a quiescent, non-proliferative and non-matrix producing states[59]. In one of their studies, they have further noted no changes in cell proliferation, alignment or matrix production between 2.5% and 10% strains[59]. Moreover, reconstituted collagen gels, such as that used in this study, behave like viscoelastic fluids prior to forming mature fibrils. Therefore, when subjected to long-term cyclic loading, they can succumb to irreversible creep, especially at higher strain amplitudes[59]. Wernig et.al., have shown that the same integrin β-1 receptors involved in cell alignment, also mediate stretch-induced apoptosis at strains greater than 10%[171]. Further, studies have also shown higher

expression of matrix degrading MMPs such as MMPs-2 with higher strain amplitudes[237-238]. While it can be argued that the presence of these MMPs might be required to initiate matrix remodeling, their activity can at the same time also adversely cause the degradation of newly synthesized elastic matrix[10, 83, 172]. In the current study, we therefore utilized lower strain values of 2.5% and varied the frequency rates to evaluate its effects on cell behavior and induced elastic matrix outcomes.

Cell densities after 21 days of treatment were found to be comparable between the static and dynamic cultures. This was in accordance with other studies that have reported similar observations within collagen gel scaffolds[28, 236]. It has been noted that under 10% strains, cell proliferation appears to be dictated by the scaffold in which the cells are grown. For example, while Kim et.al., noted increased cell proliferation at 7% strains in PGA scaffolds[57], Isenberg et.al. noted no changes in cell densities between 2.5% and 10% strains[59], or between static and dynamic cultures within tubular collagen scaffolds. In contrast to the results reported on rat cells in the previous chapter, addition of EFs did not increase cell numbers in this study.

Several studies have also shown that cyclic stretch can maintain a healthy contractile phenotype of SMCs. SMCs in culture are known to typically switch to a more synthetic, proliferative and matrix-producing phenotype, compared to that seen *in vivo*. While this phenotypic switch to produce matrix is crucial from the stand point of tissue engineering and regenerative medicine, excessive expression can also lead to abnormal proliferation and undesirable matrix output, as seen in a diseased environment such as that in AAAs. Maintaining a balance between a healthy and a synthetic phenotype is

therefore the key to carefully regulate desirable cellular response. Cyclic stretch is known to improve the expression of various contractile phenotypic markers of SMCs such as SMA, caldesmon and MHC, while at the same time, also increase matrix output. In our study, mRNA expressions of the 2 contractile markers tested- SMA and caldesmon appeared to be influenced more by change in frequency, than with the addition of EFs. While addition of EFs to static constructs did not significantly change gene expression of the above contractile markers, a bimodal trend was observed with increase in frequency of applied strain. This trend was far more pronounced in SMA gene expression, which showed a moderate 2-fold increase with stretch at 0.5 Hz, increased further up to 4-fold at 1.5 Hz, and at 3 Hz, dropped down to levels similar to that within static constructs. Caldesmon expression was moderately increased with stretch at 0.5 Hz and 1.5 Hz, but not at 3 Hz. On the other hand, gene expression of osteopontin, a marker for osteogenic differentiation of SMCs suggestive of an activated phenotype, was elevated up to 2-fold within constructs stretched at 3 Hz alone. However, no differences were noted relative to control in other constructs treated with EFs, both static and dynamic. This is in contrast to other studies that have reported that the expression of osteopontin that is generally increased within 3-D cultures, is down regulated by the addition of cyclic stretch[240]. TGF-β1 is known to induce osteogenic differentiation of SMCs at concentrations > 10 ng/ml[139]. While the doses utilized in our study were a 100-fold lower, it is likely that at frequencies as high as 3 Hz, the addition of TGF-β1 could induce such osteogenic expression. mRNA expression of elastin appeared to be influenced both by the addition of EFs and changing frequencies of cyclic stretch. While addition of EFs increased elastin

mRNA expression up to 5-fold within static constructs, a bimodal frequency-dependent change was seen under cyclic stretch. Up to a 3-fold increase was seen with stretch at 0.5 Hz, which was significantly elevated up to 6-fold at 1.5 Hz, but lowered to levels comparable to static constructs without EFs at 3Hz. Similarly, the 2-fold increase mRNA expressions of fibrillin-1 and LOX within EFs-treated static constructs, relative to control, were mirrored in stretched constructs under 1.5 Hz frequencies alone. This trend, together with that seen with variation in gene expressions of SMC markers, suggests that EF-mediated alternations in gene expressions are closely regulated under varying dynamic environments. This is further substantiated with observations made in elastic matrix output within different treatment conditions in this study. Within static constructs treated with EFs, despite the up-regulation in elastin gene expression, alkali-soluble matrix elastin content was not significantly greater than untreated controls. However, EF-treatment under cyclic strains at 1.5 Hz, significantly improved alkali-soluble matrix elastin output up to 5-fold, relative to static constructs with or without EFs. Further, while mRNA expression of elastin and genes encoding other elastic matrix proteins were lower in EF-treated constructs stretched at 0.5 Hz and 3 Hz relative to static EFs, alkali-soluble elastin content between the three groups were comparable. Moreover, despite the 2-fold increase in LOX and fibrillin-1 gene expressions seen relative to control within static EFs and EFs + 1.5 Hz constructs, we could not detect their presence at the protein levels. Fibrillin-1 is an important component of the microfibrillar scaffolds on which tropoelastin units are coecervated, and LOX is a Cu^{2+} dependent enzyme that crosslinks tropoelastin molecules. Their synthesis and activity are therefore important determinants

in generating a mature, crosslinked elastic matrix. In the light of limited synthesis of these proteins, despite increase in their gene expressions, crosslinking new elastin precursors were likely limited. This could potentially have contributed to the low levels of alkali-insoluble elastin measured in all treatment conditions.

Analysis of elastic matrix degrading gelatinases, MMPs -2 and -9, showed different trends at the gene expression level compared to that at the enzyme level. MMP-2 gene expression was up-regulated up to 2-fold relative to control in EF-treated constructs stretched at 3 Hz alone, and was comparable to static controls within all other constructs. However, both the total protein content as well as enzyme activity of MMP-2 were comparable among all treatment conditions. This finding is in contrast to that observed by other groups, wherein both gene expression and enzyme activity of MMP-2 have been reported to increase under cyclic stretch relative to static controls[237-238]. This difference could be attributed to the use of low strains of 2.5% in our studies, compared to the 10% strains used in other studies. It is also likely that at these strains, EFs-mediated decrease in MMP-2 enzyme activity is being facilitated. While the differences in protein content and enzyme activity remained insignificant, it is important to note that the thick bands corresponding to active enzyme in the zymograms indicated high levels of enzyme activity for protein concentrations as low as 5 μg/lane. On the other hand, mRNA expression of MMP-9 was uniformly low in all treatment conditions. However, moderate increase (~ 1.5 –fold) in its protein content, both zymogen and active forms, were seen in constructs treated with EFs and stretched at 1.5 Hz and 3 Hz.

The matrix ultrastructure and orientation of cells in the scaffolds were contrary to what we had hypothesized. As noted in the VVG stained slides and IF images, at the strain and frequencies provided, the cells and elastic fibers all appear to be oriented more in the longitudinal direction, than in the circumferential direction. Several studies have reported lower degrees of orientation and random alignment at 2.5% strains, compared to higher strains of 10%. However, what we note in this study is a uniform orientation in the longitudinal direction. Further, the longitudinal orientation closely resembles what was observed in the static cultures reported in **Chapter 3**. The increase in expression of various SMC contractile markers and changes in levels of matrix elastin however indicate that the cells have responded to the presence of external mechanical stimuli. The cross sectional views of constructs treated with stretch do indicate higher levels of circumferential orientation on the surface closest to the silicone tubing, compared to the regions further away from it. This indicated preliminary levels of orientation, not completely transferred to the entire thickness of the collagen gel. As a result of this orientation, the mechanical tests that were performed on ring sections of the constructs also did not show significant differences in tensile or yield properties. The low modulus of ~ 2 kPa seen in all test conditions could also be explained by the apparent influence of treatment conditions on matrix orientation more in the longitudinal direction and less in the circumferential direction.

4.5. Conclusions

In this study we have demonstrated a positive influence of application of dynamic stimulation along with EFs up to 1.5 Hz frequency. Both increases in mRNA expression of proteins involved in elastic matrix assembly as well as increase in alkali-insoluble matrix elastin content was observed and found to be highest in the constructs treated with EFs and stretched at frequency of 1.5 Hz. Alkali-insoluble matrix elastin remained unchanged with the addition of EFs along with dynamic stimulation. While a circumferential orientation was not obtained as expected, a high degree of longitudinal orientation was obtained.

CHAPTER FIVE

IMPACT OF MMP–INHIBITION ON OUTCOMES OF INDUCED ELASTOGENESIS IN STATICALLY AND DYNAMICALLY CULTURED TISSUES

5.1. INTRODUCTION

In the studies described in the previous chapters, we reported on the elastogenic benefits of TGF–β1 and HA-o to adult SMCs, both rat and human, cultured under static and dynamic conditions. In these studies, however, it was noted that the fraction of matrix elastin deposited in the highly crosslinked alkali-insoluble elastin form was low, and the expression and activity of the elastolytic enzyme MMP-2 continued to be high, regardless of the treatment condition. In an attempt to improve deposition of crosslinked mature elastic matrix and reduce its degradation, critical to enhancing accumulation and fiber formation, in this study, we sought to evaluate if suppression of MMP-2 activity in the cultured constructs improves the above mentioned synthesis.

Doxycycline (DOX) is a modified tetracycline compound that has been widely administered as a broad-spectrum antibiotic[126]. Known to be a non-specific MMP inhibitor, systemic delivery of DOX has been clinically shown to reduce the rate of AAA growth and progression of disease[45-47]. Studies exploring the mechanisms of MMP inhibition have found DOX to significantly reduce activity of both elastolytic (MMPs -2, -9) and non-elastolytic (MMPs -1,-3,-8,-12) proteases, both at the transcription and translation steps of protein synthesis[127-128]. Several groups have also specifically

evaluated its effects on gelatinases, i.e., MMPs -2 and -9, proteases that are up-regulated most in the AAA walls and are primarily responsible for elastolytic activity, both *in vivo* and *in vitro*[129-130].

Preliminary studies conducted in our lab tested effects of DOX on SMCs isolated from a $CaCl_2$ model of rat AAA, over a dose range of 0.1 μM–10 μM. The DOX was added exogenously with culture medium. Of these, the highest dose of 10 μM was found to be highly cytotoxic, while the lower doses of 0.1 μM and 1 μM did not impede cell proliferation over 21 days of culture. For this study, we therefore delivered the lower DOX doses of 0.1 μM and 1 μM, and exogenously supplemented it to the culture medium along with previously determined, effective dose combination of EFs (see **Chapter 3**). In the study described in **Chapter 4**, the dynamic conditioning regime found to promote highest elastogenic activity was 2.5% cyclic strain applied at a frequency of 1.5 Hz. The two DOX doses with EFs were therefore provided to both static HASMC-seeded tubular collagen gel constructs, and constructs stretched cyclically to 2.5% strains at 1.5 Hz for 21 days.

5.2. MATERIALS AND METHODS

All steps involved in fabrication and culture of constructs, assay time points and methods of construct harvest, methods of biochemical analysis, imaging, and statistical analysis were performed in a manner similar to that described in **Section 4.2** of **Chapter 4**. Doxycycline solutions were prepared fresh prior to each media change. Mechanical testing was not performed on these constructs.

The different treatment conditions are listed in **Table 5.1**. Of these, the static controls, static + EFs and EFs + 1.5 Hz construct samples were reused from those cultured for the study in **Chapter 4**. These samples were either 1) re-assayed along with the samples obtained from those cultured with DOX in this study (DNA assay, Fastin assay, zymography western blotting of MMPs -2 and 9), or 2) experiments for both studies were performed simultaneously (RT-PCR and western blotting for SMC phenotypic markers, fibrillin and fibulins), in order to enable direct statistical comparison.

Group	Doxycycline (μM)	TGFβ1 (0.1 ng/ml)/ HA-o (0.2 μg/ml)	Cyclic Stretch (2.5% strain, 1.5 Hz)
No EFs (Control)	-	-	-
EFs, static	-	+	-
EFs + DOX, static (1)		+	-
EFs + DOX, static (2)	0.1	+	-
EF, dynamic	1	+	+
EFs + DOX, dynamic (1)	0.1	+	+
EFs + DOX, dynamic (2)	1	+	+

Table 5.1: Experimental conditions- effect of MMP-inhibition on outcomes of induced elastogenesis

5.3. RESULTS

5.3.1. Construct Compaction

As shown in **Figure 5.1**, the aspect ratios of constructs (length : O.D) at 21 days after treatment with DOX and EFs were found to be 11 ± 2.3, similar to that seen in constructs without DOX and in no EF controls. This indicates that the degree of

contraction was higher in the transverse direction than longitudinally (as length/O.D is ~ 11, which indicates length >> O.D).

5.3.2. Cell Quantification

After 21 days of treatment, cell numbers were normalized to mg dry weights of lyophilized constructs. While cell numbers appeared to increase under dynamic stimulation in constructs with or without DOX, this increase was statistically significant only in constructs with 0.1 μM DOX ($2.01 \pm 0.62 \times 10^6$) and EFs compared to static controls without DOX or EFs ($\rho = 0.006$) (**Figure 5.2**). Differences were statistically insignificant between all other treatment conditions. This indicates that the addition of DOX with EFs under static or stretched conditions did not adversely affect cell growth, either in terms of cell proliferation or cell death, compared to untreated static controls.

5.3.3. Analysis of SMC Markers

RT-PCR (n = 6) and western blotting (n = 1) of SMC phenotypic markers were performed to analyze the effect of treatment conditions on phenotypic changes to SMC (**Figure 5.3**). mRNA expressions of contractile phenotypic markers of SMCs – SMA (early-stage marker) and caldesmon (mid-stage marker), and synthetic, activated marker, osteopontin, were analyzed in the different treatment conditions**.**

Figure 5.3 A shows the fold change in mRNA expression of SMA in the different treatment conditions compared to static constructs without EFs (control). Compared to

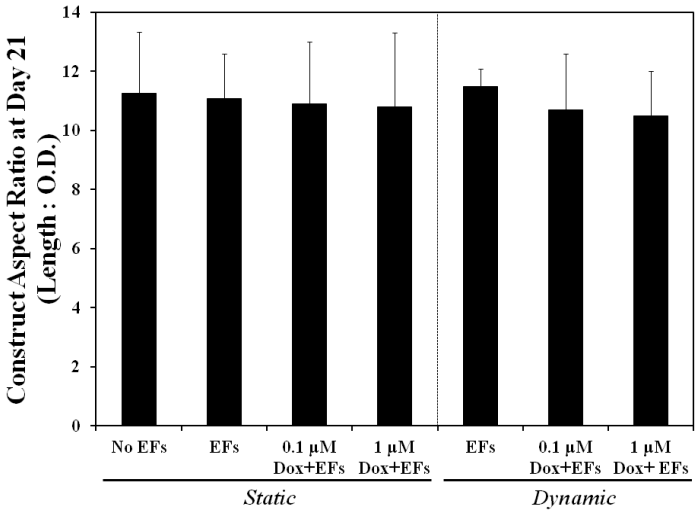

Figure 5.1: Effect of treatment conditions on construct compaction after 21 days. Graph above shows similar extents of contraction among all treated conditions, under both static and dynamic conditions

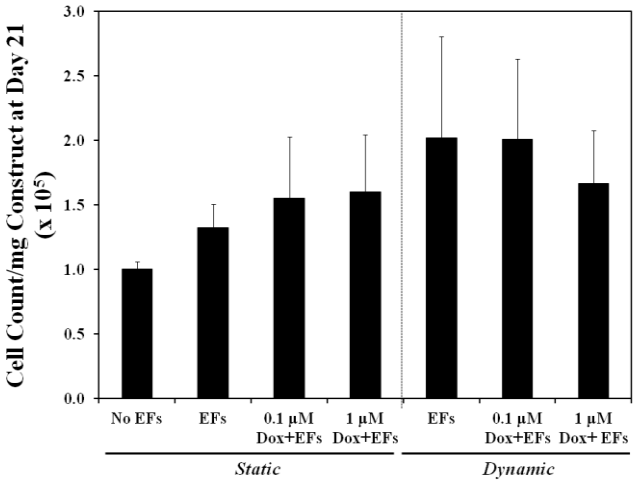

Figure 5.2: Effect of DOX + EFs on cell densities after 21 days of treatment, under static and stretched conditions. Plot above shows addition of DOX + EFs under both static and dynamic conditions did not significantly alter cell densities

ontrols, SMA mRNA expression remained unchanged in all static constructs treated with or without DOX. Addition or increasing concentration of DOX did not alter this expression ($\rho > 0.06$). On the other hand, cyclic stretch significantly increased its expression in all treatment conditions ($\rho < 0.001$ compared to static controls). This

increase was highest in dynamic constructs with EFs alone, where 4.13 ± 1 –fold increase was seen compared to controls (ρ < 0.001). This increase was also mirrored in all dynamic constructs treated with EFs or EFs + DOX, compared to their corresponding static constructs treated with similar concentrations of the same factors (ρ < 0.001). Addition of 0.1 μM DOX with EFs to stretched constructs appeared to slightly lower SMA expression compared to stretched constructs with EFs alone (ρ = 0.003). However, as was seen with static constructs, increasing concentration of DOX in stretched constructs did not alter SMA mRNA expression (ρ = 0.27).

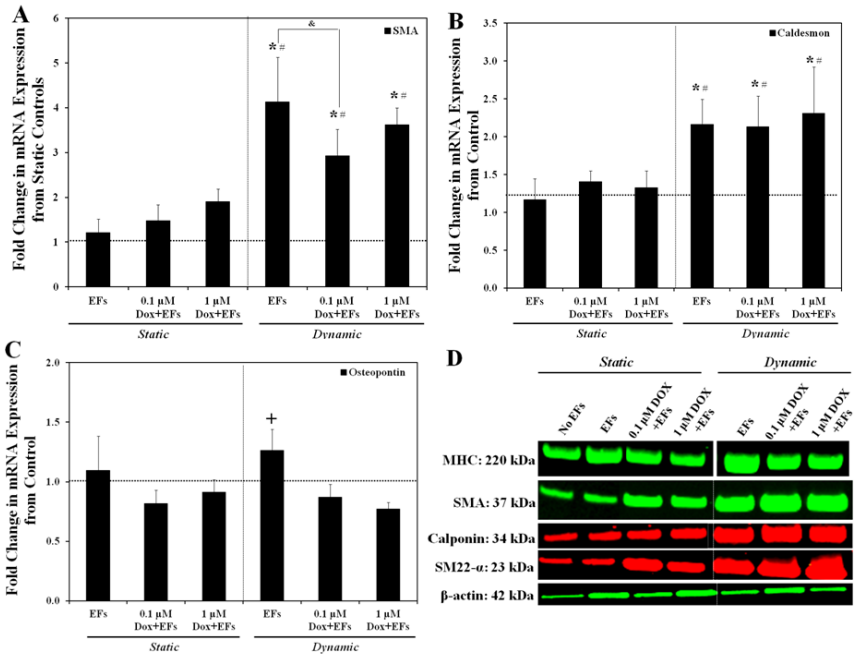

Figure 5.3: Effect of stretch on SMC phenotypic markers compared to static cultures in the presence of DOX + EFs. (A) mRNA expression of SMA significantly increased with application of stretch compared to static constructs. (B) mRNA expression of caldesmon similarly increased within cyclically stretched constructs. (C) mRNA expression of osteopontin remained unaffected in all treatment conditions, except in stretched EFs constructs alone. (D) Representative immunoblots of SMC contractile phenotypic markers showing increase in protein content with addition of stretch. Significant differences for $p \leq 0.05$ are indicated by '*' relative to control, '#' from static EFs, '&' between the groups indicated, and '+' from all DOX + EFs –treated constructs, both static and dynamic

Figure 5.3 B shows fold changes in mRNA expression of caldesmon compared to controls. Similar to the trends observed with mRNA expression of SMA, that of caldesmon remained unchanged within all statically treated constructs ($\rho > 0.49$), but increased to 2.2 ± 0.45 -fold with incorporation of stretch ($\rho < 0.001$), compared to controls. Addition or increasing concentration of DOX did not alter its expression between conditions within both static ($\rho > 0.93$) and stretched constructs ($\rho > 0.98$). However, addition of stretch to constructs treated with similar concentrations of EFs or EFs + DOX significantly increased its expression compared to corresponding static constructs ($\rho < 0.02$).

As seen in **Figure 5.3 C**, mRNA expression of the synthetic, activated SMC phenotype marker, osteopontin, was not significantly increased or decreased compared to control in any of the treatment conditions ($\rho > 0.2$). While addition of EFs alone (both static and stretched) appeared to slightly increase this expression, the differences were statistically insignificant ($\rho > 0.2$). However, compared to stretched constructs with EFs alone, addition of DOX at both doses, appeared to lower this expression, in both static ($\rho < 0.02$) as well as stretched ($\rho < 0.005$) constructs. Differences with increase in DOX concentration (both static and stretched) were insignificant ($\rho > 0.8$).

Western blotting (**Figure 5.3 D**) of contractile phenotypic markers SMA, SM22α, calponin and MHC showed an increase in band intensities in all stretched constructs compared to the static constructs. Bands for caldesmon were undetected at the protein concentrations tested (5 μg).

5.3.4. Elastic Matrix Content

RT-PCR for gene expressions of elastin, fibrillin-1, fibulin-4 and LOX, Fastin assay for quantifying matrix elastin (alkali -soluble and –insoluble), and western blotting of fibrillin-1, fibulin, and LOX were performed to evaluate the effects of the treatment conditions on elastic matrix output.

As seen in **Figure 5.4 A**, mRNA expression of elastin was significantly increased in all treatment conditions compared to control ($\rho < 0.01$). Among the static constructs, the highest increase was seen in those with 1 μM DOX + EFs (6.1 ± 0.97, $\rho < 0.001$), compared to control. However, among the 3 sets of static cultures treated with or without DOX, no statistical difference was observed ($\rho > 0.15$). The mRNA expression was pronounced to a greater extent among the stretched constructs than their static counterparts (6.7 ± 1-fold compared to control, $\rho < 0.001$). Similar to that seen with the static constructs, addition of DOX + EFs at the 2 doses to stretched constructs induced similar increases in mRNA elastin expression compared to stretched constructs with EFs alone ($\rho = 1$). As seen in **Chapter 4**, with respect to control, addition of stretch to constructs treated with EFs alone resulted in a 6.7 ± 1.5 –fold increase in elastin mRNA expression, which was significantly higher than the 4.8 ± 0.4 –fold among static EFs constructs ($\rho = 0.006$). However, addition of stretch did not improve the already high mRNA expression among the DOX-treated cultures at either doses ($\rho > 0.15$).

The mRNA expression of fibrillin-1, the microfibrillar scaffolding protein of elastic matrix, was increased to similar extents of approximately 2-fold in almost all treatment conditions compared to controls ($\rho > 0.12$), as seen in **Figure 5.4 B**. However,

this increase was statistically significant only in 3 treatment conditions compared to control- static EFs (2 ± 0.6 –fold, $\rho = 0.02$), and 0.1 µM DOX + EFs –treated constructs, both static (2.1 ± 0.6, $\rho = 0.01$) and stretched (2 ± 0.6, $\rho = 0.04$). No significant differences in expression were observed between all other treatment conditions. The mRNA expression of fibulin-4 (**Figure 5.4 C**) also remained unchanged in all treatment conditions compared to control ($\rho > 0.85$). mRNA expression of LOX appeared to be elevated in all treatment conditions (**Figure 5.4 D**). However, this increase was also significant only in 3 treatment conditions- static constructs with EFs alone (2.82 ± 1.1, $\rho = 0.004$), stretched constructs with EFs alone (2.68 ± 0.42, $\rho = 0.01$), and stretched constructs with 1 µM DOX + EFs (2.43 ± 0.42, $\rho = 0.047$). Like that observed in expressions of fibrillin-1 and fibulin-5, differences in mRNA expression of LOX between treatment conditions, both static and stretched, were insignificant ($\rho > 0.098$).

Matrix elastin content was measured in terms of the less crosslinked alkali-soluble elastin, and the highly crosslinked alkali-insoluble elastin, as seen in **Figure 5.5**. Compared to control, alkali-soluble matrix elastin content was significantly elevated in all treatment conditions, both static ($\rho < 0.047$) and stretched ($\rho < 0.001$). Within static constructs, the addition of DOX + EFs at both doses resulted in further increase in alkali-soluble elastin content compared to those with EFs alone (26.2 ± 9.5 µg/mg, $\rho = 0.05$ with 0.1 µM DOX + EFs, and 30.6 ± 9.3, $\rho = 0.001$ with 1 µM DOX + EFs). Addition of stretch further increased alkali-soluble elastin content. Up to 2-fold increase was noted in constructs treated with EFs alone (15.5 ± 1.7 µg/mg in static, compared to 32 ± 5.8 µg/ml

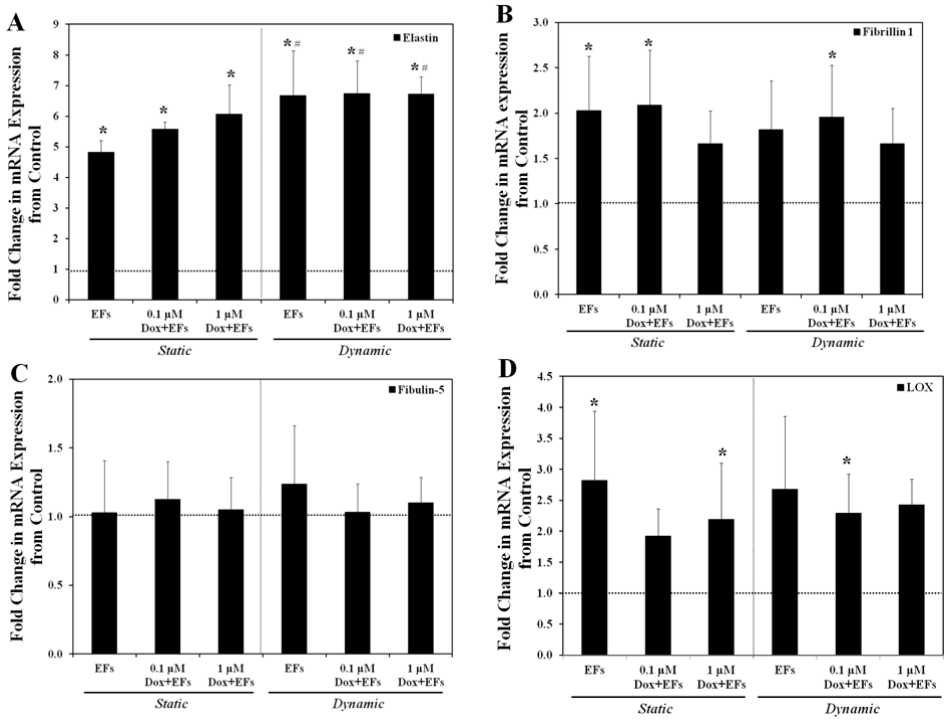

Figure 5.4: Evaluation of changes in mRNA expression of different elastic matrix proteins under static and dynamic conditions with the addition of DOX and EFs (A) elastin, (B) fibrillin-1, (C) fibulin-5, and (D) LOX. '*' represents significant difference from control and '#' from static EFs, for $p \leq 0.05$

in not improve the already high levels of alkali-soluble elastin content (> 26 μg/mg in all cases, $\rho > 0.47$ between the 4 DOX + EF –treated constructs). Similarly, among the 3 sets of stretched constructs, with or without DOX, differences were insignificant ($\rho > 0.46$). The presence of the highly crosslinked, alkali-insoluble matrix elastin content was found to be similar in almost all treatment conditions (1.9 ± 0.8 μg/mg, $\rho > 0.19$), with or without DOX or stretch. Stretched constructs with 0.1 μg/mg DOX + EFs, were the only condition that showed a significant increase in alkali-insoluble elastin content compared to all other constructs (3.8 ± 1.9, $\rho < 0.04$).

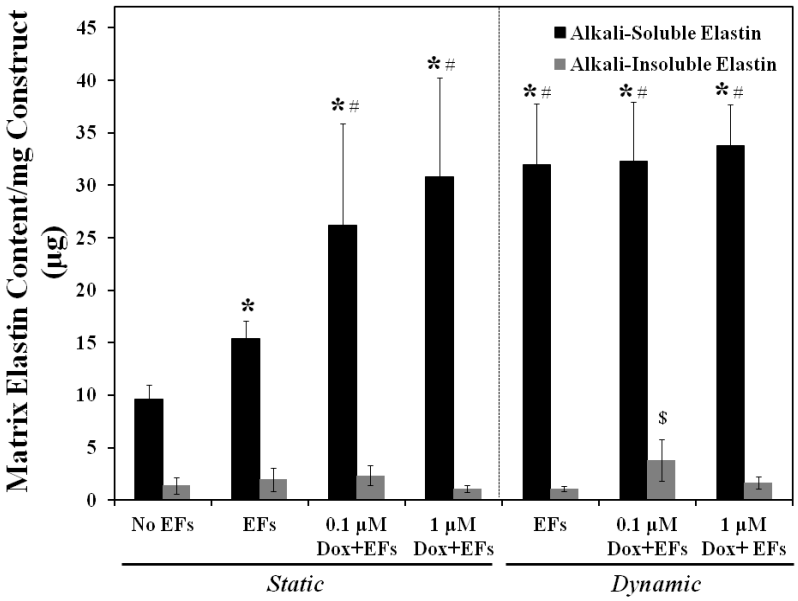

Figure 5.5: Effects of addition of DOX and EFs on elastic matrix content under static and dynamic conditions. Alkali -soluble elastin elevated in all treatment conditions compared to control. Alkali-insoluble matrix elastin remained unchanged in almost all cases, except in 0.1 M DOX + EFs. '*' represents significant difference from control, '#' from static EFs, and '$' with respect to every treatment condition, for $p \leq 0.05$)

Western blotting of the elastic matrix proteins fibrillin-1, fibulins -4 and -5, and LOX did not result in consistently detectable or quantifiable bands. This is likely due to the low protein concentrations (5 µg) that these were tested with.

5.3.5. MMP-2 Production and Activity

RT-PCR, western blotting and zymography were performed to analyze the effects of DOX + EFs under static and stretched conditions. As seen in **Figure 5.6**, constructs treated with DOX + EFs significantly decreased MMP-2 mRNA expression under both static and stretched conditions, compared to those without DOX ($\rho < 0.01$), at both the doses provided. Within static constructs, compared to control, MMP-2 mRNA expression was significantly decreased to 0.24 ± 0.05 –fold and 0.22 ± 0.1 –fold with 0.1 µM DOX

+ EFs and 1 µM DOX + EFs respectively ($\rho < 0.001$ for both). This decrease was also significant compared to static constructs treated with EFs alone ($\rho < 0.01$), whose MMP-2 mRNA expression was 0.7 ± 0.18 –fold compared to control ($\rho = 0.02$). The difference in expression between DOX-treated and –untreated constructs was significant under dynamic stimulation as well ($\rho < 0.001$ for stretched EFs compared to both doses of stretched DOX + EFs). MMP-2 mRNA expression within stretched constructs with EFs alone were comparable to control (0.98 ± 1.8 –fold, $\rho = 1$). However, with the addition of 0.1 µM DOX + EFs and 1 µM DOX + EFs, this was brought down to 0.36 ± 0.08 –fold and 0.31 ± 0.07 –fold respectively ($\rho < 0.001$ for both). While MMP-2 mRNA expression appeared to increase with stretch, this increase was significant in constructs treated with EFs alone ($\rho = 0.03$). Differences in its expression between static and dynamic constructs treated with DOX + EFs, at both DOX doses, were statistically insignificant ($\rho > 0.25$).

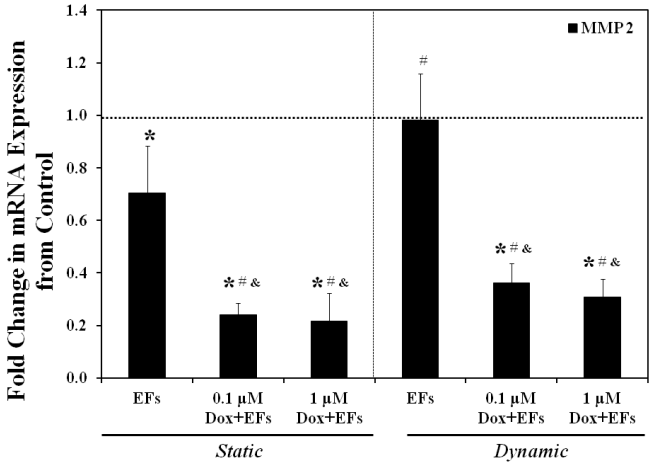

Figure 5.6: Changes in mRNA expressions of MMP-2 under static and dynamic conditions, with DOX + EFs, and EFs alone, relative to control. Significant decrease observed with addition of DOX + EFs under both static and dynamic conditions. '*' represents fold change from control, '#' from static EFs, and '&' from dynamic EFs

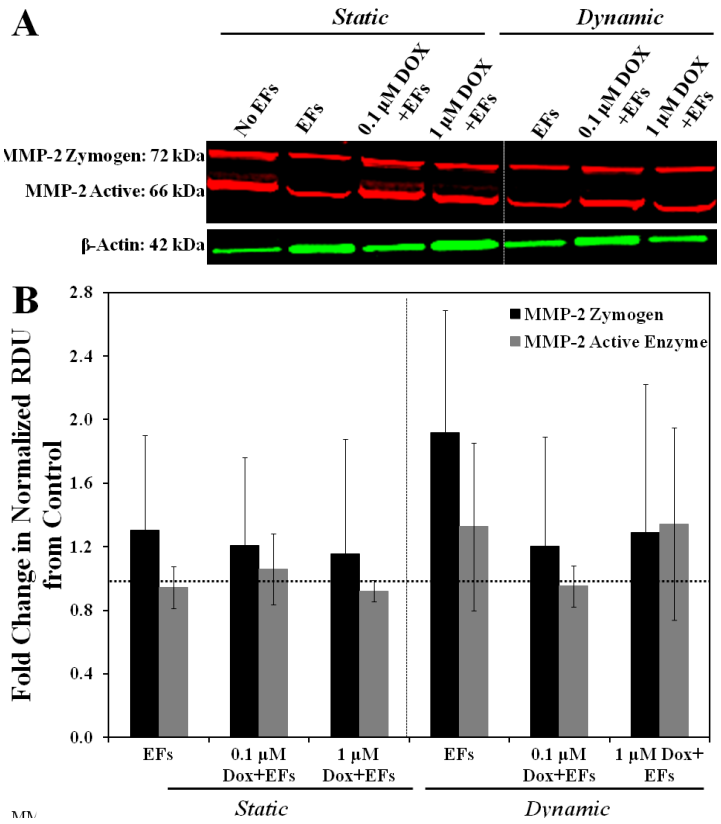

Figure 5.7: Effect of addition of DOX + EFs on MMP-2 protein content under static and dynamic conditions relative to control. (A) Representative immunoblots of active and zymogen forms of MMP-2 in all treatment conditions. (B) Semi-quantitative analysis of MMP-2 protein represented as fold change in RDU relative to control. No significant differences noted between different treatment conditions

Western blotting of MMP-2 (**Figures 5.7 A** and **B**) did not show any significant, treatment-specific differences in intensities of bands corresponding to both zymogen and active forms of the protein (ρ > 0.63). However, zymography (**Figures 5.8 A** and **B**) showed significant decrease in enzyme activity of MMP-2 as a function of DOX dose, under both static and stretched conditions. Within static constructs, fold-change in RDU

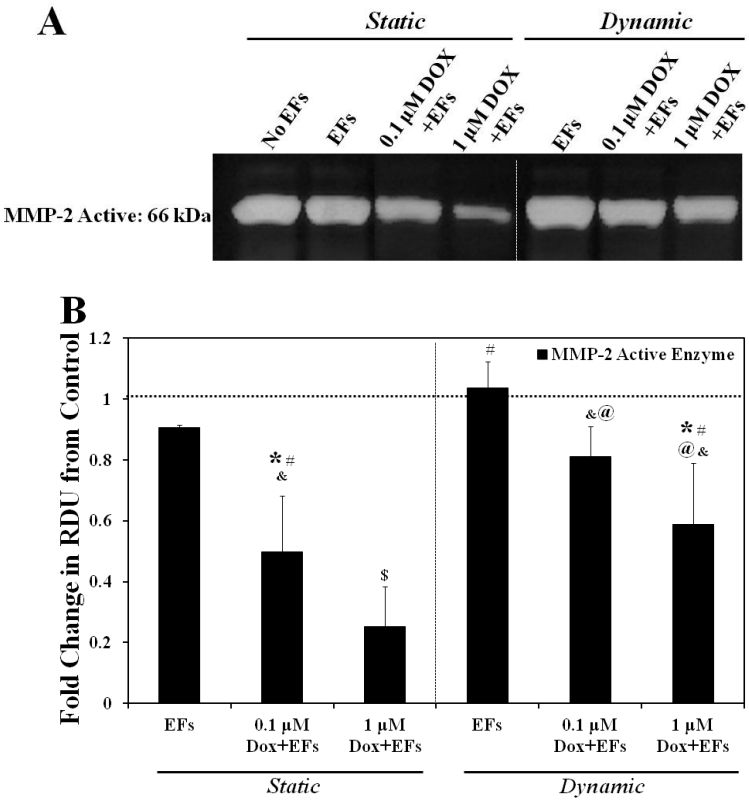

Figure 5.8: Change in MMP-2 enzyme activity with addition of DOX and EFs under static and stretched conditions relative to control. (A) Representative zymogram showing bands corresponding to active MMP-2 enzyme. Bands corresponding to zymogen form of the enzyme were undetected. (B) Fold change in MMP-2 active enzyme compared to control. Significant decrease observed proportional to increase in DOX concentration in both static and dynamic constructs. '*' represents significant difference from control, '#' from static EFs, '@' from 0.1 µM DOX + EFs static, '&' from dynamic EFs and '$' compared to every treatment condition, for $p \leq 0.05$

values of active MMP-2 enzyme bands relative to control, were significantly decreased to 0.45 ± 0.18 –fold with 0.1 µM DOX + EFs, and further decreased to 0.25 ± 0.13 –fold with 1 µM DOX + EFs ($\rho < 0.001$ for both). This decrease in MMP-2 enzyme activity under both DOX doses tested was significant relative to static constructs treated with EFs alone as well ($\rho < 0.001$). Increase in DOX dose (with EFs) to 1 µM significantly

decreased enzyme activity compared to 0.1 µM DOX + EFs (ρ = 0.008). Similarly, while application of stretch did appear to increase MMP-2 enzyme activity, this trend was mirrored under dynamic conditioning as well. Within stretched constructs, relative to control, the active enzyme band intensities were significantly decreased to 0.81 ± 0.1 –fold with 0.1 µM DOX + EFs (ρ = 0.048), and 0.59 ± 0.2 with 1 µM DOX + EFs (ρ = 0.001). Again, this decrease was significant compared to stretched constructs treated with EFs alone (ρ < 0.04) whose band intensities were comparable to control (1 ± 0.09 –fold, ρ = 0.7, relative to control). Similar to that seen within static constructs, decrease in enzyme activity within stretched constructs was also proportional to increasing DOX concentration (ρ = 0.005 between 0.1 µM and 1 µM DOX + EFs, dynamic constructs). Zymogen forms of MMP-2 (72 kDa) enzyme were undetected in all treatment conditions at the protein concentrations tested (5 µg) in both western blots and gelatin zymograms.

5.3.6. MMP-9 Production and Activity

mRNA expressions of MMP-9 for constructs in all groups were extremely low and barely above the detectable limits of the instrument, at the cDNA concentrations tested. It was therefore not possible to discern differences in its gene expression between different groups, if any existed. Western blotting of MMP-9 (**Figures 5.9 A** and **B**) showed a dose-dependent decrease in band intensities of active MMP-9 protein, with decrease in intensity being proportional to increase in DOX concentration (with EFs), under both static and dynamic conditioning. Within static constructs, relative to control, RDU values of MMP-9 active protein bands were decreased to 0.64 ± 0.16 –fold (ρ =

0.02) with 0.1 µM DOX + EFs, and further down to 0.44 ± 0.07 –fold (ρ = 0.01) with 1 µM DOX + EFs. Compared to static constructs treated with EFs alone (whose band intensities were 0.95 ± 0.01 –fold, ρ = 0.71, relative to control), significant decrease in MMP-9 active protein band intensity was observed with 1 µM DOX + EFs alone (ρ = 0.04), and it was comparable to 0.1 µM DOX + EFs (ρ = 0.1).

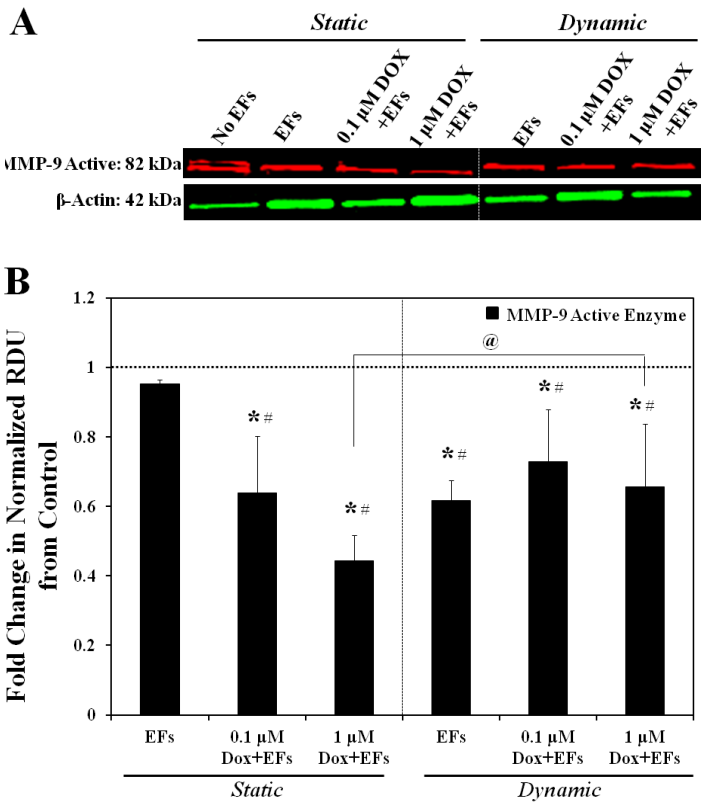

Figure 5.9: Effect of addition of DOX and EFs on MMP-9 protein content, under static and dynamic conditions. (A) Representative immunoblots of MMP-9 active protein in different treatment conditions. Bands corresponding to zymogen form of protein were undetected. (B) Semi-quantitative analysis of MMP-9 active protein represented as fold change in RDU relative to control. Significant decrease seen with addition of DOX + EFs in both static and dynamic constructs. '*' represents significant difference from control, '#' from static EFs, and '@' between conditions indicated, for $p \leq 0.05$

Application of stretch appeared to increase MMP-9 active band intensities in all constructs, relative to the corresponding static constructs treated with similar concentrations of DOX or EFs. These differences were however statistically significant in constructs with 1 μM DOX + EFs alone (ρ = 0.047 between static and dynamic). In all stretched constructs, MMP-9 intensities remained lower than control; 0.6 ± 0.06 –fold (ρ = 0.01) for EFs + stretch alone, 0.72 ± 0.15 –fold for 0.1 μM DOX + EFs + stretch (ρ = 0.048), and 0.66 ± 0.18 –fold for 1 μM DOX + EFs + stretch (ρ = 0.02). Among the 3 sets of constructs under dynamic conditioning, with or without DOX, MMP-9 band intensities were comparable (ρ > 0.8). Bands corresponding to zymogen forms of MMP-9 were undetected in western blots at the protein concentrations tested. Both active and inactive forms of MMP-9 enzyme were undetected in gelatin zymograms.

5.3.7. Matrix Ultrastructure

Matrix ultrastructure appeared similar to the static and dynamic constructs evaluated in **Chapter 4**, as seen in **Figures 5.10** through **5.12**. Cells and synthesized matrix were oriented more in the longitudinal direction, than circumferentially. Elastin and fibrillin appeared to be localized and associated with each other in most regions of all constructs.

5.4. Discussion

The studies conducted in **Chapters 3** demonstrated the elastogenic benefits of EFs to vascular SMCs cultured under static conditions within collagenous tissue

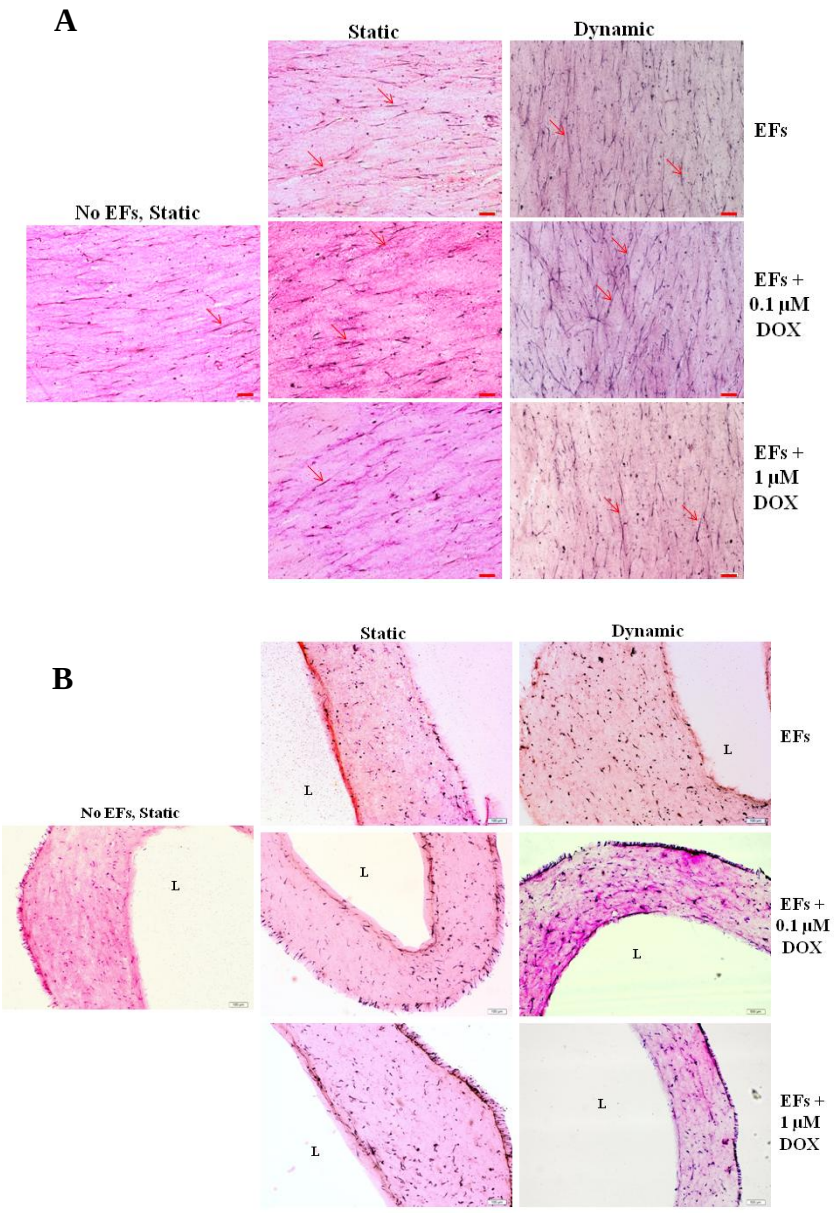

Figure 5.10: Elastic matrix assembly and orientation in response to with DOX and EFs under static and dynamic conditions. Representative (A) longitudinal- and (B) cross- sections (30 µm thick) of constructs show more elastic fibers (stained purple to black) deposited within DOX + EFs- treated constructs. Cells and matrix appear to be oriented more in the longitudinal direction, than circumferential. Scale bar denotes 100 µm. 10 × magnification

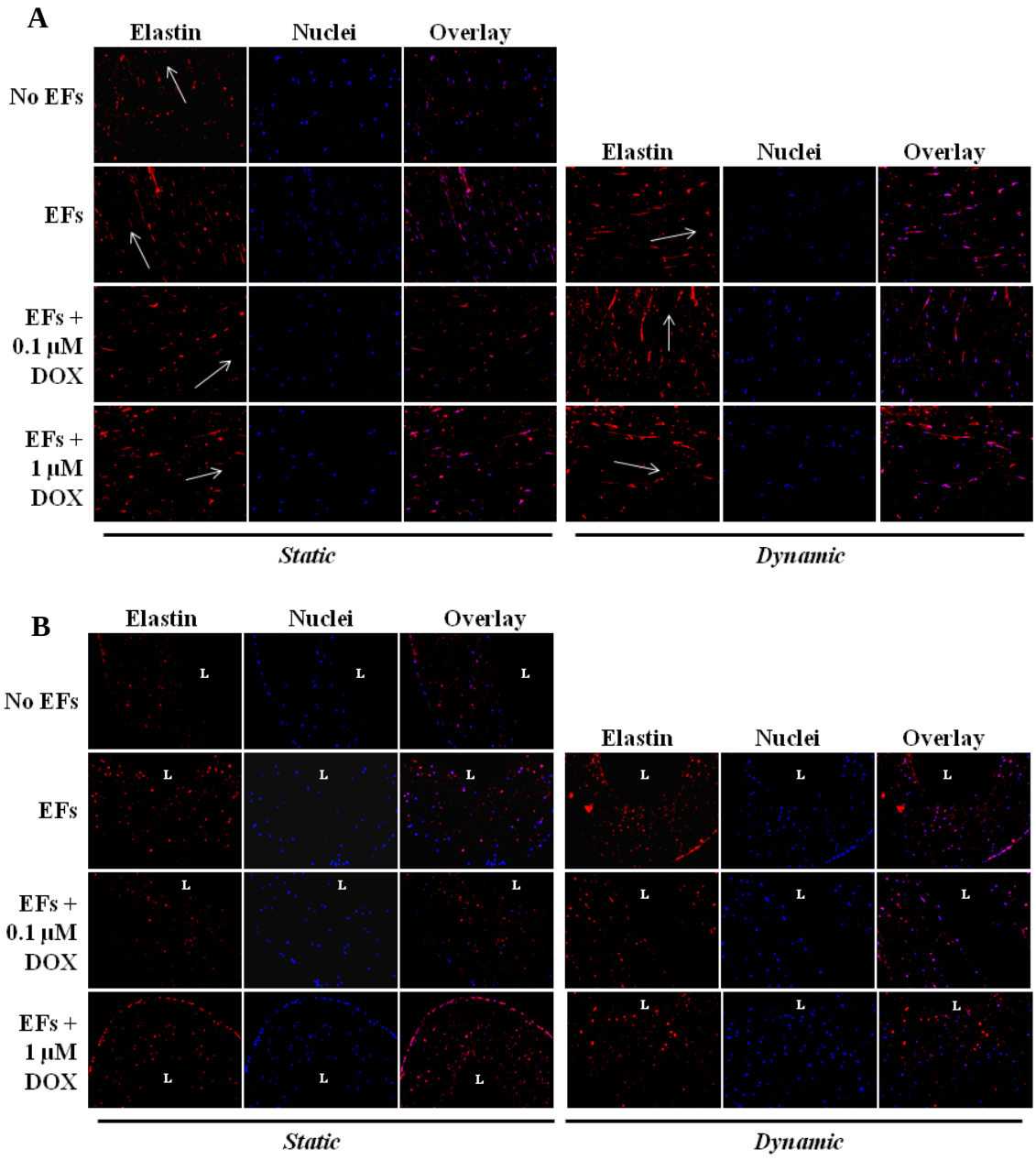

Figure 5.11: Effects of treatment with DOX, EFs and dynamic stimulation towards elastin synthesis and assembly. Representative fluorescent micrographs of 10 µm-thick (A) longitudinal- and (B) cross-sections of constructs immunolabeled with elastin (red) and nuclei (blue). Longer fibers of elastin are seen in the longitudinal sections. Addition of DOX, under both static and dynamic conditions appears to have improved elastic matrix output. **White arrows indicate longitudinal direction of constructs.** 'L' = lumen. 10 × magnification

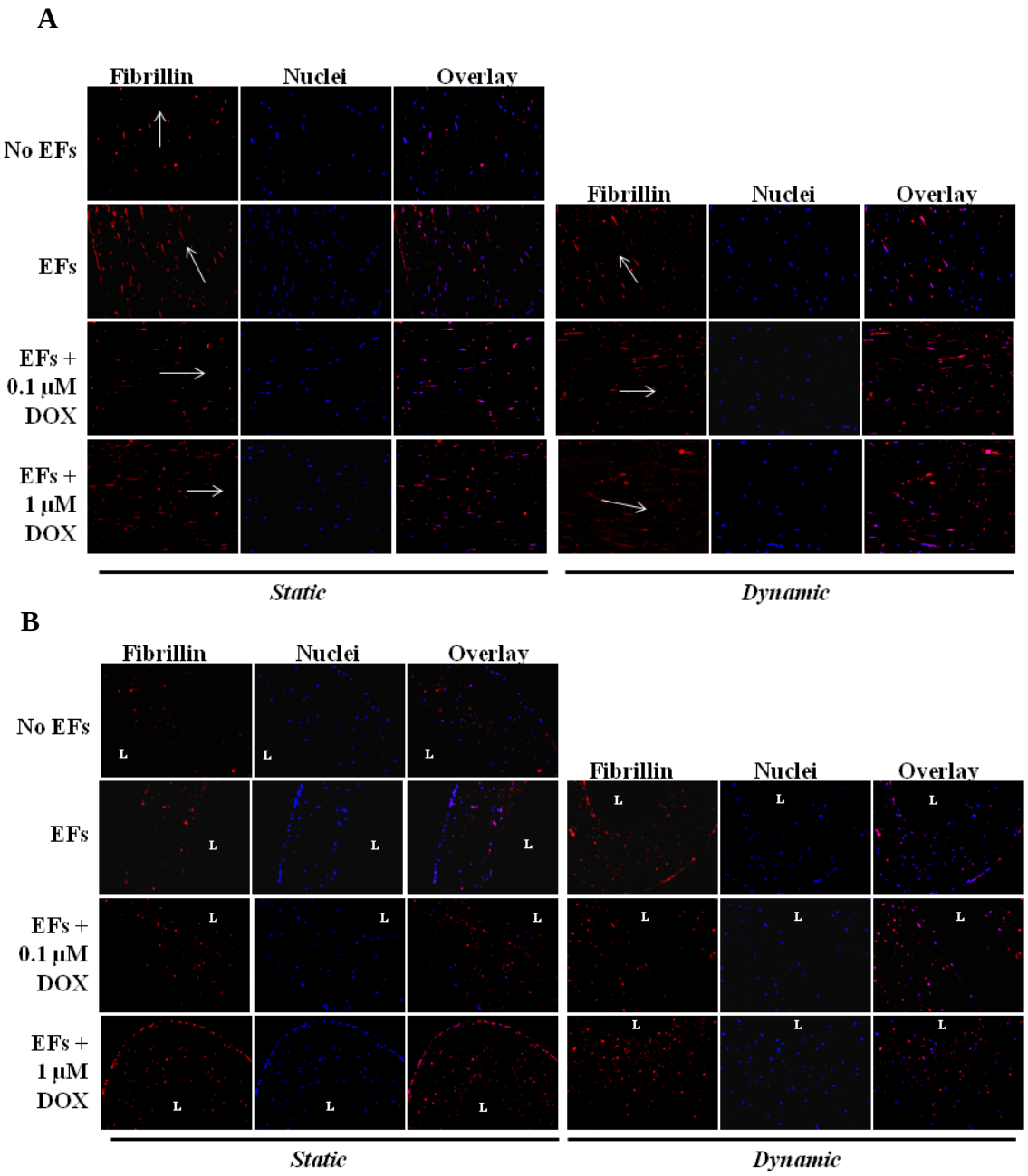

Figure 5.12: Effects of treatment with DOX, EFs and dynamic stimulation towards synthesis and assembly of fibrillin. Representative fluorescent micrographs of 10 µm-thick (A) longitudinal- and (B) cross-sections of constructs immunolabeled with fibrillin (red) and nuclei (blue). **White arrows indicate longitudinal direction of constructs.** 'L' = lumen. Magnification = 10 ×

serve to enhance net accumulation of newly synthesized elastic matrix and improve its quality, especially in the form of more mature fiber formation. In the current study, we constructs. In Chapter 4, we were able to replicate these results within adult human SMCs, and further enhance matrix alignment with the application of cyclic stretch as reported in **Chapter 4**. That these observations were made within collagenous microenvironments, not particularly conducive to elastogenesis, by inducing inherently non-elastogenic adult SMCs, is highly encouraging. One of the observed shortcomings of the tested methods was the continued lack of synthesis and organization of highly crosslinked, mature alkali-insoluble matrix elastin. At the same time, the expression, synthesis and activity of MMP-2, a major elastolytic protease[83], was found to remain consistently high in both studies. We therefore hypothesized that suppression of MMP-2 can therefore evaluated the benefits of utilizing DOX, a modified tetracycline reported to be a non-specific MMP inhibitor[130], supplemented with EFs, in improving elastic matrix outcomes via suppression of MMPs.

Progression of AAA disease appears to be related to two factors, namely, a) chronically high levels of matrix protease activity, primarily MMPs -2 and -9, initiated by inflammatory cells infiltrating the site of tissue injury[16, 55, 241], and b) the inability of the native vascular cells to preserve and restore disrupted vascular wall matrix, especially elastin[10, 18, 79]. Systemic delivery of Doxycycline has been clinically useful to attenuate MMP-mediated disruption and loss of elastic matrix[46, 126]. As a result, progression of disease is suppressed, and in a few cases even reverted, by preserving the existing elastic matrix within the AAA wall[46, 126]. Despite these benefits, systemic delivery of DOX has

also been linked to likely dose-dependent effects such as frequent gastrointestinal tract disturbances, cutaneous photosensitivity and irreversible dental discoloration[242]. Besides, systemic inhibition of MMPs is not desirable since it plays key roles in normal tissue remodeling and turnover as well[83]. Localized delivery of DOX using osmotic pumps in AAA rodent models has been attempted and showed DOX to retain therapeutic benefits at concentrations 100-fold lower than that delivered systemically[243-244]. However, when we delivered similar concentrations to SMCs in 2D cell culture, we found DOX to be cytotoxic at concentrations as low as 10 μM, but to promote cell proliferation at lower concentrations. Other studies have also indicated a dose-dependent inhibition of cell attachment and proliferation by DOX [245-246]. In the current study, at concentrations as low as 0.1 and 1 μM, we did not observe any changes in cell densities compared to those without DOX treatment, both static and stretched. These differences may be due to one or more of the following factors, namely a) reduced DOX dose on a per cell basis within the current 3D model owing to much higher cell-seeding density, compared to that in 2-D culture, b) limitation to diffusion of DOX into constructs, effectively reducing doses perceived by cells, and c) the presence of a collagenous environment that is inherently deterrent to cell proliferation, potentially normalizing the proliferative capacity of cells across treatment conditions.

DOX-mediated suppression of gelatinases has shown to be achieved by inhibition both at the level of mRNA expression of proteases[127-128], as well as during protein synthesis, and inducing irreversible loss of enzyme activity post-synthesis[131, 247]. Liu et.al. have shown that DOX destabilized MMP-2 mRNA by reducing its half life from 28 to 4

hours[248]. At the concentrations tested in our study, we witnessed a marked suppression in MMP-2 mRNA expression as well. This suppression was higher in the DOX + EFs treated cultures, than those treated with EFs alone, both under static and stretched conditions. In the static cultures, up to a 5-fold decrease in MMP-2 mRNA expression was found with the addition of 1 μM DOX, and a 4-fold suppression for 0.1 μM. Even within cyclically stretched constructs, where the stretch-induced increase in MMP-2 mRNA expressions are known to occur[170], its gene expression was found to be decreased to levels statistically similar to that found within static cultures treated with DOX + EFs. However, this decrease in expression was not found to be dose-dependent, with similar levels of MMP-2 mRNA suppression seen in both DOX doses tested, with or without stretch. It is important to note that the DOX doses tested in this study were several orders of magnitude lower than what has been shown to inhibit MMP-2 gene expression[127-128]. It is likely that within a 3D collagenous environment, where cells inherently secrete proteases for tissue remodeling[170, 237], inhibition of MMP at the level of gene expression, in the presence of such low concentrations of inhibitors, could get normalized. This normalizing effect is further substantiated by the finding that MMP-2 mRNA expression was suppressed to similar, and not proportional extents, within static and stretched constructs. On the other hand, at the protein level, both active and zymogen forms of MMP-2 were found to be similar under all treatment conditions, indicating that at the levels tested, DOX did not inhibit protein synthesis, despite the apparent decrease in MMP-2 mRNA expression. In contrast however, enzyme activity of MMP-2, as evaluated by zymography, was found to decrease proportionally with increase in DOX

concentrations, in both static and dynamic constructs. This suppression was however more pronounced within static constructs (up to 2- and 4- fold decrease with 0.1 μM and 1 μM DOX + EFs respectively), than within stretched constructs (up to 1.5- and 2- fold with 0.1 μM and 1 μM DOX + EFs respectively), likely due to increase the phenomenon of tissue remodeling-mediated increase in MMP-2 expression mentioned above. Several groups, including Liu et.al.,[248] have also shown that DOX alters the conformation of both the zymogen and the active enzyme by binding enzyme-associated Ca^{++}[131]. This makes the proteins more susceptible to proteolysis, resulting in their fragmentation into smaller molecular weight fractions and an irreversible loss of enzyme activity[131-132]. While we did not observe MMP-2 fragments in either western blots or the zymograms, our results nonetheless substantiate the hypothesis that DOX further inhibits MMP-2 activity at the enzyme-activity level as well. It is likely that the phenomenon of fragmentation occurs at higher DOX concentrations than that tested here, or that even if the fragments were formed in our study, their concentrations were too low to be detected. It is important to note that the MMP-2 gene expression and enzyme activity were far more suppressed in constructs treated with DOX + EFs, than that within EFs alone, indicating that DOX significantly enhances the anti-proteolytic activity of the treatment, above what TGF-β1[40] and HA-o[43] have also been reported to also induce.

MMP-9 mRNA expression at concentrations tested were very low to begin with, which made discerning differences between cases difficult. The low mRNA expression could also indicate why we did not observe bands corresponding to zymogen form of MMP-9 at the concentrations tested. However, western blotting did reveal differences in

total protein content of active MMP-9 enzyme. This was found to be lowered proportional to increase in DOX concentration, both in static and dynamic constructs. This further substantiates that the concentrations of DOX tested in this study were effective in suppressing protease activity.

Addition of DOX also increased mRNA expression of elastin as well as alkali-soluble matrix content, compared to untreated controls as well as constructs treated with EFs alone, in both static and dynamic constructs. Differences in mRNA expression of elastin appeared to be more pronounced between static and dynamic constructs, than between the two doses. mRNA expression of other elastic matrix proteins was found to be similarly increased (up to 2 fold) in all EF treated cultures, with or without DOX. Interestingly, unlike that seen in constructs treated with EFs alone, alkali-soluble matrix elastin content was found to be similar in all EF + DOX-treated constructs, and was not found to be influenced by varying concentration or application of stretch. This could likely be due to the similar levels of mRNA expression as well as total protein content of MMP-2 seen among all DOX + EFs –treated constructs.

Several studies have indicated that DOX-mediated suppression of MMPs additionally occurs through the suppression of JNK pathway[133, 249]. Within AAAs, suppression of JNK has also been shown increase expression and synthesis of various matrix proteins, especially LOX, via a TGFβ-1 activated pathway[250-253]. Thus, it is pertinent to expect that DOX would enhance LOX bioavailability as well. LOX expression in our study, while elevated in EF-treated constructs (both static and dynamic) relative to static control, does not appear to be enhanced further upon addition of DOX.

TGFβ-1, which is added along with DOX in this study, is also known to enhance LOX mRNA expression and improve activity of the crosslinking enzyme[38]. It is possible that any DOX-mediated regulation of LOX expression may be limited and thus be masked by the addition of TGFβ-1 in our cultures. It is also important to note that our studies were conducted on healthy SMCs and in concentrations much lower than that reported in other studies. The combined suppression of MMP activity and increase in alkali-soluble matrix elastin was translated into higher quantities of alkali-insoluble matrix elastin only in one of the treatment conditions- 0.1 μM DOX + EFs with stretch. The levels remained comparable to static controls in all other cases. It is likely that the formation of the highly crosslinked alkali-insoluble elastin requires higher expression of elastic matrix scaffolding proteins i.e., fibrillin-1, fibulins and LOX, than that obtained in our studies. Matrix ultrastructure also appeared similar to constructs treated with EFs alone. As noted in **Chapter 4** studies, cell and fiber alignment were once again in the longitudinal direction, and not in the circumferential direction. This is likely due to the low strains of 2.5% applied to the constructs in this study.

5.5. Conclusions

Supplementation of HASMC-collagen constructs with DOX and EFs improved elastic matrix output in terms of higher quantities of alkali-soluble matrix elastin. Expression and activity of both MMPs -2 and -9 were found to be suppressed in both the DOX-doses tested. Improvements in insoluble-elastin content was observed in one of the DOX treated cultures (0.1 μM DOX + EFs + stretch).

CHAPTER SIX

EVALUATION OF ELASTOGENIC EFFECTS DUE TO LOCALIZED, NANOPARTICULATE DELIVERY OF DOX AND TGF-β1 IN 3-D COLLAGEN–GEL TUBES

6.1. INTRODUCTION

In the previous chapter, we demonstrated that the treatment of adult SMCs within collagen constructs with EFs and DOX improve outcomes of induced elastogenesis. While these studies mimic an *in vivo* tissue microenvironment, the EFs and DOX were supplemented exogenously to the culture media. There are two limitations to such delivery. First, the direct translation of such exogenous delivery and its cell-regulatory outcomes cannot be achieved *in vivo* at the site of proteolysis and disease, in a manner similar to that demonstrated in these studies. Second, it is unclear whether diffusional limitations exist for EF access into the tissue constructs, and to what extent induced elastogenesis is limited by this factor. In the context of *in situ* matrix repair, it is thus important to obtain localized, controlled delivery of therapeutic agents, whose concentrations and bioavailability can be closely regulated to achieve significant and predictable cellular response. Nanoparticulate delivery of active agents via polymeric carriers has been widely used for various *in vivo* drug delivery applications[254-256]. Compared to other delivery modes such as those involving the use of microparticles, nanoparticles (NPs) offer several advantages such as higher surface area/unit volume, achieving higher release, better tissue infiltration and interaction at the cellular level due

to their nano-range sizes comparable to cells, and generation of comparatively lesser byproducts of polymeric degradation that can adversely impact activity of agents encapsulated within[257-259]. In this study, we have utilized the *in vitro* tubular collagen gel model, as optimized in the previous chapters, to evaluate the effects of localized delivery of elastogenic factors from poly (lactic-co-glycolic acid) (PLGA) nanoparticles (NPs).

It is important to note that in this study, we have evaluated the effects of co-delivery of only TGF-β1 and DOX, and excluded HA-o from the study. Nanoparticulate formulations for HA-o delivery are currently being developed in our lab, and were therefore not available to be included in this study. Accordingly, a direct comparison of the results of **Chapters 4** and **5** are therefore not possible. We have thus included in this study, an additional control case in which TGF-β1 and DOX were exogenously delivered at concentrations similar to that released from the NPs. All other culture conditions were kept constant among the different treatment cases.

6.2. MATERIALS AND METHODS

6.2.1. Synthesis of TGFβ-1 and DOX loaded Nanoparticles

Two different sets of Poly (*dl*-lactic-co-glycolic acid) nanoparticles (PLGA; 50:50 lactide : glycolide; inherent viscosity 0.95-1.20 dL/g in hexafluoroisopropanol; Durect Corporation, Birmingham, AL) nanoparticles were synthesized – one with TGF-β1 (28 kDa) (R & D Systems, Minneapolis, MN) and another with DOX (Sigma, St. Louis, MO). A double-emulsion/solvent evaporation method was utilized to obtain PLGA NPs loaded with either of the water soluble factors[213-214]. Nanoparticles were synthesized with 0.25%

w/v polyvinyl alcohol (PVA), which acts as an anionic surfactant and a stabilizer[213]. Particle size and ζ-potential were evaluated using a NICOMP 380 ZLS analyzer. Size homogeneity of the synthesized particles was confirmed using TEM. In order to obtain the target concentration of factors (as optimized in Chapters 4 and 5) released from the NPs, 2 different drug-loading concentrations for DOX, and 3 for TGF-β1 were tested. DOX was loaded at 2% and 5% w/v, while TGF-β1 was loaded at 1000 ng, 2000 ng and 5000 ng per mg of PLGA. Blank NPs were synthesized in manner similar to the factor-loaded NPs, but without the addition of any factors.

6.2.2. Release Profile of Factors from NPs

Release of DOX and TGF-β1 (**agents**) from NPs was evaluated in PBS at 37 °C over 21 days. TGF-β1 NPs were suspended in PBS at a concentration of 10 mg/ml, while DOX loaded NPs were tested at 0.2 mg/ml and 0.5 mg/ml. In order to measure the concentration of the agents released from the NPs at each time point, the nanoparticles were first centrifuged at 14,000 rpm for 30 minutes at 4 °C, and supernatants collected for analysis. Fresh, 1 ml aliquots of PBS were added post-centrifugation to replenish the volumes for further study of release. The collected aliquots of supernatant from the TGF-β1- NP preparations were frozen at -20 °C until analysis. The concentration of TGF-β1 was measured in these aliquots using a commercially available enzyme-linked immunosorbant assay (ELISA) kit (R & D Systems, Minneapolis, MN). Concentration of DOX in supernatant aliquots similarly obtained by processing DOX NPs, were not frozen but measured immediately after each centrifugation cycle using UV-spectrophotometry

(SpectraMax M2, Molecular Devices, Inc., Sunnyvale, CA) at absorbance of λ = 273 nm[259-260]. Concentrations were determined based on calibration curves of known DOX concentrations incubated in PBS for similar time points. Based on the cumulative release curves plotted for all cases, the optimum NP formulation was chosen for each factor, such that a total of 0.5 mg/ml NPs would be used to release agents within the collagen gel constructs over 21 days of culture.

6.2.3. Formulation of NP-loaded Collagen Constructs

Acid-solubilized rat-tail collagen was brought to physiological pH as detailed in **Section 4.2.2.** Following this, the 2 sets of NPs were added at a final concentration of 0.5 mg/ml. 5×10^5 HASMCs/ml were then added to this viscous mixture, mixed well by gentle pipetting, and then added to the culture chambers of the bioreactors. The bioreactors were sterilized and set up as detailed in **Sections 4.2.1** and **4.2.2.** Day 1 of culture was set to 24 hours after seeding the constructs since the factors from NPs were expected to initiate release of active agents immediately after seeding. The three treatment conditions tested, i.e. constructs with exogenous delivery (control; EDC), blank NPs (BNP) and agent-loaded NPs (ANP), and are listed in **Table 6.1**. Cyclic stretch was provided to all the 3 conditions at 2.5% strain and 1.5 Hz, as optimized in **Chapter 4**. DOX and TGF-β1 were exogenously supplementation to one set of constructs as delivery mode controls. The concentrations of exogenous delivery were equivalent to that released by the NPs at similar time points along (determined from their release curves in PBS) with DMEM/F12 (Media Core, Cleveland Clinic, Cleveland OH), 10 % v/v FBS (PAA

Scientific, Dartmouth, MA) and 1% v/v PS (Thermo Scientific, Rockford, IL). Constructs with blank NPs or agent-loaded NPs were cultured in above culture medium with no exogenous factors. Culture medium was changed every 2 days, and spent media pooled for each construct and frozen at -20 °C until analysis. Constructs were harvested 21 days after seeding, rinsed 3 × in sterile PBS, and processed for various biochemical assays.

6.2.4. Retention of NPs within Collagen Gels

In order to verify that the NPs were retained in the gels, and not eluted out during compaction of constructs, a pilot study was performed on PLGA NPs loaded with Cy5-tagged bovine serum albumin (BSA; NanoCS, New York, NY). N = 3 constructs were seeded each with 3 different NP concentrations - 0.1 mg/ml, 0.2 mg/ml and 0.5 mg/ml, and harvested at 3 time points – day 3, day 7 and day14. Constructs were visualized under a fluorescence microscope using a Cy5 filter (Olympus, Pittsburgh, PA) to gauge retention on the day of harvest. Additionally, a DNA assay was also performed at days 3, 7 and 14, to estimate the effect of NPs on cell proliferation. A minor difference between the NPs used in this pilot study, and the ones used to deliver DOX/TGF-β1, as discussed in this chapter, concerns the surfactant used to synthesize the NPs. Di-dodecyl-dimethyl-ammonium bromide (DMAB), a cationic amphiphile, that imparts a net positive charge was used to synthesize NPs in the pilot study. As will be elaborated further in the Discussion section of this chapter (**Section 6.4**), although the surfactants may not directly influence release itself, DMAB, may have associated with released TGF-β1, resulting in decreased detection with ELISA. Hence, in subsequent experiments, we used PVA, which provides a net negative charge, as a surfactant. Despite the difference in

surfactants used, we believe that the pilot study can be used as a reliable indicator to estimate NP retention within the gels. This is since removal of NPs is likely to occur either during bulk fluid exclusion during

gel compaction, or subsequently by diffusion.

Table 6.1: Experimental conditions-nanoparticulate delivery of elastogenic agents

Group	**Mode of delivery of DOX and TGF-β1**
Exogenous Delivery Control **(EDC)**	Supplemented with culture medium
Blank NPs **(BNP)**	-
Agent-loaded NPs **(ANPs)**	0.2 mg/ml DOX-NPs and 0.3 mg/ml TGF-β1-NPs

6.2.5. Compaction of Tissue Constructs

All constructs were photographed at regular intervals and compaction of constructs was calculated and represented as an aspect ratio of length : O.D. on day 21 of harvest.

6.2.6. DNA Assay for Cell Quantification

As detailed in **Section 4.2.4**, 1/4th segment of the each of the harvested constructs were flash-froze, lyophilized for 24 hrs and digested in 5 mg/ml proteinase-K (Gibco–Invitrogen, Carlsbad, CA) for 10 hours. Samples were then centrifuged at 14,000 rpm to pellet any possible NPs, and supernatants sonicated prior to performing the Hoechst 33258 dye (Gibco–Invitrogen, Carlsbad, CA) -based flourometric DNA assay[221]. Cell

numbers were calculated based on the estimate of 6 pg DNA/cell, and normalized to mg tissue weights for comparison, (n = 5/case).

6.2.7. RT-PCR for mRNA Expression of SMA Phenotypic Markers and Matrix Proteins

Rinsed segments of constructs were cut into small 1–2 mm long pieces and stored in RNAlater solution until processing, and RNA isolated using RNeasy kit (Qiagen, Valencia, CA), as detailed in **Section 4.2.5.** Briefly, samples were transferred to 500 µl RLT buffer (supplied with the kit) with 1% v/v 2-mercaptoethanol (Sigma, St. Louis, MO), homogenized using needle and syringe, and manufacturer's instructions followed to isolate RNA into 50 µl of RNAase-free water. RNA content was measured using a Ribo-green assay kit (Invitrogen, Carlsbad, CA), and 250 ng total RNA was reverse transcribed into 40µl cDNA, as detailed in **Section 4.2.5.** RT-PCR was performed for SMC markers such as SMA, caldesmon and osteopontin, elastic matrix proteins such as elastin, fibrillin-1, fibulin-5, LOX and collagen, and MMPs -2 and -9. Gene expressions were estimated in 1 µl cDNA (duplicate readings, n = 5 per sample), using the comparative threshold method with 18 s as the normalizing gene, as described in **Chapter 1**[261]. Primer sequences and source for the above genes are listed in **Table 4.2** in **Chapter 4.**

6.2.8. Fastin Assay for Elastin Content

Lyophilized construct segments were digested in 0.1 N NaOH to solubilize alkali-soluble matrix elastin, followed by in 0.25 M oxalic acid to obtain solubilized alkali-

insoluble matrix elastin, as described in **Section 4.2.6.** Digested samples were once again centrifuged at 14,000 rpm for 30 minutes to eliminate any possible contamination from NPs. Digested aliquots (250 μl) were used to assay for alkali-soluble elastin, and 175 μl for alkali-insoluble elastin using the Fastin assay kit (Accurate Scientific and Chemical Corporation, Westbury, NY), as mentioned in **Section 4.2.5**.

6.2.9. Western Blotting for Cellular and Matrix Proteins

Lyophilized segments of constructs were cut into small 1-2 mm long pieces and 500 μl of RIPA lysis buffer (Invitrogen, Carlsbad, CA) with a protease inhibitor cocktail (Thermo Scientific, Rockford, IL) was added to homogenize samples and solubilize proteins, as described in **Section 4.2.7.** A BCA assay (Thermo Scientific, Rockford, IL) was performed to measure concentration of total protein in all samples. Western blotting was performed to detect the phenotypic markers of contractile SMCs (n = 1/case) such as smooth muscle α-actin (SMA; an early-stage marker), Smooth muscle-22-α (SM22; a mid-stage marker), myosin heavy chain (MHC; a late-stage marker), and calponin and caldesmon (both mid-stage markers), elastic matrix proteins (n = 3/case) such as LOX, fibrillin-1 and fibulins -4 and -5, and matrix proteases (n = 3/case) MMPs-2 and -9. All blots were simultaneously labeled for the protein of interest and for the normalizing protein, β-actin. Protein content of 10 μg per sample was used to immunoblot the above proteins. Antibody concentrations and incubation time points corresponding to different steps in immunoblotting are detailed in **Section 4.2.7**. To semi-quantitatively represent the differences in elastic matrix proteins and proteases content between different

conditions, samples from n = 3 biological replicates per condition were assayed. Band intensities of the protein of interest calculated in RDU were first normalized to β-actin values, then normalized to the condition with exogenous factor delivery (treated as biological control), and represented as fold change in RDU values compared to the above condition.

6.2.10. Gelatin Zymography for Detection of Enzyme Activities of MMPs -2 and -9

Gelatin zymography was performed to semi-quantitatively estimate differences the enzyme activities of the proteases MMPs -2 and -9, between the treatment conditions (n = 3/case). Protein samples (10 μg) homogenized in RIPA buffer as discussed in **Section 6.2.9.**, were loaded into each lane of a 10% gelatin zymogram. As described in **Section 4.2.8.**, zymography was performed on n = 3 biological replicates, and enzyme activity was represented as a fold change in RDU values relative to EDC constructs (control).

6.2.11. Visualization of Elastic Matrix

Constructs harvested after 21 days of treatment were rinsed 3 times in PBS, and 0.5 cm long constructs were fixed in 4% w/v paraformaldehyde for 6 hours at RT and 6 hours at 4 °C. Samples were then dehydrated and embedded in paraffin wax as detailed in **Section 4.2.9.** Histology was performed on 30 μm-thick cross- and longitudinal- sections using an Elastic stain kit (Laboratories Inc., Cache, UT) to visualize the ultrastructure of elastic matrix content in the constructs. IF was performed on 10 μm cross- and

longitudinal- sections, imaged using an fluorescence microscope under Cy5 filter (Olympus, Pittsburgh, PA) to detect elastin and fibrillin. The labeled sections were mounted in Vectashield with DAPI (Vector Laboratories, INC. Burlingame, CA) to stain for nuclei, and cover-slipped prior to imaging and visualization.

Longitudinal sections (1 mm thick) of harvested constructs were fixed in 2.5% w/v gluteraldehyde and 4% w/v paraformaldehyde in sodium cacodylate buffer for 24 hours, and then processed for TEM, as described previously in **Section 4.2.9.**

6.2.12. Statistical Analysis

All experiments were performed on n = 5 biological replicates per treatment condition, unless mentioned otherwise. Histology, IF and TEM were performed on segments from n = 1 construct per condition. All quantitative and semi-quantitative results are represented as mean ± standard deviation per condition. One-way ANOVA was performed to calculate statistical significance in differences between treatment condition. Conditions were deemed to be significantly different for ρ values ≤ 0.05.

6.3. RESULTS

6.3.1. Nanoparticles Size and Release Profiles

Hydrodynamic diameters of both TGF-β1 and DOX loaded NPs, and blank NPs synthesized were found to be within 300 ± 30 nm diameter and had a surface charge of 30 ± 5 mV. **Figure 6.1** shows the release curves of DOX and TGF-β1 from NPs in PBS over 21 days. In the studies discussed in **Chapters 4 and 5**, 0.1 ng/ml of TGF-β1 with

either of the DOX concentrations of 0.1 μM or 1 μM, were found to promote the most significant elastogenic outcomes. Based on the release curves of the two agent-loaded NPs, the formulations that most closely matched these concentrations were 2000 ng/mg loading of TGF-β1 when added at 0.3 mg/ml, and 5% DOX loading when added at 0.2 mg/ml to the collagen-cell mixture. It is important to note that while the cumulative release of DOX from NPs over 21 days of treatment was similar to that optimized in exogenous delivery (5.61 μg/ml over 21 days), TGF-β1 released from the 2000 ng/mg formulation was ~ 10 fold lower. To account for this, we included exogenous delivery controls (EDC), to which DOX and TGF-β1 were supplemented exogenously to the culture medium. Equivalent concentrations corresponding to the release of TGF-β1 from 2000 ng/mg loading (**Figure 6.1 A**), and DOX from and 5% loading at 0.2 mg/ml (**Figure 6.1 B**) were added.

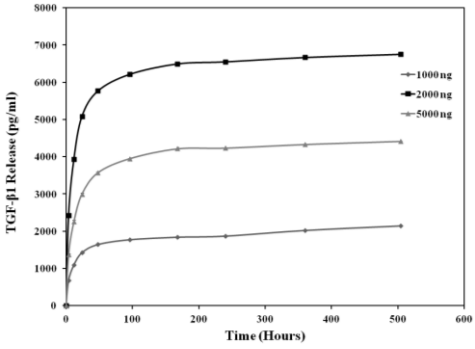

Figure 6.1 A: TGF-β1 Release Profile showing an initial burst phase followed by a sustained plateau phase. Based on the concentration released from 3 NP formulations, 2000 ng/mg loading condition was used for subsequent studies

6.3.2. Nanoparticle Retention and Effects on Cell Density

Cy5-tagged BSA loaded PLGA NPs were added at concentrations of 0.1 mg/ml,

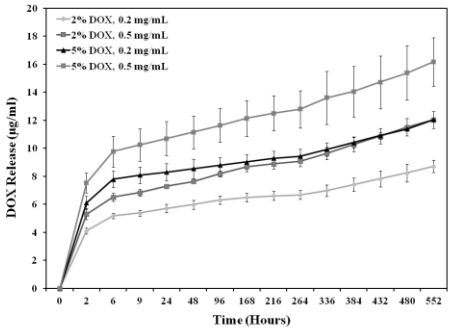

Figure 6.1 B: DOX Release Profile. Based on the concentrations released from the 2 formulations of DOX-loaded PLGA NPs, a 5% w/v loading was chosen for subsequent studies

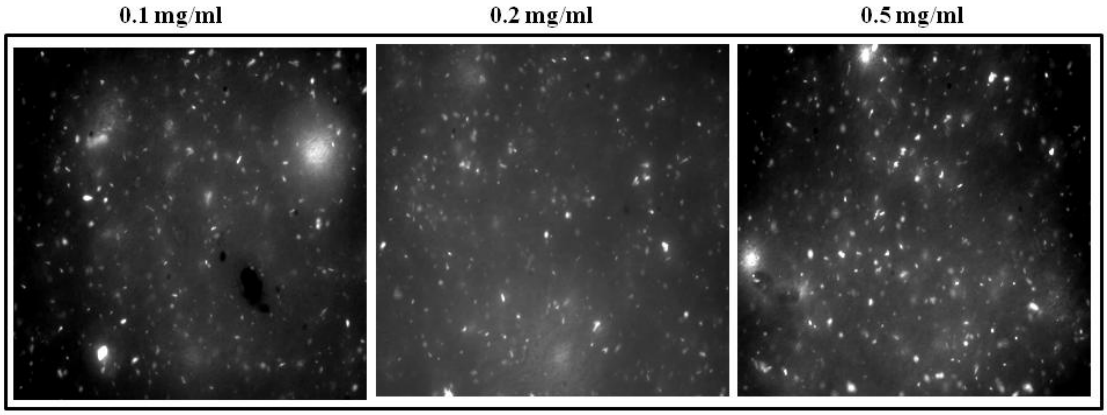

Figure 6.2: Cy5-tagged BSA NPs (white specs) retained within collagen gel tubes at day 14. NPs added at the 3 concentrations - 0.1 mg/ml, 0.2 mg/ml and 0.5 mg/ml

0.2 mg/ml and 0.5 mg/ml to HASMC-seeded collagen gel constructs, and were cultured for 3, 7 and 14 days. As seen in **Figure 6.2**, NPs at all three concentrations were retained within the gels at until day 14. DNA assay was performed to estimate cell densities at the different time points to estimate the effects of the different NP concentrations on cell proliferation (**Figure 6.3**). At day 14, cell proliferation appeared comparable in constructs

with 0.1 mg/ml and 0.2 mg/ml NPs (1.7 ± 0.05 and 1.6 ± 0.25 –fold compared to day 1 of seeding). This was slightly less pronounced in constructs with 0.5 mg/ml NPs (1.4 ± 0.16 –fold). However, the increase in cell densities with increasing culture durations in all treatment conditions indicated that the NPs did not adversely hinder cell proliferation. Based on these findings, and the results obtained from the release curves of agents from NPs (**Figure 6.1**), NP concentration of 0.5 mg/ml was chosen for further studies to test the effects of nanoparticulate delivery of DOX and TF-β1.

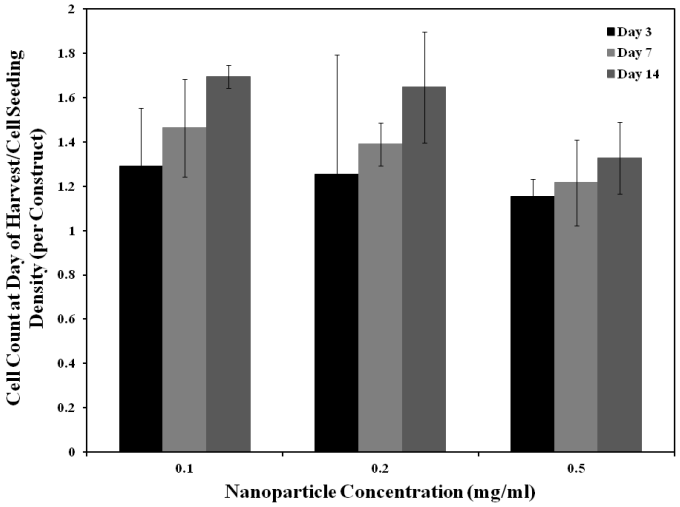

Figure 6.3: Cell density in collagen constructs with different NP concentrations, harvested at 3 time points. None of the 3 concentrations tested ha detrimental effects on proliferation rates

6.3.3. Compaction of Tissue Constructs

After 21 days, constructs in all treatment conditions were found to have a length : O.D. aspect ratio of 8.4–9.5 (**Figure 6.4)**. No significant differences were observed in the

extent of compaction between the different treatment conditions (ρ = 0.91 for both sets of NP-treated constructs, with and without factors, compared to EDC).

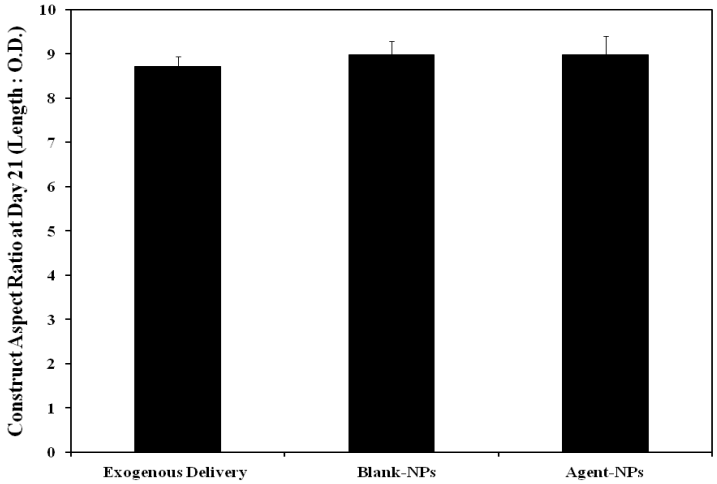

Figure 6.4: Construct compaction after 21 days of treatment. Addition of NPs did not alter aspect ratios over 21 days of treatment. Compaction was comparable among the three cases

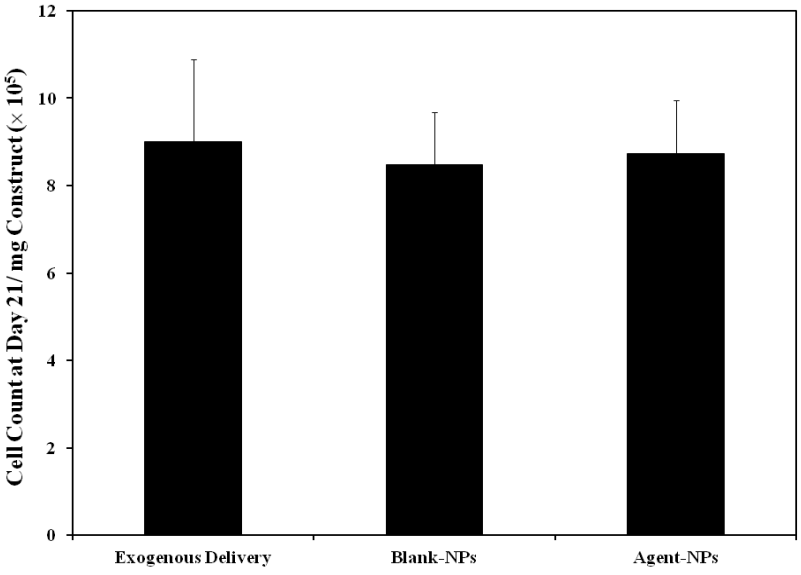

Figure 6.5: Effects of addition of NPs on cell density. No significant differences were observed in the cell densities of constructs with or without NPs

6.3.4. Cell Quantification

The cell densities after 21 days of culture were found to be similar under all treatment conditions. Addition of NPs did not seem to adversely impact cell proliferation. Average cell densities, as represented in **Figure 6.5**, were found to be around $1.5 \pm 0.25 \times 10^5$ cells/mg construct. No significant differences were observed compared to EDC ($\rho = 0.93$ for BNP, and 0.22 for ANP).

6.3.5. Analysis of SMC Markers

RT-PCR was performed to evaluate the mRNA expressions of SMA and caldesmon, the contractile SMC markers, and osteopontin, the synthetic/activated SMC phenotypic marker (**Figure 6.6**). Expression of the contractile markers was found to be maintained even with the addition of NPs compared to EDC ($\rho = 0.97$ and 0.93 for SMA, and 0.99 for caldesmon, for BNP and ANP). Osteopontin expression was also not elevated with the addition of NPs, and was not found to be statistically different from EDC ($\rho = 0.08$ for BNP and 0.07 for ANP).

Western blotting was performed to estimate the differences in synthesis of various proteins that indicated the maintenance of a contractile, non-activated phenotype of SMCs over the 21 day period– SMA, calponin, caldesmon, SM22α and MHC (**Figure 6.7**). For 10 μg protein concentrations, band intensities for all the contractile markers relative to their β-actin band intensities were found to be similar in all 3 treatment conditions. This demonstrates that a healthy contractile phenotype of cells was

maintained despite the addition of NPs, with or without the active agents (DOX and TGF-β1).

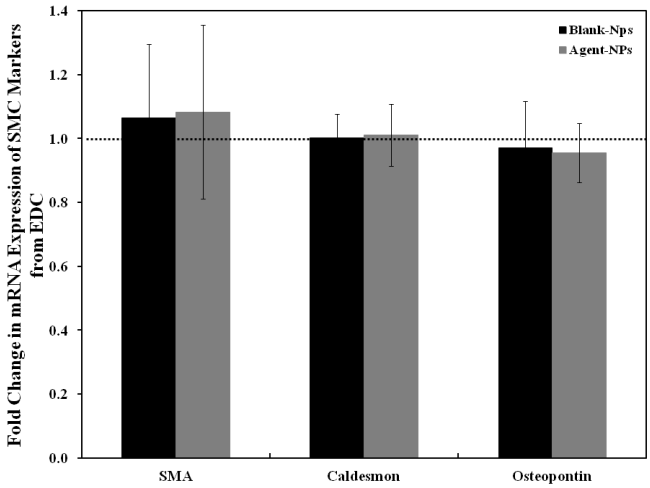

Figure 6.6: Effects of NP addition on SMC phenotypic response. mRNA expressions of SMC phenotypic markers SMA, caldesmon and osteopontin remained comparable to EDC constructs

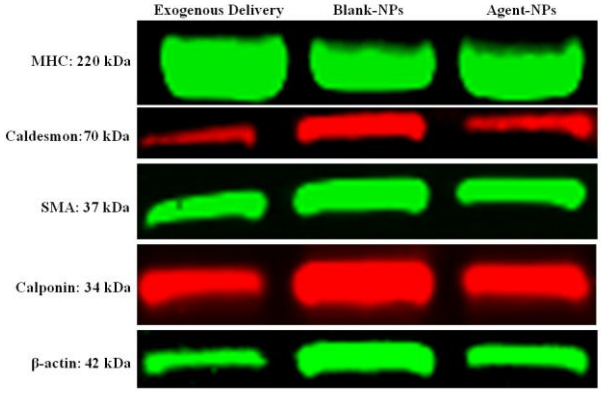

Figure 6.7: SMC phenotypic marker expression in response to NP delivery. Representative western blots of contractile SMC phenotypic markers indicate that phenotypic behavior of SMC was not altered by the addition of NPs

6.3.6. Elastic Matrix Content

The mRNA expressions of various genes corresponding to proteins constituting the elastic matrix were determined using RT-PCR –elastin, fibrillin-1, fibulin-5 and LOX (**Figure 6.8**). mRNA expression of elastin was decreased 3 ± 0.1 -fold ($\rho < 0.001$) in

BNP constructs compared to EDC. This decrease was significantly bridged in ANP constructs (ρ = 0.002 compared to BNPs), which showed only a 10% decrease in elastin expression compared to EDC. Statistical comparison of elastin expression between exogenous and NP delivery of agents revealed no significant differences (ρ = 0.512). Similar trends were seen in differences in mRNA expressions of fibrillin-1 and fibulin-4. Expression of these genes were decreased up to 4-fold in constructs with Blank NPs ($\rho <$ 0.001 compared to exogenous control for both genes). ANP constructs showed similar expression levels of fibulin-4 (ρ = 0.99), and a slight decrease in fibrillin-1 expression (1.5 ± 0.1 -fold, $\rho < 0.001$) compared to EDC constructs. The mRNA expression of LOX on the other hand, showed higher expression for both sets of constructs treated with NPs compared to EDC. While this difference was not significant in BNP constructs (1.5 ± 0.3 -fold compared to exogenous controls, ρ = 0.16), the 1.7 ± 0.5 -fold increase within ANPs was statistically significant compared to EDC (ρ = 0.05). In addition to gene expression of the above elastic matrix proteins, mRNA expression of collagen-1 was also estimated in the different treatment conditions. A slight decrease in collagen-1 expression compared to EDC was observed in constructs treated with NPs, but this decrease was statistically insignificant (ρ = 0.1 for BNP constructs and 0.19 for ANPs).

A Fastin assay was performed to estimate the elastic matrix content in terms of alkali –soluble and –insoluble elastin within the 3 sets of constructs (**Figure 6.9**). Alkali–soluble matrix elastin content within ANP constructs (20.01 ± 1.81 μg/mg) were found to be similar to that in EDC controls (20.97 ± 1.87 μg/mg, ρ = 0.73). These levels were significantly greater (up to 2-fold) than in BNP construct (9.62 ± 2.34 μg/mg, $\rho < 0.001$

compared to exogenous treatment controls). On the other hand, quantities of alkali–insoluble matrix elastin was found to be barely above the detection limits of the assay kit within the sample volumes tested (around 0.5 μg/mg for all 3 conditions). They were statistically insignificant between the 3 conditions (ρ = 0.98 for BNP constructs and 0.64 for ANP, compared to EDC).

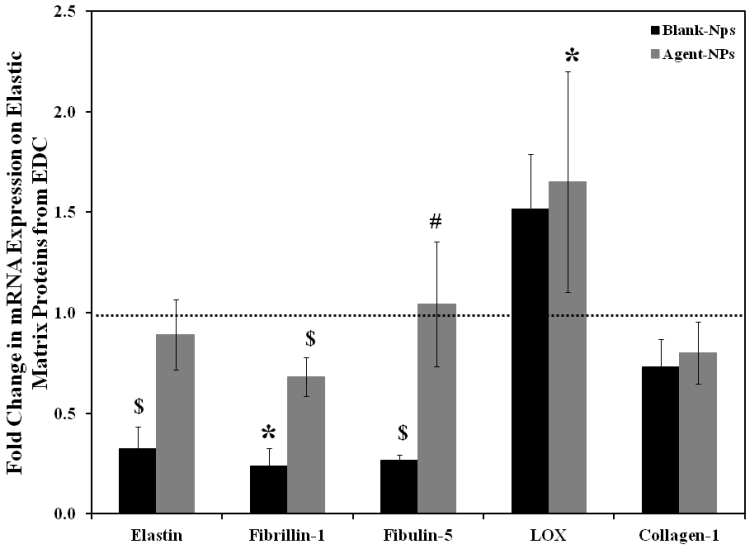

Figure 6.8: Effects of NP based delivery on mRNA expressions of elastic matrix proteins- elastin, fibrillin-1, fibulin-5, LOX and collagen-1. Expression of LOX was elevated in both BNP and ANP constructs. Expression of elastin was comparable between the 2 delivery modes, and that of fibrillin and fibulin was moderately lowered. '*' represents significant difference from EDC, '#' from BNP and '$' from every treatment condition for $p < 0.05$

Western blotting was performed to estimate the levels of LOX, fibrillin-1 and fibulin-4. As seen in **Figure 6.10**, band intensities of LOX protein were found to be significantly higher in the constructs treated with NPs, both blank and agent-loaded, compared to EDC. Their intensities for treatment controls in the 2 subsequent biological replicates were too low to be reliably quantified. Therefore statistical comparison

representing differences in LOX protein content have not been performed. At the 10 μg protein concentrations tested, fibrillin-1 and fibulin-4 were undetected.

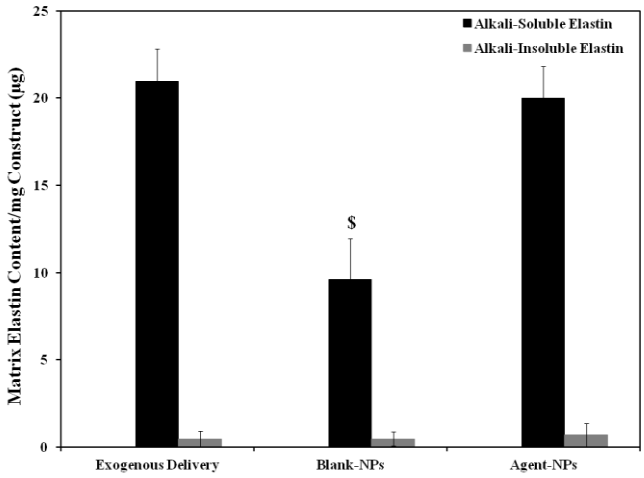

Figure 6.9: Differences in elastic matrix content between the 2 delivery modes. Elastic matrix content measured in terms of alkali -soluble and -insoluble elastin remained comparable between NP-based and exogenous delivery of agents. '$' represents significant difference from every treatment condition for $p < 0.05$

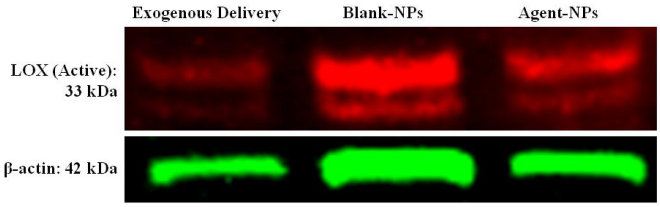

Figure 6.10: Effects of NP-based delivery on LOX protein content. Representative western blot of LOX protein in the 3 treatment conditions. LOX content appears to be significantly elevated by the addition of NPs, both in BNP and ANP constructs, relative to EDC.

6.3.7. Analysis of MMPs -2 and -9

Gene expressions of the 2 gelatinases MMP-2 and -9 were determined using RT-PCR. As seen in **Figure 6.11**, MMP-2 gene expression was significantly increased with

the addition of NPs. Constructs with Blank NPs showed an average of 4.25 ± 0.6 -fold increase in MMP–2 expression compared to EDC ($\rho < 0.001$). The addition of factors within NPs lowered this expression 1.8-fold compared to Blank NPs ($\rho < 0.001$). MMP–2 expression was 2.4 ± 0.3 -fold higher in ANP compared to EDC ($\rho < 0.001$). On the other hand, expression of MMP–9 was decreased in both sets of constructs treated with NPs. However this decrease was not statistically significant ($\rho = 0.06$ for BNP constructs, and 0.18 for ANP). It is important to note that the Ct values for MMP–9 were only slightly above the reliable detection limits of the instrument for the cDNA concentrations tested. MMP-2 gene expression was in general much higher than that for MMP-9.

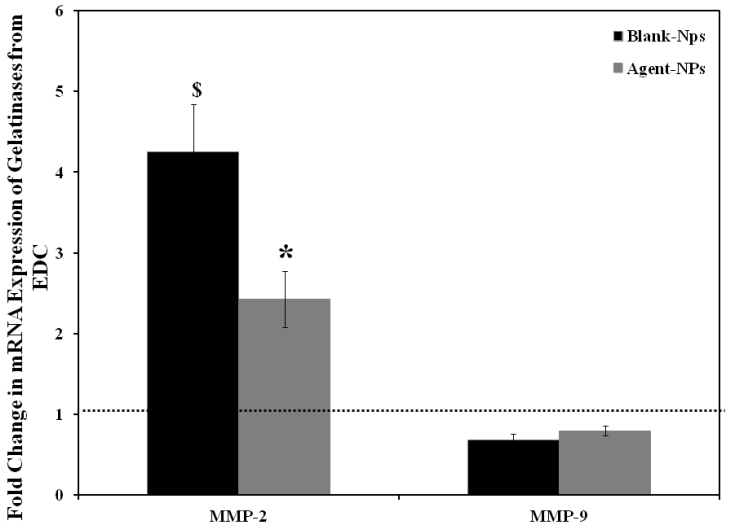

Figure 6.11: Outcomes in mRNA expression of MMPs -2 and -9 with delivery mode. A significant upregulation in MMP-2 is seen with the incorporation of NPs, while MMP-9 expression appears to have been suppressed. '*' represents significant difference from EDC, '$' with every treatment condition, for $p < 0.05$

Western blotting was performed to estimate the amount of MMP protein present in the constructs. As seen in **Figures 6.12 A and C**, the zymogen form of MMP–2

corresponding to the 72 kDa bands, was found to be lower in BNP constructs compared to other 2 treatment conditions (3 ± 0.9 -fold compared to EDC, $\rho = 0.03$). Differences in band intensities between the 2 sets of constructs with NPs, with and without factors, were found to be insignificant ($\rho = 0.19$). In contrast, the band intensities for active MMP–2 enzyme corresponding to 66 kDa were found to be higher in both sets of NP-treated constructs (1.7 ± 0.4 fold increase, $\rho = 0.05$ for BNP constructs, compared to EDC). No statistical difference in band intensities of active MMP–2 between exogenous and NP delivery of factors was observed (1.5 ± 0.4 fold increase, $\rho = 0.27$ for Factor-NPs).

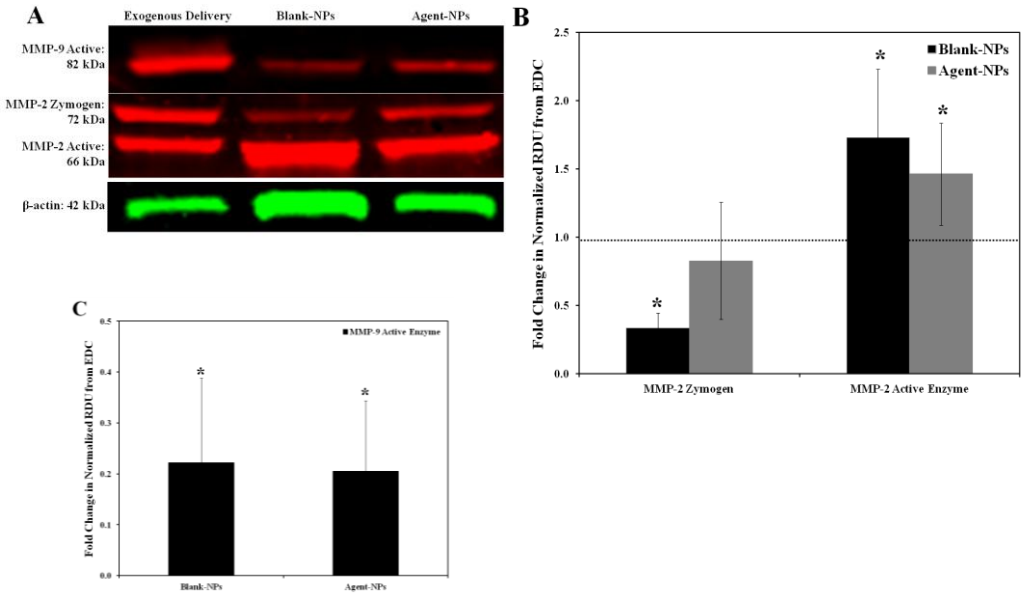

Figure 6.12: Outcomes in protein quantities of MMPs -2 and -9 in response to agent delivery mode. (A) Representative immunoblots of MMPs -2 and -9 along with normalizing protein β-actin. Semi-quantificatitative comparison of zymogen and active forms of MMP-2 protein (B) show an increase relative to EDC. However incorporation of agents within NPs appears to have brought down these levels relative to BNP. However, and MMP-9 active enzyme (C) levels are significantly attenuated with the addition of NPs.

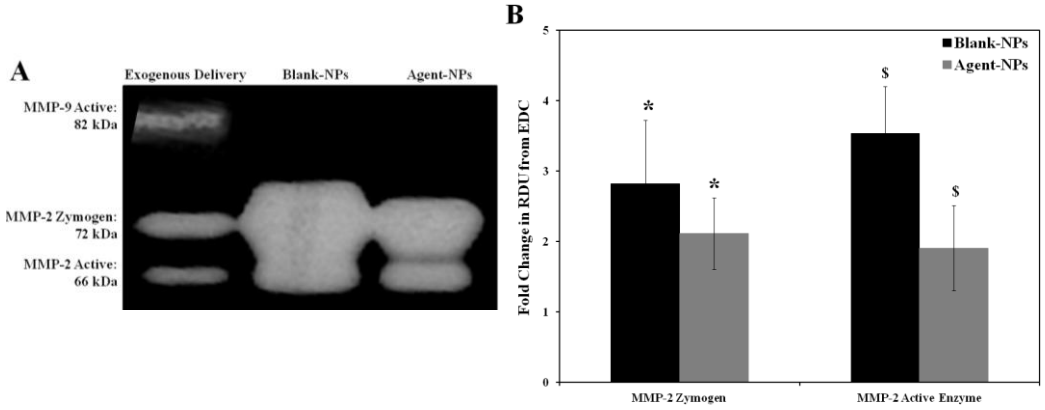

Figure 6.13: Zymography of MMPs -2 and -9. (A) Representative zymograms showing both active and inactive forms of MMP-2 enzyme, and only active form of MMP-9 enzyme. (B) Semi-quantitative comparison of zymogen and active forms of MMP-2

On the other hand, as seen in **Figures 6.12 B and C** band intensities corresponding to the 82 kDa active MMP–9 enzyme were found to be significantly decreased to similar extents in both sets of NP-treated constructs compared to exogenous supplementation (4.5-fold with $\rho = 0.001$ for both NP-treated constructs with and without agents). Zymogen forms of MMP–9 protein were undetected at the concentrations tested.

Zymography was performed to estimate the activity of the gelatinases present in the constructs (**Figure 6.13**). The enzyme activity of MMP–2 was found to be significantly elevated in the constructs with NPs compared to EDC. A 2.8 ± 0.9 fold increase ($\rho = 0.03$) in MMP–2 zymogen, and 3.5 ± 0.5 fold increase ($\rho = 0.001$) in active enzyme was found in BNP constructs compared to EDC. This activity was decreased with the delivery of agents in ANP constructs, where up to a 2-fold increase was found in the intensities of both zymogen ($\rho = 0.2$) and active enzyme ($\rho = 0.01$), compared to EDC. On the other hand, as seen in **Figure 6.13 A** and **B**, at the protein concentrations

tested, bands corresponding to active MMP–9 enzyme were detected only in EDC constructs. They were not detected in either of the NP-treated constructs in any of the 3 biological replicates tested. Zymogen bands of MMP–9 enzyme were undetected in all 3 conditions.

6.3.8. Matrix Ultrastructure

Elastic matrix components elastin and fibrillin-1 were immunolabeled in 10 μm cross and longitudinal sections of the 3 treatment conditions, and visualized using a fluorescence microscope under a Cy5 filter. As seen in **Figures 6.14** and **6.15**, cells and elastic matrix fibers appeared to be far more oriented in the longitudinal direction than circumferentially, in all treatment conditions. Signs of circumferential orientation were observed in the regions closer to the lumen of the constructs. Clumps of elastin and fibrillin were found in both cross and longitudinal sections, indicating that the synthesized fibers might be oriented in all directions. Elastin and fibrillin appeared to be mostly co-localized. Appearance and orientation of elastic fibers as seen in IF, were confirmed in the 30 μm sections that were stained for elastin using a modified VVG staining kit. Elastic matrix was undetected in the longitudinal sections imaged using TEM.

6.4. DISCUSSION

In studies discussed in the previous chapters, and in prior work conducted in our lab, we have demonstrated the elastogenic inductibility of adult vascular SMCs by various exogenously supplemented EFs (TGF-β and HA-o)[37, 173, 184]. While the use of

these EFs have shown tremendous potential in stimulating *de novo* synthesis of elastic matrix in culture, it is important to evaluate strategies for their controlled and sustained delivery in a localized manner for final clinical application of regenerative repair of elastic matrix at sites of proteolytic disease such as AAA.

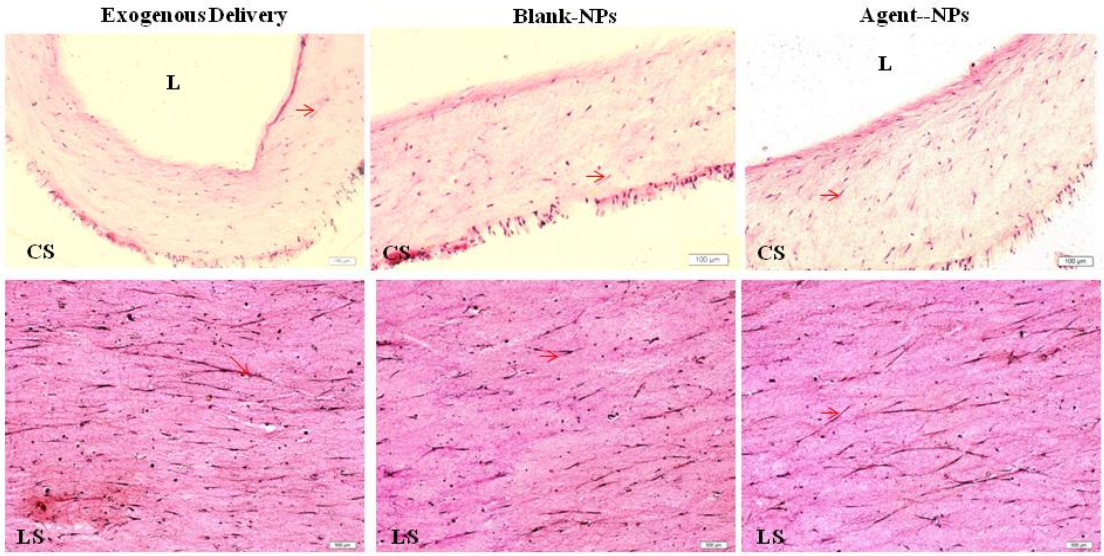

Figure 6.14: Representative images of Elastic staining of 30 μm thick cross- (CS) and longitudinal- (LS) sections of collagen (stained pink) constructs after 21 days of treatment. Orientation of cells and elastic fibers (stained purple/black, indicated by red arrows) seen in the logitunal direction. Cells and matrix appear to orient in the circumferential direction closer to the lumen (L) in the corss-sections

This evaluation is crucial especially since the outcomes of factors we have evaluated in our studies are highly dose-dependent. For example, the regulatory effects of growth factors like TGF-β are critically dependent on precise control of delivered dose as they can induce extremely contrasting outcomes depending on the concentration[220]. While at concentrations below 10 ng/ml, it can suppress abnormal cell proliferation and aid in synthesis and assembly of elastin and elastic matrix components[37, 262], at higher concentrations it can induce a synthetic, osteogenic switch of SMC phenotype and induce

rapid calcification[139]. Moreover, the outcomes of TGF-β supplementation is also highly site dependent[185]. For example, while the use of TGF-β has positively influenced elastic matrix synthesis by SMCs from AAA disease models, TGF-β at similar concentrations has been shown to adversely impact thoracic AAs[60-61]. In fact, the use of TGF-β antagonists such as losartan has been shown to regress thoracic AAs[263-264].

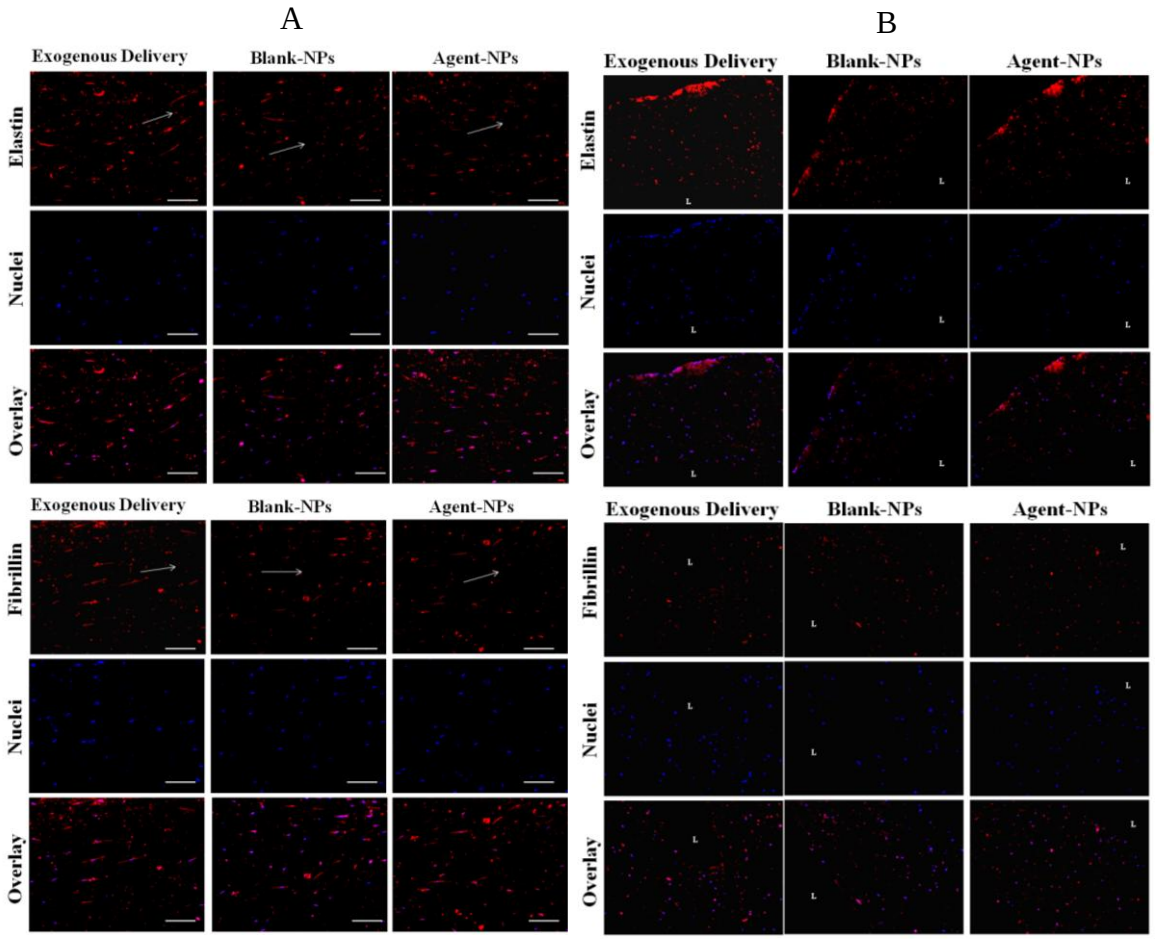

Figure 6.15: Effect of agent delivery mode on outcomes of elastic matrix assembly and ultrastructure. Representative fluorescent micrographs of 10 µm thick (A) longitudinal- and (B) cross –sections of constructs immunolabeled for elastin (red, top panel), fibrillin (red, bottom panel) and nuclei (blue). All three treatment conditions showed detectable levels of both proteins. Both fibrillin and elastin distribution appears comparable between EDC and ANP constructs. Orientation in the longitudinal direction appeared more than circumferentially. **White arrows indicate longitudinal direction of constructs**. 'L' = lumen. Magnification = 10 ×

Several studies have also demonstrated substantial benefits in therapeutic outcomes of localized, controlled delivery of factors over systemic delivery. For example, many groups have evaluated various localized delivery methods for DOX, and have shown pronounced decrease in MMP activity and preservation of elastic matrix at concentrations even 100 fold lower than that used for systemic delivery[243, 253]. This has the potential to overcome several undesirable side effects of systemic delivery of DOX for AAA treatment[242, 245]. Moreover, systemic inhibition of MMPs is undesirable since they participate in normal matrix remodeling and turnover as well[83].

In the current study, we have therefore utilized the tubular collagen model optimized in the previous chapters, to evaluate the outcomes of localized delivery of DOX and TGF-β from nanoparticles, over their exogenous delivery. This *in vitro* model allowed the benefits of assessing the direct response of SMCs to polymer-based delivery of previously optimized elastogenic factors in a controlled microenvironment. PLGA (50:50 blend) chosen as the polymeric nano-carrier of factors, offers several benefits as an ideal drug delivery vehicle.

PLGA is one of the most biocompatible polymers widely used for a variety of drug delivery applications[265-267]. It undergoes hydrolytic degradation into lactic acid and glycolic acid, which have not shown to induce adverse cell response, both *in vivo* and *in vitro*[259, 268]. PLGA is also easy to formulate and characterize[258], and has been shown to be compatible for delivery of both DOX[269-270] and TGF-β[271-272]. It is also one of the very few biomaterials approved by FDA for a variety of clinical applications[265].

The surface charge of nanoparticles has shown to play a role in mediating the bioavailability of factors as well as in regulating cellular response, both *in vitro* and *in vivo*. Various studies have pointed towards the benefits of utilizing cationically surface-charged nanoparticles for vascular applications[213-214], especially from the standpoint of enhancing elastic matrix deposition. It has been suggested that the presence of cationic amphiphiles attract the negatively charged LOX molecules, while at the same time repel positively charged elastases[215]. This has been further illustrated in studies that have utilized cationic amphiphiles such as DMAB which were shown to increase LOX protein synthesis and significantly suppress expression and activity of proteases such as MMPs -2 and -9[216, 273]. In the current study, we thus initially formulated and tested DMAB-modified PLGA NPs. However, the concentration of TGF-β1 released from these NPs was extremely low, possibly due to interaction between the DMAB particles and the growth factor. However, we were able to overcome this problem and obtain detectable and consistent quantities of TGF-β1 released from anionically modified NPs. Accordingly, in this study we have utilized anionic nanoparticles for the delivery of both DOX and TGF-β1. While surface charge modification did not affect DOX release profiles, DOX-loaded NPs were also synthesized using PVA to maintain consistency between the NPs releasing both these agents.

Likely due to their failure to repel elastases, anionic NPs (both with and without agents) resulted in a marked increase in the mRNA expression, protein synthesis as well as enzyme activity of MMP–2. However, it was also observed that the delivery of agents from the NPs resulted in a marked decrease in overall MMP–2 mRNA expression relative

to BNP constructs, and a decrease in protein content of active MMP-2 enzyme to levels seen in EDC constructs, This suggests a positive influence of addition of agent-loaded NPs. The MMP-2 enzyme activity was similarly lowered in ANP constructs compared to BNP constructs, but remained higher than those with exogenous factor treatment.

In contrast however, the mRNA expression, total protein content and enzyme activity of MMP-9 was found to be significantly lowered with the addition of NPs, with or without agents. Zymogen bands for MMP-9 enzyme were completely undetected in both sets of the NP-treated constructs. In addition to this, the lack of difference in the MMP-9 protein levels, as seen in immunoblots (**Figure 6.10**) between blank and agent-loaded NPs suggests that MMP-9 inhibition may be influenced significantly more by the PVA-modified anionic NPs, than the addition of agents. This finding is contrary to what has been suggested in the literature regarding the positive influence of cationic amphiphiles for elastic matrix deposition, and therefore in corollary a negative influence of anionic amphiphiles.

On the same lines, LOX protein content was found to be significantly higher in constructs treated with NPs, both with or without agents. Protein bands corresponding to LOX in our immunoblots showed extremely low to negligent quantities in constructs with exogenous factor delivery. This was consistent with the mRNA expression of LOX, which also showed higher expression in constructs with NPs. While mRNA expression was not significantly different between BNP and EDC, their comparable expression levels combined with the significantly higher levels of active LOX protein within NP-treated constructs seems to suggest that LOX production is also somehow triggered by

the PVA modified NPs. It is likely that the decrease in MMP-9 mRNA expression as well as its diminished enzymatic activity has in a way improved LOX protein availability. To our knowledge, no direct correlation between MMP-9 inhibition or LOX up-regulation with the use of PLGA NPs or its surface modification with anionic amphiphiles has been reported in literature so far. Further investigation in is regard is warranted and its understanding would definitely help improve targeted *in situ* matrix repair strategies.

Similarly, alkali-soluble matrix elastin content was found to be similar in both exogenous and NPs delivery of factors. While these levels were 2 fold lower in constructs with Blank-NPs, it is important to note that the ~ 9 μg/mg levels of alkali-soluble matrix elastin content was similar to that observed in constructs evaluated in the previous chapters that were cultured without EFs or DOX. This contrasting observation however, seems similar to proposed physical effects of Hyaluronic acid (HA) in elastic matrix assembly[274-275]. Native HA is a highly anionic glycosaminoglycan (GAG) present in the ECM of various tissues[95]. It facilitates synthesis of fibrillin microfibrils and directs elastic fiber assembly by binding versican (a proteoglycan) with elastin-associated proteins[42, 160]. HA also appears to stabilize elastin fibers against elastase degradation, once formed[43]. In addition to this, HA is known to enhance formation of mature matrix elastin by 1) coacervating soluble tropoelastin via their positive lysine residues and 2) facilitating lysyl oxidase (LOX)-mediated oxidation and crosslinking of tropoelastin into insoluble elastic fibers[42-43]. Studies from our lab have also confirmed such up-regulation and demonstrated elastogenic synergy between HA oligomers (~ 756 Da) and growth factors such as TGF-β1[37, 44]. It is likely that the anionic NPs behave in a manner similar to anionic HA.

However, despite the increase in LOX content and comparable levels of alkali-soluble matrix elastin, the mature alkali-insoluble matrix elastin content was found to be extremely low and statistically similar under all treatment conditions. This is likely due to the low mRNA expressions of fibrillin-1 and fibulin-4, the microfibrillar proteins key to elastic fiber assembly, combined with the high expression and enzymatic activity of MMP-2. The low alkali-insoluble matrix elastin yields could also be contributed by the fact that the concentration of TGF-β1 delivered in this study was ~ 10 fold less than that we previously showed to be elastogenic. Concurrently, analysis of matrix ultrastructure of constructs did not reveal obvious differences between the three treatment conditions. Similar to that observed in **Chapters 4** and **5**, the ultrastructure of all constructs showed a higher degree of longitudinal orientation than circumferential alignment, again likely due the application of low strains. Circumferential alignment of cells and matrix were found in regions closer to the lumen of the constructs.

Addition of NPs did not adversely affect cell proliferation or the expression of contractile phenotypic markers of SMC. These levels were comparable in all treatment conditions.

One of the limitations of this study was the lack of direct visualization of NPs in the cultured constructs, since they were not tagged with any dyes in order to minimize the effects of any external influences. NPs were assumed to be retained in the constructs based on the pilot study performed with DMAB NPs at similar concentrations. Moreover, the significant differences in results which were consistent across all experimental methods analyzed, suggest that the NPs were retained and that the factors released from

NPs were bio-available and bioactive. Culturing an additional set of constructs with NPs loaded with vital dyes, in parallel and under similar culture conditions detailed in this study would help in providing a visual distribution of NPs in the constructs. This would also help in better understanding of NP behavior such as its retention and degradation profiles within such a collagenous microenvironment.

Another limitation of this study at present is the lack of knowledge of accurate release profiles of the factors from NPs within the collagen constructs. While PLGA is known to undergo only hydrolytic degradation, and therefore their release profiles can be expected to be similar within different aqueous environments at similar pH, studies have indicated that degradation of PLGA can be accelerated by the presence of enzymes in serum and that released by cells in culture[276-277]. However, there is lack of consistency and clarity with respect to enzymatic degradation of PLGA. Degradation of PLGA, and generation of acidic pH is also known further increase polymeric degradation[278]. However, the frequent media change performed every 2 days can aid in minimizing the effects of increase in pH. Therefore a certain level of inequality in concentrations of factors delivered exogenously and via NPs in this study is bound to exist. A more systematic analysis of properties of NP-treated constructs, the concentration of un-released agents retained within NPs at the end of culture period, and examining its degradation profiles over a time-dependent manner would aid in normalizing these uncertainties and help in developing more efficient strategies for elastogenic response by adult cells.

6.5. Conclusions

Treatment of HASMCs within tubular collagen constructs with DOX- and TGF-β1- loaded PLGA NPs positively influenced overall elastogenic outcomes. Addition of NPs, both with and without factors did not adversely affect cell proliferation or expression of contractile SMA phenotype, compared to exogenously agent-treated constructs. The agents released from the NPs were found to be bioactive, as warranted by the positive differences in results obtained between agent-loaded and no-agent NPs, primarily in terms of elastic matrix outcomes. While the mRNA expression of elastic matrix proteins such as elastin and fibrillin-1 were less with NP-delivery compared to exogenous delivery, the quantity of alkali-soluble matrix elastin synthesized by cells under both conditions was comparable. Levels of insoluble elastin were uniformly low under all treatment conditions. LOX mRNA expression as well as active protein quantities were significantly elevated in NP-treated constructs, both with and without agents. Similarly, mRNA expression, protein synthesis as well as enzyme activity of MMP-9 was significantly suppressed within both NP-treated constructs, with and without agents. Expression and activity of MMP-2 on the other seemed to be elevated with the addition of NPs. The level of expression and enzyme activity was however lowed in constructs with agent-loaded NPs compared to those with blank NPs, indicating bioactivity of encapsulated agents.

Overall, this model demonstrates that the effects of agents delivered from PLGA NPs appeared to be comparable to their exogenously delivery, warranting that further

studies with similar strategies can greatly benefit *in situ* elastic matrix repair within diseased tissues such as AAAs.

CHAPTER SEVEN

CONCLUSIONS AND FUTURE OUTLOOK

7.1. OVERALL CONCLUSIONS

The concurrent delivery of TGF-β1 and HA-o to adult SMC cultures evaluated in previous studies in our lab has successfully demonstrated the elastogenic potential of these factors. However, cells, especially SMCs behave very differently in a 2D cell culture environment, where their response to external stimuli is often different from that seen *in vivo*. The overall goal of this thesis was to therefore develop an *in vitro* model system, where cellular response to induced elastogenesis will be similar to what can be replicated *in vivo*. The presence of a collagenous matrix is centric to replicating vascular tissue architecture and mechanics, and vascular cells, regardless of the choice of scaffolds, robustly synthesize collagen. Moreover, collagenous microenvironments are known to promote a quiescent phenotype, similar to that seen *in vivo*, which is often not conducive to elastogenesis. Examining the impact of a pre-existing collagenous microenvironment on the ability of the cells to synthesize fibrous elastic matrix on their own, and also their response to provided elastogenic factors, would be pertinent for a relevant *in vitro* system. We therefore chose a 3D collagen gel model, widely been evaluated for vascular tissue engineering applications.

In the first set of studies, we demonstrated that the elastogenic potential of TGF-β1 - HA-o combination could be replicated within RASMCs seeded in 3D collagen gels, maintained under static tension. We tested six dose combinations - 0.1 ng/ml, 1 ng/ml

and 10 ng/ml TGF-β, each with 0.2 μg/ml and 2 μg/ml HA-o, which were exogenously supplemented to RASMCs within 3D collagen constructs. Relative to untreated control, all constructs receiving the doses were found to induce elastogenesis. While mRNA expression of elastin remained unchanged relative to control, all 6 dose combinations up-regulated mRNA expression of LOX, with highest of up to 2-fold being in constructs with 10 ng/ml TGF-β, with both doses of HA-o. Similarly, while tropoelastin protein quantities in all cases were comparable to untreated controls, significant increase was seen in the presence of alkali-soluble matrix elastin. Highest quantities of the alkali-soluble matrix elastin content were seen in constructs receiving 0.1 ng/ml TGF-β with 0.2 μg/ml HA-o. However, quantities of the more crosslinked, alkali-insoluble matrix elastin were elevated only in constructs with 10 ng/ml TGF-β and 0.2 μg/ml HA-o treatment conditions, where LOX protein content was also moderately elevated relative to other treatment conditions (~ 1.5-fold from constructs with 0.1 ng/ml TGF-β 0.2 μg/ml HA-o). MMP-2 enzyme activity on the other hand, was elevated in all treatment conditions, which likely contributed to the low alkali-soluble matrix elastin content. MMP-9 protein content, both active and zymogen forms, was suppressed in all conditions receiving treatment, with lowest levels seen in constructs with 0.1 ng/ml and 10 ng/ml TGF-β, with respective doses of HA-o. These results were confirmed with histology and IF analysis, where a high no. of aligned elastic fibers were found in all treatment conditions, with the highest of more than 2 fold being in those with 0.1 ng/ml TGF-β and 0.2 μg/ml HA-o. However, induced elastogenesis did not have a significant impact on the mechanical properties of the constructs. Tensile modulus was comparable in the select 4 treatment

conditions that were tested (~ 60 kPa). This is likely due to the fact that the elastic fibers synthesized, though aligned, were mostly discontinuous, and were not present in their highly crosslinked, mature forms. Their contribution to the mechanical properties would therefore be very minimal. Constructs that received 0.1 ng/ml TGF-β1 and 0.2 μg/ml HA-o (termed EFs) were concluded to be most elastogenic; since they induced the synthesis of highest quantities of alkali-soluble matrix elastin as well has the highest no. of aligned fibers.

In the next set of studies, our goal was to achieve circumferential orientation of EF-treated cells and the synthesized matrix, similar to that needed *in vivo* within elastic arteries. Different from that used in the previous study, we adopted a tubular collagen gel model seeded with human SMCs. Since cyclic strains are known have profound impact towards this orientation, we developed a bioreactor capable of delivering circumferential cyclic strains to cells with the tubular collagen gels. An important consideration for the choice of cyclic strain parameters was its impact on MMP synthesis and enzyme activity, since it can negatively impact accumulation and assembly of newly synthesized elastic matrix. We therefore chose to use low strains of 2.5% which induces relatively lower levels of undesirable protease activity. These were tested under 3 frequencies of 0.5 Hz, 1.5 Hz and 3 Hz, another important parameter equally contributing to cell and matrix alignment. EFs were added to all three sets of stretched constructs over 21 days of culture, and results were compared with static tubular constructs with and without EFs. Cell densities were found to be similar under all test conditions, indicating that none of the treatment conditions adversely impacted cell growth. A bimodal trend with increasing

frequencies was observed in outcomes of contractile SMC phenotypic markers and elastic matrix components, with highest levels observed in constructs stretched under 1.5 Hz. For gene expression and protein synthesis of contractile SMC markers, change in frequency appeared to have a greater impact than addition of EFs. For example, while no changes were found in the static constructs with addition of EFs, SMA mRNA expression increased progressively up to 1.5 Hz, where it peaked at 4-fold relative to static constructs, and was lowered to 2-fold within constructs stretched at 0.5 and 3 Hz. Compared to static constructs, contractile phenotypic markers were elevated in all stretched constructs. Application of stretch at 3Hz frequency alone appeared to induce an osteogenic switch in SMCs, which showed ~ 2-fold increase in osteopontin mRNA expression relative to all other conditions.

Elastic matrix outcomes were most pronounced in constructs receiving EFs with stretch at 1.5 Hz, in terms of both mRNA expressions and matrix content. In these constructs, up to a 7-fold increase was seen in elastin mRNA expression, and up to a 5-fold increase in alkali-soluble matrix elastin content, relative to static controls. Constructs stretched at 0.5 Hz showed similar levels of gene expression and matrix outputs as that of EF-treated static constructs, which were both higher than untreated static controls. Application of strains at 3 Hz frequency did not show improvement in elastic matrix output, and its levels were comparable to that of untreated static control. Addition of EFs or strains did not significantly influence gene expressions or protein content of other elastic matrix proteins (fibrillin, fibulins and LOX), relative to control. Perhaps as a

consequence, levels of alkali-insoluble matrix content were uniformly low in all constructs.

MMP-9 gene expressions remained extremely low, but its protein content was moderately elevated at higher strain frequencies. Application of strains at all 3 frequencies did not adversely affect gene expressions or protein content of MMP-2. These levels were comparable in all constructs, both static and dynamic. While its enzyme activity was also similar in all conditions, their band intensities were extremely high even at low protein concentrations, indicating high levels of enzyme activity. This could also be a contributive factor for the low alkali-insoluble matrix elastin outcomes.

In our next set of studies, we therefore tested the supplementation of Doxycycline (DOX), along with EFs, in order to improve elastic matrix outcomes by suppressing MMP-2 enzyme activity. We tested two doses of DOX – 0.1 μM and 1 μM, along with EFs, in HASMC-seeded tubular collagen gel constructs. These doses were tested on static constructs, and those stretched at 2.5% strain at 1.5 Hz (which was shown to promote elastogenesis the most in the previous study). Addition of DOX at both doses with EFs was effective in significantly suppressing mRNA expression of MMP-2, under both static (up to 4-fold) and dynamic (up to 3-fold) conditions, relative to control. While its protein content remained unchanged relative to other conditions, MMP-2 enzyme activity was lowered to similar levels at both DOX concentrations (up to 2-fold under static and up to 1.5 fold under dynamic conditions). All DOX + EFs-treated constructs significantly increased alkali-soluble matrix content to similar levels, at both DOX concentrations, under static and dynamic conditions. Up to 3-fold increase was seen relative to static

control, and up to 2.5-fold relative to static constructs treated with EFs alone. Addition of 0.1 μM DOX with EFs significantly increased synthesis of the mature, highly crosslinked alkali-insoluble matrix elastin (up to 2-fold) relative to other treatment conditions. Its quantities were similar in all other conditions. mRNA expression and quantities of other elastic matrix components remained unchanged.

Overall, in the 3 studies discussed above we demonstrated induction of significant levels of elastogenesis in adult cells from both rat and humans. EFs, together with DOX and 2.5% cyclic strains at 1.5 Hz, significantly improved elastic matrix outcomes, both at the mRNA and protein levels. However, its translation to an *in vivo* scenario is limited by its highly dose-depended induction of outcomes. In the next set of studies we therefore examined if a targeted, nanoparticle-based delivery of these factors would induce elastogenesis to similar levels as that seen with exogenous delivery. TGF-β1 and DOX were encapsulated separately within PLGA nanoparticles (NPs), and incorporated within HASMC-seeded tubular collagen gel constructs, subjected to 2.5% strain at 1.5 Hz (ANP). These were compared to constructs with blank NPs (BNP), and those treated with exogenous supplementation of TGF-β1and DOX to culture medium, both stretched similarly (EDC). Interestingly, while gene expressions of elastin and fibulin were comparable to EDC, that of LOX was up-regulated to 1.5-fold relative to EDC. This is likely due to the presence of anionic NPs, since a moderate increase in LOX expression was seen even in BNP constructs. This was reflected at the protein levels as well, where both NP-treated constructs showed significantly larger quantities of LOX. Matrix elastin content, both alkali-soluble and –insoluble, in EDC and ANP were comparable, both 4-

fold higher than BNP constructs. Gene expression, protein content as well as enzyme activity of MMP-2 were significantly elevated in NP-treated constructs, relative to EDC. These levels however appeared to be lowered within ADC (vs. BNP), indicating that the bioactivity of encapsulated agents was maintained. In contrast however, relative to EDC, the gene expression, protein content and enzyme activity were significantly lowered in both NP-treated constructs, indicating an influence of NPs themselves. Addition of NPs did not affect cell densities or SMC phenotype, and these were comparable in all three conditions. It is important to note that these results were obtained at TGF-β1 concentrations 10-fold lower than what was optimized in the previous studies. Overall, we were able to successfully demonstrate that localized delivery of TGF-β1 and DOX is able to mirror the elastogenic benefits of their exogenous delivery, without causing any adverse effects.

One of the limitations of the studies conducted at 2.5% strain was its effects on cell and matrix orientation. They appeared to be oriented more in the longitudinal direction, than circumferentially, as was expected. At higher frequencies of 1.5 Hz and 3 Hz, higher degree of circumferential orientation was observed in regions closer to the inner silicone tubing (lumen). Perhaps as a result, compared to other conditions, these constructs also showed lesser degree of longitudinal orientation. Any contribution of the different treatment conditions to the mechanical properties of the constructs therefore is likely to be reflected more in the longitudinal direction than circumferentially. We therefore did not record any significant differences in the tensile properties (tested on constructs in second set of studies alone) tested on ring segments of the constructs treated

under different frequencies, or between static and dynamic. Regardless, we have been able to adequately demonstrate the positive influence of various factors on elastogenic induction of adult HASMCs.

Results from these studies demonstrate how even within a quiescent, collagenous environment, TGF-β1, HA-o and DOX can be utilized to induce de novo synthesis of elastic matrix. These will prove most beneficial in developing efficient strategies for *in vivo* translation of the above factors to repair and rebuild compromised elastic matrices.

7.2. FUTURE OUTLOOK

Overall results evaluated in this thesis sufficiently demonstrate positive outcomes of elastogenic induction of adult vascular cells using several parameters within a relevant *in vitro* model. However, there are several factors that can be addressed in the future studies to develop more efficient strategies for induced elastogenesis.

1) One of the primary limitations of *in vitro* induction of elastogenesis, is the insufficient synthesis of matrix elastin, especially the highly crosslinked form, in absolute quantities. While various parameters discussed in the study significantly improve these quantities relative to untreated controls, these levels are insufficient when compared to what is present *in vivo* within elastic aortae. This is perhaps also contributed to by the low levels of other elastic matrix components such fibrillin, fibulins and LOX, all of which play an equally important role in regenerating and repairing compromised elastic matrix. Strategies that target at improving outcomes of these components, in addition to that needed for elastin

synthesis, will significantly improve elastic matrix outcomes for *in vivo* applications.

2) The cyclic strains of 2.5% utilized in this study were below the 10% strains popularly used to demonstrate call and matrix orientation. We hypothesized that since strain frequencies play an equally important role in matrix alignment, lowering strains levels to suppress negative impact of strain-induced MMP activity, and at the same time testing various frequencies, would improve orientation. While we were able to effectively suppress increase in strain-induced MMP-2 enzyme activity and achieve some degree of circumferential orientation at higher frequencies, the degree of orientation is insufficient. Future studies conducted at higher strain levels, at the optimized frequency of 1.5 Hz, along with the utilization of DOX for MMP suppression, can contribute to improving elastic matrix quantities and orientation.

3) Viability of cells across the thickness of the constructs were not evaluated extensively. It is likely that the cells closer to the lumen, where the stress concentrations are higher, will be more apoptotic than those further away from it. Though results obtained from live-dead assays performed on test constructs cultured for 2 days, DNA assay after 21-day treatment, and construct compaction ratios indicate overall cell viability, they did not elucidate effect of varying stress concentrations across the construct thickness on cell viability, which is also likely to affect matrix output. Examining this parameter will be pertinent, especially when higher strain amplitudes are utilized.

4) When TE vascular grafts are implanted *in vivo,* the cells within such grafts will be subjected to both cyclic stretch (circumferential and longitudinal), as well as shear stress due to flow of blood. The bioreactor constructed in our studies was capable of delivering cyclic stretch, but did not incorporate the component of flow due to the presence of the central silicone tube. The cellular response and final matrix outcomes are therefore reflective only of effects of cyclic stretch, and not flow. In future studies, it would be pertinent to study the effects of flow along with cyclic stretch. However, directly subjecting the collagen gels to pulsatile flow without the presence of a central supporting mandrel can have 2 adverse consequences,1) irreversible creep of viscous, and insufficiently contracted gels, and 2) apoptotic response of SMCs to shear stress which would in turn compromise sufficient synthesis of elastic matrix. Incorporating the parameter of flow after the gels have substantially contracted and have synthesized elastic matrix over 3 weeks, will overcome the above consequences, while at the same time also reflect on the effects of shear on TE vascular grafts.

5) If the future direction of this work is towards developing purely tissue-engineered strategies for vascular matrix repair, or even to better understand cell-regulatory factors in induced elastogenesis, pre-aligned scaffolds such as electrospun tubular collagen can be utilized. Similar parameters of strain, frequency, and EF and Dox delivery optimized in this thesis can be then be applied. This would be an alternative to improve cell and matrix orientation at low strains, and at the same time suppress MMP-induced elastic matrix degradation.

6) In the studies utilizing NP-delivery of factors, we were able to demonstrate how localized delivery mirrors effects of exogenous delivery. However, the release kinetics of factors from NPs in a serum-rich, cellular, and hydrogel/collagenous environment is poorly understood. Studies conducted in a time-dependent manner to better understand release kinetics in such an environment would profoundly help in efficiently strategizing better delivery vehicles that can induce optimum cellular response. NP-based delivery and in-situ repair is a great strategy for inducing elastogenesis *in vivo*. Better understanding of parameters that contribute to their outcomes can therefore prove advantageous and profitable for future applications.

REFERENCES

1. Rodgers UR, Weiss AS. Cellular interactions with elastin. Pathologie Biologie2005 Sep;53(7):390-8.

2. Li DY, Brooke B, Davis EC, Mecham RP, Sorensen LK, Boak BB, Eichwald E, Keating MT. Elastin is an essential determinant of arterial morphogenesis. Nature1998 May 21;393(6682):276-80.

3. Rosenbloom J, Abrams WR, Mecham R. Extracellular matrix 4: the elastic fiber. FASEB J1993 Oct;7(13):1208-18.

4. Kelleher CM, McLean SE, Mecham RP. Vascular extracellular matrix and aortic development. Curr Top Dev Biol2004;62:153-88.

5. Wagenseil JE, Mecham RP. Vascular extracellular matrix and arterial mechanics. Physiol Rev2009 Jul;89(3):957-89.

6. Kozel BA, Rongish BJ, Czirok A, Zach J, Little CD, Davis EC, Knutsen RH, Wagenseil JE, Levy MA, Mecham RP. Elastic fiber formation: a dynamic view of extracellular matrix assembly using timer reporters. J Cell Physiol2006 Apr;207(1):87-96.

7. Pasquali-Ronchetti I, Baccarani-Contri M. Elastic fiber during development and aging. Microsc Res Tech1997 Aug 15;38(4):428-35.

8. Wagenseil JE, Mecham RP. New insights into elastic fiber assembly. Birth Defects Res C Embryo Today2007 Dec;81(4):229-40.

9. Faury G, Pezet M, Knutsen RH, Boyle WA, Heximer SP, McLean SE, Minkes RK, Blumer KJ, Kovacs A, Kelly DP, Li DY, Starcher B, Mecham RP. Developmental adaptation of the mouse cardiovascular system to elastin haploinsufficiency. J Clin Invest2003 Nov;112(9):1419-28.

10. Patel A, Fine B, Sandig M, Mequanint K. Elastin biosynthesis: The missing link in tissue-engineered blood vessels. Cardiovasc Res2006 Jul 1;71(1):40-9.

11. Nordon IM, Hinchliffe RJ, Loftus IM, Thompson MM. Pathophysiology and epidemiology of abdominal aortic aneurysms. Nat Rev Cardiol2011 Feb;8(2):92-102.

12. Keeling WB, Armstrong PA, Stone PA, Bandyk DF, Shames ML. An overview of matrix metalloproteinases in the pathogenesis and treatment of abdominal aortic aneurysms. Vasc Endovascular Surg2005 Nov-Dec;39(6):457-64.

13. The Molecular Biology and Pathology of Elastic Tissues. Symposium proceedings. Nairobi, Kenya, 1-3 November 1994. Ciba Found Symp1995;192:1-361.

14. Kielty CM. Elastic fibres in health and disease. Expert Rev Mol Med2006;8(19):1-23.

15. Milewicz DM, Urban Z, Boyd C. Genetic disorders of the elastic fiber system. Matrix Biol2000 Nov;19(6):471-80.

16. Daugherty A, Cassis LA. Mechanisms of abdominal aortic aneurysm formation. Curr Atheroscler Rep2002 May;4(3):222-7.

17. Aggarwal S, Qamar A, Sharma V, Sharma A. Abdominal aortic aneurysm: A comprehensive review. Exp Clin Cardiol2011 Spring;16(1):11-5.

18. Li DY, Brooke B, Davis EC, Mecham RP, Sorensen LK, Boak BB, Eichwald E, Keating MT. Elastin is an essential determinant of arterial morphogenesis. Nature1998 May 21;393(6682):276-80.

19. Karnik SK, Brooke BS, Bayes-Genis A, Sorensen L, Wythe JD, Schwartz RS, Keating MT, Li DY. A critical role for elastin signaling in vascular morphogenesis and disease. Development2003 Jan;130(2):411-23.

20. Rentschler M, Baxter BT. Pharmacological approaches to prevent abdominal aortic aneurysm enlargement and rupture. Ann N Y Acad Sci2006 Nov;1085:39-46.

21. McPhee JT, Hill JS, Eslami MH. The impact of gender on presentation, therapy, and mortality of abdominal aortic aneurysm in the United States, 2001-2004. J Vasc Surg2007 May;45(5):891-9.

22. Rabkin DJ. Techniques in Vascular and Interventional Radiology. Introduction. Tech Vasc Interv Radiol2008 Sep;11(3):155.

23. Wilt TJ, Lederle FA, Macdonald R, Jonk YC, Rector TS, Kane RL. Comparison of endovascular and open surgical repairs for abdominal aortic aneurysm. Evid Rep Technol Assess (Full Rep)2006 Aug(144):1-113.

24. Salacinski HJ, Goldner S, Giudiceandrea A, Hamilton G, Seifalian AM, Edwards A, Carson RJ. The mechanical behavior of vascular grafts: a review. J Biomater Appl2001 Jan;15(3):241-78.

25. Droc I, Raithel D, Calinescu FB. Endovascular treatment of abdominal aortic aneurysms: indications and results. Minim Invasive Ther Allied Technol2011 Apr;20(2):117-24.

26. Lederle FA, Freischlag JA, Kyriakides TC, Padberg FT, Jr., Matsumura JS, Kohler TR, Lin PH, Jean-Claude JM, Cikrit DF, Swanson KM, Peduzzi PN. Outcomes following endovascular vs open repair of abdominal aortic aneurysm: a randomized trial. JAMA2009 Oct 14;302(14):1535-42.

27. Mitchell SL, Niklason LE. Requirements for growing tissue-engineered vascular grafts. Cardiovasc Pathol2003 Mar-Apr;12(2):59-64.

28. Long JL, Tranquillo RT. Elastic fiber production in cardiovascular tissue-equivalents. Matrix Biol2003 Jun;22(4):339-50.

29. L'Heureux N, Paquet S, Labbe R, Germain L, Auger FA. A completely biological tissue-engineered human blood vessel. FASEB J1998 Jan;12(1):47-56.

30. Kim BS, Mooney DJ. Engineering smooth muscle tissue with a predefined structure. J Biomed Mater Res1998 Aug;41(2):322-32.

31. Shaikh FM, Callanan A, Kavanagh EG, Burke PE, Grace PA, McGloughlin TM. Fibrin: a natural biodegradable scaffold in vascular tissue engineering. Cells Tissues Organs2008;188(4):333-46.

32. Swartz DD, Russell JA, Andreadis ST. Engineering of fibrin-based functional and implantable small-diameter blood vessels. Am J Physiol Heart Circ Physiol2005 Mar;288(3):H1451-60.

33. Zhang X, Baughman CB, Kaplan DL. In vitro evaluation of electrospun silk fibroin scaffolds for vascular cell growth. Biomaterials2008 May;29(14):2217-27.

34. Ramamurthi A, Vesely I. Evaluation of the matrix-synthesis potential of crosslinked hyaluronan gels for tissue engineering of aortic heart valves. Biomaterials2005 Mar;26(9):999-1010.

35. Gao J, Crapo P, Nerem R, Wang Y. Co-expression of elastin and collagen leads to highly compliant engineered blood vessels. J Biomed Mater Res A2008 Jun 15;85(4):1120-8.

36. Liu JY, Swartz DD, Peng HF, Gugino SF, Russell JA, Andreadis ST. Functional tissue-engineered blood vessels from bone marrow progenitor cells. Cardiovasc Res2007 Aug 1;75(3):618-28.

37. Kothapalli CR, Taylor PM, Smolenski RT, Yacoub MH, Ramamurthi A. Transforming growth factor beta 1 and hyaluronan oligomers synergistically enhance elastin matrix regeneration by vascular smooth muscle cells. Tissue Eng Part A2009 Mar;15(3):501-11.

38. Shanley CJ, Gharaee-Kermani M, Sarkar R, Welling TH, Kriegel A, Ford JW, Stanley JC, Phan SH. Transforming growth factor-beta 1 increases lysyl oxidase enzyme activity and mRNA in rat aortic smooth muscle cells. J Vasc Surg1997 Mar;25(3):446-52.

39. Gacheru SN, Thomas KM, Murray SA, Csiszar K, Smith-Mungo LI, Kagan HM. Transcriptional and post-transcriptional control of lysyl oxidase expression in vascular smooth muscle cells: effects of TGF-beta 1 and serum deprivation. J Cell Biochem1997 Jun 1;65(3):395-407.

40. Dai J, Losy F, Guinault AM, Pages C, Anegon I, Desgranges P, Becquemin JP, Allaire E. Overexpression of transforming growth factor-beta1 stabilizes already-formed aortic aneurysms: a first approach to induction of functional healing by endovascular gene therapy. Circulation2005 Aug 16;112(7):1008-15.

41. Losy F, Dai J, Pages C, Ginat M, Muscatelli-Groux B, Guinault AM, Rousselle E, Smedile G, Loisance D, Becquemin JP, Allaire E. Paracrine secretion of transforming growth factor-beta1 in aneurysm healing and stabilization with endovascular smooth muscle cell therapy. J Vasc Surg2003 Jun;37(6):1301-9.

42. Wu WJ, Vrhovski B, Weiss AS. Glycosaminoglycans mediate the coacervation of human tropoelastin through dominant charge interactions involving lysine side chains. J Biol Chem1999 Jul 30;274(31):21719-24.

43. Fornieri C, Baccarani-Contri M, Quaglino D, Jr., Pasquali-Ronchetti I. Lysyl oxidase activity and elastin/glycosaminoglycan interactions in growing chick and rat aortas. J Cell Biol1987 Sep;105(3):1463-9.

44. Joddar B, Ramamurthi A. Fragment size- and dose-specific effects of hyaluronan on matrix synthesis by vascular smooth muscle cells. Biomaterials2006 May;27(15):2994-3004.

45. Abdul-Hussien H, Hanemaaijer R, Verheijen JH, van Bockel JH, Geelkerken RH, Lindeman JH. Doxycycline therapy for abdominal aneurysm: Improved proteolytic balance through reduced neutrophil content. J Vasc Surg2009 Mar;49(3):741-9.

46. Lindeman JH, Abdul-Hussien H, van Bockel JH, Wolterbeek R, Kleemann R. Clinical trial of doxycycline for matrix metalloproteinase-9 inhibition in patients with an abdominal aneurysm: doxycycline selectively depletes aortic wall neutrophils and cytotoxic T cells. Circulation2009 Apr 28;119(16):2209-16.

47. Thompson RW, Baxter BT. MMP inhibition in abdominal aortic aneurysms. Rationale for a prospective randomized clinical trial. Ann N Y Acad Sci1999 Jun 30;878:159-78.

48. Huffman MD, Curci JA, Moore G, Kerns DB, Starcher BC, Thompson RW. Functional importance of connective tissue repair during the development of experimental abdominal aortic aneurysms. Surgery2000 Sep;128(3):429-38.

49. Weinberg CB, Bell E. A blood vessel model constructed from collagen and cultured vascular cells. Science1986 Jan 24;231(4736):397-400.

50. Kanda K, Matsuda T. In vitro reconstruction of hybrid arterial media with molecular and cellular orientations. Cell Transplant1994 Nov-Dec;3(6):537-45.

51. Seliktar D, Black RA, Vito RP, Nerem RM. Dynamic mechanical conditioning of collagen-gel blood vessel constructs induces remodeling in vitro. Ann Biomed Eng2000 Apr;28(4):351-62.

52. Kim BS, Nikolovski J, Bonadio J, Smiley E, Mooney DJ. Engineered smooth muscle tissues: regulating cell phenotype with the scaffold. Exp Cell Res1999 Sep 15;251(2):318-28.

53. Song J, Rolfe BE, Hayward IP, Campbell GR, Campbell JH. Effects of collagen gel configuration on behavior of vascular smooth muscle cells in vitro: association with vascular morphogenesis. In Vitro Cell Dev Biol Anim2000 Oct;36(9):600-10.

54. Higgins SP, Solan AK, Niklason LE. Effects of polyglycolic acid on porcine smooth muscle cell growth and differentiation. J Biomed Mater Res A2003 Oct 1;67(1):295-302.

55. Annambhotla S, Bourgeois S, Wang X, Lin PH, Yao Q, Chen C. Recent advances in molecular mechanisms of abdominal aortic aneurysm formation. World J Surg2008 Jun;32(6):976-86.

56. Thie M, Schlumberger W, Semich R, Rauterberg J, Robenek H. Aortic smooth muscle cells in collagen lattice culture: effects on ultrastructure, proliferation and collagen synthesis. Eur J Cell Biol1991 Aug;55(2):295-304.

57. Kim BS, Nikolovski J, Bonadio J, Mooney DJ. Cyclic mechanical strain regulates the development of engineered smooth muscle tissue. Nat Biotechnol1999 Oct;17(10):979-83.

58. Kim BS, Mooney DJ. Scaffolds for engineering smooth muscle under cyclic mechanical strain conditions. J Biomech Eng2000 Jun;122(3):210-5.

59. Isenberg BC, Tranquillo RT. Long-term cyclic distention enhances the mechanical properties of collagen-based media-equivalents. Ann Biomed Eng2003 Sep;31(8):937-49.

60. Jones JA, Spinale FG, Ikonomidis JS. Transforming growth factor-beta signaling in thoracic aortic aneurysm development: a paradox in pathogenesis. J Vasc Res2009;46(2):119-37.

61. Guo DC, Papke CL, He R, Milewicz DM. Pathogenesis of thoracic and abdominal aortic aneurysms. Ann N Y Acad Sci2006 Nov;1085:339-52.

62. Kielty CM, Sherratt MJ, Shuttleworth CA. Elastic fibres. J Cell Sci2002 Jul 15;115(Pt 14):2817-28.

63. Balazs EA. Chemistry and molecular biology of the intercellular matrix. London, New York,: Academic Press; 1970.

64. Baccaranicontri M, Vincenzi D, Cicchetti F, Mori G, Pasqualironchetti I. Immunocytochemical Localization of Proteoglycans within Normal Elastin Fibers. Eur J Cell Biol1990 Dec;53(2):305-12.

65. Hoeve CA, Flory PJ. The elastic properties of elastin. Biopolymers1974 Apr;13(4):677-86.

66. Trask TM, Trask BC, Ritty TM, Abrams WR, Rosenbloom J, Mecham RP. Interaction of tropoelastin with the amino-terminal domains of fibrillin-1 and fibrillin-2 suggests a role for the fibrillins in elastic fiber assembly. J Biol Chem2000 Aug 11;275(32):24400-6.

67. Berman I. Color atlas of basic histology. 3rd ed. New York: Lange Medical Books/McGraw-Hill; 2003.

68. Robert L, Hornebeck W. Elastin and elastases. Boca Raton, Fla.: CRC Press; 1989.

69. Foster JA, Bruenger E, Gray WR, Sandberg LB. Isolation and amino acid sequences of tropoelastin peptides. J Biol Chem1973 Apr 25;248(8):2876-9.

70. Sage H, Gray WR. Studies on the evolution of elastin--I. Phylogenetic distribution. Comp Biochem Physiol B1979;64(4):313-27.

71. Fazio MJ, Mattei MG, Passage E, Chu ML, Black D, Solomon E, Davidson JM, Uitto J. Human elastin gene: new evidence for localization to the long arm of chromosome 7. Am J Hum Genet1991 Apr;48(4):696-703.

72. Indik Z, Yeh H, Ornstein-Goldstein N, Sheppard P, Anderson N, Rosenbloom JC, Peltonen L, Rosenbloom J. Alternative splicing of human elastin mRNA indicated by sequence analysis of cloned genomic and complementary DNA. Proc Natl Acad Sci U S A1987 Aug;84(16):5680-4.

73. Mecham RP, Whitehouse L, Hay M, Hinek A, Sheetz MP. Ligand affinity of the 67-kD elastin/laminin binding protein is modulated by the protein's lectin domain: visualization of elastin/laminin-receptor complexes with gold-tagged ligands. J Cell Biol1991 Apr;113(1):187-94.

74. Hinek A, Mecham RP, Keeley F, Rabinovitch M. Impaired elastin fiber assembly related to reduced 67-kD elastin-binding protein in fetal lamb ductus arteriosus and in cultured aortic smooth muscle cells treated with chondroitin sulfate. J Clin Invest1991 Dec;88(6):2083-94.

75. Csiszar K. Lysyl oxidases: a novel multifunctional amine oxidase family. Prog Nucleic Acid Res Mol Biol2001;70:1-32.

76. Rucker RB, Murray J. Cross-linking amino acids in collagen and elastin. Am J Clin Nutr1978 Jul;31(7):1221-36.

77. Narayanan AS, Page RC, Kuzan F, Cooper CG. Elastin cross-linking in vitro. Studies on factors influencing the formation of desmosines by lysyl oxidase action on tropoelastin. Biochem J1978 Sep 1;173(3):857-62.

78. Gacheru SN, Trackman PC, Shah MA, Ogara CY, Spacciapoli P, Greenaway FT, Kagan HM. Structural and Catalytic Properties of Copper in Lysyl Oxidase. Journal of Biological Chemistry1990 Nov 5;265(31):19022-7.

79. Chadwick D, Goode J, Ciba Foundation. The molecular biology and pathology of elastic tissues. Chichester ; New York: J. Wiley; 1995.

80. Visser A. The molecular biology and pathology of elastic tissues - Robert,L. Patient Educ Couns1996 Jul;28(2):231-.

81. Ye S, Humphries S, Henney A. Matrix metalloproteinases: implication in vascular matrix remodelling during atherogenesis. Clin Sci1998 Feb;94(2):103-10.

82. Pasnik J, Moll JA, Szalowska DA, Baj Z, Moll J, Moll M, Sysa A, Zeman K. Matrix metallo protein ases and tissue inhibitors of metaloproteinases may be may act as proinflammatory markers after cardiopulmonary bypass in children. Inflamm Res2005 Aug;54:S204-S.

83. Galis ZS, Khatri JJ. Matrix metalloproteinases in vascular remodeling and atherogenesis: the good, the bad, and the ugly. Circ Res2002 Feb 22;90(3):251-62.

84. Robert L. The molecular biology and pathology of elastic tissues. Ciba F Symp1995;192:1-3.

85. Larsen M, Artym VV, Green JA, Yamada KM. The matrix reorganized: extracellular matrix remodeling and integrin signaling. Curr Opin Cell Biol2006 Oct;18(5):463-71.

86. Bazzoni G. Endothelial tight junctions: permeable barriers of the vessel wall. Thromb Haemost2006 Jan;95(1):36-42.

87. Kielty CM, Stephan S, Sherratt MJ, Williamson M, Shuttleworth CA. Applying elastic fibre biology in vascular tissue engineering. Philos Trans R Soc Lond B Biol Sci2007 Aug 29;362(1484):1293-312.

88. Hungerford JE, Owens GK, Argraves WS, Little CD. Development of the aortic vessel wall as defined by vascular smooth muscle and extracellular matrix markers. Dev Biol1996 Sep 15;178(2):375-92.

89. Thyberg J. Differentiated properties and proliferation of arterial smooth muscle cells in culture. Int Rev Cytol1996;169:183-265.

90. Thyberg J, Hedin U, Sjolund M, Palmberg L, Bottger BA. Regulation of differentiated properties and proliferation of arterial smooth muscle cells. Arteriosclerosis1990 Nov-Dec;10(6):966-90.

91. Hoofnagle MH, Wamhoff BR, Owens GK. Lost in transdifferentiation. J Clin Invest2004 May;113(9):1249-51.

92. Prockop DJ, Kivirikko KI. Collagens: molecular biology, diseases, and potentials for therapy. Annu Rev Biochem1995;64:403-34.

93. Kagan HM, Li W. Lysyl oxidase: properties, specificity, and biological roles inside and outside of the cell. J Cell Biochem2003 Mar 1;88(4):660-72.

94. Steve Berg. Synthesis of Collagen. Available from: http://course1.winona.edu/sberg/308s02/Lec-note/11-new.htm

95. Varki A. Essentials of glycobiology. 2nd ed. Cold Spring Harbor, N.Y.: Cold Spring Harbor Laboratory Press; 2009.

96. Imberty A, Lortat-Jacob H, Perez S. Structural view of glycosaminoglycan-protein interactions. Carbohydr Res2007 Feb 26;342(3-4):430-9.

97. Iozzo RV. Basement membrane proteoglycans: from cellar to ceiling. Nat Rev Mol Cell Biol2005 Aug;6(8):646-56.

98. Mochizuki S, Brassart B, Hinek A. Signaling pathways transduced through the elastin receptor facilitate proliferation of arterial smooth muscle cells. J Biol Chem2002 Nov 22;277(47):44854-63.

99. Rodgers UR, Weiss AS. Cellular interactions with elastin. Pathol Biol (Paris)2005 Sep;53(7):390-8.

100. Ito S, Ishimaru S, Wilson SE. Inhibitory effect of type 1 collagen gel containing alpha-elastin on proliferation and migration of vascular smooth muscle and endothelial cells. Cardiovasc Surg1997 Apr;5(2):176-83.

101. Fulop T, Khalil A, Larbi A. The role of elastin peptides in modulating the immune response in aging and age-related diseases. Pathol Biol (Paris)2012 Feb;60(1):28-33.

102. Brooke BS, Bayes-Genis A, Li DY. New insights into elastin and vascular disease. Trends Cardiovas Med2003 Jul;13(5):176-81.

103. Basalyga DM, Simionescu DT, Xiong WF, Baxter T, Starcher BC, Vyavahare NR. Elastin degradation and calcification in an abdominal aorta injury model - Role of matrix metalloproteinases. Circulation2004 Nov 30;110(22):3480-7.

104. Fulop T, Jacob MP, Wallach J, Hauck M, Seres I, Varga Z, Robert L. [The elastin-laminin receptor]. J Soc Biol2001;195(2):157-64.

105. Spofford CM, Chilian WM. The elastin-laminin receptor functions as a mechanotransducer in vascular smooth muscle. Am J Physiol Heart Circ Physiol2001 Mar;280(3):H1354-60.

106. Fulop T, Jr., Douziech N, Jacob MP, Hauck M, Wallach J, Robert L. Age-related alterations in the signal transduction pathways of the elastin-laminin receptor. Pathol Biol (Paris)2001 May;49(4):339-48.

107. Kunecki M, Nawrocka A. Elastin-laminin receptor and abdominal aortic aneurysms. New subject to study? A review. Pathol Biol (Paris)2001 May;49(4):333-8.

108. O'Connell MK, Murthy S, Phan S, Xu C, Buchanan J, Spilker R, Dalman RL, Zarins CK, Denk W, Taylor CA. The three-dimensional micro- and nanostructure of the aortic medial lamellar unit measured using 3D confocal and electron microscopy imaging. Matrix Biol2008 Apr;27(3):171-81.

109. Apter JT. Correlation of visco-elastic properties with microscopic structure of large arteries. IV. Thermal responses of collagen, elastin, smooth muscle, and intact arteries. Circ Res1967 Dec;21(6):901-18.

110. Dobrin PB, Conway M, Canfield T. Elastin, Collagen and the Biaxial Elastic Properties of Dog Carotid-Artery. Fed Proc1980;39(3):384-.

111. Segura AM, Luna RE, Horiba K, Stetler-Stevenson WG, McAllister HA, Willerson JT, Ferrans VJ. Immunohistochemistry of matrix metalloproteinases and their inhibitors in thoracic aortic aneurysms and aortic valves of patients with Marfan's syndrome. Circulation1998 Nov 10;98(19):Ii331-Ii7.

112. Hanada K, Vermeij M, Garinis GA, de Waard MC, Kunen MG, Myers L, Maas A, Duncker DJ, Meijers C, Dietz HC, Kanaar R, Essers J. Perturbations of vascular homeostasis and aortic valve abnormalities in fibulin-4 deficient mice. Circ Res2007 Mar 16;100(5):738-46.

113. Francke U. Williams-Beuren syndrome: genes and mechanisms. Hum Mol Genet1999;8(10):1947-54.

114. Curran ME, Atkinson DL, Ewart AK, Morris CA, Leppert MF, Keating MT. The Elastin Gene Is Disrupted by a Translocation Associated with Supravalvular Aortic-Stenosis. Cell1993 Apr 9;73(1):159-68.

115. Tantcheva-Poor I, Schuster A, Kornak U, Chelius K, Mauch C. [Congenital Autosomal Recessive Cutis laxa Type II A Wrinkly-Skin-Syndrome.]. Klin Padiatr2012 Jul 20.

116. Brooke BS, Bayes-Genis A, Li DY. New insights into elastin and vascular disease. Trends Cardiovasc Med2003 Jul;13(5):176-81.

117. Motwani JG, Topol EJ. Aortocoronary saphenous vein graft disease: pathogenesis, predisposition, and prevention. Circulation1998 Mar 10;97(9):916-31.

118. Saito A, Motomura N, Kakimi K, Ono M, Takai D, Sumida S, Takamoto S. Cryopreservation does not alter the allogenicity and development of vasculopathy in post-transplant rat aortas. Cryobiology2006 Apr;52(2):251-60.

119. Wilson GJ, Courtman DW, Klement P, Lee JM, Yeger H. Acellular matrix: a biomaterials approach for coronary artery bypass and heart valve replacement. Ann Thorac Surg1995 Aug;60(2 Suppl):S353-8.

120. Allaire E, Bruneval P, Mandet C, Becquemin JP, Michel JB. The immunogenicity of the extracellular matrix in arterial xenografts. Surgery1997 Jul;122(1):73-81.

121. Allaire E, Mandet C, Bruneval P, Bensenane S, Becquemin JP, Michel JB. Cell and extracellular matrix rejection in arterial concordant and discordant xenografts in the rat. Transplantation1996 Sep 27;62(6):794-803.

122. Lai L, Prather RS. Progress in producing knockout models for xenotransplantation by nuclear transfer. Ann Med2002;34(7-8):501-6.

123. Lederle FA, Kane RL, MacDonald R, Wilt TJ. Systematic review: repair of unruptured abdominal aortic aneurysm. Ann Intern Med2007 May 15;146(10):735-41.

124. Chambers D, Epstein D, Walker S, Fayter D, Paton F, Wright K, Michaels J, Thomas S, Sculpher M, Woolacott N. Endovascular stents for abdominal aortic aneurysms: a systematic review and economic model. Health Technol Assess2009 Oct;13(48):1-189, 215-318, iii.

125. Kadoglou NP, Liapis CD. Matrix metalloproteinases: contribution to pathogenesis, diagnosis, surveillance and treatment of abdominal aortic aneurysms. Curr Med Res Opin2004 Apr;20(4):419-32.

126. Dodd BR, Spence RA. Doxycycline inhibition of abdominal aortic aneurysm growth: a systematic review of the literature. Curr Vasc Pharmacol2011 Jul 1;9(4):471-8.

127. Hanemaaijer R, Visser H, Koolwijk P, Sorsa T, Salo T, Golub LM, van Hinsbergh VW. Inhibition of MMP synthesis by doxycycline and chemically modified tetracyclines (CMTs) in human endothelial cells. Adv Dent Res1998 Nov;12(2):114-8.

128. Uitto VJ, Firth JD, Nip L, Golub LM. Doxycycline and chemically modified tetracyclines inhibit gelatinase A (MMP-2) gene expression in human skin keratinocytes. Ann N Y Acad Sci1994 Sep 6;732:140-51.

129. Franklin IJ, Harley SL, Greenhalgh RM, Powell JT. Uptake of tetracycline by aortic aneurysm wall and its effect on inflammation and proteolysis. Br J Surg1999 Jun;86(6):771-5.

130. Curci JA, Mao D, Bohner DG, Allen BT, Rubin BG, Reilly JM, Sicard GA, Thompson RW. Preoperative treatment with doxycycline reduces aortic wall expression and activation of matrix metalloproteinases in patients with abdominal aortic aneurysms. J Vasc Surg2000 Feb;31(2):325-42.

131. Smith GN, Jr., Brandt KD, Hasty KA. Activation of recombinant human neutrophil procollagenase in the presence of doxycycline results in fragmentation of the enzyme and loss of enzyme activity. Arthritis Rheum1996 Feb;39(2):235-44.

132. Smith GN, Jr., Brandt KD, Hasty KA. Procollagenase is reduced to inactive fragments upon activation in the presence of doxycycline. Ann N Y Acad Sci1994 Sep 6;732:436-8.

133. Petrinec D, Liao S, Holmes DR, Reilly JM, Parks WC, Thompson RW. Doxycycline inhibition of aneurysmal degeneration in an elastase-induced rat model of abdominal aortic aneurysm: preservation of aortic elastin associated with suppressed production of 92 kD gelatinase. J Vasc Surg1996 Feb;23(2):336-46.

134. Xiong W, Knispel RA, Dietz HC, Ramirez F, Baxter BT. Doxycycline delays aneurysm rupture in a mouse model of Marfan syndrome. J Vasc Surg2008 Jan;47(1):166-72; discussion 72.

135. Boyle JR, McDermott E, Crowther M, Wills AD, Bell PR, Thompson MM. Doxycycline inhibits elastin degradation and reduces metalloproteinase activity in a model of aneurysmal disease. J Vasc Surg1998 Feb;27(2):354-61.

136. Wills A, Thompson MM, Crowther M, Brindle NP, Nasim A, Sayers RD, Bell PR. Elastase-induced matrix degradation in arterial organ cultures: an in vitro model of aneurysmal disease. J Vasc Surg1996 Oct;24(4):667-79.

137. Nakashima H, Aoki M, Miyake T, Kawasaki T, Iwai M, Jo N, Oishi M, Kataoka K, Ohgi S, Ogihara T, Kaneda Y, Morishita R. Inhibition of experimental abdominal aortic aneurysm in the rat by use of decoy oligodeoxynucleotides suppressing activity of nuclear factor kappaB and ets transcription factors. Circulation2004 Jan 6;109(1):132-8.

138. Teckman JH, Lindblad D. Alpha-1-antitrypsin deficiency: diagnosis, pathophysiology, and management. Curr Gastroenterol Rep2006 Feb;8(1):14-20.

139. Simionescu A, Philips K, Vyavahare N. Elastin-derived peptides and TGF-beta1 induce osteogenic responses in smooth muscle cells. Biochem Biophys Res Commun2005 Aug 26;334(2):524-32.

140. Thie M, Schlumberger W, Semich R, Rauterberg J, Robenek H. Aortic smooth muscle cells in collagen lattice culture: effects on ultrastructure, proliferation and collagen synthesis. Eur J Cell Biol1991 Aug;55(2):295-304.

141. Li S, Lao J, Chen BP, Li YS, Zhao Y, Chu J, Chen KD, Tsou TC, Peck K, Chien S. Genomic analysis of smooth muscle cells in 3-dimensional collagen matrix. FASEB J2003 Jan;17(1):97-9.

142. Foster JA, Rich CB, Miller M, Benedict MR, Richman RA, Florini JR. Effect of age and IGF-I administration on elastin gene expression in rat aorta. J Gerontol1990 Jul;45(4):B113-8.

143. Noguchi A, Nelson T. IGF-I stimulates tropoelastin synthesis in neonatal rat pulmonary fibroblasts. Pediatr Res1991 Sep;30(3):248-51.

144. Rich CB, Goud HD, Bashir M, Rosenbloom J, Foster JA. Developmental regulation of aortic elastin gene expression involves disruption of an IGF-I sensitive repressor complex. Biochem Biophys Res Commun1993 Nov 15;196(3):1316-22.

145. McGowan SE, McNamer R. Transforming growth factor-beta increases elastin production by neonatal rat lung fibroblasts. Am J Respir Cell Mol Biol1990 Oct;3(4):369-76.

146. Mauviel A, Chen YQ, Kahari VM, Ledo I, Wu M, Rudnicka L, Uitto J. Human recombinant interleukin-1 beta up-regulates elastin gene expression in dermal fibroblasts. Evidence for transcriptional regulation in vitro and in vivo. J Biol Chem1993 Mar 25;268(9):6520-4.

147. Zhang G, Suggs LJ. Matrices and scaffolds for drug delivery in vascular tissue engineering. Adv Drug Deliv Rev2007 May 30;59(4-5):360-73.

148. Kothapalli CR, Ramamurthi A. Lysyl oxidase enhances elastin synthesis and matrix formation by vascular smooth muscle cells. J Tissue Eng Regen Med2009 Dec;3(8):655-61.

149. Kothapalli CR, Ramamurthi A. Copper nanoparticle cues for biomimetic cellular assembly of crosslinked elastin fibers. Acta Biomater2009 Feb;5(2):541-53.

150. Hayashi A, Suzuki T, Tajima S. Modulations of elastin expression and cell proliferation by retinoids in cultured vascular smooth muscle cells. J Biochem1995 Jan;117(1):132-6.

151. Tukaj C, Trzonkowski P, Pikula M, Hallmann A, Tukaj S. Increased migratory properties of aortal smooth muscle cells exposed to calcitriol in culture. J Steroid Biochem Mol Biol2010 Jul;121(1-2):208-11.

152. Tukaj C, Kubasik-Juraniec J, Kraszpulski M. Morphological changes of aortal smooth muscle cells exposed to calcitriol in culture. Med Sci Monit2000 Jul-Aug;6(4):668-74.

153. Toole BP, Wight TN, Tammi MI. Hyaluronan-cell interactions in cancer and vascular disease. J Biol Chem2002 Feb 15;277(7):4593-6.

154. Toole BP. Hyaluronan and its binding proteins, the hyaladherins. Curr Opin Cell Biol1990 Oct;2(5):839-44.

155. Laurent TC, Fraser JR. Hyaluronan. FASEB J1992 Apr;6(7):2397-404.

156. Aruffo A, Stamenkovic I, Melnick M, Underhill CB, Seed B. CD44 is the principal cell surface receptor for hyaluronate. Cell1990 Jun 29;61(7):1303-13.

157. Underhill CB. The interaction of hyaluronate with the cell surface: the hyaluronate receptor and the core protein. Ciba Found Symp1989;143:87-99; discussion 100-6, 281-5.

158. Orlidge A, D'Amore PA. Cell specific effects of glycosaminoglycans on the attachment and proliferation of vascular wall components. Microvasc Res1986 Jan;31(1):41-53.

159. Culty M, Miyake K, Kincade PW, Sikorski E, Butcher EC, Underhill C. The hyaluronate receptor is a member of the CD44 (H-CAM) family of cell surface glycoproteins. J Cell Biol1990 Dec;111(6 Pt 1):2765-74.

160. Wight TN. Versican: a versatile extracellular matrix proteoglycan in cell biology. Curr Opin Cell Biol2002 Oct;14(5):617-23.

161.Rossler A, Hinghofer-Szalkay H. Hyaluronan fragments: an information-carrying system? Horm Metab Res2003 Feb;35(2):67-8.

162. Joddar B, Ibrahim S, Ramamurthi A. Impact of delivery mode of hyaluronan oligomers on elastogenic responses of adult vascular smooth muscle cells. Biomaterials2007 Sep;28(27):3918-27.

163. Joddar B, Ramamurthi A. Elastogenic effects of exogenous hyaluronan oligosaccharides on vascular smooth muscle cells. Biomaterials2006 Nov;27(33):5698-707.

164. Haga JH, Li YS, Chien S. Molecular basis of the effects of mechanical stretch on vascular smooth muscle cells. J Biomech2007;40(5):947-60.

165. Kanda K, Matsuda T. Behavior of arterial wall cells cultured on periodically stretched substrates. Cell Transplant1993 Nov-Dec;2(6):475-84.

166. Kona S, Chellamuthu P, Xu H, Hills SR, Nguyen KT. Effects of cyclic strain and growth factors on vascular smooth muscle cell responses. Open Biomed Eng J2009;3:28-38.

167. Liu B, Qu MJ, Qin KR, Li H, Li ZK, Shen BR, Jiang ZL. Role of cyclic strain frequency in regulating the alignment of vascular smooth muscle cells in vitro. Biophys J2008 Feb 15;94(4):1497-507.

168. Qu MJ, Liu B, Wang HQ, Yan ZQ, Shen BR, Jiang ZL. Frequency-dependent phenotype modulation of vascular smooth muscle cells under cyclic mechanical strain. J Vasc Res2007;44(5):345-53.

169. Lee KW, Stolz DB, Wang Y. Substantial expression of mature elastin in arterial constructs. Proc Natl Acad Sci U S A2011 Feb 15;108(7):2705-10.

170. O'Callaghan CJ, Williams B. Mechanical strain-induced extracellular matrix production by human vascular smooth muscle cells: role of TGF-beta(1). Hypertension2000 Sep;36(3):319-24.

171. Wernig F, Mayr M, Xu Q. Mechanical stretch-induced apoptosis in smooth muscle cells is mediated by beta1-integrin signaling pathways. Hypertension2003 Apr;41(4):903-11.

172. Seliktar D, Nerem RM, Galis ZS. Mechanical strain-stimulated remodeling of tissue-engineered blood vessel constructs. Tissue Eng2003 Aug;9(4):657-66.

173. Venkataraman L, Ramamurthi A. Induced elastic matrix deposition within three-dimensional collagen scaffolds. Tissue Eng Part A2011 Nov;17(21-22):2879-89.

174. Xie SZ, Fang NT, Liu S, Zhou P, Zhang Y, Wang SM, Gao HY, Pan LF. Differentiation of smooth muscle progenitor cells in peripheral blood and its application in tissue engineered blood vessels. J Zhejiang Univ Sci B2008 Dec;9(12):923-30.

175. Ramamurthi A, Vesely I. Smooth muscle cell adhesion on crosslinked hyaluronan gels. J Biomed Mater Res2002 Apr;60(1):195-205.

176. Xu ZC, Li H, Zhou GD, Li G, Liu Y, Zhang WJ, Cui L, Liu W, Cao YL. [Constructing of smooth muscle layers of tissue engineered blood vessel in a bioreactor]. Zhonghua Zheng Xing Wai Ke Za Zhi2008 May;24(3):220-4.

177. Iwasaki K, Kojima K, Kodama S, Paz AC, Chambers M, Umezu M, Vacanti CA. Bioengineered three-layered robust and elastic artery using hemodynamically-equivalent pulsatile bioreactor. Circulation2008 Sep 30;118(14):S52-S7.

178. Lin S, Sandig M, Mequanint K. Three-dimensional topography of synthetic scaffolds induces elastin synthesis by human coronary artery smooth muscle cells. Tissue Eng Part A2011 Jun;17(11-12):1561-71.

179. Cheng ST, Chen ZF, Chen GQ. The expression of cross-linked elastin by rabbit blood vessel smooth muscle cells cultured in polyhydroxyalkanoate scaffolds. Biomaterials2008 Nov;29(31):4187-94.

180. Bashur CA, Ramamurthi A. Aligned electrospun scaffolds and elastogenic factors for vascular cell-mediated elastic matrix assembly. J Tissue Eng Regen Med2011 Sep 23.

181. Crapo PM, Wang Y. Physiologic compliance in engineered small-diameter arterial constructs based on an elastomeric substrate. Biomaterials2010 Mar;31(7):1626-35.

182. Keire PA, L'Heureux N, Vernon RB, Merrilees MJ, Starcher B, Okon E, Dusserre N, McAllister TN, Wight TN. Expression of versican isoform V3 in the absence of ascorbate improves elastogenesis in engineered vascular constructs. Tissue Eng Part A2010 Feb;16(2):501-12.

183. Bashur CA, Venkataraman L, Ramamurthi A. Tissue engineering and regenerative strategies to replicate biocomplexity of vascular elastic matrix assembly. Tissue Eng Part B Rev2012 Jun;18(3):203-17.

184. Kothapalli CR, Gacchina CE, Ramamurthi A. Utility of hyaluronan oligomers and transforming growth factor-beta1 factors for elastic matrix regeneration by aneurysmal rat aortic smooth muscle cells. Tissue Eng Part A2009 Nov;15(11):3247-60.

185. Ghosh J, Murphy MO, Turner N, Khwaja N, Halka A, Kielty CM, Walker MG. The role of transforming growth factor beta1 in the vascular system. Cardiovasc Pathol2005 Jan-Feb;14(1):28-36.

186. Davis ME, Hsieh PCH, Grodzinsky AJ, Lee RT. Custom design of the cardiac microenvironment with biomaterials. Circ Res2005 Jul 8;97(1):8-15.

187. Lee K, Silva EA, Mooney DJ. Growth factor delivery-based tissue engineering: general approaches and a review of recent developments. J R Soc Interface. [Review]. 2011 Feb;8(55):153-70.

188. Lutolf MP, Hubbell JA. Synthetic biomaterials as instructive extracellular microenvironments for morphogenesis in tissue engineering. Nat Biotech2005 Jan;23(1):47-55.

189. Allen TM, Cullis PR. Drug delivery systems: Entering the mainstream. Science2004 Mar 19;303(5665):1818-22.

190. Panyam J, Labhasetwar V. Biodegradable nanoparticles for drug and gene delivery to cells and tissue. Adv Drug Deliv Rev2003;55(3):329-47.

191. Pitsillides CM, Joe EK, Wei XB, Anderson RR, Lin CP. Selective cell targeting with light-absorbing microparticles and nanoparticles. Biophys J2003 Jun;84(6):4023-32.

192. Sarikaya M, Tamerler C, Jen AKY, Schulten K, Baneyx F. Molecular biomimetics: nanotechnology through biology. Nat Mater2003 Sep;2(9):577-85.

193. Altman GH, Diaz F, Jakuba C, Calabro T, Horan RL, Chen JS, Lu H, Richmond J, Kaplan DL. Silk-based biomaterials. Biomaterials2003 Feb;24(3):401-16.

194. Drury JL, Mooney DJ. Hydrogels for tissue engineering: scaffold design variables and applications. Biomaterials2003 Nov;24(24):4337-51.

195. Hutmacher DW. Scaffolds in tissue engineering bone and cartilage. Biomaterials2000 Dec;21(24):2529-43.

196. Lee KY, Mooney DJ. Hydrogels for tissue engineering. Chem Rev2001 Jul;101(7):1869-79.

197. Li WJ, Laurencin CT, Caterson EJ, Tuan RS, Ko FK. Electrospun nanofibrous structure: A novel scaffold for tissue engineering. J Biomed Mater Res2002 Jun 15;60(4):613-21.

198. Matthews JA, Wnek GE, Simpson DG, Bowlin GL. Electrospinning of collagen nanofibers. Biomacromolecules2002 Mar-Apr;3(2):232-8.

199. Goldberg M, Langer R, Jia X. Nanostructured materials for applications in drug delivery and tissue engineering. J Biomater Sci Polym Ed2007 Mar;18(3):241-68.

200. Kim SS, Park MS, Jeon O, Choi CY, Kim BS. Poly(lactide-co-glycolide)/hydroxyapatite composite scaffolds for bone tissue engineering. Biomaterials2006 Mar;27(8):1399-409.

201. Chen RR, Silva EA, Yuen WW, Brock AA, Fischbach C, Lin AS, Guldberg RE, Mooney DJ. Integrated approach to designing growth factor delivery systems. FASEB J2007 Dec;21(14):3896-903.

202. Chen RR, Silva EA, Yuen WW, Mooney DJ. Spatio-temporal VEGF and PDGF delivery patterns blood vessel formation and maturation. Pharm Res2007 Feb;24(2):258-64.

203. Nguyen KT, West JL. Photopolymerizable hydrogels for tissue engineering applications. Biomaterials2002 Nov;23(22):4307-14.

204. Ratner BD, Bryant SJ. Biomaterials: Where we have been and where we are going. Annu Rev Biomed Eng2004 2004;6:41-75.

205. Silva EA, Mooney DJ. Spatiotemporal control of vascular endothelial growth factor delivery from injectable hydrogels enhances angiogenesis. J Thromb Haemost2007 Mar;5(3):590-8.

206. Silva EA, Mooney DJ. Synthetic extracellular matrices for tissue engineering and regeneration. Curr Top Dev Biol2004 2004;64:181-205.

207. Ahmann KA, Weinbaum JS, Johnson SL, Tranquillo RT. Fibrin degradation enhances vascular smooth muscle cell proliferation and matrix deposition in fibrin-based tissue constructs fabricated in vitro. Tissue Eng Part A2010 Oct;16(10):3261-70.

208. Chau Y, Tan FE, Langer R. Synthesis and characterization of dextran-peptide-methotrexate conjugates for tumor targeting via mediation by matrix metalloproteinase II and matrix metalloproteinase IX. Bioconjug Chem2004 Jul-Aug;15(4):931-41.

209. Lutolf MR, Weber FE, Schmoekel HG, Schense JC, Kohler T, Muller R, Hubbell JA. Repair of bone defects using synthetic mimetics of collagenous extracellular matrices. Nat Biotechnol2003 May;21(5):513-8.

210. Safran SA, Gov N, Nicolas A, Schwarz US, Tlusty T. Physics of cell elasticity, shape and adhesion. Physica a-Statistical Mechanics and Its Applications2005 Jul 1;352(1):171-201.

211. Flemming RG, Murphy CJ, Abrams GA, Goodman SL, Nealey PF. Effects of synthetic micro- and nano-structured surfaces on cell behavior. Biomaterials1999 Mar;20(6):573-88.

212. Ji W, Sun Y, Yang F, van den Beucken JJ, Fan M, Chen Z, Jansen JA. Bioactive electrospun scaffolds delivering growth factors and genes for tissue engineering applications. Pharm Res2011 Jun;28(6):1259-72.

213. Labhasetwar V, Song C, Humphrey W, Shebuski R, Levy RJ. Arterial uptake of biodegradable nanoparticles: effect of surface modifications. J Pharm Sci1998 Oct;87(10):1229-34.

214. Song CX, Labhasetwar V, Murphy H, Qu X, Humphrey WR, Shebuski RJ, Levy RJ. Formulation and characterization of biodegradable nanoparticles for intravascular local drug delivery. Journal of Controlled Release1997 Jan 18;43(2-3):197-212.

215. Gertler A. The non-specific electrostatic nature of the adsorption of elastase and other basic proteins on elastin. Eur J Biochem1971 Jun 29;20(4):541-6.

216. Kagan HM, Simpson DE, Tseng L. Substrate-directed modulation of elastin oxidation by lysyl oxidase. Connect Tissue Res1981;8(3-4):213-7.

217. Gacchina CE, Ramamurthi A. Impact of pre-existing elastic matrix on TGFbeta1 and HA oligomer-induced regenerative elastin repair by rat aortic smooth muscle cells. J Tissue Eng Regen Med2010 Jul 23.

218. Shi Y, Vesely I. Fabrication of mitral valve chordae by directed collagen gel shrinkage. Tissue Eng2003 Dec;9(6):1233-42.

219. Juncosa-Melvin N, Boivin GP, Galloway MT, Gooch C, West JR, Sklenka AM, Butler DL. Effects of cell-to-collagen ratio in mesenchymal stem cell-seeded implants on tendon repair biomechanics and histology. Tissue Eng2005 Mar-Apr;11(3-4):448-57.

220. Battegay EJ, Raines EW, Seifert RA, Bowen-Pope DF, Ross R. TGF-beta induces bimodal proliferation of connective tissue cells via complex control of an autocrine PDGF loop. Cell1990 Nov 2;63(3):515-24.

221. Labarca C, Paigen K. A simple, rapid, and sensitive DNA assay procedure. Anal Biochem1980 Mar 1;102(2):344-52.

222. Livak KJ, Schmittgen TD. Analysis of relative gene expression data using real-time quantitative PCR and the 2(-Delta Delta C(T)) Method. Methods2001 Dec;25(4):402-8.

223. Lee JS, Basalyga DM, Simionescu A, Isenburg JC, Simionescu DT, Vyavahare NR. Elastin calcification in the rat subdermal model is accompanied by up-regulation of degradative and osteogenic cellular responses. Am J Pathol2006 Feb;168(2):490-8.

224. Loria RM, Kos WL, Campbell AE, Madge GE. Suppression of aortic elastic tissue autofluorescence for the detection of viral antigen. Histochemistry1979 Jun 18;61(2):151-5.

225. Bashur CA, Dahlgren LA, Goldstein AS. Effect of fiber diameter and orientation on fibroblast morphology and proliferation on electrospun poly(D,L-lactic-co-glycolic acid) meshes. Biomaterials2006 Nov;27(33):5681-8.

226. 95. Dawson-Saunders`, B. and Trapp`, R.G.`, 1994. Estimating and comparing proportions. In: Dawson-Saunders`, B.`, Editor`, 1994. Basic and Clinical Biostatistics`, Appleton & Lange`, East Norwalk`, pp. 143–161.

227. Long JL, Tranquillo RT. Elastic fiber production in cardiovascular tissue-equivalents. Matrix Biol2003 Jun;22(4):339-50.

228. Johnson DJ, Robson P, Hew Y, Keeley FW. Decreased elastin synthesis in normal development and in long-term aortic organ and cell cultures is related to rapid and selective destabilization of mRNA for elastin. Circ Res1995 Dec;77(6):1107-13.

229. L'Heureux N, Germain L, Labbe R, Auger FA. In vitro construction of a human blood vessel from cultured vascular cells: a morphologic study. J Vasc Surg1993 Mar;17(3):499-509.

230. Kothapalli CR, Ramamurthi A. Induced elastin regeneration by chronically activated smooth muscle cells for targeted aneurysm repair. Acta Biomater2010 Jan;6(1):170-8.

231. Grainger DJ, Kemp PR, Witchell CM, Weissberg PL, Metcalfe JC. Transforming growth factor beta decreases the rate of proliferation of rat vascular smooth muscle cells by extending the G2 phase of the cell cycle and delays the rise in cyclic AMP before entry into M phase. Biochem J1994 Apr 1;299 (Pt 1):227-35.

232. Gacchina CE, Deb PP, Barth J, Ramamurthi A. Elastogenic Inductability of Smooth Muscle Cells from a Rat Model of Late-Stage Abdominal Aortic Aneurysms. Tissue Eng Part A2011 Feb 22.

233. Ibrahim S, Joddar B, Craps M, Ramamurthi A. A surface-tethered model to assess size-specific effects of hyaluronan (HA) on endothelial cells. Biomaterials2007 Feb;28(5):825-35.

234. Shi Y, Vesely I. Characterization of statically loaded tissue-engineered mitral valve chordae tendineae. J Biomed Mater Res A2004 Apr 1;69(1):26-39.

235. Gupta V, Grande-Allen KJ. Effects of static and cyclic loading in regulating extracellular matrix synthesis by cardiovascular cells. Cardiovasc Res2006 Dec 1;72(3):375-83.

236. Schutte SC, Chen Z, Brockbank KG, Nerem RM. Cyclic strain improves strength and function of a collagen-based tissue-engineered vascular media. Tissue Eng Part A2010 Oct;16(10):3149-57.

237. Seliktar D, Nerem RM, Galis ZS. The role of matrix metalloproteinase-2 in the remodeling of cell-seeded vascular constructs subjected to cyclic strain. Ann Biomed Eng2001 Nov;29(11):923-34.

238. Grote K, Flach I, Luchtefeld M, Akin E, Holland SM, Drexler H, Schieffer B. Mechanical stretch enhances mRNA expression and proenzyme release of matrix metalloproteinase-2 (MMP-2) via NAD(P)H oxidase-derived reactive oxygen species. Circ Res2003 Jun 13;92(11):e80-6.

239. Gacchina C, Brothers T, Ramamurthi A. Evaluating smooth muscle cells from CaCl2-induced rat aortal expansions as a surrogate culture model for study of elastogenic induction of human aneurysmal cells. Tissue Eng Part A2011 Aug;17(15-16):1945-58.

240. Nikolovski J, Kim BS, Mooney DJ. Cyclic strain inhibits switching of smooth muscle cells to an osteoblast-like phenotype. FASEB J2003 Mar;17(3):455-7.

241. Blanchard JF. Epidemiology of abdominal aortic aneurysms. Epidemiol Rev1999;21(2):207-21.

242. Baxter BT, Pearce WH, Waltke EA, Littooy FN, Hallett JW, Jr., Kent KC, Upchurch GR, Jr., Chaikof EL, Mills JL, Fleckten B, Longo GM, Lee JK, Thompson RW. Prolonged administration of doxycycline in patients with small asymptomatic abdominal aortic aneurysms: report of a prospective (Phase II) multicenter study. J Vasc Surg2002 Jul;36(1):1-12.

243. Bartoli MA, Parodi FE, Chu J, Pagano MB, Mao D, Baxter BT, Buckley C, Ennis TL, Thompson RW. Localized administration of doxycycline suppresses aortic dilatation in an experimental mouse model of abdominal aortic aneurysm. Ann Vasc Surg2006 Mar;20(2):228-36.

244. Sho E, Chu J, Sho M, Fernandes B, Judd D, Ganesan P, Kimura H, Dalman RL. Continuous periaortic infusion improves doxycycline efficacy in experimental aortic aneurysms. J Vasc Surg2004 Jun;39(6):1312-21.

245. Bendeck MP, Conte M, Zhang M, Nili N, Strauss BH, Farwell SM. Doxycycline modulates smooth muscle cell growth, migration, and matrix remodeling after arterial injury. Am J Pathol2002 Mar;160(3):1089-95.

246. Franco C, Ho B, Mulholland D, Hou G, Islam M, Donaldson K, Bendeck MP. Doxycycline alters vascular smooth muscle cell adhesion, migration, and reorganization of fibrillar collagen matrices. Am J Pathol2006 May;168(5):1697-709.

247. Golub LM, Ramamurthy NS, McNamara TF, Greenwald RA, Rifkin BR. Tetracyclines inhibit connective tissue breakdown: new therapeutic implications for an old family of drugs. Crit Rev Oral Biol Med1991;2(3):297-321.

248. Liu J, Xiong W, Baca-Regen L, Nagase H, Baxter BT. Mechanism of inhibition of matrix metalloproteinase-2 expression by doxycycline in human aortic smooth muscle cells. J Vasc Surg2003 Dec;38(6):1376-83.

249. Kim HS, Luo L, Pflugfelder SC, Li DQ. Doxycycline inhibits TGF-beta1-induced MMP-9 via Smad and MAPK pathways in human corneal epithelial cells. Invest Ophthalmol Vis Sci2005 Mar;46(3):840-8.

250. Ventura JJ, Kennedy NJ, Flavell RA, Davis RJ. JNK regulates autocrine expression of TGF-beta1. Mol Cell2004 Jul 23;15(2):269-78.

251. Schlumberger W, Thie M, Rauterberg J, Robenek H. Collagen synthesis in cultured aortic smooth muscle cells. Modulation by collagen lattice culture, transforming growth factor-beta 1, and epidermal growth factor. Arterioscler Thromb1991 Nov-Dec;11(6):1660-6.

252. Yoshimura K, Aoki H, Ikeda Y, Fujii K, Akiyama N, Furutani A, Hoshii Y, Tanaka N, Ricci R, Ishihara T, Esato K, Hamano K, Matsuzaki M. Regression of abdominal aortic aneurysm by inhibition of c-Jun N-terminal kinase. Nat Med2005 Dec;11(12):1330-8.

253. Yamawaki-Ogata A, Hashizume R, Satake M, Kaneko H, Mizutani S, Moritan T, Ueda Y, Narita Y. A doxycycline loaded, controlled-release, biodegradable fiber for the treatment of aortic aneurysms. Biomaterials2010 Dec;31(36):9554-64.

254. Soppimath KS, Aminabhavi TM, Kulkarni AR, Rudzinski WE. Biodegradable polymeric nanoparticles as drug delivery devices. Journal of Controlled Release2001 Jan 29;70(1-2):1-20.

255. Lee KY, Peters MC, Anderson KW, Mooney DJ. Controlled growth factor release from synthetic extracellular matrices. Nature2000 Dec 21-28;408(6815):998-1000.

256. Allen TM, Cullis PR. Drug delivery systems: entering the mainstream. Science2004 Mar 19;303(5665):1818-22.

257. Flemming RG, Murphy CJ, Abrams GA, Goodman SL, Nealey PF. Effects of synthetic micro- and nano-structured surfaces on cell behavior. Biomaterials1999 Mar;20(6):573-88.

258. Wu XS. Synthesis, characterization, biodegradation, and drug delivery application of biodegradable lactic/glycolic acid polymers: Part III. Drug delivery application. Artif Cells Blood Substit Immobil Biotechnol2004;32(4):575-91.

259. Shive MS, Anderson JM. Biodegradation and biocompatibility of PLA and PLGA microspheres. Adv Drug Deliv Rev1997 Oct 13;28(1):5-24.

260. Mitic SS, Miletic GZ, Kostic DA, Naskovic-Dokic DC, Arsic BB, Rasic ID. A rapid and reliable determination of doxycycline hyclate by HPLC with UV detection in pharmaceutical samples. J Serb Chem Soc2008;73(6):665-71.

261. Livak KJ, Schmittgen TD. Analysis of relative gene expression data using real-time quantitative PCR and the 2(T)(-Delta Delta C) method. Methods2001 Dec;25(4):402-8.

262. Stegemann JP, Nerem RM. Altered response of vascular smooth muscle cells to exogenous biochemical stimulation in two- and three-dimensional culture. Exp Cell Res2003 Feb 15;283(2):146-55.

263. Matt P, Habashi J, Carrel T, Cameron DE, Van Eyk JE, Dietz HC. Recent advances in understanding Marfan syndrome: should we now treat surgical patients with losartan? J Thorac Cardiovasc Surg2008 Feb;135(2):389-94.

264. Radonic T, de Witte P, Baars MJ, Zwinderman AH, Mulder BJ, Groenink M. Losartan therapy in adults with Marfan syndrome: study protocol of the multi-center randomized controlled COMPARE trial. Trials2010;11:3.

265. Makadia HK, Siegel SJ. Poly Lactic-co-Glycolic Acid (PLGA) as Biodegradable Controlled Drug Delivery Carrier. Polymers (Basel)2011 Sep 1;3(3):1377-97.

266. Lu JM, Wang X, Marin-Muller C, Wang H, Lin PH, Yao Q, Chen C. Current advances in research and clinical applications of PLGA-based nanotechnology. Expert Rev Mol Diagn2009 May;9(4):325-41.

267. Danhier F, Ansorena E, Silva JM, Coco R, Le Breton A, Preat V. PLGA-based nanoparticles: An overview of biomedical applications. J Control Release2012 Jul 20;161(2):505-22.

268. Astete CE, Sabliov CM. Synthesis and characterization of PLGA nanoparticles. J Biomater Sci Polym Ed2006;17(3):247-89.

269. Wang XY, Xu H, Zhao YQ, Wang SN, Abe H, Naito M, Liu YL, Wang GQ. Poly(lactide-co-glycolide) encapsulated hydroxyapatite microspheres for sustained release of doxycycline. Mater Sci Eng B-Adv2012 Mar 15;177(4):367-72.

270. Patel RS, Cho DY, Tian C, Chang A, Estrellas KM, Lavin D, Furtado S, Mathiowitz E. Doxycycline delivery from PLGA microspheres prepared by a modified solvent removal method. J Microencapsul2012;29(4):344-52.

271. Lu L, Stamatas GN, Mikos AG. Controlled release of transforming growth factor beta1 from biodegradable polymer microparticles. J Biomed Mater Res2000 Jun 5;50(3):440-51.

272. Jaklenec A, Hinckfuss A, Bilgen B, Ciombor DM, Aaron R, Mathiowitz E. Sequential release of bioactive IGF-I and TGF-beta 1 from PLGA microsphere-based scaffolds. Biomaterials2008 Apr;29(10):1518-25.

273. Kagan HM, Tseng L, Simpson DE. Control of elastin metabolism by elastin ligands. Reciprocal effects on lysyl oxidase activity. J Biol Chem1981 Jun 10;256(11):5417-21.

274. Wu WJ, Vrhovski B, Weiss AS. Glycosaminoglycans mediate the coacervation of human tropoelastin through dominant charge interactions involving lysine side chains. Journal of Biological Chemistry1999 Jul 30;274(31):21719-24.

275. Bartholomew JS, Anderson JC. Investigation of Relationships between Collagens, Elastin and Proteoglycans in Bovine Thoracic Aorta by Immunofluorescence Techniques. Histochem J1983;15(12):1177-90.

276. Alexis F. Factors affecting the degradation and drug-release mechanism of poly (lactic acid) and poly [(lactic acid)-co-(glycolic acid)] Polym Int. 2005`;54:36–46.

277. Lu L, Peter SJ, Lyman MD, Lai HL, Leite SM, Tamada JA, Uyama S, Vacanti JP, Langer R, Mikos AG. In vitro and in vivo degradation of porous poly(DL-lactic-co-glycolic acid) foams. Biomaterials2000 Sep;21(18):1837-45.

278. Zolnik BS, Burgess DJ. Effect of acidic pH on PLGA microsphere degradation and release. J Control Release2007 Oct 8;122(3):338-44.